



**CHARACTERIZATION OF THE HYDROGEOLOGY OF THE LODWAR ALLUVIAL
AQUIFER SYSTEM, TURKANA COUNTY, KENYA**

BY;

FLORENCE JEROTICH TANUI


I80/51693/2017

A THESIS SUBMITTED IN FULFILLMENT OF THE REQUIREMENTS FOR THE AWARD
OF THE DEGREE OF DOCTOR OF PHILOSOPHY IN GEOLOGY OF THE UNIVERSITY
OF NAIROBI

2021

DECLARATION

I declare that this thesis is my original work and has not been submitted elsewhere for examination, award of degree or publication. Where other people's work or my own work has been used, this has been properly acknowledged and referenced in accordance with the University of Nairobi's requirements.


Signature.......... Date..... **December 03, 2021**

Florence Jerotich Tanui


I80/51693/2017

Department Earth and Climate Sciences
University of Nairobi

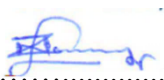
This thesis is submitted for examination with our approval as research supervisors:


Prof Daniel Olago Signature..... Date..... **December 03, 2021**

Department of Earth and Climate Sciences
University of Nairobi
P.O box 30197-00100
Nairobi Kenya


Dr Gilbert Ouma Signature..... Date..... **December 03, 2021**

Department of Earth and Climate Sciences
University of Nairobi
P.O box 30197-00100
Nairobi Kenya


Dr Zachariah Kuria Signature..... Date..... **December 03, 2021**

Department of Earth and Climate Sciences
University of Nairobi
P.O box 30197-00100
Nairobi Kenya

DEDICATION

I dedicate this research to my family. A special feeling and gratitude to my loving parents, my mother Alice for your prayers and to my late father William Rutto for the unique inspiration to my hard work and to all my siblings for being incredible cheerleaders throughout the entire doctorate program. Special dedication to my loving husband, who encouraged me to pursue my dreams and finish my thesis, and to my son and daughter for being the constant source of joy. Finally, to the Almighty God for good health throughout the study period.

ACKNOWLEDGEMENTS

The REACH Program, funded by UK Aid from the UK Foreign, Commonwealth and Development Office (FCDO) for the benefit of developing countries, provided funding for this study (Program Code 201880), covering tuition fees, data collection and analysis, and a monthly stipend. However, the opinions expressed and the information provided therein are not necessarily those endorsed by the FCDO, which cannot accept any liability for or reliance on such views or information.

I acknowledge the members of the REACH programme in all the partner countries, Kenya, Ethiopia, Bangladesh and the University of Oxford, who inspired the new research dimension related to water security. My appreciation goes to the REACH Kenya fraternity for the invaluable support in logistics and assistance during the data collection. The writing of this thesis would not have been successful without the invaluable support of my University Supervisors for technical guidance and exemplary supervision, especially Prof Daniel Olago, who was my lead supervisor. Special thanks go to my family for your constant support and motivation, especially for allowing me to go for my fieldworks, conferences, and workshops pertaining to my studies. I will forever be grateful for all your prayers throughout my study period.

ABSTRACT

Drylands account for more than a third of the world's land area and are characterized by less than 250 mm of rainfall per year. In these regions, groundwater is a strategic resource and plays a key role in economic development, especially in sub-Saharan Africa, where it is responsible for improving livelihoods. Lodwar town depends primarily on a poorly studied groundwater system for its municipal water supplies. The aim of this research was to establish the sustainability of this aquifer system through a comprehensive study of its hydrogeological characteristics, sensitivity to climate variability, and the influence of natural and anthropogenic processes, all of which are currently unknown yet critical for its sustainable management. The methods used were: detailed geological mapping and rock analysis (petrography and X-ray fluorescence); remote sensing (digital elevation models and vegetation cover maps) and drone mapping of Lodwar town for stream lineament analysis; evaluation of borehole drilling datasets including yields, static water levels, water rest levels, drawdowns, transmissivities, and borehole depth; geophysical surveys involving vertical electrical soundings for evaluation of the hydrogeological characteristics; aquifer hydrogeochemistry of surface (river, scoop holes, water pans) and groundwater, where field measurements included pH, Temp, and EC using hand-held Combo Tester HI98129 while, turbidity, total hardness, alkalinity, Ca^{2+} , Mg^{2+} , Na, K^+ , Fe^{2+} , Mn^{2+} , Cl^- , F^- , HCO_3^- , SO_4^{2-} and CO_3^{2-} NO_3^- , NO_2^- were measured at the Water Resources Central Laboratory based standard analytical procedures. Furthermore, stable isotopic analyses of oxygen-18, deuterium and tritium in water samples was done at Elemtex Lab, United Kingdom to establish the rainfall-surface water-groundwater interactions, groundwater age and recharge sources. The multifaceted dataset was analysed using descriptive and inferential statistics, including principal component analysis (PCA), hierarchical cluster analysis (HCA), the software PHREEQC for analysis of the water chemistry data, and all together, to develop the first conceptual aquifer model for this system. The findings of this research revealed that Lodwar and its surroundings are underpinned by three different and interconnected freshwater ($<1000\mu\text{S}/\text{cm}$) aquifers (shallow alluvial aquifer (SAA), the intermediate aquifer (IA) and the deep aquifer (DA)) that are collectively referred to as the Lodwar Alluvial Aquifer System (LAAS). The fourth, the Turkana Grit Shallow Aquifer (TGSA), is highly saline with electrical conductivity $> 5000\mu\text{S}/\text{cm}$ and fluoride values between 2.20 to 18.74 mg/L. The dominant water types are: Ca- HCO_3 (SAA and Turkwel river), Na- HCO_3 (IA), Ca- HCO_3 (Napuu Bh) and Na- HCO_3 (DA) and NaCl (TGSA). The petrographical, geochemical, isotopic and inferential statistical analyses indicate that rock-water interaction, Turkwel river recharge, and oxidation reactions control the SAA chemistry, while dissolution and evaporation are key factors affecting TGSA. The dominant processes in the IA include dissolution, ion exchange, and dilution. Elevated concentrations of NO_3^- and SO_4^{2-} in the wet as compared to the dry seasons, but still within WHO recommended limits, tritium values ranging from 1.10 to 2.24 in the SAA, IA and DA, and the isotopic values of surface water and groundwater, reflect strong links to modern rainfall and the Turkwel river, indicating that the LAAS is highly susceptibility to climate variability and pollution. The decreasing d-excess values from the SAA (2.18‰) to the intermediate aquifer (-6.81‰) and TGSA (-8.14‰) indicate that they are interlinked and isotope fractionation occurs during the lateral groundwater flow away from the Turkwel River. The study has attributed recharge of the LAAS to diffuse recharge by the Turkwel River and from the surface water of the Kawalase River during the wet season, as well as direct infiltration during rainfall events. This study provides comprehensive approaches for investigating the groundwater resources in data-scarce regions for their sustainable use and management.

TABLE OF CONTENTS

DECLARATION.....	ii
DEDICATION.....	iii
ACKNOWLEDGEMENTS	iv
ABSTRACT.....	v
TABLE OF CONTENTS	vi
LIST OF FIGURES	x
LIST OF TABLES	xviii
LIST OF ABBREVIATIONS AND ACRONYMS	xxii
DEFINITION OF TERMS.....	xxv
CHAPTER ONE: INTRODUCTION.....	1
1.1 Background	1
1.1.1 Global Perspectives.....	1
1.1.2 Regional Perspectives	2
1.1.3 National Perspectives.....	3
1.2 Statement of the Problem	5
1.3 General and Specific Objectives	7
1.3.1 General Objective	7
1.3.2 Specific Objectives	7
1.3.3 Research Questions.....	7
1.4 Justification and Significance.....	8
1.4.1 Justification	8
1.4.2 Significance.....	9
1.5 Scope and Limitation of the Study.....	10
1.6 The Layout of the Thesis.....	11

CHAPTER TWO: LITERATURE REVIEW	13
2.1 Introduction	13
2.2 Hydrogeological Characteristics of Aquifers	13
2.2.1 A global review of aquifer types.....	15
2.2.2 Aquifer characteristics and groundwater flow	18
2.3 Hydrogeochemical Characteristics of Volcano-Sedimentary and Alluvial Aquifers	20
2.3.1 Determinants of natural groundwater quality and vulnerability of alluvial aquifers to pollution20	
2.3.2 Hydrochemical facies and rock water interactions	21
2.4 Rainfall-Surface Water-Groundwater Linkages and Recharge Estimation	23
2.4.1 Rainfall - surface water – groundwater interactions	23
2.4.2 Recharge estimation with particular reference to ASALs	26
2.4.3 Age of groundwater	32
2.5 Conceptual Aquifer Geometry Modelling.....	34
2.6 Current Approaches to Sustainable Groundwater Management	34
2.7 Summary	35
CHAPTER THREE: STUDY AREA AND METHODS.....	37
3.1 Introduction	37
3.2 Description of the Study area	37
3.2.1 Location of the Study area	37
3.2.2 Demographics	38
3.2.3 Geological setting	40
3.2.4 Physiography and Drainage	45
3.2.5 Vegetation.....	47
3.2.6 Climate.....	48
3.2.7 Land Use	50

3.2.8	Water Resources	50
3.3	Research Design.....	52
3.4	Research Methodology.....	53
3.4.1	Hydrogeology of the Lodwar Alluvial Aquifer System	53
3.4.2	Hydrogeochemistry and Aquifer Susceptibility to Pollution.....	69
3.4.3	Rainfall-Surface Water-Groundwater Interactions and Groundwater Recharge	80
3.4.4	Development of aquifer conceptual model	86
CHAPTER FOUR: RESULTS AND DISCUSSION.....		88
4.1	Introduction	88
4.2	Results	88
4.2.1	Hydrogeological characteristics of the LAAS	88
4.2.2	Hydrogeochemistry and Water Quality	144
4.2.3	Rainfall-Surface Water-Groundwater Interactions and Groundwater Recharge ..	180
4.2.4	Development of Conceptual aquifer model	192
4.3	Discussion	198
4.3.1	Lodwar Alluvial Aquifer System.....	198
4.3.2	Implications for sustainable groundwater use, demand, and aquifer protection...	206
CHAPTER FIVE: CONCLUSIONS AND RECOMMENDATIONS		208
5.1	Conclusions	208
5.2	Recommendations	211
5.3	Recommendations For Future Research	213
REFERENCES.....		215
APPENDICES.....		249
	Appendix 3.1: Analytical rationale – hydrogeological characteristics of the LAAS.....	249
	Appendix 3.2 Analytical rationale – hydrogeochemistry of the LAAS	253

Appendix 3.3: Analytical rationale – Rainfall-Surface water -Groundwater Interactions.....	259
Appendix 4.1: Field description for the quartzo-feldspathic gneiss.....	259
Appendix 4.2: Field description of the Turkana grits samples collected from the study area	260
Appendix 4.3: Field description of the Holocene sediments between Napuu and Lolupe, east of Lodwar, Natir and at Turkwel Riverbank at Kakwanyang area.....	261
Appendix 4.4: Field description of the Sandstone outcrops in the study area	262
Appendix 4.5: Field description of conglomerate and grainstone samples.....	262
Appendix 4.6: Field description of volcanic rocks (augite basalt, nepheline-phonolite, and dolerite dyke found in Turkana grits and basement rocks	263
Appendix 4.7: Results of the whole rock analysis for samples collected from the study area (1645 -3858).....	264
Appendix 4.8: Results of the major elements obtained from X-fluorescence spectrometry (XRF) at ICRAF lab (1648-3858); the results have been arranged in order of rock samples where “nd” refers to not detected while “-“ were not measured.....	267
Appendix 4.9: Results of the trace elements obtained from X-fluorescence spectrometry (XRF) at ICRAF lab (1648-3858); the results have been arranged in order of rock samples where “nd” refers to not detected while “-“were not measured	269
Appendix 4.10: Results of the vertical electrical soundings for VES 1 to VES 15	272
Appendix 4.11: Results of the vertical electrical soundings of VES 16 to VES 27	273
Appendix 4.12: VES graphs for VES 17 to 20 carried out on section A of the LAAS around Nadapal and Naoyatira areas.....	274
Appendix 4.13: VES graphs carried out in section B of the LAAS between Kakemera and Nachomin areas.....	275
Appendix 4.14: VES graphs for section C of the LAAS around Kakwanyang and Nang'omo areas	276
Appendix 4.15: VES graphs of section d of the LAAS covering Napuu, Lolupe and Nayuu areas	

Appendix 4.16: Results for oxygen-18, deuterium and tritium for rainfall and surface water (Turkwel River = TR, Kawalase River = KR, water pans = pan, scoop holes = SH, Eliye sprong and Lake Turkana = LT) samples in Lodwar and its environs.....	278
Appendix 4.17: Results for oxygen-18, deuterium and tritium for groundwater samples in shallow alluvial aquifer (SAA), Turkana grit shallow aquifer (TGSA), intermediate aquifer (IA), deep aquifer (DA), and for wells with unknown depth (DU); (nm = not measured).....	279
Appendix 4.18: Groundwater samples in the SAA, IA, DA and for wells with unknown depth (DU) used in the calculation of age of groundwater in the LAAS.....	283

LIST OF FIGURES

Figure 1.1: Layout of the thesis	12
Figure 2.1: Schematic illustration of the confined and unconfined aquifers (source: Salako and Adepelumi, 2018)	15
Figure 2.2: Diagrammatic representation of the hydrological cycle, including rain-fed and irrigated farming with potential abstraction of groundwater (Source: Green 2016).....	24
Figure 2.3: Summary of hydrologic processes in rainfall - surface water - groundwater systemic interactions.....	25
Figure 3.1: Location of the study area within the Turkwel River watershed	38
Figure 3.2: Geological map of Turkana county showing the location of the study within the Turkwel River Basin (Partly modified from the Ministry of Energy and Regional Development 1987)	41
Figure 3.3: Geological map of Turkwel River Basin (Geological Map of Kenya (MERD), 1987)	42
Figure 3.4: Physiography and drainage map of Lodwar and its environs	47

Figure 3.5: Vegetation cover map of the study area within the mid-Turkwel watershed.....	48
Figure 3.6: Deviation of mean annual rainfall percentage based on 1950-2012 long-term mean (Opiyo et al., 2015).....	49
Figure 3.7: Long-term rainfall data for Lodwar met station based on CHIRP (2018) dataset indicating increasing rainfall in recent years	49
Figure 3.8: Research Design for Lodwar Alluvial Aquifer System.....	53
Figure 3.9: Location of rock samples collected during the geological mapping	57
Figure 3.10: Flight paths for the drone during the flight mission in Lodwar town overlaid on the ESRI satellite imagery	58
Figure 3.11: Grid pattern for the image collection points within the boundray of Lodwar town.	59
Figure 3.12: Schlumberger array configuration used in the study area	60
Figure 3.13: Image showing Schlumberger array configuration used during the fieldwork for the vertical electrical soundings.....	60
Figure 3.14: VES Locations within the Lodwar Alluvial Aquifer System.....	61
Figure 3.15: Workflow for processing drone-acquired images using Pix4D photogrammetric software (Hawkins, 2016).....	65
Figure 3.16: Surface water and groundwater sources in the mid-Turkwel River watershed.....	70
Figure 3.17: Distribution of surface water and groundwater isotope samples within the mid-Turkwel watershed.....	82
Figure 3.18: Simple schematic diagram of TC/EA-IRMS for determination of $\delta^2\text{H}$ and $\delta^{18}\text{O}$	83
Figure 4.1: Geological map of the area showing the distribution groundwater abstraction sources in Lodwar town and its environs.....	89

Figure 4.2: Exposures of Turkana Grit (a) calcite-cemented grit at Naiwaitorong area, (b) an exposure of the Turkana grit formation, (c) grits at Naotin intercalated with a sandstone unit, and (d) grit showing graded bedding (Field Photo May, 2018)	91
Figure 4.3: Exposed Holocene sediments illustrating thick deposits and erosional features at Napuu-Nayuu areas, Turkana county	92
Figure 4.4: STRM of the study area within the Turkwel River watershed.....	94
Figure 4.5: Drainage lineaments map of the area extracted from the STRM-based DEM.....	95
Figure 4.6: Digital terrain model of Lodwar town produced from drone-acquired images that excluding the airport section.....	96
Figure 4.7: Five-meter contour map of Lodwar town obtained from the drone-acquired images	97
Figure 4.8: Comparison between (a) drone-based DEM and (b) STRM-based DEM for Lodwar town.....	98
Figure 4.9: Comparisons between (a) UAV drone-based slope angle map and (b) STRM-based slope angle map.....	98
Figure 4.10: Orthomosaic image obtained from the processing of the drone-acquired images. The Mapping exercise did not cover Lodwar airport which is demarcated as a no-fly zone for drones	99
Figure 4.11: Zooming inside the red rectangle within the orthomosaic image	99
Figure 4.12: Textured 3D model for Lodwar municipality excluding the airport area (original model too large to be included in the report).....	100
Figure 4.13: Microphotograph of the nepheline-phonolite (sample 1650) observed under (a) PPL and (b) XPL showing the prismatic nepheline crystals and euhedral hematite grains, with cataclastic deformation of plagioclase was observed in the thin section.....	103

Figure 4.14: Microphotograph of the dolerite dyke rock within the Turkana grits shows fracturing in PPL and with no fluid inclusion entrapment observed, in XPL, possible twinning of is observed. However, this can be further evaluated in a slice < 30 μ	104
Figure 4.15: Microphotograph of the conglomerate sample (3857) under (a) PPL and (b) XPL showing sub-rounded quartz grains and prismatic nepheline crystal with distinct cleavages	105
Figure 4.16: Microphotographs for the medium-grained gravelly sandstone (sample 1659) under (a) PPL and (b) XPL, compact altered sandstone shown in PPL (b) and XPL (c); coarse-grained gravelly-sandstone (sample 3858) shown in PPL (e) and XPL (f)	106
Figure 4.17: Microphotographs of the Turkana grit samples showing zoning features (a and b) calcite-cemented matrix on quartz and feldspars minerals (b and c).....	107
Figure 4.18: Microphotographs of the quartzo-feldspathic gneiss adjacent to the dolerite intrusion showing highly deformed surfaces (a and b) and fine-grained surface of quartz and feldspars further away from the intrusion (c and d)	108
Figure 4.19: (a) An-Ab-Or normative classification based on O'Connor (1965) and 9b) AFM diagram for the quartzo-feldspathic gneiss showing high Na ₂ O and K ₂ O content (after Irvine and Baragar, 1971).....	110
Figure 4.20: Variations of the chemical compositions of the major elements among the clusters of Turkana grits	112
Figure 4.21: Sandstone classification diagram after Herron (1988).....	124
Figure 4.22: Variations of major and trace elements in the conglomerate at Lodwar town (1677) and Natir area (3857)	125
Figure 4.23: Variations in compositions of major elements in Grainstone samples	126
Figure 4.24: Distribution of the major elements in the rock samples of the nepheline-phonolite at Lodwar town, grit contact and at Kanamkemer.....	127

Figure 4.25: Occurrence of major and trace elements in the augite basalt with a cumulative frequency curve showing their distribution	128
Figure 4.26: Compositions of major elements in the dolerite dyke in the Turkana grits and in the Basement system.....	129
Figure 4.27: TAS classification diagram for the volcanic rocks	130
Figure 4.28: AFM classification diagram After Irvine et al., 1971 showing augite basalt and dolerite in the Turkana grit being cacl-alkaline while the nepheline-phonolite, and the dolerite in the Basement system as tholeiitic in nature	131
Figure 4.29: Pseudo-cross-section and resistivity cross-section between VES 18, 19 and 20 where VES 17 was omitted from the pseudo section since it was not in the straight path with the three selected points.....	132
Figure 4.30: Pseudo-cross-section and resistivity cross-section between Kakemera (east) and Nachomin (west) areas (VES 13, 15,16, 24, and 23).....	134
Figure 4.31: Pseudo-cross-section and resistivity cross-section of VES 21 and VEs 22 between Kakwanyang and Nang’omo areas	135
Figure 4.32: Pseudo-cross-section from west to east of Section D of the LAAS (a) and from south to north (b) toward the Turkwel River.....	136
Figure 4.33: Variations in electrical resistivities values with depth (ρ_1 to ρ_4) based on the 26 VES locations	137
Figure 4.34: Resistivity values of the inferred aquifer layer in the study area showing values <10 Ohm-m indicating possible saline groundwater	138
Figure 4.35: Distribution of secondary data points in the study area with depth information - the majority of shallow boreholes are along the Turkwel River and are mainly concentrated within Lodwar town.....	140

Figure 4.36: Spatial distribution of transmissivity values in the study area based on secondary data obtained from the WRA database	143
Figure 4.37: Piezometric surface map of the study area determined from static water levels ...	144
Figure 4.38: Seasonal variations in the physico-chemical parameters in the river water (RW), shallow alluvial aquifer (SAA) intermediate aquifer (IA), Turkana Grit Shallow Aquifer (TGSA) and the deep aquifer (DA).....	157
Figure 4.39: Seasonal variations in the major cations in the river water (RW), shallow alluvial aquifer (SAA) intermediate aquifer (IA), Turkana Grit Shallow Aquifer (TGSA) and the deep aquifer (DA).....	158
Figure 4.40: Seasonal variations in the major anions in the river water (RW), shallow alluvial aquifer (SAA) intermediate aquifer (IA), Turkana Grit Shallow Aquifer (TGSA) and the deep aquifer (DA).....	159
Figure 4.41: Spatial variation of the physicochemical parameters (EC, PH, temperature and turbidity) for the river water (RW), shallow alluvial aquifer (SAA) intermediate aquifer (IA), Turkana Grit Shallow Aquifer (TGSA) and the deep aquifer (DA)	161
Figure 4.42: Groundwater and surface water piper diagram (a) in the wet season and in (b) the dry season	163
Figure 4.43: Changes in 58 groundwater samples collected in the wet season (May 2018) and in the dry season (February 2019) in the hydrochemical facies	164
Figure 4.44: Variations in the water quality index values during the (a) wet season and in the (b) dry season showing improved water quality in all the aquifers in the dry season.....	166
Figure 4.45 WQI map for the study area based on the 94 groundwater samples of the wet season	166
Figure 4.46: Factor loadings for PC 1 and PC 2 during (a) wet season and during (b) dry season for the SAA; TGSA (c) wet season and during (d) dry season; IA during (e) wet season and during	

(f) dry season and for the wells without the drilled depth information (g) wet season and during (h) dry season..... 169

Figure 4.47: Dendrogram (a) in the wet season and (b) in the dry season for groundwater samples, showing three main clusters in the wet season and four main groups in the dry season, based on aquifer mineralization levels..... 171

Figure 4.48: Saturation indices of minerals in the wet season (May) and in the February - dry season for (a) SAA; (b) TGSA; (c) IA; (d) DA and wells without drilled depth information.. 173

Figure 4.49: Plots for Na^+/Cl^- in groundwater in the (a) wet season and (b) dry season and for the relationship between $[\text{Ca}^{2+} + \text{Mg}^{2+} - \text{SO}_4^{2-} - \text{HCO}_3^-]$ and $[\text{Na}^+ - \text{Cl}^-]$ (c) and (d) in the surface water, shallow alluvial aquifer (SAA), intermediate aquifer (IA), Turkana grit shallow aquifer (TGSA) and the deep aquifer (DA) (Fisher and Mullican, 1997)..... 175

Figure 4.50: Nitrate levels across the Turkwel river samples indicating elevated levels for the samples within the Lodwar Municipal boundary in the dry season of February 2018..... 177

Figure 4.51: Heat map for NO_3 within Lodwar Municipal boundary indicating areas of elevated concentrations across the Lodwar municipality..... 179

Figure 4.52: Isotope signatures of (a) $\delta^{18}\text{O}$ and (b) $\delta^2\text{H}$ in river water (KR and TR), water pans, scoop holes (SH), spring and lake samples, as well as groundwater samples from the shallow alluvial aquifer (SAA), intermediate aquifer (IA), Turkana grit shallow aquifer (TGSA) and the deep aquifer (DA) 181

Figure 4.53: Regression lines of $\delta^2\text{H}$ versus $\delta^{18}\text{O}$ for the nearby GNIP stations; Kericho, Moyale and Soroti with their respective regression statistics 185

Figure 4.54: Relationship between $\delta^{18}\text{O}$ and $\delta^2\text{H}$ for the rain sample, Turkwel River, Kawalase River, scoop holes, water pans and springs in the study area..... 186

Figure 4.55: Regression analysis for $\delta^{18}\text{O}$ and $\delta^2\text{H}$ for SAA (<30m), IA (31-100m), and the TGSA(<30m) in relation to the Soroti LMWL and the GMWL. The graph also shows the position

of the rain sample, Turkwel River samples, spring sample, samples of the DA (>100), and the TGSA samples	187
Figure 4.56: Tritium trend in the groundwater of the LAAS between 2004 and 2018, indicating ^3H values approaching pre-bomb levels.....	189
Figure 4.57: Spatial distribution of tritium in groundwater in the Lodwar Alluvial Aquifer System (LAAS); older groundwater is saline unless within the proximity of the Turkwel River while the younger groundwater is fresh.....	190
Figure 4.58: Spatial distribution of (a) $\delta^{18}\text{O}$ and (b) $\delta^2\text{H}$ for all the groundwater samples showing isotope enrichment along the Turkwel River, suggesting diffuse recharge.....	192
Figure 4.59: Cross-section lines (AB, CD, EF, and GH) representing different part of the study area indicating variations in surface geology and topography.....	194
Figure 4.60: Geological cross-sections along for selected profiles in the study area, showing changes in the surface geology with depth	195
Figure 4.61: Conceptual aquifer model of the Lodwar Alluvial Aquifer System showing the three sub-systems; shallow alluvial aquifer (SAA), intermediate aquifer (IA) and deep aquifer (DA). The SAA is unconfined while the IA and DA are semi-confined and are separated by semi-impervious layers (aquitard)	197

LIST OF TABLES

Table 3.1: Constituency population and population density in Turkana County (Source: KNBS, 2009; 2019).....	39
Table 3.2: Population census of the major urban centres in Turkana County (Source: KNBS, 2009;2019).....	40
Table 3.3: Desktop study data sources in the area and their specific contribution to the hydrogeological of the study area.....	55
Table 3.4: VES orientation;(east (E), west (W), north (N), south (S), probing depth (m), elevation (m asl), and length of the AB line at each sounding location of the vertical electrical sounding (VES)	61
Table 3.5: Representative values of porosity and specific yield for different geological materials (Brassington, 2010).....	66
Table 3.6: Typical values of hydraulic conductivity in various geological materials	68
Table 3.7: Atomic masses and oxidation states of cations and anions tested.....	72
Table 3.8: The rating weights (wi) and unit weight (Wi) assigned to the water quality parameters	74
Table 3.9: Water quality rating based on WQI.....	76
Table 3.10: Samples submitted for stable isotope analysis at Elemtex lab, United Kingdom	81
Table 4.1: Comparison of STRM-based and drone-based digital elevation models and slope angle maps	97
Table 4.2: Results for the major oxides, major elements and trace metals in the quartzo-feldspathic gneiss (three rock samples, see Appendix 4-7 to 4-9 for detailed results per sample).....	110

Table 4.3: Description of the different clusters of the Turkana grits based K Means Clustering Algorithm.....	111
Table 4.4: Class centroids for each cluster based on the compositions of the major elements in the rock samples.....	112
Table 4.5: Description of the major oxides, major and trace elements of the four clusters of the Turkana grits	113
Table 4.6: Descriptive statistics for the major elements (Cluster 1 to 4)for the different groups of Turkana grits samples (SD – standard deviation).....	114
Table 4.7: Results and summary statistics for the major oxides, major and trace elements of the Holocene sediments East of Lodwar town.....	115
Table 4.8: Results and summary statistics for the major oxides, major and trace elements of the Holocene sediments at Napuu/Lolupe area.....	117
Table 4.9: Results and summary statistics for the major oxides, major and trace elements of the Holocene sediments at Turkwel River bank near Kakwanyang area	118
Table 4.10: Results and summary statistics for the Major oxides, major and trace elements of the Holocene sediments at Natir	119
Table 4.11: Ratio of $\text{SiO}_2 / \text{Al}_2\text{O}_3$ showing the maturity of Holocene sedimentsin the study area while the ratio of $\text{K}_2\text{O} / \text{Al}_2\text{O}_3$ indicating the pelitic origin of the sediments.....	121
Table 4.12: Results and summary statistics for the major oxides in the (a) fine-grained sandstone and (b) coarse-grained sandstone in the study area	122
Table 4.13: Results and summary statistics for the major elements in the (a) fine-grained sandstone and (b) coarse-grained sandstone in the study area	123
Table 4.14: Calculated aquifer properties based on geological mapping, secondary data and geophysics covering the proposed aquifer sections	139

Table 4.15: Minimum and maximum porosity values of various geological materials based on Todd, 1980	142
Table 4.16: Physico-chemical results for samples collected in the dry season of February 2018 for the Turkwel River shaded fields are values that exceed guideline values for drinking water, and 'nd' refers to not detected. The samples were arranged (left to right) from upstream to downstream	146
Table 4.17: Physico-chemical parameters results during the February 2018 dry season for the SAA and IA (2452 and 2460); (the shaded values exceed the drinking water guidelines of KEBS (2014) and WHO (2011))	148
Table 4.18: Physicochemical parameters for the SAA in the wet season (shaded fields indicate values that exceed the guidelines for drinking water)	149
Table 4.19: Physico-chemical parameters for the SAA in the dry season (February 2019 - shaded values exceed the KEBS and WHO guidelines for drinking water).....	150
Table 4.20: Physico-chemical parameters for the TGSA during the wet and dry seasons (shaded values exceed the KEBS (2014) and WHO (2011) guidelines for drinking water).....	152
Table 4.21: Results for the intermediate aquifer physico-chemical parameters in the wet season (the shaded fields are values that exceed guideline values for drinking water of KEBS (2014) and WHO (2011))	154
Table 4.22: Results for the intermediate aquifer measured water quality parameters of February 2019 (the shaded values exceed the drinking water guidelines of KEBS (2014) and WHO (2011))	155
Table 4.23: Water quality parameters for the deep aquifer during the dry and wet seasons (highlighted values exceed the KEBS (2014) and WHO (2011) guideline value for drinking water)	156
Table 4.24: Groundwater samples with variations in hydrochemical facies between the wet and the dry season.....	163

Table 4.25: Water quality index (a) in the wet season and (b) in the dry season for the SAA, IA, TGS and the DA, and for the boreholes and handpumps with an unknown depth.....	165
Table 4.26: Institutional groundwater supply sources with NO ₃ levels >5.0 mg/L in the wet and dry seasons	178
Table 4.27: Descriptive statistics for $\delta^{18}\text{O}$ and $\delta^2\text{H}$ in rainfall and surface water in the Lodwar and its environs (n/a for median and standard deviation values represent one sample available for analysis)	182
Table 4.28: Descriptive statistics Results for oxygen-18, ² H and ³ H groundwater samples in the SAA, TGSA, IA, DA, and for wells with unknown depth (DU).....	184
Table 4.29: Regression results from the shallow alluvial aquifer (SAA), Turkana grits shallow aquifer (TGSA), intermediate aquifer and for the wells with unknown depth (DU) relative to the GMWL and LWML.....	192

LIST OF ABBREVIATIONS AND ACRONYMS

Abbreviation	Meaning
AAS	Atomic Absorption Spectroscopy
Al	Aluminium
As	Arsenic
ASAL	Arid and semi-arid land
asl	Above Sea Level
BCM	Billion cubic meters
Bh	Borehole
Ca	Calcium
CF	Continuous flow
CKR	Central Kenyan Rift
Co	Cobalt
Cr	Cromium
Cu	Copper
DA	Deep aquifer
DEM	Digital elevation model
EC	Electrical Conductivity
EPA	Environmental Protection Agency
FAO	Food Agricultural Organization
GMWL	Global meteoric water line
GNIP	Global Network of Isotopes in Precipitation
GPS	Geographic Positioning System
GSD	Ground Sampling Distance
HCA	Hierarchical Cluster Analysis
Hp	Hand pump
IA	Intermediate Aquifer
IAEA	International Atomic Energy Agency
ICRAF	International Centre of Agriculture and Forestry
IRMS	isotope ratio mass spectrometer
JICA	Japanese International Corporation Agency
K	Potassium
KEBS	Kenya Bureau of Standards
KISEDIP	Kalobeyei Integrated Socio and Economic Development Programme
Km ²	Square kilometre
KNBS	Kenya National Bureau of Statistics
KPHC	Kenya Population and Housing Census
LAAS	Lodwar Alluvial Aquifer System
LMWL	Local meteoric Water Line

LOWASCO	Lodwar Water and Sewerage Company
LSC	Liquid scintillation counter
m ²	Square meter
MCM	Million Cubic Meter
Mg	Magnesium
mg/L	Milligram per litre
Mn	Manganese
Mo	Molybdenum
MWI	Ministry of water and Irrigation
MWL	Meteoric Water Line
Na	Sodium
NAS	Nairobi Aquifer System
NDMA	National Drought Management Authority
NE	North East
NGO	Non-Governmental Organization
Ni	Nickel
NKR	Northern Kenyan Rift
NW	North West
P	Phosphorous
Pb	Lead
PCA	Principal Component Analysis
PPL	Plane polarised light
RTI	Radar Technologies International
S	Sulphur
SAA	Shallow Alluvial Aquifer
SDD	Silicon Drift Detector
SE	South East
Se	Selenium
SPA	Service Provision Agreement
SPSS	Statistical Package for Social Sciences
SSA	Sub-Saharan African
SWC	soil water content
TC/EA	Temperature conversion elemental analyser
TCG	Turkana County Government
TGSA	Turkana Grit Shallow Aquifer
Ti	Titanium
TU	Tritium units
UAV	Unmanned-aerial vehicles
UNESCO	United Nations Educational, Scientific and Cultural Organization
UNHCR	United Nations High Commission for Refugees
USA	United States

VES	Vertical Electrical Sounding
WHO	World Health Organization
WQI	Water Quality Index
WRA	Water Resources Authority
WTF	Water table fluctuation
XPL	Crossed polarised light
XRF	X-ray fluorescence
Zn	Zinc

DEFINITION OF TERMS

Term	Definition
Aquiclude	An impervious layer that overlays an aquifer (Mook, 2000)
Aquifer	An aquifer is defined as a rock or unconsolidated sediment body with adequate permeability to allow water to flow through it. (Chilton and Seiler, 2006)
Aquitard	An aquitard is a body that, such as a lump of clay, a till, or a poorly fractured igneous or metamorphic rock does not allow a significant amount of water to be transferred (Salako and Adepelumi, 2018)
Artesian Well	A well drilled in a confined aquifer where water rises above the surface of the ground and flows out if it is not capped (Salako and Adepelumi, 2018)
Darcy's Law	States that the rate of flow is directly proportional to the hydraulic gradient (Chilton and Seiler, 2006)
Electrical Conductivity (EC)	It is an aqueous solution measurement of the dissolved material, which relates to the material's ability to conduct electrical current through it.
Groundwater	Groundwater refers to water in the saturated region beneath the water table (Salako and Adepelumi, 2018)
Groundwater Vulnerability	The pollution vulnerability of groundwater tends or is likely to occur after being introduced in some location above the uppermost part of the aquifer at a specified location in the groundwater system (Ghosh <i>et al.</i> , 2015)
Hydraulic Conductivity (K)	It refers to the water transmitting property of the aquifer, also known as the permeability coefficient (Chilton and Seiler, 2006).
Hydraulic Head	The hydraulic head denotes a 'piezometric level' for confined aquifers and 'water table' for unconfined aquifers (Chilton and Seiler, 2006)
Hydraulic Head	The height of the water level in the aquifer in an observation well or borehole (Chilton and Seiler, 2006).
Lagga	Same as <i>Wadis</i> - A large stream channel that carries water during the rainfall events mostly dry up a few days following the rains (JICA, 2012)
Net Recharge	The amount of water that penetrates per unit area from the surface to the groundwater table (Salako and Adepelumi, 2018)
Perched Water Table	The upper boundary of a confined aquifer that comprises the water table (Chilton and Seiler, 2006)
Perched Aquifer	An aquifer type in which water is present under conditions of the water table forming the perched water table (Chilton and Seiler, 2006)

Porosity	Porosity within unconsolidated sediments or sedimentary rocks refers to the percentage of open space. In sediments or sedimentary rocks, primary porosity often refers to the spaces between grains, while secondary porosity refers to porosity that developed after the rock was formed, i.e. fractures. The porosity of volcanic rock is often associated with vesicles, whereas limestone may have additional porosity associated with fossil cavities (Chilton and Seiler, 2006).
Recharge	The entry of water into the saturated zone (Mook, 2000)
Recharge	Recharge refers to as the entry of water into the saturated zone (Mook, 2000)
Specific Storage	Specific storage refers to the amount of water released or taken into storage from the aquifer per unit volume of the aquifer and per unit change in the hydraulic head (Chilton and Seiler, 2006).
Specific Yield (S_y)	Specific yield refers to the drainable porosity of an aquifer and is represents the ratio of the volume of water drained by gravity after saturation (Salako and Adepelumi, 2018)
Storage Coefficient	Aquifer Storage Coefficient or Storativity (S) is the volume of water released from storage per unit area of an aquifer per unit change in the hydraulic head (Mook, 2000).
Storativity	The amount of water discharged from storage per unit of aquifer or aquitard surface area per unit of hydraulic head decline (Salako and Adepelumi, 2018)
Transmissivity	The aquifer's transmissivity (T) refers to the amount of water transmitted laterally through the aquifer unit by full saturation of the aquifer under the hydraulic gradient (Salako and Adepelumi, 2018).
Unsaturated Zone	Refers to the part of the subsurface that is above the water table level and is partially saturated, i.e. in the pore spaces between sediment grains, contains both air and liquid water (Chilton and Seiler, 2006).
Wadis	A channel of a watercourse that is dry except during periods of rainfall (Aboubaker <i>et al.</i> , 2013)
Point source pollution	Point sources of pollution refer to the discharge of contaminants into the groundwater through a pipe, ditch, discrete fissure, tunnels, concentrated animal feed, and municipal wastewater (Garba Abdullahi <i>et al.</i> , 2014; Islam <i>et al.</i> , 2017)
Non-point source pollution	Nonpoint sources may result from agricultural chemicals (fertilizers and pesticides) through surface runoff, precipitation, atmospheric deposition, seepage, drainage, or hydrological modification (Islam <i>et al.</i> , 2017).

CHAPTER ONE: INTRODUCTION

1.1 Background

Groundwater resources have recently gained much attention globally as an important source of water supply for domestic, industrial and agricultural water demands (Al-Ruwaih, 2017; Tlili-zrelli *et al.*, 2018; Wu *et al.*, 2015). Groundwater supplies account for one-third of all freshwater consumption worldwide, with an estimated consumption of 36%, 42% and 27% for domestic, agricultural and industrial uses, respectively (Taylor *et al.*, 2012). Today, about half of the megacities in the world and hundreds of major cities on all continents rely on groundwater for the above major uses (Jaroslav and Van der Gun, 2004), while rural communities and small towns rely on it to supply domestic water, particularly in arid areas (UNESCO, 1998). The hydrogeological setting of groundwater systems across the globe is unique to every region (Jaroslav and Van der Gun, 2004; Liu *et al.*, 2018; Shirazi *et al.*, 2015).

Studies have revealed that the natural groundwater quality and geochemical characteristics of aquifers are consistent with the geology of the area (Chae *et al.*, 2004). Generally, shallow groundwater systems are more vulnerable to natural and anthropocentric factors (Khatri and Tyagi, 2014) that affect both groundwater quality and quantity. Climate influences groundwater systems directly through recharge from precipitation and indirectly by variations in groundwater use (i.e. increased abstraction during droughts) (Andrés-Doménech *et al.*, 2015; Taylor *et al.*, 2012). Increased human activities have led to land-use changes that have modified the climate, resulting in increased variability in precipitation (Tague *et al.*, 2008), soil moisture, surface and groundwater (Taylor *et al.*, 2012). In addition, sustainable groundwater development is continuously threatened by a population increase, competing demands for water, and climate change (Dennehy *et al.*, 2015). Therefore, sustainable groundwater management strategies require interdisciplinary science that provides accurate knowledge and tools for informed decision-making.

1.1.1 Global Perspectives

Globally, groundwater resources are still poorly assessed and, in many cases, are not managed in a sustainable manner (Famiglietti, 2014). Four major hydrogeological settings define the distribution of groundwater resources in the world; basement, sedimentary basins, high relief folded mountain and volcanic regions (Jaroslav and Van der Gun, 2004). Unlike deep

groundwater, shallow groundwater systems are common in most places (Famiglietti, 2014; Jaroslav and Van der Gun, 2004).

In arid areas worldwide, alluvial aquifers in wadis and river plains are important groundwater resources (Van der Gun, 2010). Alluvial aquifers are often limited in width and thickness and are the easiest to exploit of all the aquifer systems due to the shallow water table, good drinking water quality and significantly high yields. Most alluvial aquifers comprise sand and gravel and mostly unconfined. In ASAL regions, alluvial aquifers in the valleys of seasonal or ephemeral streams often have permanent subsurface flows (Jaroslav and Van der Gun, 2004). These aquifers may also receive additional recharge by infiltration of excess irrigation water, sometimes contributing the most recharge (González-Trinidad *et al.*, 2017). Thus, they are highly vulnerable to human-induced pollution (Goni *et al.*, 2019; D. Zhang *et al.*, 2019). Furthermore, strong hydraulic links with rivers and streams characterize alluvial aquifers, resulting in the exchange of water between seasons; i.e. streams recharge the aquifers in the wet season and are drained in the dry season (Jaroslav and Van der Gun, 2004). This process makes the alluvial aquifers vulnerable to rainfall and streamflow variability (Van der Gun, 2010). Sustainable development of groundwater sources in alluvial aquifers, therefore, requires a detailed understanding of their hydrogeological characteristics (Liu *et al.*, 2018; Shirazi *et al.*, 2015), water quality and groundwater chemistry (Abid *et al.*, 2011; Aghazadeh *et al.*, 2017), as well as their interactions with the river systems (Atuahene, 2017; Hinzman *et al.*, 2000; Teng *et al.*, 2018).

1.1.2 Regional Perspectives

Groundwater is a vital source of water supply in Africa (MacDonald and Adelana, 2008), especially in ASALs, where surface water resources are limited (Adelana *et al.*, 2011). Indeed, sub-Saharan Africa is a region that depends largely on groundwater (Lapworth *et al.*, 2017; Xu *et al.*, 2019) and has extensive drought-prone areas (Foster *et al.*, 2012) such as Somalia, Burundi, Niger, Ethiopia, Mali and Chad (Shiferaw *et al.*, 2014). Therefore, the successful development of sustainable groundwater supplies is crucial for the continent's future supply of safe water, economic growth, and food security (MacDonald and Adelana, 2008). The major setback, however, to achieving sustainable groundwater development and management is the lack of scientific understanding of the groundwater resources (MacDonald *et al.*, 2012; Xu *et al.*, 2019) indicated that the groundwater resources in Africa are distributed unevenly with the largest aquifers being the North Africa's sedimentary aquifers, including Algeria, Libya, Egypt and what

was then Sudan (current Sudan and South Sudan). Alluvial aquifers hosted in unconsolidated sediments form the vast majority of the sedimentary aquifers (MacDonald and Davies, 2000). They occur in riparian zones of ephemeral and perennial rivers and comprise important groundwater resources in sub-Saharan Africa (Lapworth *et al.*, 2017).

In terms of water quality, urban groundwater is generally susceptible to human pollution. Due to insufficient waste management, the shallow urban groundwater in Africa is often very poor (Lapworth *et al.*, 2017) and source protection (Ochungo *et al.*, 2019), posing a significant health risk to users (Varol and Şekerci, 2018). Although alluvial aquifers are essential resources in Africa (MacDonald and Adelana, 2008), they are the least investigated (Lapworth *et al.*, 2017). Few studies of alluvial aquifers have been undertaken in the northern, western and southern African regions and very few in the East African region (Xu *et al.*, 2019).

1.1.3 National Perspectives

Groundwater resources in Kenya are becoming increasingly important due to the increasing population (Falkenmark, 2019), infrastructural development, pollution of surface water (Bai *et al.*, 2016) and increased droughts caused by climate change (Taylor *et al.*, 2012). About 80% of the country is covered by arid and semi-arid lands faced with significant water scarcity (NDMA, 2016; World Bank, 2018). The rainfall ranges from less than 200 mm in northern Kenya to more than 1800 mm in the region of Mt. Kenya, with an annual average of 630 mm (Koskei *et al.*, 2018; Opiyo *et al.*, 2015). It is estimated that the 2016-2017 drought affected about 3.4 million people living in arid and semi-arid areas across 23 of the 47 counties in the country (NDMA, 2016). The recent drought events in the country (NDMA, 2016) have resulted in an increased focus on the development of the country's groundwater (REACH, 2015) to expand the existing water supplies. Generally, the groundwater resources are unevenly distributed both in time and space, a situation that has been exacerbated by climate variability (World Bank, 2018). Besides, very few studies have been undertaken to understand groundwater resources (World Bank, 2018) accurately.

The occurrence and distribution of the groundwater resources in Kenya are controlled majorly by geology (Kuria, 2011). Intrusive rocks and volcanic flows cover the Rift Valley and Central Kenya; sedimentary rocks characterize coastal and northern Kenya, while metamorphic rocks are localized in eastern Kenya (Kuria, 2011). Groundwater is confined within the Rift Valley by lacustrine sediments, weathered and fractured zones in volcanic rocks, and sediments interbedded

between volcanic rocks (Kuria, 2013). According to Kuria (2013), the rift valley's aquifers include the Turkana aquifer, the Baringo-Bogoria aquifer, the Nakuru aquifer, and the Magadi aquifer. There is no single identified aquifer with significant groundwater in the areas covered by the basement rocks. The piezometric map indicates that the aquifer within the basement rocks is localized; examples of these aquifers can be found near Isiolo, Meru, Embu, Wote, and Kitui (Kuria, 2013). Under the geological conditions of the basement terrains, groundwater occurs in weathered zones above the crystalline basement rocks, fractured zones within the crystalline bedrock, and alluvial deposits along the main drainage channels. (Kuria, 2011).

The major sedimentary aquifers in Kenya include; Lotikipi and Lodwar aquifers (Up to 80 deep), Tiwi aquifer (<70 m deep), Gongoni-Msambweni aquifer (40-100 m deep), Baricho aquifer (25-60 m deep), and the Merti aquifer 110-180 m deep) (Kuria, 2011). The renewable groundwater in the country is estimated at 1.04 BCM per annum, and about 0.18 BCM (17%) is currently being utilized (MWI, 2013; World Bank, 2018). Kuria (2011) plotted a transmissivity map using data from the national groundwater database. This map shows that the transmissivities of groundwater in drilled boreholes in Kenya range from <1.2 to 1598.7 m²/day, with the largest values observed within the sedimentary aquifers. The Lotikipi, Lodwar and Tiwi aquifers are sedimentary (consolidated/unconsolidated) aquifers with transmissivities ranging from 10 to 600 m²/d (Kuria, 2011).

Although the groundwater resources in Kenya have the potential to boost water supplies, its exploitation is limited due to naturally poor water quality (Kuria, 2011; MWI, 2013; World Bank, 2018), pollution in urban centres (Ochungo *et al.*, 2019; Olago, 2018), saline intrusion in coastal areas (Ochungo *et al.*, 2019), and limited knowledge of the occurrence of the groundwater in the country (Olago, 2018; World Bank, 2018). Understanding the aquifer chemistry and identifying the various sources of the chemical components in the groundwater is important for its geochemical characterization (Chenini *et al.*, 2010; Selvakumar *et al.*, 2017). However, in Kenya, very few studies investigating aquifer hydrogeochemistry have been undertaken in volcanic (Kanda and Suwai, 2013; Karegi *et al.*, 2018; Maina and Gaciri, 2010) and sedimentary areas (Comte *et al.*, 2017; Muthuka, 1994), and fewer in metamorphic areas. Hove and Ongweny (1974) investigated Kenya's groundwater quality based on total dissolved solids. Olaka *et al.* (2016) investigated the groundwater fluoride enrichment within the Central Kenya Rift - an active rift

setting. Groundwater quality studies have also been conducted in coastal regions of Kenya (Makokha, 2019; Muthuka, 1994; Mzuga *et al.*, 2001).

Rainfall-surface water interactions of alluvial aquifers have not been studied, yet such knowledge is important in the understanding of aquifers recharge characteristics and for the determination of impacts of rainfall and streamflow variability on groundwater. However, few studies have focused on the investigation of groundwater isotopes in Kenya (Avery and Tebbs, 2018; Doust and Sumner, 2007; Henkes *et al.*, 2018; Nyende, 2013; Nyilitya *et al.*, 2020; Ochungo *et al.*, 2019; Oiro *et al.*, 2018; Sklash and Mwangi, 1991), and none has been carried out in Turkana county.

1.2 Statement of the Problem

Turkana County, situated in the north-western Kenya, is classified as an arid and semi-arid land (ASAL) with very erratic, low (263 mm/yr.) and unreliable rainfall throughout the year (Opiyo, 2014). The County majorly depends on groundwater resources for water supply (JICA, 2012). The steadily increasing demand for water from the rapid growth of urban populations, businesses and emerging oil development operations has resulted in an unprecedented high demand for water in an arid region (Olago, 2018). With this regard, the understanding of the groundwater resources within Lodwar municipality and its environs is critical for the development of safe and reliable groundwater supplies.

Groundwater sources (boreholes and handpumps) in Turkana County are developed mainly along the major rivers (Turkwel and Kerio Rivers) and major laggas (JICA, 2012). Within Lodwar Municipality, boreholes and handpumps have been developed on the riparian zones of the Turkwel River (Hirpa *et al.*, 2018; Olago, 2018) to abstract groundwater from the alluvial aquifer whose hydrogeological characteristics are not fully understood (Olago, 2018). According to RTI (2013), a shallow aquifer, within multi-layered fresh and weathered volcanic structures juxtaposed with river sediments and Turkana grits close to the basement, underlies Napuu village east of Lodwar town. The storage capacity of the Napuu shallow Lodwar aquifer was estimated to be 10 billion cubic meters (BCM) per year, with an estimated recharge of 1.2 BCM/year (RTI, 2013). These values are extremely high, necessitating a detailed study in the area to obtain accurate aquifer storage and recharge estimates. UNESCO drilled three confirmatory boreholes (RTI 1, RTI 2 and RTI 3) and conducted test pumping. Of these, RTI 1 is within the current study area and was drilled to a depth of 47 m with an aquifer thickness of 20 m between 27- 47 m below ground level.

Although the findings of this study have been widely criticised owing to the methodology used and unrealistic storage and recharge estimates (Avery, 2013), the drilling and test pumping results provide important hydrogeological information of Lodwar and its environs that was initially unknown. The analysis of the cross-sections revealed a possible replenishment correlation dynamic between the Lodwar Aquifer and the Turkwel River (RTI, 2013). The surface water-groundwater dynamics in Lodwar and its environs require further investigation to determine specific correlations. A further study will unveil the aquifer's structure and geometry, hydrogeological characteristics, accurate storage estimates and delineation of aquifer boundaries.

The ten boreholes used for drinking water supplies in Lodwar are all located within a radius of 10 km from the town area (Olago, 2018), indicating that some parts of the municipality lie on top of its groundwater resource. Currently, Lodwar municipality has no sewerage facility and a functional waste disposal system (Hirpa *et al.*, 2018), posing a risk of pollution of the shallow alluvial aquifer. Lack of a proper sewage system contributes greatly to nitrate and faecal contamination of shallow groundwater (Heiß *et al.*, 2020). Further, no comprehensive water quality studies have been undertaken to date for the shallow aquifer in Lodwar and its environs. Although Turkwel River has been hypothesised to replenish the groundwater of the Lodwar alluvial aquifer, the geochemical correlation and seasonal groundwater chemistry dynamics need to be established. The hydrogeochemistry and vulnerability to pollution status of this aquifer is unknown, and thus an urgent need for the determination of prevailing water quality, hydrochemical characterization, and the determination of natural and human-induced pollution.

An aquifer system's rainfall-surface water-groundwater interaction provides data on the amount of recharge attributed to rainfall and surface water (Atuahene, 2017; Meng *et al.*, 2019; Teng *et al.*, 2018). It provides an opportunity to measure and quantify base flows and influxes between the groundwater and surface water. Seasonal water table changes in the Lodwar aquifer is unknown, and it is currently not possible to determine the extent to which climate variability influences the system (Newman, 2019; Subramani *et al.*, 2009; Xi *et al.*, 2018). The quasi-perennial Turkwel River that originates from Mt. Elgon region has been suspected to be the main source of recharge to the shallow aquifer within Lodwar (Hirpa *et al.*, 2018; JICA, 2012; Olago, 2018). However, the specific recharge sites, and the effects of the 'drying-up' periods every year (Hirpa *et al.*, 2018), are unknown. Further, increasing populations, the planned expansion of irrigation activities (Odra, 2015), warming temperatures and reduced precipitation linked to global warming may also

upsurge the risk of water scarcity in the Turkwel, resulting in reduced surface water and a subsequent decrease in the groundwater recharge (Hirpa *et al.*, 2018). The uncertainties surrounding the systemic interaction between the Turkwel River and the underlying Lodwar Alluvial Aquifer needs to be determined. Besides, no study has been undertaken in the study area related to groundwater interaction regimes.

1.3 General and Specific Objectives

1.3.1 General Objective

The main objective of the study was to establish the hydrogeological characteristics of the Lodwar Alluvial Aquifer System (LAAS) and its vulnerability to climate variability and anthropogenic risks and uncertainties in the context of sustainable management.

1.3.2 Specific Objectives

The specific objectives for the research are to: -

1. Determine the hydrogeological characteristics of the Lodwar Alluvial Aquifer System;
2. Characterize the aquifer hydrogeochemistry, and to determine its susceptibility to pollution;
3. Establish rainfall-surface water-groundwater interaction and recharge characteristics of the aquifer; and
4. Develop a conceptual aquifer geometry model

1.3.3 Research Questions

The following research questions were formulated for this research:

1. What are the hydrogeological characteristics of the Lodwar Alluvial Aquifer System?
2. What are the hydrogeochemical characteristics of the LAAS and its susceptibility to pollution?
3. What are the rainfall-surface water-groundwater interaction dynamics and recharge characteristics in the LAAS?
4. Can we develop a conceptual aquifer geometry model using the derived datasets from this research?

1.4 Justification and Significance

1.4.1 *Justification*

In the initial stages of the preparation of a sustainable groundwater development plan, scientific understanding of the hydrogeological characteristics of an aquifer has an important role. These include groundwater occurrence and distribution in its geological setting, and aquifer characteristics such as extent, lithology, aquifer media, transmissivity, yields, depths, storage, specific capacity, recharge, and discharge characteristics. These characteristics have not been studied on a spatial scale in the Lodwar Alluvial Aquifer System (LAAS), although it is being abstracted for water supplies; there are only point source data on aquifer characteristics from drilled boreholes in the area which on their own cannot inform on aspects such as aquifer extent, recharge and discharge characteristics. Furthermore, delineation of aquifer boundaries based on the scientific understanding of the hydrogeological characteristics are critical tools for aquifer protection, sustainable groundwater management, and land-use planning (Alam and Ahmad, 2014).

The geochemistry of groundwater is an essential factor in determining its geochemical evolution (Hamlat and Guidoum, 2018) and use for several purposes, such as domestic, irrigation, and industrial uses (Mostafa *et al.*, 2017). Aquifer hydrogeochemistry contributes to the understanding of the groundwater facies and aquifer processes in a region and reveals the sources of chemical components in groundwater and its quality. The shallow nature and highly permeable geology overlying this aquifer make it extremely important to both understand its vulnerability to pollution and to delineate potential pollution sources. Thus, the spatial and temporal characterization of the hydrogeochemistry of the Lodwar Alluvial Aquifer System will not only make it possible to assess its suitability for domestic, drinking, industrial and irrigation purposes but also to determine the geochemical processes underpinning its characteristics, thus providing the much-needed evidence necessary for successful development and management of safe water supplies.

Rainfall - surface water - groundwater interactions are crucial components of alluvial aquifer systems. The estimation of modern-day aquifer recharge rates for shallow aquifers is critical when evaluating the sustainability of groundwater resource development (Chilton and Seiler, 2006; Jaroslav and Van der Gun, 2004), the recharge and discharge characteristics of the LAAS are currently unknown. Several studies have proposed potential linkages between the Turkwel River

and the LAAS (Hirpa *et al.*, 2018; JICA, 2012; Olago, 2018; RTI, 2013), but the current evidence is insufficient for informed decision-making for the development and protection of the aquifer. In addition, an understanding of aquifer recharge mechanisms and associated land-use linkages is required for resource catchment-scale assessments, which form essential components for integrated water resource management (Foster and Chilton, 2003). Isotopic analyses of oxygen-18, deuterium and tritium in rainfall, surface water and groundwater samples are useful tools for confirming the existing linkages among these systems, and to quantify the recharge from rainfall and surface water. This kind of study has not done in the area; further, the impacts of current and future climate variability and risks remain uncertain for the Lodwar Alluvial Aquifer System.

Currently, no aquifer conceptual model is available for the area of study. The aquifer conceptual model for the LAAS will help to illustrate the hydrogeological and geochemical conditions controlling the quantity and quality of its groundwater. The aquifer conceptual model derived from the understanding of the hydrogeology, hydrogeochemistry, and the evaluation of the rainfall-surface water-groundwater interaction is a tool that can be utilized by decision-makers in both county and national levels for sustainable use and management of groundwater resources.

1.4.2 *Significance*

The elucidation of the hydrogeological characteristics of the Lodwar Alluvial Aquifer System will provide the evidence-base for sustainable management of the system. Accurate information on the aquifer storativity, recharge, and discharge mechanisms are crucial in planning current abstraction to minimize future risks of water supply in Lodwar and its environs. Aquifer identification, delineation, and protection of recharge zones is part of Vision 2030 environmental protection goals, especially in arid and semi-arid regions of Kenya. This study will also contribute to the ongoing groundwater studies in arid environments, especially in the sub-Saharan Africa region, where knowledge of groundwater resources is much needed to ensure access to safe drinking water supplies and achieve sustainable management.

Characterization of the hydrogeochemistry of the LAAS will help to discriminate natural and anthropogenic influences on groundwater quality in the aquifer system. It will, therefore, facilitate early detection, mitigation and elimination of contamination sources by the Turkana county government to ensure that its people get sustainable access to safe water. The provision of clean and safe drinking water to its citizens is a constitutional directive of the Government of Kenya.

Therefore, the findings of this study will contribute to its full realization in Lodwar and its environs. The seasonal water quality monitoring conducted by this study and the accompanying water quality index maps would form the basis for long-term groundwater monitoring and development by the Water Resources Authority (WRA) and other agencies in the area. Developed countries such as the United States, United Kingdom, Denmark, amongst others, have developed the groundwater vulnerability maps for their entire countries. This study is a step for Kenya to develop such maps for its groundwater resources. Identifying areas of good groundwater quality contributes to SDG 6 of clean water and sanitation in the contexts of communities in Lodwar and its environs. Furthermore, the key features of groundwater relevant to the SDGs that this study aims to elucidate are its use, management, and sustainability.

Knowledge of the extent, recharge and discharge characteristics of the aquifer will help the Turkana County Government to not only know the sustainable supply limits of the aquifer but also to protect it and to plan the urban expansion into non-recharge and abstraction zones. This information would enable the Turkana county government to plan for sustainable supply and to adopt management options that consider the impacts of climate variability in the region. Very few studies involving rainfall-surface water-groundwater interaction have been carried out globally, especially in Sub-Saharan Africa, and this study will provide additional knowledge in future studies. Lastly, the conceptual aquifer geometry model for the LAAS will be an excellent tool for decision making in terms of monitoring, development, management, and protection of the aquifer system.

1.5 Scope and Limitation of the Study

The study area covered the mid-section of the Turkwel watershed, centred on Lodwar municipality and extending to its environs. Secondary data on groundwater quality, geological logs of drilled wells, and test pumping data were obtained from the regional and sub-regional offices of the Water Resources Authority (WRA) and from the water practitioners in the Turkana region, such as Oxfam and the Catholic Diocese of Lodwar. Field geological and geophysical studies were undertaken, and rock and water samples (groundwater, river and rainfall) were collected within the 1040 km² study area. Recharge characteristics and groundwater interaction processes were determined using isotopic compositions of deuterium, oxygen-18 and tritium in water.

The major limitations of this study were data scarcity and inaccessibility. The hydrogeological data of the area are generally limited, while that available contained numerous gaps. Missing information for most borehole records included; geographic coordinates, drilled depth, borehole logs, tested yields, water rest levels, and water quality information. Water table monitoring data was available only for two boreholes (LOWASCO Bh 9 and Napuu Bh) for nine and six months, respectively, limiting the application of the water table fluctuation method in this study. Inaccessibility of boreholes and handpumps in some parts of the study area for water sampling was also a challenge – the ongoing land tenure system has led to fencing off land areas and privatization of water points.

1.6 The Layout of the Thesis

This study is presented in five chapters, as illustrated in the thesis layout (Figure 1.1). Chapter 1 provides the background of the study, including the global, regional and local perspectives of groundwater, statement of the problem, study objectives, as well as justification and significance. Chapter two describes the study areas in terms of location, geology and structures, climate, groundwater and surface water resources, and land use activities, as well as a detailed literature review of the thematic areas covered by the study. Chapter 3 presents the various methodologies used for each specific objective, while Chapter 4 summarizes the research findings. Chapter 5 provides the main conclusions from all the chapters, implications for practice, and potential areas for future research based on the critical findings of this study.

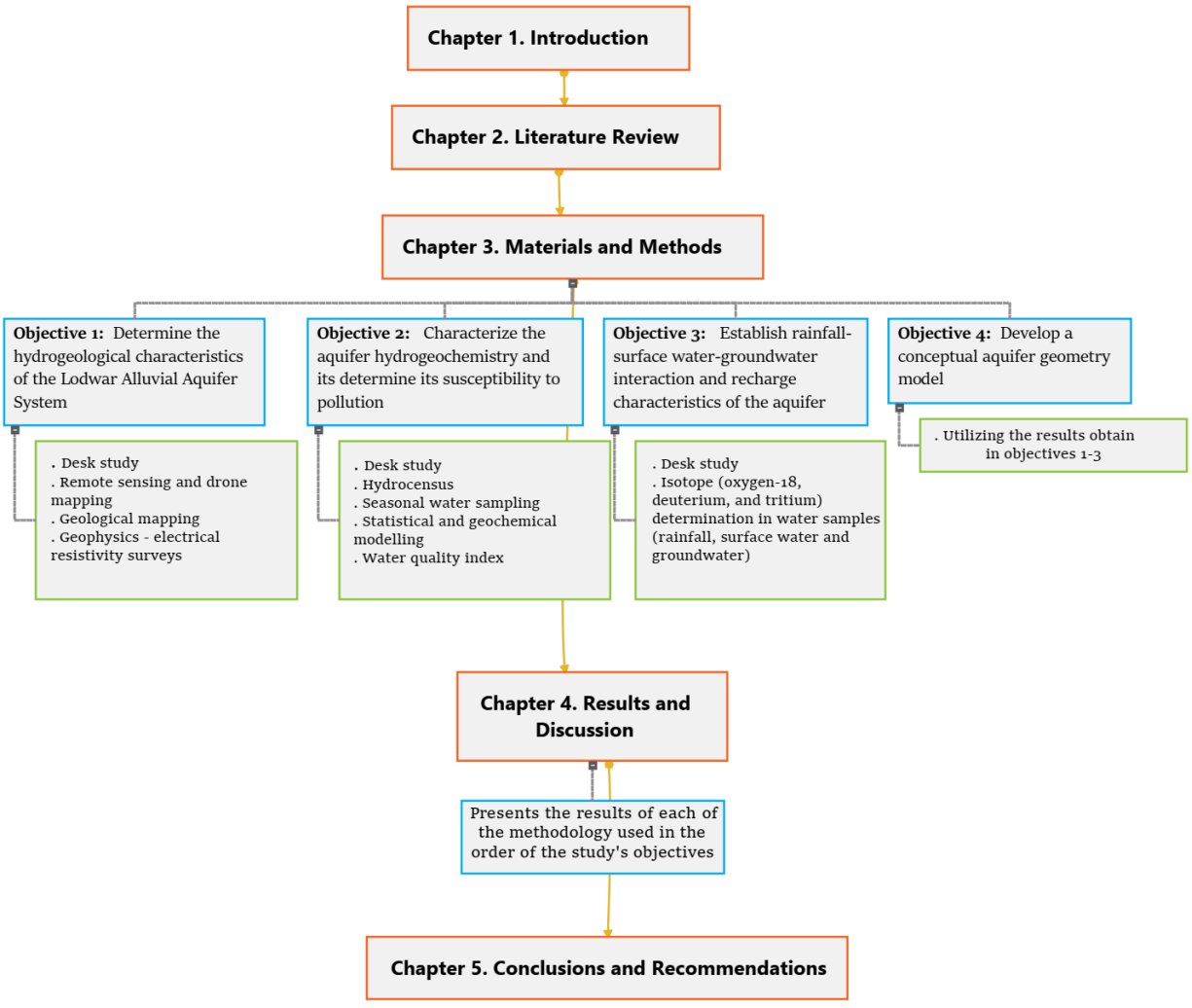


Figure 1.1: Layout of the thesis

CHAPTER TWO: LITERATURE REVIEW

2.1 Introduction

This chapter presents a detailed literature review of groundwater systems, with a particular focus on volcano-sedimentary and alluvial aquifers. These aquifers comprise the hydrogeological contexts of the research study area as specified in Chapter 1, section 1.2, and relate to the research objectives of the thesis. The first part covers a global review of aquifer settings, types, characteristics and geometries in volcano-sedimentary and alluvial terrains. The second part covers the hydrogeochemistry and hydrochemical facies, aquifer processes, and vulnerability to pollution within volcano-sedimentary aquifers and alluvial systems. Part three includes rainfall-surface water-groundwater interactions, recharge estimation and age of groundwater, while part four provides details of aquifer geometry modelling. An additional section of current approaches to sustainable groundwater management comprises part five. Lastly, a summary of this chapter with key highlights and gaps is presented.

2.2 Hydrogeological Characteristics of Aquifers

The lithological characteristics and hydraulic properties of an area control the groundwater development within that area (Ahmed *et al.*, 1998); therefore, hydrogeological conditions are unique to every region around the world (Jaroslav and Van der Gun, 2004). The successful development of groundwater and its optimum utilization requires an accurate understanding of prevailing aquifer characteristics and properties (Ahmed *et al.*, 1998; Chilton and Seiler, 2006).

An aquifer is a reservoir of groundwater composed of permeable geological units saturated with water to provide usable quantities of water. Aquifers transport groundwater from recharge to discharge zones and serve as a storage medium for current and future use. Globally, two major types of aquifers exist; confined and unconfined. A confined aquifer is underlain by an aquiclude and is mostly unconfined at its outcropping edges that contribute a significant amount of recharge during rainfall events (Chilton and Seiler, 2006). Confined aquifers may also receive recharge through upper and lower leaky confining layers. The groundwater in a confined aquifer is subjected to hydrostatic pressure that induces increased pore pressure that is higher than atmospheric pressure (Ahmed *et al.*, 1998), causing the water in a well to rise beyond the upper level of the

aquifer. In instances where there is enough pressure to force the water to flow at the land surface, these are referred to as artesian wells. As a result, the well's or aquifer's response to changes in atmospheric pressure is variable and directly proportional to the degree of aquifer confinement (pore pressure) containment, as well as hydraulic and storage characteristics. Confined aquifers often have low storativity values ranging from 0.01 to 0.0001 (Salako and Adepelumi, 2018). Unconfined aquifers, also known as phreatic aquifers, do not have upper impermeable layers but are underlain by an aquiclude (Chilton and Seiler, 2006; Salako and Adepelumi, 2018). Thus, they can be recharged locally from rainfall by infiltration and percolation of the rainwater through interconnected pores. In comparison with confined aquifers, groundwater in an unconfined aquifer is more susceptible to anthropogenic pollution, linked to the possibility of direct migration of dissolved pollutants to recharge water. Unconfined aquifers have storativity values > 0.01 (Salako and Adepelumi, 2018). Schematic illustration of confined and unconfined aquifers is given in Figure 2-1. Perched aquifers are distinct types of unconfined aquifers occurring above the regional water table (Salako and Adepelumi, 2018). Thus, when a low-permeability layer prevents the downward water movement above it, they always exist above an unconfined aquifer or a confined aquifer in the vadose zone. Perched aquifers are generally small and may not have sufficient storage to support substantially good production.

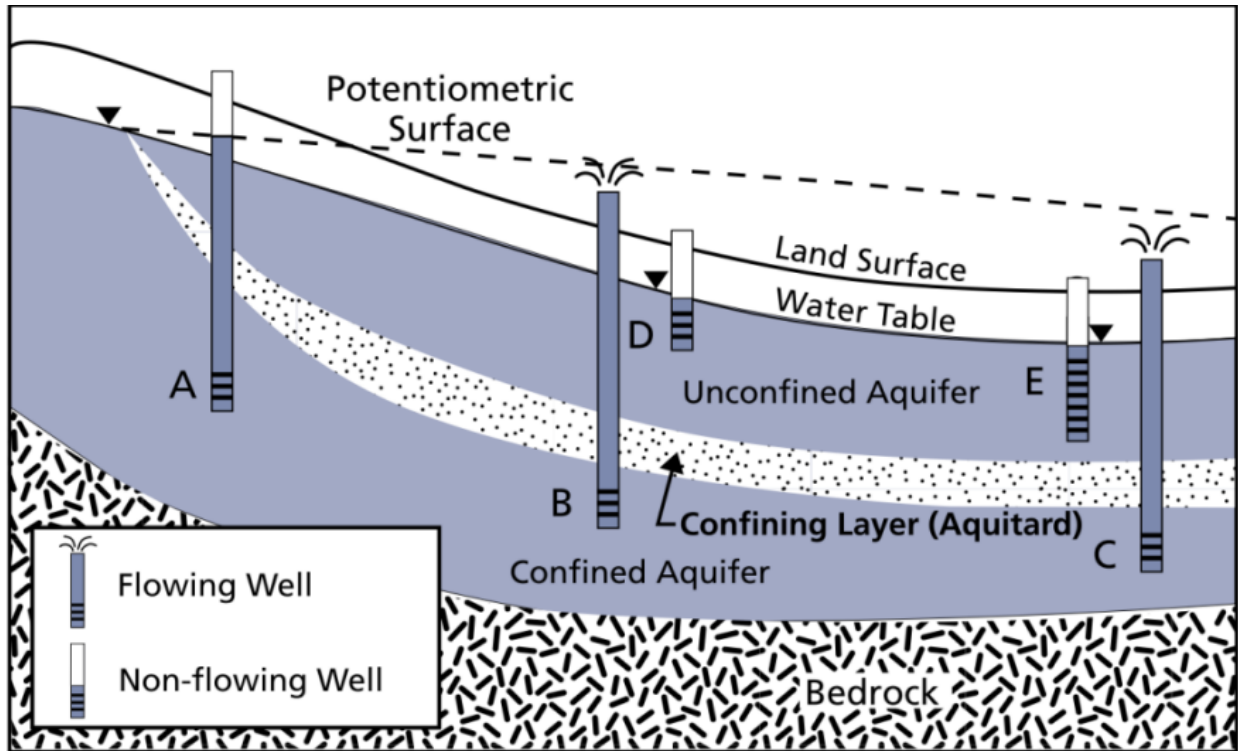


Figure 2.1: Schematic illustration of the confined and unconfined aquifers (source: Salako and Adepelumi, 2018)

2.2.1 A global review of aquifer types

Groundwater occurrence primarily depends on geology, geomorphology, weathering, and adequate rainfall (both current and historical) (MacDonald *et al.*, 2012). There are four geological provinces for groundwater occurrence around the world: Precambrian “basement” rocks, volcanic rocks, consolidated sedimentary rocks, and unconsolidated sediments (alluvial aquifers) (Chilton and Seiler, 2006; Macdonald *et al.*, 2016; Mook, 2000).

2.2.1.1 Precambrian “basement” aquifers

Precambrian basement aquifers develop within overlying weathered materials and fractured bedrock of metamorphic and or intrusive origin (Wright, 1992). In tropical and sub-tropical regions (Wright, 1992), deeply weathered crystalline bedrock aquifer systems occur within low-latitude regions of Africa, South America and Asia (Taylor and Howard, 2000). About 40 % of sub-Saharan Africa is underlying these aquifers (MacDonald *et al.*, 2012) and are a significant source of water for a quarter of a billion people in the region (MacDonald and Adelana, 2008; Taylor *et al.*, 2009). Across the tropics, including East Africa, weathered crystalline basement

aquifers maintain water supplies (Maurice *et al.*, 2018). Transmissivities of crystalline basement aquifers investigated by Maurice *et al.* (2018) in Tanzania and Uganda ranged from 10–1,000 m²/day, which were higher than observed in the majority of deeply weathered crystalline bedrock aquifers (<10 m²/day). Generally, the basement aquifer systems are highly heterogeneous (Taylor and Howard, 2000) and are characterized by considerably low yields (Wright, 1992).

2.2.1.2 *Volcanic rock aquifers*

In North America, especially Columbia Basin in the NW of the USA and parts of the Deccan Plateau in India, volcanic aquifers are widespread around the world and are important groundwater resources. These aquifers form in basin-like structures formed in volcanic regions with extensive basalt-lava flows (Mook, 2000). Limited groundwater resources are often provided by volcanic aquifers (Jaroslav and Van der Gun, 2004; Kebede *et al.*, 2008). Increased groundwater abstraction from deep artesian aquifers may reduce piezometric levels, resulting in mixing with shallow groundwater overlying the aquifer (Mook, 2000). Volcanic rocks cover only 6% of the land area in SSA and are mostly confined to eastern Africa (MacDonald *et al.*, 2012) and were formed during the Cainozoic period, associated with the opening of the rift valley in East Africa. The region's volcanic aquifers include thick, complicated sequences of lava flows, sheet basalts, and pyroclastic rock such as agglomerate and ash (MacDonald *et al.*, 2012).

2.2.1.3 *Sedimentary rock aquifers*

Consolidated sediments make up some of the major aquifers in the world, consisting primarily of younger Paleogene and Neogene and older Mesozoic or Palaeozoic formations of sandstone and limestone (Chilton and Seiler, 2006; Mook, 2000). Aquifers are found in consolidated sediments all over the world, including mountain belts such as the Andean, Alpine-Himalayan, and North American cordilleras, as well as lowlands and plateau areas in northern Europe and Central China (Chilton and Seiler, 2006; Foster and Chilton, 2003). Massive sedimentary aquifers in North Africa contain a significant portion of Africa's groundwater (MacDonald *et al.*, 2012), with the largest groundwater reserves in Libya, Algeria, Sudan, Egypt, and Chad (MacDonald *et al.*, 2012; Mook, 2000).

Depending on the degree of cementation, Paleogene and Neogene sandstones can range from loose to highly consolidated rock (Chilton and Seiler, 2006). In such cases, secondary porosity caused by fracture development can provide adequate permeability and storage to form productive aquifer

(Mook, 2000). On the other hand, limestones show solution enhancement of such fractures (karst) in arid and semi-arid areas and coastal regions that make them prolific aquifers (Chilton and Seiler, 2006; Foster and Chilton, 2003). Due to both the main porosities and fractures enhanced by weathering and dissolution, sandstone and limestone have high to very high permeability, respectively (Chilton and Seiler, 2006). In sandstone and calcareous aquifers, the combination of primary and secondary porosities results in rapid groundwater movement with velocities often above 100 m / day (Chilton and Seiler, 2006; Mook, 2000).

2.2.1.4 Alluvial aquifers

Quaternary deposits occurring in alluvial plains and fans, river deltas, and glacio-fluvial deposits usually consist of unconsolidated sediments that host numerous aquifers (Mook, 2000). Gravel and sand dominate the formations with intercalations of silt, mud, and clay. The unconsolidated sediments form some of the most important aquifers globally, hosting enormous volumes of groundwater (Chilton and Seiler, 2006). The great examples of unconsolidated sedimentary aquifers include, the Mekong, the Lower Indus and Ganges Brahmaputra valleys, the north European plain, the Tigris-Euphrates, and the Nile valley (Chilton and Seiler, 2006; Macdonald *et al.*, 2016). In east Africa, the South Coast aquifer system (SC) is an excellent example comprising unconsolidated coastal sediments (Oiro *et al.*, 2018). These deposits are located in the world's largest cities, such as Bangkok, Beijing, Cairo, Calcutta, Dhaka, Hanoi, Lima, Madras, and Shanghai, and are supplied by groundwater from unconsolidated strata (Chilton and Seiler, 2006).

Aquifers are seldom simple homogeneous systems in unconsolidated strata but mainly composed of discontinuous permeable layers of productive gravels and sands separated by less permeable aquitard layers of clay and silt, reflecting the complex deposition history (Chilton and Seiler, 2006; Hinkle and Survey, 1997). In such sequences, the shallowest aquifer may be the easiest and cheapest to exploit, but it is also the most vulnerable to contamination (Chilton and Seiler, 2006). Intricate groundwater flow patterns may be created by the presence of aquitards (Mook, 2000), but the permeable layers may still have a degree of hydraulic continuity (Egan and Price, 2014), such that pumping from one layer will affect the others, generating significant vertical head gradients and leakage (Chilton and Seiler, 2006).

2.2.1.5 Heterogeneous composite “volcano-sedimentary” aquifers

Volcanic and sedimentary aquifers (volcano-sedimentary) comprise 55% (Jaroslav and Gun, 2004) of the Worlds’ groundwater resources and are mainly distributed in ASALs. Aquifers of these types include lavas and pyroclastic rocks coupled with alluvial-volcanic and alluvial fan deposits (Chilton and Seiler, 2006). In the Horn of Africa (Djibouti), alluvial aquifers exist in the valleys of wadis (intermittent streams), and they form complex volcano-sedimentary aquifers when they approach volcanic aquifers (Aboubaker *et al.*, 2013). In the Kenyan rift system, volcano-sedimentary aquifers exist in the Turkana basin and within the Mesozoic sediments in the Dawa basin at the Kenya-Ethiopia border (Kebede, 2005) located in the northern part of the country. Sedimentary aquifers in the country are in northern Kenya and the coastal region (Kuria, 2011). Turkana aquifer, Nakuru aquifer, Baringo-Bogoria aquifer, and Magadi aquifer are the aquifers in the country's rift system (Kuria, 2011), where the Turkana aquifer includes a volcano-sedimentary system. Within the Paleogene and Neogene volcanics, the volcano-sedimentary aquifers in the northern parts of Kenya, and thick Miocene to Quaternary sediments are (Kebede *et al.*, 2010a).

2.2.2 Aquifer characteristics and groundwater flow

Groundwater is rarely static, but rather moves slowly through aquifers (Chilton and Seiler, 2006) due to changes in hydraulic head and differences in groundwater levels or pressure and is primarily controlled by the permeability of the aquifer material (Shekhar, 2017). Darcy’s Law governs the flow of groundwater through an aquifer. Darcy’s Law gives an accurate description of the flow of groundwater in most naturally occurring hydrogeological conditions. Its relationship with hydraulic gradient can be expressed as;

$$\frac{Q}{A} = q = \frac{-K(h_1-h_2)}{l} = -K(\Delta h/\Delta l) \quad \text{Equation 2.1}$$

Where, Q is the rate of flow through area A, K is the hydraulic conductivity, h1 – h2 is the hydraulic head difference between two measuring points, $\Delta h/\Delta l$ is the hydraulic gradient, and q is the volumetric flow per unit surface area.

The direction of groundwater flow in an aquifer is perpendicular to equal-head lines (Chilton and Seiler, 2006). Groundwater flow may occur in, for instance, a jointed sandstone or limestone through fractures or spaces between the grains or a combination of the two (Egan and Price, 2014).

Borehole test pumping data is used to accurately determine aquifer parameters and lithological characteristics (Shirazi *et al.*, 2015) as well as to evaluate its potential (Jimenez and Chávez, 2004). Specific characteristics of each aquifer in time and space can be defined based on aquifer properties such as porosity, specific yield, aquifer storage, transmissivity, and hydraulic conductivity. The hydraulic conductivity, flow path and gradient are significantly controlled by aquifer media, according to Shirazi *et al.* (2015). Groundwater movement is usually due to variations in the hydraulic head of an aquifer. Hydraulic heads are commonly measured in relation to an arbitrary datum, which is frequently sea level (Chilton and Seiler, 2006).

Alluvial aquifers occur within the depositional basins of perennial and ephemeral streams in arid and semi-arid areas, and the aquifer materials usually comprise sand, silts and gravel (Foster and Chilton, 2003). Because of the high porosity of unconsolidated sediments in the range of 0.25 to 0.35 and the generally low horizontal hydraulic gradients of the alluvial plains, groundwater velocities in the range of 0.003-0.1 m/day are common (Chilton *et al.*, 2006). These low velocities, combined with the significant distances travelled (tens to hundreds of kilometers), suggest that much of the deeper groundwater in thick alluvial sequences was recharged several hundred to several thousand years ago, resulting in old groundwater in such systems (Chilton and Seiler, 2006).

Natural groundwater discharge occurs in springs, in arid and semi-arid areas, and in some basins, sub-surface flow into another basin can discharge significant amounts of groundwater into stream channels, wetlands, and seasonal lakes. Abstracting groundwater can also contribute significantly to groundwater discharge from water wells (Calvache *et al.*, 2011; Yang *et al.*, 2018). The groundwater potential in an aquifer is a function of rock types constituting them (Ashraf *et al.*, 2018). In basement systems, groundwater potential is due to a combination of fractures and weathered rock systems (Ashraf *et al.*, 2018; MacDonald *et al.*, 2012). In volcanic systems, the groundwater potential depends mainly on the presence of fractures (Macdonald *et al.*, 2016; Oiro *et al.*, 2018). In sedimentary systems, the main types of water-bearing rocks are usually sand, sandstone, fractured or karstic limestone and dolomite (Ashraf *et al.*, 2018). Generally, in most arid and semi-arid terrains, limited groundwater recharge contrasts with vast groundwater reserves created during the Pluvial periods of the Pleistocene (Jaroslav and Gun, 2004).

2.3 Hydrogeochemical Characteristics of Volcano-Sedimentary and Alluvial Aquifers

Groundwater chemistry is governed by factors such as rock water interaction – the formation through which water flows, evaporation and concentration, dilution due to precipitation that may result in changes in chemical compositions of groundwater (Ansari and Umar, 2019; Ashraf *et al.*, 2018; Maurice *et al.*, 2018). The hydrogeochemistry of shallow alluvial aquifers in arid and semi-arid areas is linked to the cumulative consequence of the rock-water interaction, dissolution of soluble minerals, and nature and intensity of anthropogenic activities (Ansari and Umar, 2019; Elango and Kannan, 2007; Vasu *et al.*, 2017).

2.3.1 *Determinants of natural groundwater quality and vulnerability of alluvial aquifers to pollution*

Groundwater quantity and quality, coupled with the climate change effects, are of major concern for meeting the increasing demand for freshwater (Shirazi *et al.*, 2015). Natural groundwater quality varies significantly through periodic aquifer profile as a result of geology and the physical and chemical processes that can affect salinity, temperature, pH levels, heavy metals, and organic substances in the aquifer (Afzali *et al.*, 2015; Aghazadeh *et al.*, 2017; Ansari and Umar, 2019). Physical and chemical processes that can have an impact on water quality include;

- During groundwater movement along the flow path, dissolved rocks and minerals are transported and redeposited;
- Evaporation may cause an increased concentration of minerals and salts in the groundwater;
- Chemical reactions in the aquifer leading to altered groundwater chemistry

Knowledge of prevailing groundwater quality plays a significant role in the early stages of a groundwater sustainable development plan (Shirazi *et al.*, 2015). Groundwater quality in volcanic environments is a problem in most cases due to high fluoride concentrations above 1.5 mg/L (Macdonald *et al.*, 2016). Fluoride concentrations are high in volcanic rocks in Ethiopia's Rift Valley. More generally, high fluoride groundwaters in the rift valley regions of Kenya and Tanzania have led to health associated problems (Ashley *et al.*, 2004; Coetsiers *et al.*, 2009; Mbithi *et al.*, 2017; Olaka *et al.*, 2016). Because of the rapid burial of alluvial sediments, groundwater with high arsenic (As) levels has been associated with sedimentary rocks in reducing conditions typical of alluvial and deltaic environments (Vivona *et al.*, 2007). The most likely mechanism for

As release into groundwater in this environment is reductive dissolution of As-rich Fe oxyhydroxide (Vivona *et al.*, 2007).

Groundwater pollution is a constant concern globally because aquifers, especially shallow alluvial aquifers, are vulnerable (Kumar *et al.*, 2014), especially those in the vicinity of urban areas (Al-Shaibani, 2008). Nitrate is the most prevalent groundwater contaminant in shallow urban groundwater (Kuroda and Fukushi, 2008). Nitrate in groundwater originates from agricultural runoff from the use of fertilizers upstream of the aquifers. However, in urban areas where agricultural fertilizers are absent, the common sources of nitrates are leaky sewage, septic tanks, landfills and industrial spillage (Goudarzi *et al.*, 2017; Kuroda and Fukushi, 2008). Contaminants other than nitrogen in urban groundwater include fluoride (Ayenew, 2008; Brindha *et al.*, 2011), arsenic (Acharyya, 2002), heavy metals (Twarakavi and Kaluarachchi, 2005) and volatile organic carbons (Kuroda and Fukushi, 2008).

The term “*aquifer pollution vulnerability*” was used by (Foster *et al.*, 2012) to characterise the intrinsic characteristics that determine the sensitivity of the groundwater system to being adversely affected by an imposed pollutant load. However, the approach of Foster *et al.* (2012) also distinguishes pollution vulnerability from pollution risk because pollution risk can stem from both the aquifer's natural vulnerability and the pollution load that is or will be applied to the earth's subsurface by human activities. As a result, an aquifer may be highly vulnerable while posing no risk due to the absence of significant pollution loading, and vice versa (Jang *et al.*, 2017).

2.3.2 *Hydrochemical facies and rock water interactions*

Complex water types have been observed in volcano-sedimentary aquifers (Aboubaker *et al.*, 2013). Evaluation of Na/Cl ratios reveal that halite dissolution is not the only source of Na⁺ and Cl⁻ ions in volcano-sedimentary aquifers in arid areas (Aboubaker *et al.*, 2013). Other sources of Na and Cl in alluvial aquifers are weathering of silicate minerals (Ashraf *et al.*, 2018; Ramesh and Gowri, 2012) and ion-exchange processes in the soil and aquifer matrix (Martínez and Bocanegra, 2002; Ramesh and Gowri, 2012). The dominant water types in volcanic aquifers are Na-HCO₃, Na-Mg-Ca-HCO₃, and Na-Ca-HCO₃ water types due to rock-water interactions (Morán-Ramírez *et al.*, 2016). In alluvial aquifers, Ca-HCO₃ is a common water type (Al-Shaibani, 2008; González-Trinidad *et al.*, 2017; Hinkle and Survey, 1997; B. D. Li *et al.*, 2015). Other dominant water types in arid alluvial aquifers are Ca + Mg-HCO₃ and Na + K-HCO₃ (Ansari and Umar, 2019).

Groundwater from sedimentary aquifers has a good correlation between Ca and HCO_3 ($R^2 = >0.7$) due to their high concentrations in the rocks, while volcanic aquifers often show weak correlations between Ca and HCO_3 ($R^2 = <0.1$) (Vivona *et al.*, 2007).

Fluoride concentrations in groundwater are higher, particularly in arid and semi-arid regions (Adimalla *et al.*, 2020). In volcano-sedimentary aquifers, F^- concentrations exceeding the guideline value for drinking water (1.5 mg/L) is a common challenge in groundwater (Adimalla *et al.*, 2020; Brindha *et al.*, 2011; B. D. Li *et al.*, 2015). Various variables, including rock chemistry, residence time, well depth, preferential pathways to control the occurrence of high fluoride in groundwater for the upward movement of deep groundwater. Fluoride-rich minerals (fluorite or fluorspar (CaF_2), fluorapatite [$\text{Ca}_5(\text{OH}, \text{F})(\text{PO}_4)_3$] and cryolite (Na_3AlF_6)) can release F^- into groundwater through weathering and rock-water interaction processes (Adimalla *et al.*, 2020). Other fluoride-bearing minerals include glaucophane, riebeckite and asbestos (chrysotile, actinolite, anthophyllite) minerals from the biotite, muscovite, tourmaline, lepidolite, hornblende series (Edmunds and Smedley, 2013). The processes of retention and leaching directly affect the migration and exchange of fluoride from the soil to the water (Ansari and Umar, 2019). Apart from high fluoride in groundwater, volcano-sedimentary aquifers exhibit very high iron exceeding 0.3 mg/L and manganese (> 0.1 mg/L) concentrations related to a strong anoxic condition caused by the thick silt bed (Chae *et al.*, 2004). Rock-water interaction is a process that strongly affects hydrochemical facies; solid phases (organic and inorganic) are the main sources of dissolved constituents in groundwater in this process (Elango and Kannan, 2007) and, as groundwater moves from recharge to discharge areas, a variety of chemical reactions with the solid phases occur. Expected chemical reactions depend on the original chemical nature of the water, geological formations, and residence time (Elango and Kannan, 2007). The chemical processes involved during rock-water interactions are precipitation and dissolution, ion exchange processes, oxidation, and reduction. Investigation of hydrogeochemistry of an aquifer helps to determine the factors controlling the groundwater quality and the geochemical processes in an aquifer system (Chae *et al.*, 2004; B. D. Li *et al.*, 2015; Subramani *et al.*, 2009). Studies have revealed that the groundwater quality and the geochemical characteristics of volcano-sedimentary and alluvial aquifers are consistent with the geology of the area (Chae *et al.*, 2004).

2.4 Rainfall-Surface Water-Groundwater Linkages and Recharge Estimation

The fresh groundwater resources of the world are hosted in shallow aquifers (Jaroslav and Van der Gun, 2004) recharged by modern rainfall (Green, 2016). In addition to the associated impacts of the natural environment and human activities (Green, 2016), changes in the global climate are expected to affect the hydrological cycle, alter surface water levels, and replenish groundwater systems (Taylor, 2013). The challenges of understanding the impacts of climate change on groundwater systems are unique because these changes can, directly and indirectly, affect groundwater resources and hydrogeological processes (Green, 2016; Taylor, 2013). Limited observation data in many areas has made it difficult to accurately determine the extent and direction of groundwater change due to climate impacts (Taylor 2013). Still, where they do exist, they show that groundwater, along with surface water, is vulnerable to climate variability (Z. Chen *et al.*, 2004). Further research is required to support integrated groundwater management and improve the understanding of climate and groundwater interactions.

2.4.1 *Rainfall - surface water – groundwater interactions*

The groundwater-surface water interaction in a basin plays a crucial role in understanding and managing an aquifer system. Surface water and groundwater interact in two ways: rivers gaining water from the groundwater flowing through the riverbed (base flows) and rivers losing water as it flows out of the riverbed into a groundwater system (Taylor and Howard, 1996). Atmospheric water vapour, rainfall and evapotranspiration patterns, soil water content (SWC) and temperature, and surface runoff and river discharge (Bates *et al.*, 2008) are the elements of the surface hydrologic cycle (Figure. 2.1) that are impacted by climate change. Such changes in the components of the global hydrological cycle's atmospheric and surface components are likely to result in changes in the hydrological cycle of the subsurface within the world's soil, vadose zone, and aquifers (van Dijk *et al.*, 2017). The potential climate change effects on groundwater and its sustainability are, however, poorly understood (Gleeson *et al.*, 2012; Kotchoni *et al.*, 2018). Evapotranspiration and precipitation are particularly important because they directly affect groundwater recharge and eventually affect human groundwater abstractions (Green, 2016). In arid and semi-arid regions, minor changes in rainfall may lead to great recharge changes (Green, 2016). High temperatures, on the other hand, are likely to increase evapotranspiration, which may, in turn, reduce the moisture content of the soil.

Current vulnerabilities in shallow groundwater resources in ASALs are strongly correlated with precipitation variability (Green, 2016; Kundzewicz *et al.*, 2008). The overall impacts of climate variability on groundwater resources can be determined through an investigation of rainfall-surface water-groundwater interactions. The interaction of these systems is gaining attention globally, especially in the SSA region, due to increasing rainfall variability (Kebede *et al.*, 2008). Piezometric observations and stable-isotope ratios are useful approaches for investigating groundwater interactions with rainfall and surface water (Taylor, 2013; Taylor and Howard, 1996).

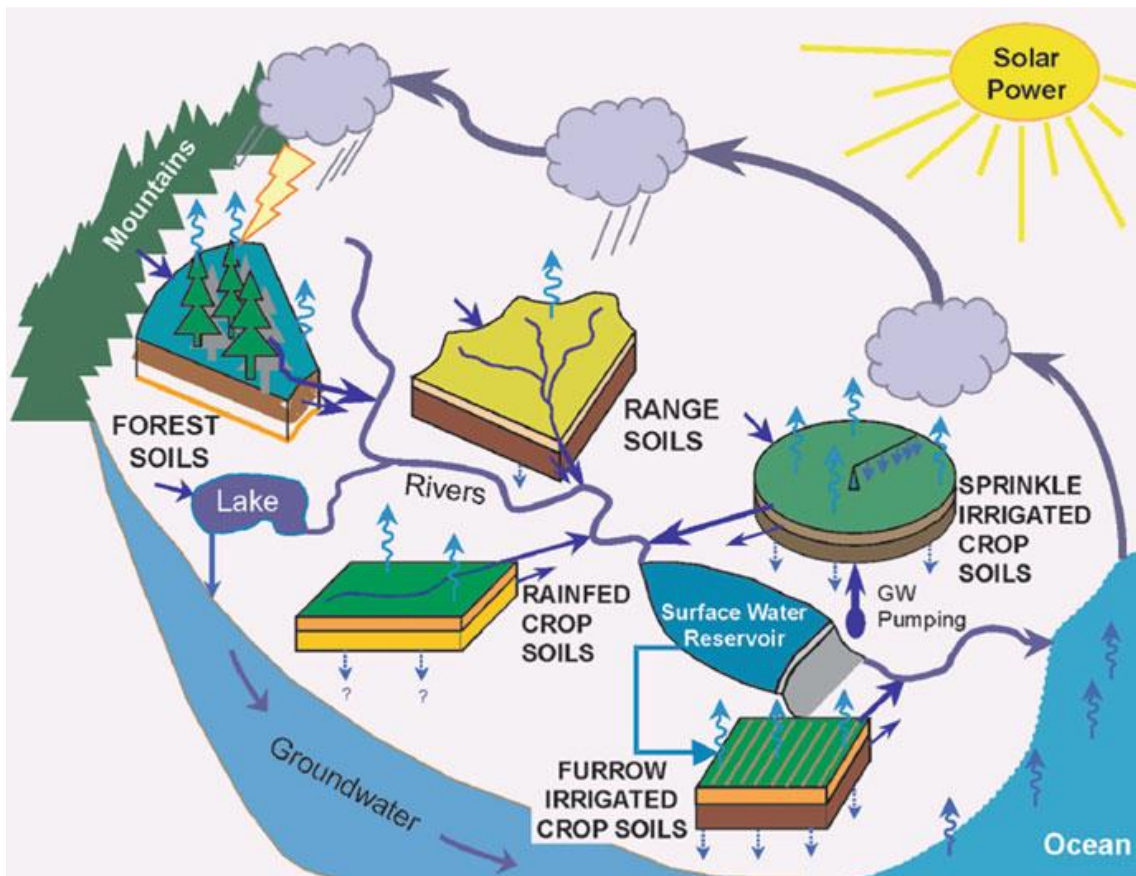


Figure 2.2: Diagrammatic representation of the hydrological cycle, including rain-fed and irrigated farming with potential abstraction of groundwater (Source: Green 2016)

Hydrologic Cycle Processes

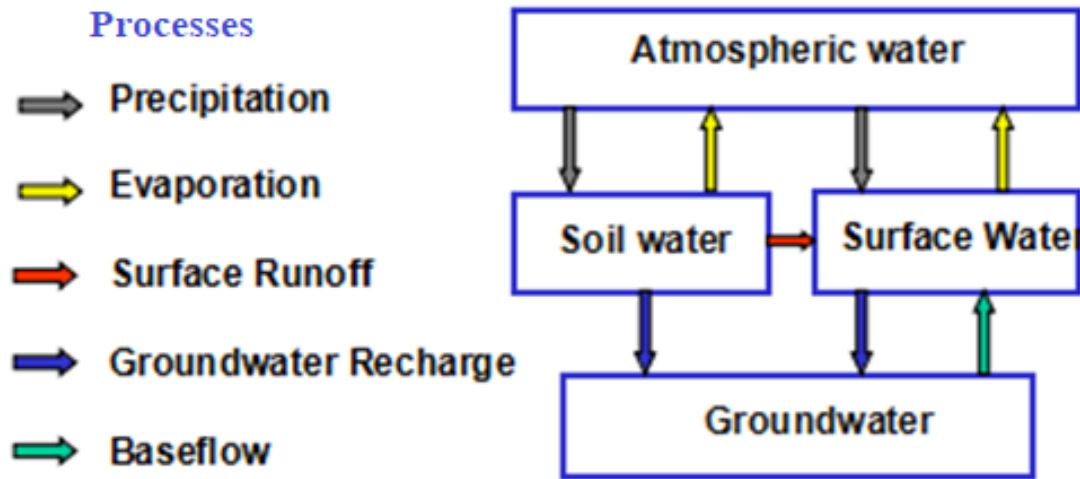


Figure 2.3: Summary of hydrologic processes in rainfall - surface water - groundwater systemic interactions

The analysis of stable isotope ratios of water ($\delta^{18}\text{O}$ and $\delta^2\text{H}$) is useful for investigating rainfall - surface water - groundwater interaction (Kebede, 2005). The distinction between the isotopic content of evaporated and unevaporated waters allows for the detection of flow paths between water bodies. When water evaporates from water bodies, isotope fractionation of the oxygen and hydrogen that make up the water occurs, resulting in the enrichment of the water body by heavy water isotopes of oxygen and hydrogen (Kebede *et al.*, 2008). Unevaporated water bodies will have lighter isotopic compositions than evaporated water bodies. In their study (Kebede, 2005) noted progressive northward enrichment of $\delta^{18}\text{O}$ and $\delta^2\text{H}$ along the River Nile, illustrating en-route water loss in the Nile channel.

Furthermore, the isotopic compositions of the shallow groundwater in the Nile basin reflected the regional mean isotopic composition of rainfall and that of the Nile River (Kebede *et al.*, 2008). Aboubaker *et al.* (2013) investigated the isotopic compositions of the Dalha volcano-sedimentary aquifer in the Horn of Africa (Djibouti). The results revealed that the ^2H and O^{18} of the aquifer depicted meteoric origin, where the first percolation of rainwater occurred in the volcanic systems (Aboubaker *et al.*, 2013).

2.4.2 Recharge estimation with particular reference to ASALs

Natural groundwater recharge (or replenishment of the water stored in an aquifer) occurs as a result of percolation of precipitation through the unsaturated zone and across the water table and from the influx of the overlying surface water bodies such as rivers, lakes, wetlands, and ocean (Faye *et al.*, 2019). Anthropogenic recharge sources include agricultural irrigation, recharge wells, and drainage systems from the engineering works (Sophocleous, 2002; Winter *et al.*, 2005). As a result, groundwater response to climate variability is complex since it is influenced by factors other than climate, such as vegetation, land use, soil types, and geology. As a result, regional climatic and local topographic, hydrogeologic, and biospheric conditions define recharge and discharge zones (Lee *et al.*, 2006; Vandecasteele *et al.*, 2007; Xu and Tonder, 2001).

A small percentage of rainfall infiltrates deeply enough to reach the water table in arid and semi-arid regions, resulting in groundwater recharge (Gates *et al.*, 2008). Most of the moisture falling as precipitation is evaporated at or near the land surface due to higher evaporation rates over precipitation (Gates *et al.*, 2008). As a result, accurate estimation of groundwater recharge is a critical factor in groundwater system management to ensure their sustainability under current and future risks (Faye *et al.*, 2019). However, recharge estimation in arid and semi-arid areas is neither straightforward nor easy due to variations in precipitation, and spatial variability in soil characteristics, topography, vegetation, and land use (Xu and Beekman, 2003). Furthermore, recharge amounts are typically insignificant in comparison to the resolution of the investigation methods. Several methods are used to estimate recharge in arid and semi-arid areas (Kebede *et al.*, 2010), and the objective of the recharge study guides the selection of the appropriate method for quantifying recharge (Xu and Beekman, 2003). Groundwater resource assessment, for example, would require large spatial and temporal recharge information. Assessments of aquifer vulnerability to pollution, on the other hand, would necessitate more detailed information on local and shorter time scales (Sophocleous, 2002; Xu and Beekman, 2003; Yang *et al.*, 2018). The standard techniques of recharge approximation in arid and semi-arid areas include; chloride mass balance (CMB) (Russell and Kluesner, 2007; Subyani and Sen, 2006), groundwater modelling (Bekesi and Mcconchie, 1998; Taylor and Howard, 1996), water table fluctuation (WFT) (Águila *et al.*, 2019; Yang *et al.*, 2018), water balance determination (Birkle *et al.*, 1998; Dhungel and Fiedler, 2016; Taylor and Howard, 1996), and stable isotopes of ^2H and ^{18}O (Shamsuddin *et al.*, 2018; H. Yeh *et al.*, 2014).

(a) Chloride mass balance

The rainfall and infiltration components of the hydrological cycle in arid regions are characterized by random and sporadic temporal and spatial variations. Consequently, the chloride concentration in rainfall has a similar behaviour (Subyani and Sen, 2006). It can, therefore, be used as an inert tracer since its degree of enrichment in the unsaturated zone as a result of water loss (Gates *et al.*, 2008) can be determined in wet and dry periods as total chloride deposition (Subyani and Sen, 2006). Due to its conservative behaviour in the unsaturated zone (Allison and Hughes, 1978) and relative abundance in rainfall (Subyani and Sen, 2006), Cl⁻ can be used in recharge estimation. Its application as a groundwater recharge tracer necessitates the exclusion of solid-phase Cl⁻ sources and low-permeability sediments at the study site, as well as the hypothesis that all Cl⁻ in the pore moisture is atmospherically resulting and transmitted through the unsaturated zone similar to water flow rate (Faye *et al.*, 2019; Gaye and Edmunds, 1996; Russell and Kluesner, 2007; Subyani and Sen, 2006). Its application is straightforward and is based on an understanding of annual precipitation, Cl⁻ concentrations in rainfall, and groundwater storage. The Cl⁻ mass balance in the unsaturated zone can be expressed as follows;

$$PC_p = RC_R \quad \text{Equation 2.2}$$

where P is the mean precipitation rate L/T, and C_p is the mean Cl concentration in precipitation (M/L³) over the period of record, R is recharge rate (L/T), and C_R is measured Cl concentration of potential pore water recharge (Allison and Hughes, 1978).

The left side of the equation represents total Cl⁻ inputs and must be adjusted if any other Cl⁻ sources are other than from rainfall are present (Gates *et al.*, 2008). Recharge is determined to be inversely proportional to pore water Cl⁻ concentration C_R .

(b) Groundwater modelling

Groundwater recharge modelling is a useful tool for determining spatially distributed recharge, mostly to unconfined aquifers (Thomas and Tellam, 2006). This technique of groundwater recharge estimation is widely applied in regional recharge investigation (Batelaan and Smedt, 2001; Bekesi and Mcconchie, 1998; Raiber *et al.*, 2008). The recharge model includes the

estimation of both direct (rainfall infiltration) and indirect (surface water infiltration) recharge (Thomas and Tellam, 2006). The groundwater recharge model input data includes;

- 1) Land use / land cover map with the attributes of runoff and water quality;
- 2) Geological map of both bedrock and surface deposits with attributes of hydraulic property;
- 3) Data from meteorology;
- 4) In grid form, ground surface elevation data; and
- 5) The elevation map of the water table.

The expected model output includes surface runoff distribution, infiltration, potential recharge, the slope at ground level, interflow, and actual recharge (Batelaan and Smedt, 2001; Hemker and Bakker, 2005; Thomas and Tellam, 2006).

(c) Water balance determination

Because of their simplicity, water balance methods are commonly used to estimate recharge. (Xu and Adams, 2005). To determine and analyze long-term average water recharge, the water balance method based on empirical evapotranspiration and runoff model is used (Xu and Adams, 2005). It is a useful method of recharge estimation, especially in areas with limited data, which makes it impossible to apply other methods. The water balance method requires readily available data such as rainfall, runoff, water levels, evapotranspiration, river channel water balance, soil moisture balance and temperature (Xu and Adams, 2005). It calculates recharge as the sum of all other fluxes such as rainfall, runoff, evapotranspiration, and storage change (Lerner *et al.*, 1990; Xu and Adams, 2005). Long-term recharge is modelled as a function of the regional interaction of site conditions like climate, soil, geology, and topography (Lee *et al.*, 2006; Xu and Adams, 2005) and allows for quantification of the actual evapotranspiration, direct runoff and recharge amounts. Usually, this method used yields a point estimate that is then extrapolated to the whole area under investigation (Xu and Adams, 2005) and may not be very useful in heterogeneous systems. The accuracy of the water balance method is often dependent on the quantity and quality of input data such as; spread of boreholes over an aquifer, frequency of water level and abstraction data, the correctness of the aquifer conceptual model and designated boundary condition (Xu and Beekman, 2003).

(d) Water table fluctuation method

Most research studies use water table fluctuation in aquifers to estimate the impacts of climate variability (Águila *et al.*, 2019; Yang *et al.*, 2018) on shallow aquifers. Rainfall and groundwater level monitoring help to establish the relationship between rainfall and recharge into a shallow aquifer. The water table fluctuation (WTF) method has been applied to estimate recharge in various arid and semi-arid regions (Brears and Post, 2014; Jassas and Merkel, 2014; Subramani *et al.*, 2009) due to its simplicity and insensitivity to the processes by which water travel in the unsaturated zone (Healy, 2010). The WTF method is applied in shallow water tables that respond rapidly to rainfall events (USGS, 2007). Chen *et al.* (2004) observed that groundwater levels of a carbonate aquifer in Manitoba, Canada responded to precipitation variability with spatial differences observed from well to well. For example, water tables at some aquifer locations responded to high-frequency precipitation. At the same time, groundwater levels in other areas did not react to high-frequency precipitation (Z. Chen *et al.*, 2004), demonstrating the presence of highly permeable channels or preferential-flow paths from the land surface to the water table. Besides, the observed groundwater level variation like precipitation indicates an indirect relationship between the water level variations and recharge (Chen *et al.*, 2004). The difference in thickness of the unsaturated zone may also be attributed to observed variations between wells (Russell and Kluesner, 2007).

The long-term water table data in semi-arid tropics has demonstrated a non-linear association between recharge and rainfall (Taylor, 2013). However, other studies in a shallow alluvial aquifer in the Sahel in West Africa (Tirogo *et al.*, 2016) and in three common geological environments (crystalline rocks, Mio-Pliocene sandstone and Quaternary sands) in Benin and other parts of West Africa (Kotchoni *et al.*, 2018) showed a linear relationship between rainfall events and recharge. These contrasting data indicate that the rainfall – groundwater recharge relationship is not always straightforward because of differences in the settings and characteristics of groundwater systems. The WTF method is, nevertheless, a useful approach to estimating the amount of aquifer recharge that is attributable to rainfall.

(e) *Recharge estimation using ^2H and ^{18}O isotopes*

Environmental isotope tracers are useful tools for understanding the hydrologic processes (González-Trinidad *et al.*, 2017; Yeh *et al.*, 2014) such as precipitation, basin hydrology, groundwater recharge and surface water - groundwater interactions (Cloutier *et al.*, 2006; Gaye and Edmunds, 1996; Joshi *et al.*, 2018; H. Yeh *et al.*, 2014; Yusuf *et al.*, 2018). Variations in oxygen and hydrogen isotopes in rainfall are caused by isotope fractionation due to hydrological processes such as evaporation and condensation, resulting in phase transformation (B. P. Singh, 2017). Other factors that cause variations in the isotopic composition of rainfall include; altitude, latitude, inland distance, source vapour, environmental conditions, and humidity (González-Trinidad *et al.*, 2017). A comparison of the isotopic compositions of oxygen and hydrogen in rainfall and groundwater provides an excellent tool for evaluating the recharge mechanism (Yeh *et al.*, 2014). Furthermore, effective groundwater resource management necessitates determining the sources of groundwater recharge (Yeh *et al.*, 2014).

The ^{18}O and ^2H have been used extensively in catchment studies to establish groundwater recharge, flow regimes, and water flow paths (Adomako *et al.*, 2010; González-Trinidad *et al.*, 2017). In arid and semi-arid regions, deuterium and oxygen-18 isotope enrichment due to evaporation through the soil surface is more prominent than rainfall infiltration (González-Trinidad *et al.*, 2017), allowing for the determination of evaporation rates in soil water. Recharge estimation using stable isotopes of ^{18}O and ^2H is a qualitative approach as opposed to quantitative approaches such as water balance and water table fluctuation methods due to their conservative nature (Xu and Beekman, 2003). A specific relationship governing the compositions of oxygen and hydrogen isotope values in rainfall exists: Craig (1961) used a linear regression method to analyze oxygen and hydrogen isotopic compositions in rainfall, snow melt, and river water from all over the world. His finding established the Global Meteoric Water Line (GMWL) expressed as;

$$\delta D = 8 \delta^{18}\text{O} + 10 \quad \text{Equation 2.3}$$

A later study by the International Atomic Energy Agency (IAEA) that used water samples from the global rainfall stations (Gat, 1980) showed similar results:

$$\delta D = (8.17 \pm 0.08) \delta^{18}\text{O} + (10.56 \pm 0.64) \quad \text{Equation 2.4}$$

When condensation occurs, the slope of the meteoric water line of oxygen and hydrogen isotopes represents the ratio of the temperature relationship between δD and $\delta^{18}O$; the intercept value is based on the evaporative conditions in the region of the water source (Yeh *et al.*, 2014). Also called deuterium excess or d-excess, the intercept is expressed as:

$$d = \delta D - 8 \delta^{18}O \quad \text{Equation 2.5}$$

Variations in rainfall evaporation or source evaporation conditions in various air masses result in different slopes and intercepts for various regions (Yeh *et al.*, 2014), resulting in Local Meteoric Water Lines (LMWL). Higher intercepts greater than 10‰ indicate rapid evaporation or evaporated rainfall (Yeh., 2014). Therefore, the d-excess value allows the air mass source of meteoric water to be identified and the groundwater recharge source to be defined (Gaye and Edmunds, 1996; Yeh *et al.*, 2014).

Various studies have used stable isotopes of ^{18}O and 2H to evaluate recharge characteristics of the shallow alluvial aquifers in arid and semi-arid areas (Faye *et al.*, 2019; González-Trinidad *et al.*, 2017; Joshi *et al.*, 2018; Oiro *et al.*, 2018; H. Yeh *et al.*, 2014). The study of Yeh *et al.* (2014) considered the isotopic compositions of river water and for water samples of the alluvial aquifer in the Hualian River basin. The results indicated that rainfall was the primary source of the river water, while the isotopic composition of the alluvial aquifer in the Hualian River basin indicated recharge from rainfall and river water (Yeh *et al.*, 2014). In their research (Yeh *et al.* (2014), the composition of alluvial groundwater was similar to that of river water, indicating that the recharge of river water was greater than the infiltration of rainfall in the Hualian basin. González-Trinidad *et al.* (2017) used stable isotopes of ^{18}O and 2H to determine groundwater recharge sites and to identify groundwater flow processes of Calera alluvial aquifer, Mexico. It was determined that streamflow play a significant role as a source of local recharge to the aquifer (González-Trinidad *et al.*, 2017).

In SSA, Faye *et al.* (2019) used isotopes of oxygen (^{16}O , ^{18}O) and hydrogen (1H , 2H) compiled from several other studies to trace natural groundwater recharge in the Thiaroye aquifer of Dakar, Senegal. The study concluded that shallow groundwater of this aquifer is primarily derived from isotopically depleted rainfall that occurs in the latter part of the monsoon (September) (Faye *et al.*, 2019). Values of $\delta^{18}O$ and δ^2H in groundwater ranged from >4 and 20‰, respectively (Faye *et al.*, 2019), indicating large variability in evaporative enrichment prior to recharge (Xu *et al.*, 2019). In

East Africa, Oiro *et al.* (2018) used $^{16,18}\text{O}$ and $^1,^2\text{H}$ stable isotopes to identify spatiotemporal controls on groundwater recharge in two contrasting aquifer systems; Nairobi Aquifer System (NAS) (volcanic) and South Coast aquifer (S.C.) (sedimentary). The isotopic composition of the NAS showed no similarity between river water and sampled groundwater, implying the existence of little or no direct infiltration of river channels into the groundwater system (Oiro *et al.*, 2018). The study revealed that recharge into the NAS is through the infiltration of surface water from human-made surface water bodies with longer residence times and with evaporation signatures (Oiro *et al.*, 2018). The SC, on the other hand, indicated recharge into the aquifer majorly through the infiltration of river water (Oiro *et al.*, 2018). It was also established that increasing groundwater abstraction in the SC aquifer and tidal backflows into the rivers has led to the mixing of fresh groundwater and seawater, as shown by marine isotopic signatures in groundwater samples.

2.4.3 Age of groundwater

The radioactive hydrogen isotope, tritium (^3H), has 12.4 years half-life (Kendall and Holland, 2003). Measurements of tritium are often used to calculate recharge rates, rates or directions of subsurface flow, and residence times of groundwater (Kendall and Holland, 2003; Zhang and Satake, 2003) within a period of less than 100 years. ^3H content is expressed in tritium units (TU, where 1 TU equals 1 ^3H atom in 10^{18} atoms of hydrogen). The natural tritium concentration peaked in the 1960s (Zhang and Satake, 2003) following atomic and hydrogen bomb testing carried out in the 1950s (Motzer, 2007). Since then, the atmospheric tritium has gradually decreased from 30 TU to almost 5 TU, approaching the pre-nuclear testing values (Gaye and Edmunds, 1996; Zhang and Satake, 2003).

Since groundwater tritium concentrations frequently reflect atmospheric tritium levels when the water was last in contact with the atmosphere, ^3H can be used to date groundwater recharge (Motzer, 2007; J. Zhang and Satake, 2003). Groundwaters that have evaporated before, during or after recharge can easily be identified by their composition of isotopes (Aggarwal and Froehlich, 2016). The age of groundwater is important in understanding aquifer mineralization and recharge regimes (Gaye and Edmunds, 1996). At its most fundamental level of interpretation, the presence of tritium in groundwater is an indication of modern recharge (Ghaffar *et al.*, 2017). The estimation of groundwater age using tritium only provides the following semi-quantitative values (Clark and Fritz, 1997; Moore, 2011; Motzer, 2007);

- < 0.8 TU indicates sub-modern water (< 1950s)
- 0.8 to 4 TU depicts a mix of sub-modern and modern water
- 5 to 15 TU suggests modern water (<5 to 10 years)
- 15 to 30 indicates recharge in the 1980s to < 1990s (Atwood, 2013; Zhao *et al.*, 2018)
- >30 TU indicates recharge occurred in the 1960s to 1970s
- >50 TU recharge in the 1950s to 1960s

The detection of tritium in shallow groundwater is a modern charging fingerprint, indicating recent replenishment (Aggarwal and Froehlich, 2016). Modern recharge is an important factor of shallow groundwater management, especially in arid and semi-arid regions where groundwater, in most cases, represents a non-renewable resource (Aggarwal and Froehlich, 2016). Recent studies have used tritium to determine the age of groundwater in arid and semi-arid areas (Abiye *et al.*, 2018; Appleyard and Cook, 2009; Casanova *et al.*, 2016; Faye *et al.*, 2019; Ghaffar *et al.*, 2017; Joshi *et al.*, 2018). Tritium measurement in an arid region of Pakistan indicated tritium levels between 5 and 14 TU, suggesting groundwater recharge by rainfall from the 1960s and 1970s, less than ten years after the atomic bomb (Ghaffar *et al.*, 2017). Ghaffar *et al.* (2017) also identified tritium levels between 17 to 25 TU and attributed it to the mixing of modern and 1960s to 1970s recharge. In SSA, tritium analysis for Thiaroye shallow alluvial aquifer in Dakar, Senegal, revealed tritium >2 TU, indicating recharge predominantly from modern rainfall (Faye *et al.*, 2019). The study also revealed that tritium distribution in groundwater was consistent with its flow paths to seasonal lakes and wetlands (Faye *et al.*, 2019). In central Africa, the shallow groundwater of the Ndop plain in northwest Cameroon showed tritium levels between 2.4 to 3.1 TU, implying modern rainfall recharge under low relative humidity regimes and negligible evaporation effects (Wirmvem *et al.*, 2017). Very few groundwater studies involving tritium have been carried out in East Africa. The study of Sklash and Mwangi (1991) used isotopes to evaluate recharge sources for groundwater supplies in the Eastern Province of Kenya. The study revealed that groundwater in highland areas is recharged from direct rainfall infiltration in humid highland areas where significant evaporation occurs during precipitation (Sklash and Mwangi, 1991). In lowland areas, groundwater recharge is from ephemeral streams and possibly from lateral groundwater flow from the highland regions (Sklash and Mwangi, 1991). Although tritium is a comprehensive tool for dating groundwater, its application in groundwater recharge is almost coming to an end (Ghaffar *et al.*, 2017) because its levels in various media are approaching the pre-bomb levels (Moore,

2011), thus making it difficult to distinguish between recharge before or after the 1950s (Ghaffar *et al.*, 2017).

2.5 Conceptual Aquifer Geometry Modelling

Hydrogeological modelling is an excellent approach for sub-surface visualization of aquifers in a given area (Alam and Ahmad, 2014; Zaheeruddin and Khurshid, 2004). Groundwater modelling is also a powerful tool for groundwater management and for predicting the future behaviour of aquifers (Baalousha, 2011). Hydrogeological data should be sufficient and reliable to build an accurate aquifer conceptual model (Baalousha, 2011). A conceptual model is an illustrative representation of a groundwater system that includes a geological and hydrological interpretation (Alam and Ahmad, 2014; Baalousha, 2011; Zaheeruddin and Khurshid, 2004). An aquifer conceptual model requires accurate information on geology, hydrology, boundary conditions, aquifer parameters (hydraulic conductivity, porosity and storativity), and hydraulic parameters (Zaheeruddin and Khurshid, 2004). It is also important to consider the depth to the water table and geological structures within an aquifer (Kaufmann, 2009). Knowledge of recharge and discharge areas of an aquifer provide critical clues of groundwater flow (Zaheeruddin and Khurshid, 2004). Bedrock data is important in aquifer conceptualization studies. However, where there are no drill-to-bedrock data, electrical resistivity, seismic reflection and gravity methods are employed to determine the aquifer geometry (Alam and Ahmad, 2014).

2.6 Current Approaches to Sustainable Groundwater Management

Groundwater resources supply freshwater to many populations in arid and semi-arid environments, and especially to small cities in SAA (Moridi *et al.*, 2018; Prinz and Singh, 2000; Subramani *et al.*, 2009). Groundwater protection and conservation measures have been generally overlooked in the majority of environmental management practices (Al-Shaibani, 2008). In arid and semi-arid areas, sustainable groundwater management may be more complicated than in other regions due to scarce human and financial resources, and excessive withdrawals (Moridi *et al.*, 2018), inadequate knowledge of groundwater resources (Comte *et al.*, 2016; Joshi *et al.*, 2018; Lautze *et al.*, 2018; Y. Xu *et al.*, 2019), lack of long-term monitoring network, and inadequate information transfer from stakeholders to users (Moridi *et al.*, 2018). In most countries, water shortages and poor water quality are primary concerns (Comte *et al.*, 2016).

Integrated groundwater management and planning involves careful assessment and understanding of the area's climate variability (Green, 2016). The success of the sustainable groundwater management of groundwater in arid and semi-arid areas require an interdisciplinary and holistic approach that incorporates all the stakeholders, policymakers, water professionals, more in-depth understanding of local specific environmental issues and hydrogeological conditions, indigenous methods of water conservation and usage (Comte *et al.*, 2016). Sustainable management accountability requires a practical policy framework that considers all the multidimensional aspects of water scarcity and overexploitation.

2.7 Summary

Groundwater occurrence and distribution is unique to its hydrogeologic setting, which influences aquifer potential and productivity. Globally, four types of aquifers exist based on their hydrogeologic setting; Precambrian basement aquifers, Volcanic aquifers, Sedimentary aquifers and Alluvial aquifers. Volcano-sedimentary aquifers comprise approximately 55% of the world's groundwater resources and are mainly distributed in arid and semi-arid areas. Specific characteristics of each aquifer in time and space can be defined based on aquifer properties such as porosity, specific yield, aquifer storage, transmissivity, and hydraulic conductivity. Darcy's Law accurately describes groundwater flow in most natural hydrogeological conditions. Volcano-sedimentary aquifers have received little attention, with only a few studies conducted in East Africa.

Many factors control the groundwater chemistry; aquifer composition through which water flows, recharge source, ion exchange processes, contamination through land-use activities, mixing processes and groundwater age. Understanding the hydrogeochemistry of an aquifer helps determine the factors controlling groundwater quality and its associated geochemical processes. High fluoride, iron and manganese concentrations are the major concerns of alluvial aquifers. In volcanic aquifers, the dominant water types identified by research studies include; Na-HCO₃, Na-Mg-Ca-HCO₃, and Na-Ca-HCO₃, while Ca-HCO₃ is the dominant water type in the alluvial aquifers. Alluvial aquifers are identified as the most vulnerable to pollution, mainly when they occur in the vicinity of urban centres. Determination of nitrate concentration in groundwater is a commonly used approach for the identification of anthropogenic pollution.

It is anticipated that changes in the global climate will affect the hydrological cycle, altering the level of surface water and recharging groundwater systems. Limited observation data in many areas has made it difficult to accurately determine the extent and direction of groundwater change as a result of climate impacts. Further studies to guide integrated groundwater management at all levels, from local to regional contexts, is required to understand climate and groundwater interactions. Isotope techniques and the water table fluctuation method are considered excellent techniques for identifying the recharge sources and recharge rates in arid and semi-arid areas, especially in regions with limited observation data. The water table fluctuation method requires long-term groundwater time-series for both rainfall and groundwater for its successful application, a requirement that presents a major limitation to this study. The age of groundwater provides important information regarding aquifer mineralization, recharge rates and its vulnerability to pollution. Groundwater with a high ^3H level depicts greater potential of its replenishment and indicates its vulnerability to pollution – an important knowledge for sustainable groundwater development.

Inadequate knowledge of groundwater resources, water scarcity and poor quality are the major concerns of groundwater use in Africa. Increasing water demands also provoke overexploitation of groundwater, which adversely impacts the quality and quantity of the available groundwater reservoirs. The impacts of climate variability also threaten the future availability of groundwater resources. Consequently, informed groundwater management strategies are urgently required for the protection and conservation of groundwater resources, especially in arid areas.

CHAPTER THREE: STUDY AREA AND METHODS

3.1 Introduction

This chapter has three main parts; study area description, research design and research methodologies. Study area description includes the general context of the location, demographic and social-economic characteristics, geological setting (both regional and local geology), and other physiographic characteristics such as physiography and drainage, soils, climate, vegetation, land use and resources as well as surface water and the groundwater resources of the area. Part two (section 3.3) deals with study design, including case study approach, exploratory and longitudinal research designs, while Part 3 (section 3.4) describes the research methodologies for each specific objective starting with desktop studies, field data collection, laboratory techniques and data analysis. A summary of this chapter (section 3.5) details the major highlights of the study area as well as the application of selected methods in aquifer studies.

3.2 Description of the Study area

3.2.1 Location of the Study area

Turkana County is the second largest among the 47 counties of Kenya after Marsabit County, located in the north-western Kenya. The borders of the Turkana county give it a unique geographical setting among the rest of the counties. The county borders three countries; Uganda to the west, South Sudan and Ethiopia to the north and Lake Turkana to the east. The adjacent counties to the south include the West Pokot, Baringo, Samburu and Marsabit county on the eastern shore of Lake Turkana. The study area is in the downstream section of the Turkwel river within Lodwar municipality and its environs and covers a total area of 1040 km² and is bounded by longitude 35° 32.0' to 35° 48. 0' and latitudes 3° 0.0' to 3°15.0' (Figure 3.1).

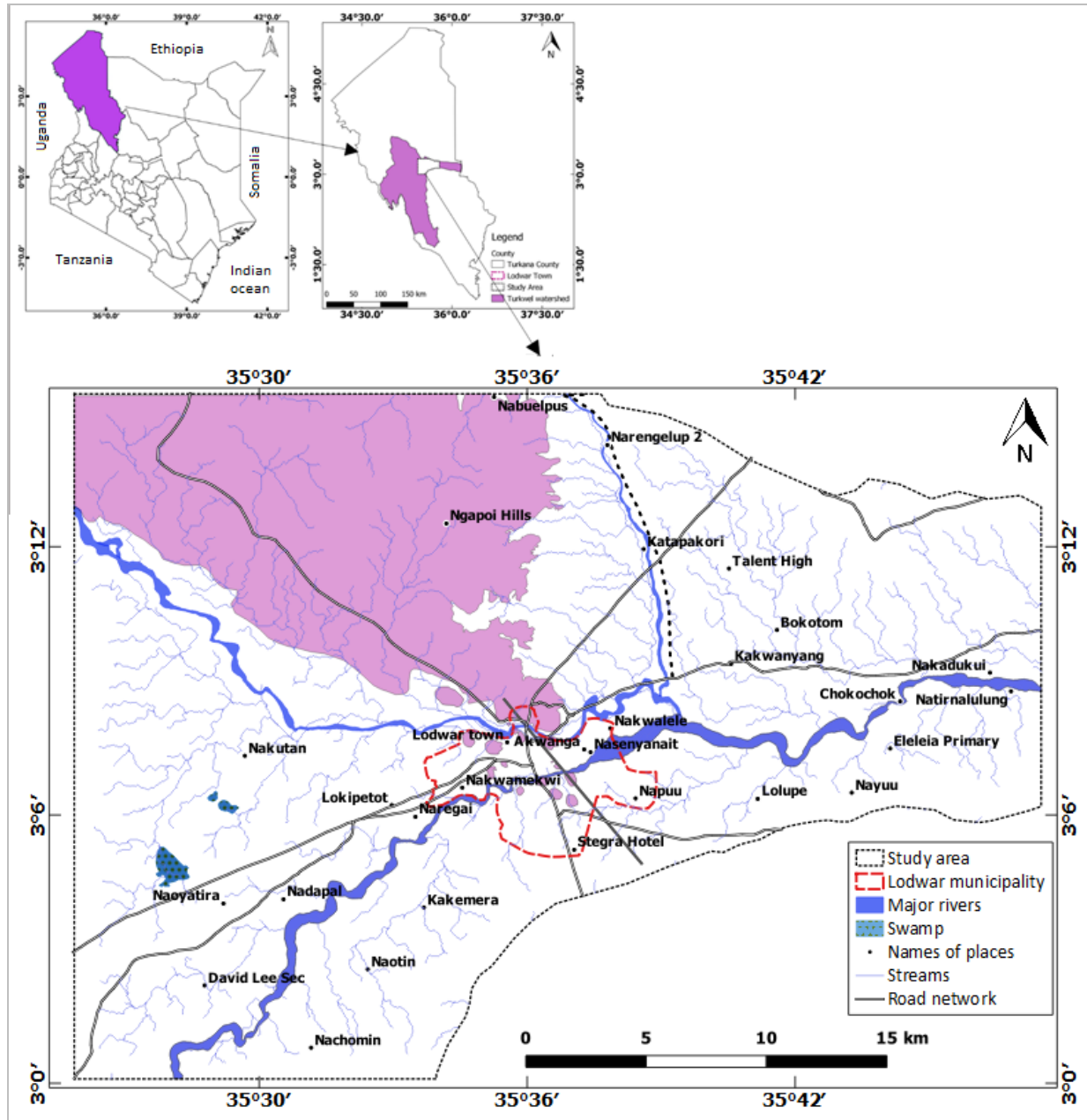


Figure 3.1: Location of the study area within the Turkwel River watershed

3.2.2 Demographics

The total population of Turkana county based on the Kenya Population and Housing Census (KPHC) of 2019 was 926, 976 (KNBS, 2019), which is about 8.37% more than that recorded in 2009 (855,399) (KNBS, 2009). The study area is in Turkana Central Constituency, which has the highest population density (29 persons/Km²) in Turkana County (KNBS, 2019) and has recorded the highest population growth since 2009 (+38%). Lodwar town, which is in the centre of the study

area, is the most populated (82, 970) of the major urban centres in Turkana county (Table 3.2). According to the 2019 population census, the increase in population of men (+86%) and women (+80%) in Lodwar town is more than double that observed in 2009. Overall, Kakuma and Lokichoggio experienced negative population trends of -28 and -34%, respectively, between 2009 and 2019 and may be linked to the establishment of Kalobeyei Integrated Socio and Economic Development Programme (KISED P) between Kakuma and Lokichoggio has led to the growth of Kalobeyei urban centre (UNHCR, 2018). The population decline can also be ascribed to more people seeking employment and the availability of infrastructure and social facilities in Lodwar town (Turkana County, 2017). In addition, the intended closure of the Kakuma refugee camp in 2016 by the Kenya government resulted in a decline in new registration of refugees and subsequent withdrawal of key NGOs in the area such as Oxfam and World Vision (UNHCR, 2018).

Generally, population increase in Turkana county will result in increased settlement and subsequent need for increased social amenities and growth of commercial enterprises to provide sanitation facilities, food and employment opportunities (Turkana County, 2017) and ultimately expansion in water supplies. More than half (61%) of rural households use unimproved water sources, with the majority relying on unprotected wells and streams (MWI, 2013).

Table 3.1: Constituency population and population density in Turkana County (Source: KNBS, 2009; 2019)

Constituencies	2009 (Census)		2019 (Census)	
	Total	No. Per/ Sq. Km	Total Pop.	No. Per/ Sq.Km
Turkana Central	134,674	24	185305	29
Turkana North	129,087	7	65218	9
Turkana West	245,327	14	239,627	14
Loima	119,932	13	107795	22
Turkana East	90,466	5	138526	12
Turkana South	135,913	18	153736	12
Kibish			36769	4
Total	855,399		926,976	

Table 3.2: Population census of the major urban centres in Turkana County (Source: KNBS, 2009;2019)

Major Urban Centres in Turkana County	Gender	Lodwar	Kakuma	Lokichoggio	Total
2009 (Census)	M	22,349	16,820	9,313	48,482
	F	23,019	15,142	8,382	46,543
	Total	45,368	31,962	17,695	95,025
2019 (Census)	M	41,583	12,050	5,915	59,548
	F	41,387	10,934	5,711	58,032
	Total	82,970	22,984	11,626	117,580
% Δ in population since 2009	Female	80	-28	-32	25
	Male	86	-28	-36	23
	Total	83	-28	-34	24

3.2.3 Geological setting

3.2.3.1 Regional geology

The main geological formations in the wider region (Figure 3.2) (Dodson, 1971; Feibel, 2011; Muia, 2015; Rhemtulla, 1970; Walsh, and Dodson, 1969) range, from oldest to youngest, as follows: (1) Precambrian basement system rocks (gneisses, granulites, quartzites and limestones with metamorphosed/non-metamorphosed/anatectic intrusive rocks such as granites, aplites, pegmatites, norites and gabbros); (2) Cretaceous-Palaeogene-Neogene sediments (Cretaceous sandstones and conglomerates of the Lapur Formation, and Turkana grits series; (3) Paleogene and Neogene volcanics (basalts, pyroclastic volcanic rocks, phonolites, trachy-andesites and nephelinites with numerous intrusive rocks of nephelinite, dolerite, teschenite, lamprophyre and microfoyaite compositions), and (4) Superficial deposits of Plio-Pleistocene to Recent age (aeolian sands, alluvial soils and gravels, lacustrine shales, shelly limestones and coarse grits) that cover most of the central and north-eastern parts of the county.

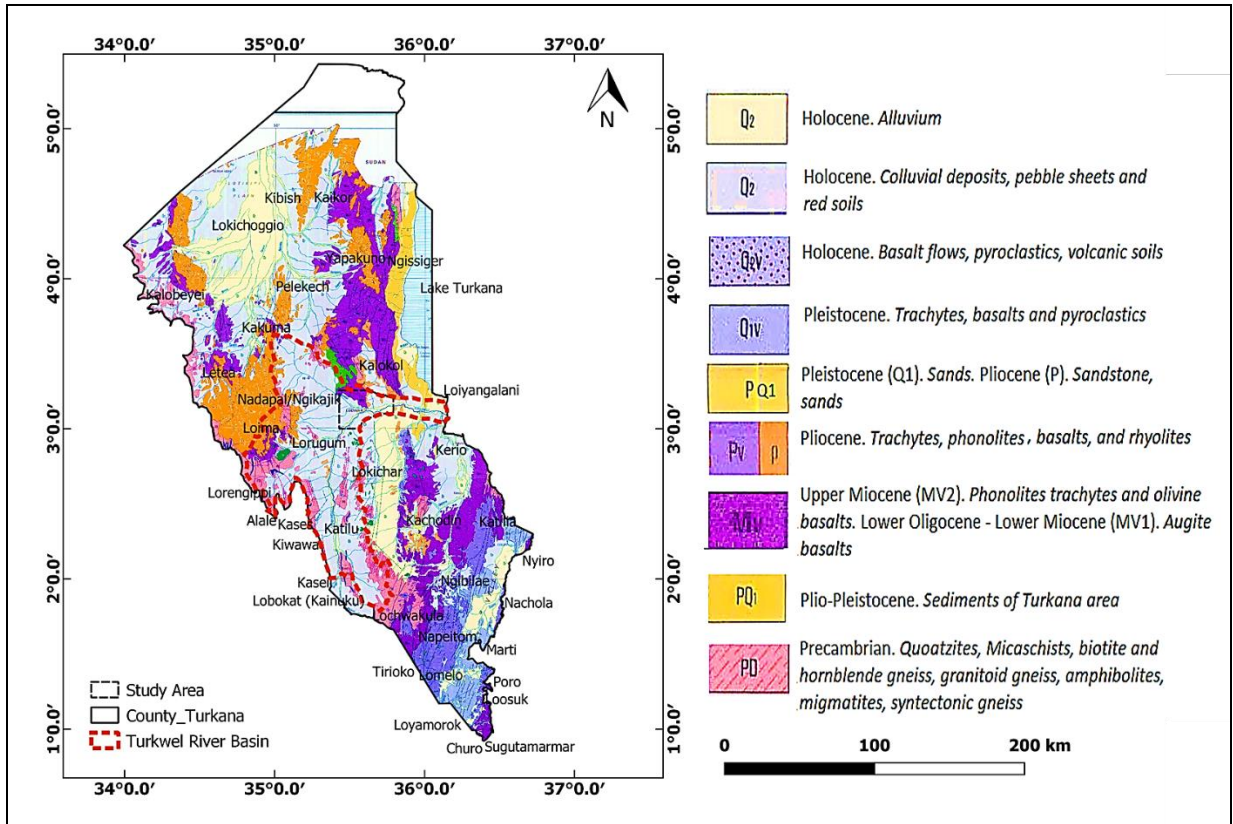


Figure 3.2: Geological map of Turkana county showing the location of the study within the Turkwel River Basin (Partly modified from the Ministry of Energy and Regional Development 1987)

3.2.3.2 Geology of the Turkwel River basin

It is important to consider the river basin scale geology (and its structures) as it bears the hydrogeology and hydrogeochemistry of the aquifers within it. The geology of the Turkwel River basin is typical of that of Turkana county (see section 3.3.1.1, Figures 3-1 and 3-2). The major formations comprise Precambrian basement systems rocks (mainly quartzo-feldspathic gneiss, biotite gneiss), sedimentary rocks (Turkana grits and Holocene sediments), volcanic rocks (nepheline phonolites and augite basalts), and alluvial deposits along laggas and streams in the study area.

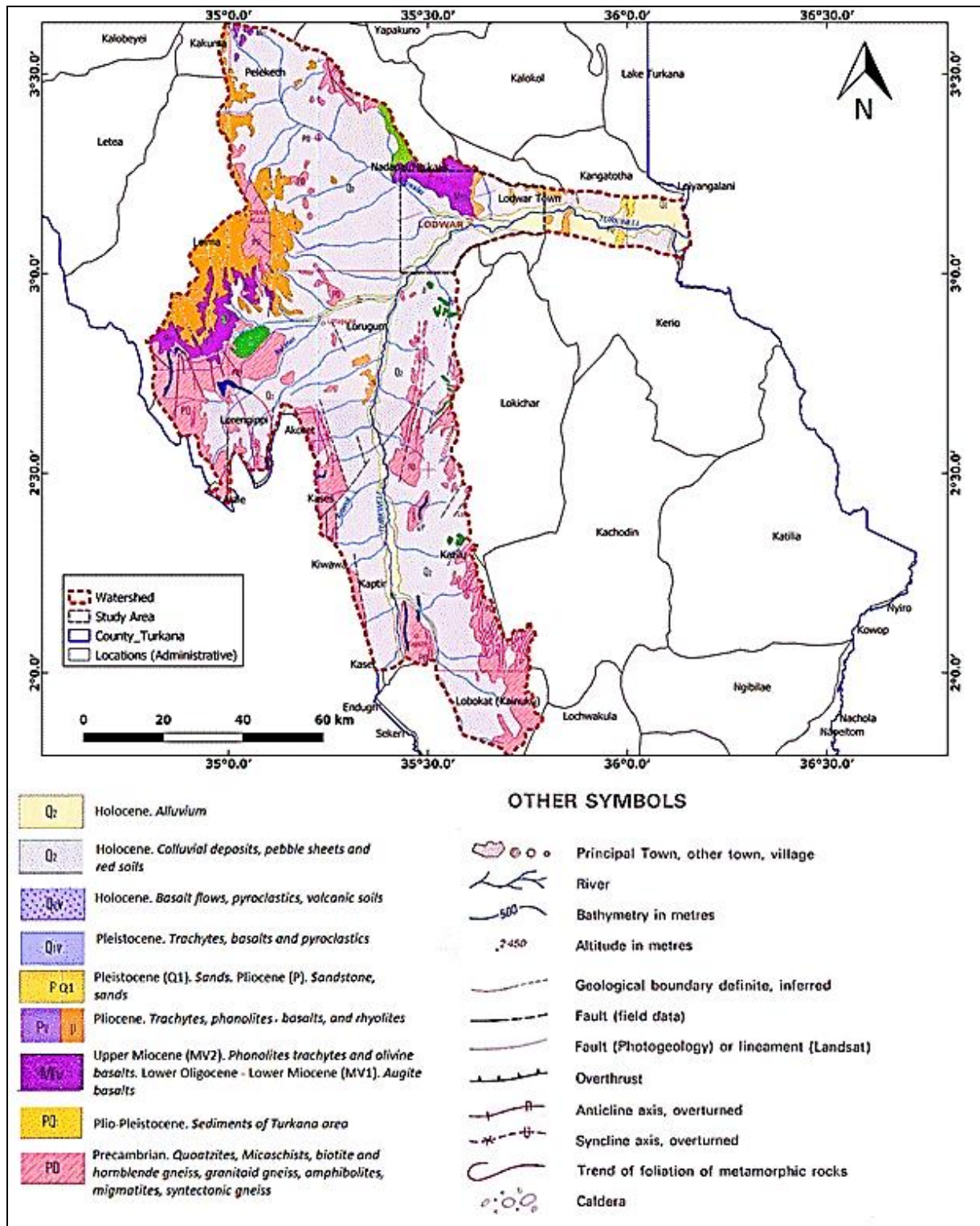


Figure 3.3: Geological map of Turkwel River Basin (Geological Map of Kenya (MERD), 1987)

(a) Basement System

The metamorphic basement in the Turkwel River basin is exposed in almost all its margins with the majority of the outcrops occurring on the western and south-eastern parts (Figure 3.3). They comprise various types of gneisses, schist, and marbles that have formed from metamorphosed sediments - grits, sandstones, limestone, and shales. Most of the exposed rock is highly weathered, often to a condition in which their original constituents are almost completely altered, with the soft, friable nature of the outcrops often preventing detailed mapping (Dodson, 1971). Biotite gneisses account for an appreciable proportion of the Basement System succession in the Turkwel River basin. Cataclastic rocks cover the western parts of the Turkwel basin forming series of well-drained hills or ridges composed of fault breccia. These rocks are fine-grained and highly faulted, consisting of angular fragments of quartz and other resistant minerals (Walsh, and Dodson, 1969).

(b) Sedimentary formations

Walsh and Dodson (1969) describe the Turkana Grit as a succession of sediments that locally exceed 152.4 m (500 feet) in thickness and unconformably overlie the Basement System rocks, from which they are derived (Mason and Gibson, 1957; Muia, 2015). The ‘Turkana Grit’ was first identified as azoic sediments found within the Northern Kenyan Rift (NKR) and Central Kenyan Rift (CKR) by Hughes, (1933). However, these studies did not investigate and described the Grit due to the absence of fossils that resulted in a principally mystifying history of many sedimentary basins in these parts of the Kenya Rift. The “Turkana Grit” is described as a series of quartzites, conglomerate, sandstone and minor shales that thin out northwards and westwards from the Lake region, meeting the younger lavas that overlie the Basement System (Walsh and Dodson, 1969; Muia, 2015) while Feibel (2011) further considers it as a Cretaceous to Pleistocene assemblage of prominent quartzo-feldspathic sandstones that transitioned into the “Turkana Grits”. Except for the Lapur Sandstone, where dinosaur remains were discovered in its lowermost part (Arambourg, 1933; Arambourg and Wolff, 1969; Wescott *et al.*, 1993) and the Lokone Sandstone, where the oldest mammalian faunas in East Africa were recently discovered, the majority of the “Turkana Grits” are still considered azoic (Ducrocq *et al.*, 2010). Exposures of the Turkana grits are only to the eastern and south-eastern parts of the Turkana County, with identified exposures around Lapur Hills, Muruangapoi, Lothidok Hills, and Lokitaung Gorge (JICA, 2012; Muia, 2015; Walsh, and Dodson, 1969).

(c) Paleogene and Neogene volcanics

Volcanic rocks occur in the Turkwel River basin south of Loima hills and at Lodwar town. The tertiary volcanics comprise phonolites, phonolitic agglomerates, nephelinites, and olivine nephelinites (Walsh and Dodson, 1969). The lowermost lava occurring at Muruangapoi hills near Lodwar has a dark grey colour, buff fine-grained groundmass, and conspicuous phenocrysts (JICA 2012). The Lodwar cone has nephelinite capping consisting of black coarsely porphyritic rock, which appears in thin sections as phenocrysts of purple-grey titanite with green outer zones with a core (Walsh and Dodson, 1969; Dodson, 1971). The main characteristics of the olivine basalts are coarse porphyritic texture, medium to coarse-textured, dark blue-grey, or black with phenocrysts of up to 0.5 cm (Dodson, 1971). In the entire Turkwel Basin, these outcrops occur at the Muruangapoi hills in Lodwar and as volcanic cones within Lodwar town and its environs (Dodson, 1971). In the study area, augite and analcime basalts outcrop within the central and north-western parts of Lodwar municipality (JICA 2012).

(d) Superficial deposits

The superficial Plio-Pleistocene to Recent age deposits in the Turkwel River basin is comprised mainly of fluvial materials that have accumulated along drainage channels (Feibel, 2011; Muia, 2015; Olago, 2018) in an extensive integrated depositional system due to subsidence (Feibel, 2011), with intercalated lacustrine deposits in areas adjacent to the present lake (Dodson, 1971). Most of the alluvial/fluvial deposits are derived from the underlying Basement System rocks, forming gravelly angular fragments that are usually well sorted (Dodson, 1971). Downstream parts of the Turkwel River Basin are covered by wind-blown sand found in small accumulations. The sand predominantly comprises quartz grains which exhibit a high degree of rounding (Dodson, 1971).

3.2.3.3 Geological structures

The Turkwel River basin is part of the subsidence feature in the formation of the greater Turkana basin (Feibel, 2011). The basin covers an area of 23,740 Km² (Hirpa *et al.*, 2018) and the prominent geological structures comprise erosional and sedimentary deposition features. Erosional surfaces are linked to exposures of the Turkana Grits, while the depositional features are related to the fluvial deposition. Generally, crests and troughs structures are observed in the major drainage features (Turkwel, Kawalase, and Monti), reflecting that lineament is controlled by folded

Precambrian Basement System (Dodson 1971). Fluvial deposits have filled the troughs while the erosional surfaces characterize the crests where Turkana grits are usually exposed. According to Hughes (1933), the Turkana grits are punctuated by dolerite dykes from volcanic activity within Lodwar town oriented in an NW-SE plane (Dodson, 1971). The dykes are eroded more readily than the bearing grits, forming linear trenches (Rhemtulla, 1970). The volcanic lavas that followed the regional subsidence led to the occurrence of volcanic dykes within the Turkana Basin and its environs cutting through the Basement system rocks and the sedimentary formations (Walsh and Dodson, 1969).

3.2.3.4 Soils

The arid climate of north-western Kenya contributes greatly to the type of landforms and soils in the region (Touber, 1990). Due to wind erosion and frequent floods, the soils in the Turkwel River basin are not well developed (Turkana County, 2017). Many studies have investigated the types and chemical characteristics of soils in Turkana county, including the Turkwel River basin (Engelen, 1984; RTI, 2013; Sombroek *et al.*, 1982; Touber, 1990). Sombroek *et al.* (1982) indicated that the Turkwel River Basin falls under Zone VI (non-arable) and Zone VII (non-arable and unsuitable for irrigation) agro-climatic zones reflecting the semi-arid and arid conditions, respectively. Engelen (1984) determined that the alluvial deposits of the Turkwel river at Nakwamoru area ranged from loamy sand to clayey texture. Touber (1990) associated the types of soils to geology and as follows; floodplains and low terrace riverine deposits occur along major rivers and range from stratified, fine sandy and clayey micaceous sediments of high fertility; alluvial and colluvial deposits are derived mostly from the undifferentiated basement system rocks; wind-blown sandy deposits cover extensive plains; bare to very shallow soils with angular quartz and gravel cover areas with Basement System rocks while younger Piedmont plains surrounding the Basement System Hills comprise deep sandy and loamy sediments supporting the dwarf shrub vegetation, and the volcanic hills consist of shallow, rocky and stony soils supporting the wooded and bushed grasslands. RTI (2013) determined that the riparian areas of the Turkwel River near Lodwar town have a high potential for agriculture due to the area's highly productive shallow alluvial aquifers and deep fertile soils.

3.2.4 Physiography and Drainage

The main physiographic features in the study area are the prominent Lodwar Hills located north-west of the Lodwar municipality and the extensive Ngapoi Hills comprising basalts and nepheline-

phonolites (Figure 3.4). The Nepheline phonolites are resistant to erosion and, thus, the reason for the cone-shaped hills in the area (Rhemtulla, 1970; Dodson, 1971; Feibel, 2011). The average height of the volcanic hills ranges between 900 m to 1150 m asl (Dodson, 1971), while the surrounding plains have elevations ranging from 450 to 600 m asl.

Turkwel, Kawalase, and Monti rivers comprise the main drainage features in the study area (Figure 3.4). Turkwel River basin is the only perennial drainage basin in Turkana County and covers an area of 23,740 km² (Hirpa *et al.*, 2018). Apart from the Turkwel River that has a perennial flow upstream of the Turkwel Dam (Hirpa *et al.*, 2018), Kawalase and Monti *laggas* have seasonal to ephemeral flow. The Kawalase River, emanating from the Loima Hills in the western parts of the study area, is the biggest tributary of the Turkwel River. Nakutan lagga follows an east-northeast direction to join with Kawalase River at Nakutan village. Elevation values of Kawalase and Turkwel Rivers range from 258 to 450 m asl. Monti *lagga* drains the northern parts of Lodwar and meets with the massive Kawalase River south of Kakwanyang before joining the Turkwel River. Four streams - Nang'omo, Chokchok, Nakadukui, and Lomopus laggas - drain the northeast part of the study area, and all flow south-eastwards into the Turkwel River (Figure 3.4).

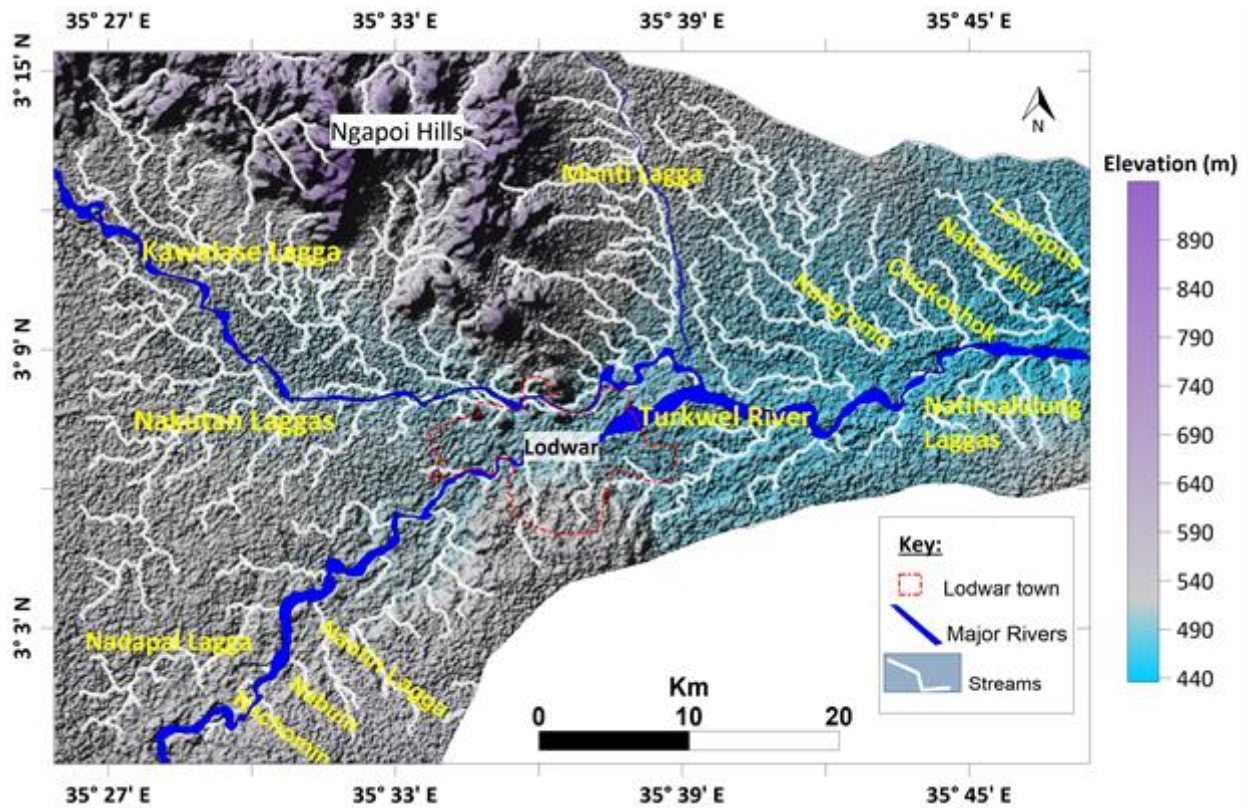


Figure 3.4: Physiography and drainage map of Lodwar and its environs

3.2.5 Vegetation

Like in the vast Turkana county, vegetation cover in the Turkwel River Basin is governed by climate, soil types, landforms, and land-use changes (JICA, 2012). Generally, the vegetation in the area is scanty, and cutting of trees for charcoal burning has negatively impacted on the distribution of vegetation cover (Dodson, 1971). Vegetation density in the Turkwel River basin is strongly correlated with distance to the river channel, with vegetation cover becoming less dense away from the Turkwel River (Stave *et al.*, 2005). Within the investigated area, tall and dense vegetation cover comprising acacias and thorny bushes occurs along the Turkwel River and on the northern part of the Kawalase River (flood plains). Thick euphorbia bushes also cover large parts of Lodwar Municipality (Walsh and Dodson, 1969). Extensive Turkana Grit surfaces are generally bare while the bases of volcanic hills northeast of Lodwar supports sparse growth of thorny scrubs while the upper parts are rocky and barren (Figure 3.5) (Dodson, 1971).

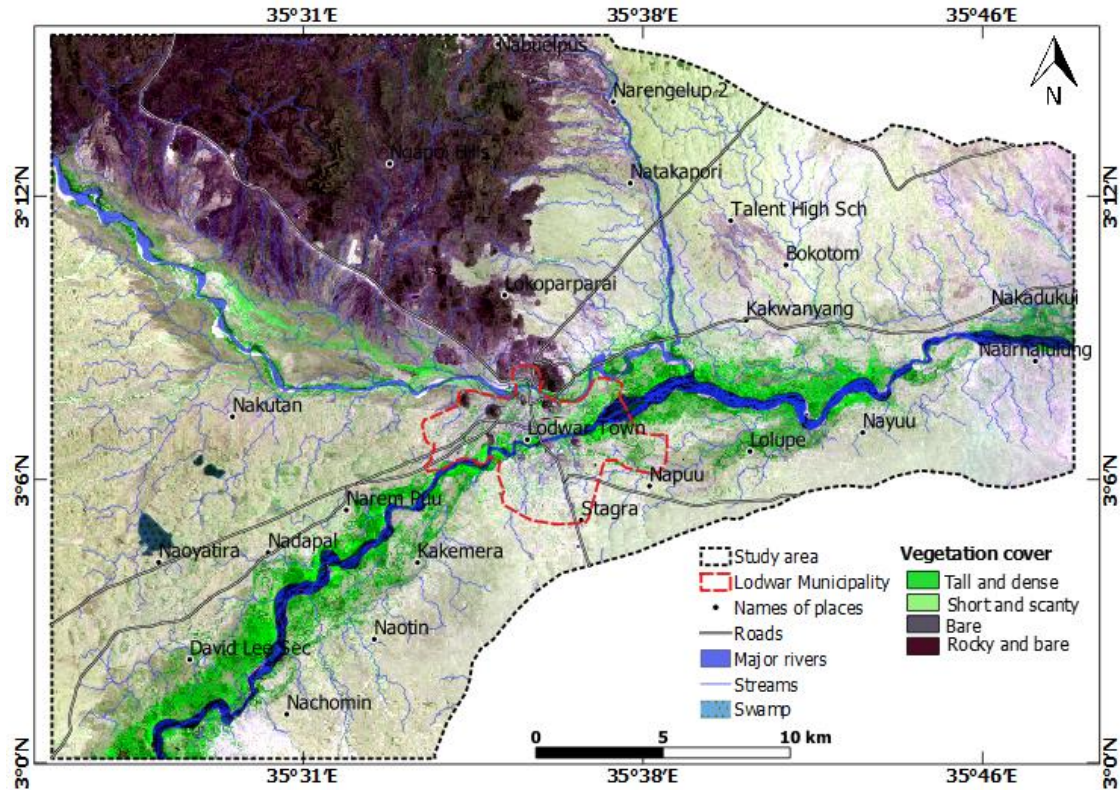


Figure 3.5: Vegetation cover map of the study area within the mid-Turkwel watershed

3.2.6 Climate

The Turkwel River Basin has an intricate hydroclimate with highly variable topography and distinct rainfall gradients from south-west to north-east (Hirpa *et al.*, 2018). Rainfall varies from 200 mm in the drought-prone north-east part of the basin (Opiyo *et al.*, 2015) to 1749 mm/year in the southern highlands (Hirpa *et al.*, 2018). Lodwar municipality, with a mean annual rainfall of 217 mm (Figure 3.6, Opiyo *et al.*, 2015), receives the lowest rainfall in entire Turkana County, and it is unreliable with a bimodal distribution where the first cycle in March, April, and May and less precipitation in October, November, and December. The surface runoff (Opiyo *et al.*, 2014) and potential evaporation rates are high (Olago, 2018), ranging from 1650 – 2800 mm/year (NDMA, 2016). The mean maximum temperatures in the Lodwar area range from 28.0 to 38.0 °C with a long term mean of 30.0 °C (Opiyo *et al.*, 2015) while the minimum temperatures range between 19.1 °C and 25.0 °C with a long-term mean of 20.9 °C (Opiyo *et al.*, 2015). In general, the county has suffered from seasonal rain failure for the last two and a half decades, with evaporation rates always surpassing the average monthly rainfall (NDMA, 2016). Drought spells may lead to a reduction in water levels or complete drying of water sources (NDMA, 2016), the

most recent of which occurred in the period 2015-2017 (FAO, 2018). However, 2006, 2007, and 2011 witnessed higher than anticipated rainfall that led to life-threatening flash floods, with losses of livestock and pasture in many parts of the county (Turkana County, 2018).

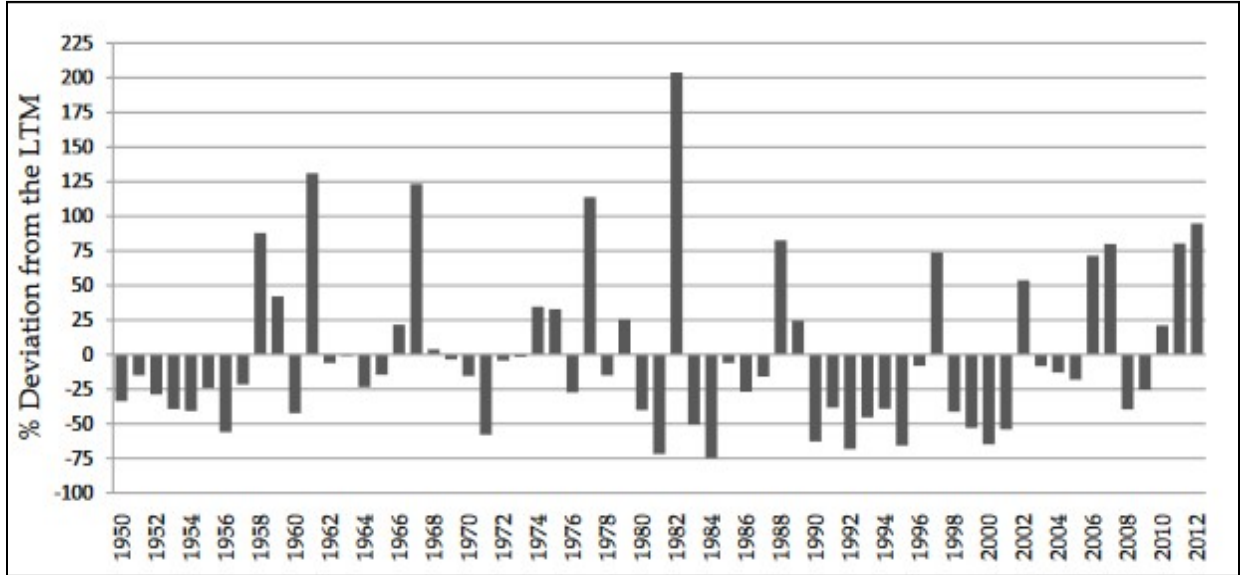


Figure 3.6: Deviation of mean annual rainfall percentage based on 1950-2012 long-term mean (Opiyo et al., 2015)

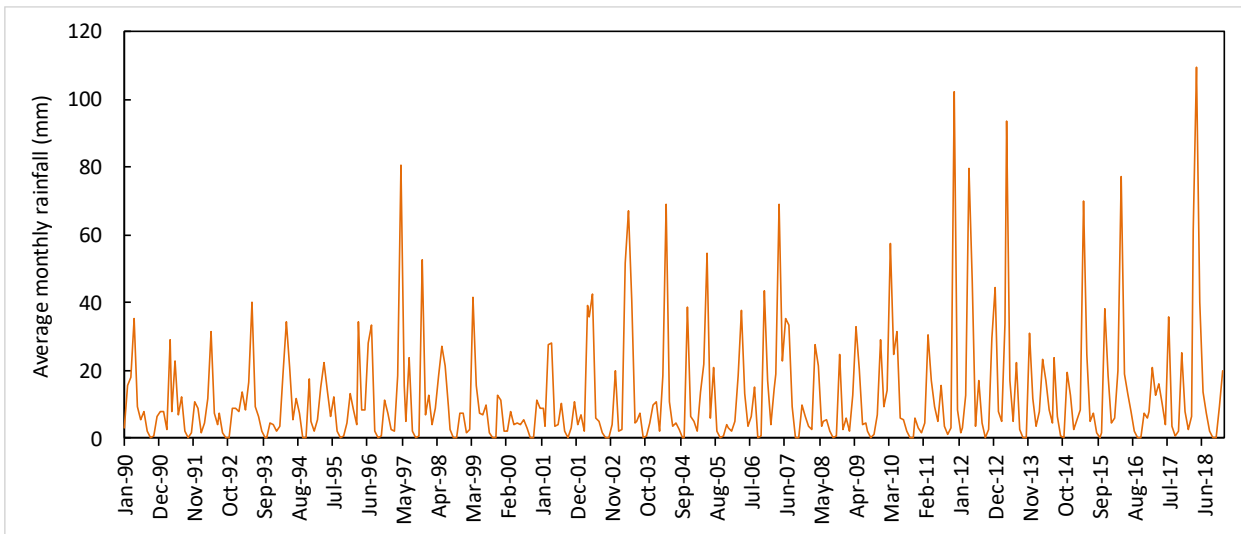


Figure 3.7: Long-term rainfall data for Lodwar met station based on CHIRP (2018) dataset indicating increasing rainfall in recent years

3.2.7 *Land Use*

Mount Elgon and the Loima Hills in the Turkwel River basin support vital economic activities such as honey production, dry-season grazing, wood production, and charcoal production. (Turkana County, 2017). Dwarf shrubs and grassland dominate the open plains and provide livestock forage during and shortly after the rainy season. At the commencement of the dry season, however, this forage dries quickly (NDMA, 2016). The Turkwel River has a high potential for crop production in the county through irrigation if properly utilized (NDMA, 2016). Currently, upstream irrigation is about 2,000 Ha and the proposed expansion of irrigated land targets approximately 10,000 Ha (Ocro, 2015) also in the upstream section. Upstream irrigation does threaten not only the quantity of surface water downstream but also the quality of groundwater in the shallow alluvial aquifer (Hirpa *et al.*, 2018). Oil exploration and the growth of commercial establishments have led to urbanization. Most rural populations are abandoning pastoral practices and moving to major urban centres, especially into Lodwar municipality where they can access social services.

3.2.8 *Water Resources*

Surface water and groundwater resources in the Turkwel River basin are abstracted mainly for domestic, livestock, irrigation, and industrial uses (JICA, 2012; Turkana County, 2018). The surface water sources other than rivers and the numerous ephemeral laggas include dams, water pans, subsurface dams, springs and rock catchments, while the groundwater sources are mainly boreholes, handpumps and hand-dug wells (JICA, 2012).

3.2.8.1 *Surface water resources*

Turkwel dam, the only dam in the Turkwel River basin, was constructed between 1986 to 1991 and is used for hydroelectric power generation (JICA, 2012). Water pans have been dug along laggas in areas with slope <3% to hold water temporarily during the rainy seasons for livestock watering (JICA, 2012). A total of 22 water pans are within the Turkwel River basin, and only two are in the research study area, namely, Nakutan and Monti water pans. There are no sub-surface dams and rock catchments constructed in the Turkwel river basin as well as in the research study area. Open access management is a major concern in the utilization of surface water resources for ensuring reliable and safe water supply for livestock and domestic use (UNICEF, 2006). Among the 23 springs of the Turkana county, only Eliye Springs is within the Turkwel River Basin (JICA,

2012) and has high fluoride content (MWI, 2013). Springs are often contaminated by site-washing and animal watering (UNICEF, 2006).

3.2.8.2 Groundwater resources

A total of 153 operational groundwater sources were identified within the Turkwel river basin, comprising 42% of all those mapped in the entire county (JICA, 2012). Of these, 29 were recorded to have dried up (19%) (JICA, 2012), reflecting the impacts of climate variability in the basin. Generally, most of these groundwater sources have been sunk in the riparian areas of the Turkwel River (Hirpa *et al.*, 2018; Olago, 2018). In terms of water quality, 90 freshwater sources (59 per cent) were reported; 42 were mildly saline (27 %), and 21 were too saline (14%). Groundwater quality presented by WRA in May 2017 indicated that boreholes located in the vicinity of the Turkwel River have EC values ranging from 276 to 330 $\mu\text{S} / \text{cm}$, whereas boreholes located further away have EC values $> 700 \mu\text{S} / \text{cm}$. Most wells in the Turkwel basin are < 20 m deep and are built along seasonal rivers during dry seasons and abandoned during wet seasons (JICA, 2012). Low water levels, low yields, collapse, vandalism and high salinity are the main challenges associated with hand-dug wells (UNICEF 2006). A total of 77 hand-dug wells were identified in the Turkwel watershed (JICA, 2012).

3.2.8.3 Urban and rural water supply

The Lodwar Water and Sanitation Company (LOWASCO) is a corporate entity recognised in 2007 under the Companies Act, Cap 286 Laws of Kenya with the sole purpose of ensuring the provision of efficient and affordable water and sewerage services to the populations of its service area area as defined in the Service Provision Agreement (SPA) (Turkana County, 2017). By 2016, LOWASCO served approximately 33,000 households – just under half of the coverage area in Lodwar municipality and its environs and where nine (9) boreholes are situated along River Turkwel. The total number of water supply connections based on the latest Water Services Regulatory Board WASREB Impact Report was 6,947, out of which 6,630 (WASREB, 2018) were active (NDMA, 2016; Turkana County, 2017). The distance to the nearest water points outside the municipality of Lodwar varies depending on the areas, with an average walking distance of 5 to 20 km from the water source (Turkana County, 2017).

3.2.8.4 Groundwater and development

JICA (2012) presents groundwater as the most reliable source of water supply for domestic, irrigation and industrial uses in Turkana County. This knowledge has made the county administration to plan the drilling of approximately 200 boreholes to expand the water supplies and to improve the sanitation facilities in the region (Turkana County, 2013).

3.3 Research Design

This study used a variety of research design(s); case study design, exploratory design and limited longitudinal design. The case study design was used to review and compile all existing information and data in the study area through in-depth desk study and secondary data collection. The case study methodology was also useful in recognizing differences in scientific knowledge and in formulating the research questions discussed in this report. The approach also helps in examining the validity of selected methods used for each of the specific objectives as well to define the extent of the study area and to establish the hypotheses surrounding groundwater occurrence, water quality and recharge in the study area. The exploratory research design was employed to bring out new scientific evidence within the study area, such as the hydrogeological characteristics of the Lodwar Alluvial Aquifer System, origin and age of groundwater, as well as establish the surface water-groundwater interactions within this aquifer. This design was implemented through reconnaissance study, geological field mapping, geophysics, and isotope analysis for rain, surface water and groundwater samples. The exploratory research findings will form the basis for future scientific studies in the study area. The longitudinal design was used to establish seasonal trends in quality and chemistry of groundwater in the study area where major observations were spread over three seasons comprising two dry seasons (February 2018 and 2019) and one wet season (May 2018). Understanding the seasonal differences in water quality helps to determine not only the underlying aquifer processes but also possible safe water supply interventions. To test the hypothesis surrounding groundwater occurrence (JICA, 2012; RTI, 2013), and the possible links between the Turkwel River and the shallow alluvial aquifer (Hirpa *et al.*, 2018; Olago 2018), longitudinal research has been beneficial in the application of several geochemical methods in data analysis and interpretation. The research process was implemented, as indicated in Figure 3.8 below.

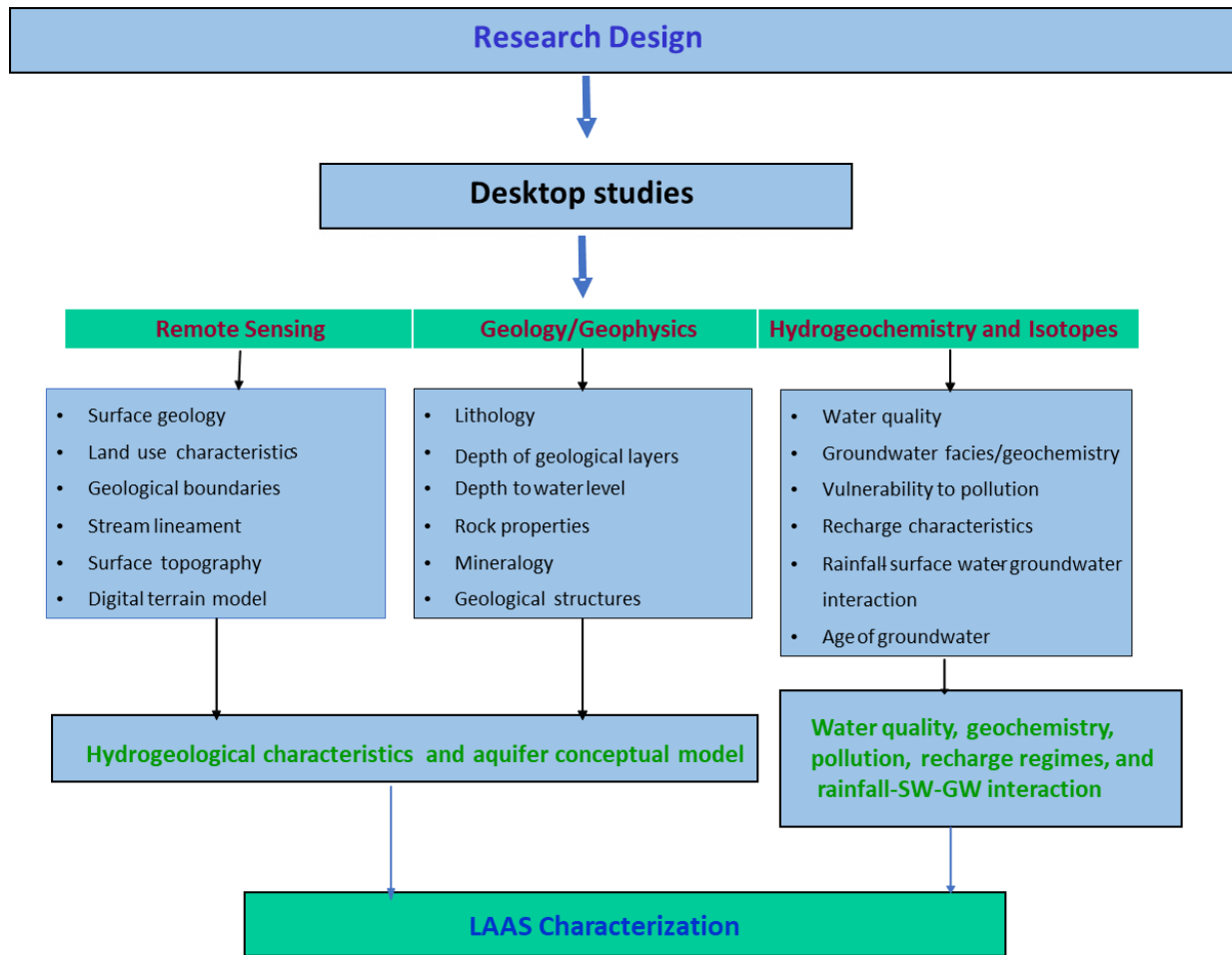


Figure 3.8: Research Design for Lodwar Alluvial Aquifer System

3.4 Research Methodology

3.4.1 Hydrogeology of the Lodwar Alluvial Aquifer System

The methods described in this section are for investigation of the hydrogeological characteristics of the Lodwar Alluvial Aquifer System. Each method and the fieldwork procedures are presented, and the analytical rationale is provided in Appendix 3-1.

3.4.1.1 Desktop studies

Preliminary examination of the hydrogeology of Lodwar and its environs using all the available information was carried out extensively prior to planning data collection from the study area (Cobbing, 2020). Distribution of all the surface water and groundwater supplies in Turkana county, including the Lodwar and its environs, was obtained from JICA (2012).

Secondary data were obtained from LOWASCO, Water Resources Authority (WRA), Oxfam, Catholic Diocese of Lodwar, where the information about the depth of the boreholes, test pumping yields, water rest levels, static water levels, and location details were extracted. Following a validation process, a total of 50 sites were identified from the database from the various boreholes and handpumps. This dataset was used in the determination of the following aquifer characteristics of Lodwar aquifers; transmissivity, hydraulic conductivity, water table, permeability, and yield. The static water levels and water rest levels from acquired secondary data were compiled and analysed to determine the groundwater flow direction and piezometric surfaces. These datasets were also plotted on the topographic maps using Golden Software Surfer Version 16 to in order to relate the groundwater and surface water flow directions. The data also contributed to the estimation of the geometry of the Lodwar Alluvial Aquifer System.

The digital terrain model for the study area (30 m) resolution was downloaded from the USGS website (<https://earthexplorer.usgs.gov/>) and was used for watershed delineation as well as analysis of the stream lineament in the study area. High definition images of the area obtained from Google maps were used to determine preliminary geological boundaries for the rock types in the area prior to field verification.

All the existing information of the study area were consolidated and used to prepare an initial site conceptual model for the area.

Table 3.3: Desktop study data sources in the area and their specific contribution to the hydrogeological of the study area

No	Data Type	Primary sources of information	Specific sources	Activity
1	Site geology	Published geological maps and reports	Walsh, and Dodson, (1969), Rhemtulla, (1970), Dodson, (1971), Ministry of Environment (1987), Feibel, (2011) Muia, (2015)	Define surface geology and geological structures of the area
2	Topography, surface water occurrence and drainage patterns	Published literature and remote sensing	JICA (2012), WRA database, Google maps and USGS Explorer satellite imagery	<ul style="list-style-type: none"> - Occurrence and distribution of surface water supplies - Drainage lineaments and surface topography
3	Groundwater occurrence	Published Hydrological and hydrogeological studies	JICA (2012), RTI, (2013), Kuria, (2013), MWA database, Catholic Diocese, Oxfam database, LOWASCO, MWI database and other published literature of the study area	<ul style="list-style-type: none"> - Determine the distribution of groundwater resources - Evaluate aquifer characteristics - Obtain groundwater flow direction - Relate groundwater occurrence with geological and surface topography - Determine aquifer types - Identify existing data gaps
4	Initial conceptual model for the study area	Utilize information gathered from the desk study	Data from sources 1, 2 and 3 above	Initial site conceptual model for Lodwar and its environs

3.4.1.2 Fieldwork

The geological site survey was conducted in a three-phase fieldwork area; Phase 1 involved a reconnaissance study to identify major outcrops in the area in February 2017; Phase 2 was a detailed geological mapping to determine the characteristics of surface geology, geological structures and the geological boundaries in May 2018, and Phase 3 involved geophysical site investigation using vertical electrical soundings (27) in February 2019. Apart from the identification of rock types and collection of roc samples, physical properties and thicknesses of rock formations were described.

(a) Rock sample collection

A total of 69 rock samples were obtained within the study area and at 5-8 km downstream during both the reconnaissance (32 samples) and the detailed geological fieldwork (37 samples) for laboratory analysis (Figure 3.9). Two to three drops of 10% hydrochloric acid were used to identify carbonate rocks in the area. Dip directions and dip angles were measured for the Basement system rocks using Branton Compass, while their geographic locations were recorded using Garmin geographic positioning system (GPS). Field description of the rock samples was carried out with the help of hand lenses (x20 and x10), while field photographs of the outcrops were taken using GPS enabled camera (Nikon Coolpix Camera). Eastwing geological hammers were used to break down representative rock samples to desirable sizes for laboratory analysis. In total, all the 69 rock samples were marked for wholerock analysis, petrographic analysis 12 samples, while 54 rock samples were marked for major (Na, Mg, Al, P, S, K, Ca, Ti, Mn) and trace (Cr, Co, Ni, Cu, Zn, As, Se, Mo, and Pb) element analyses. The 15 rock samples excluded in the major and trace element analysis were represented in the 54 samples.

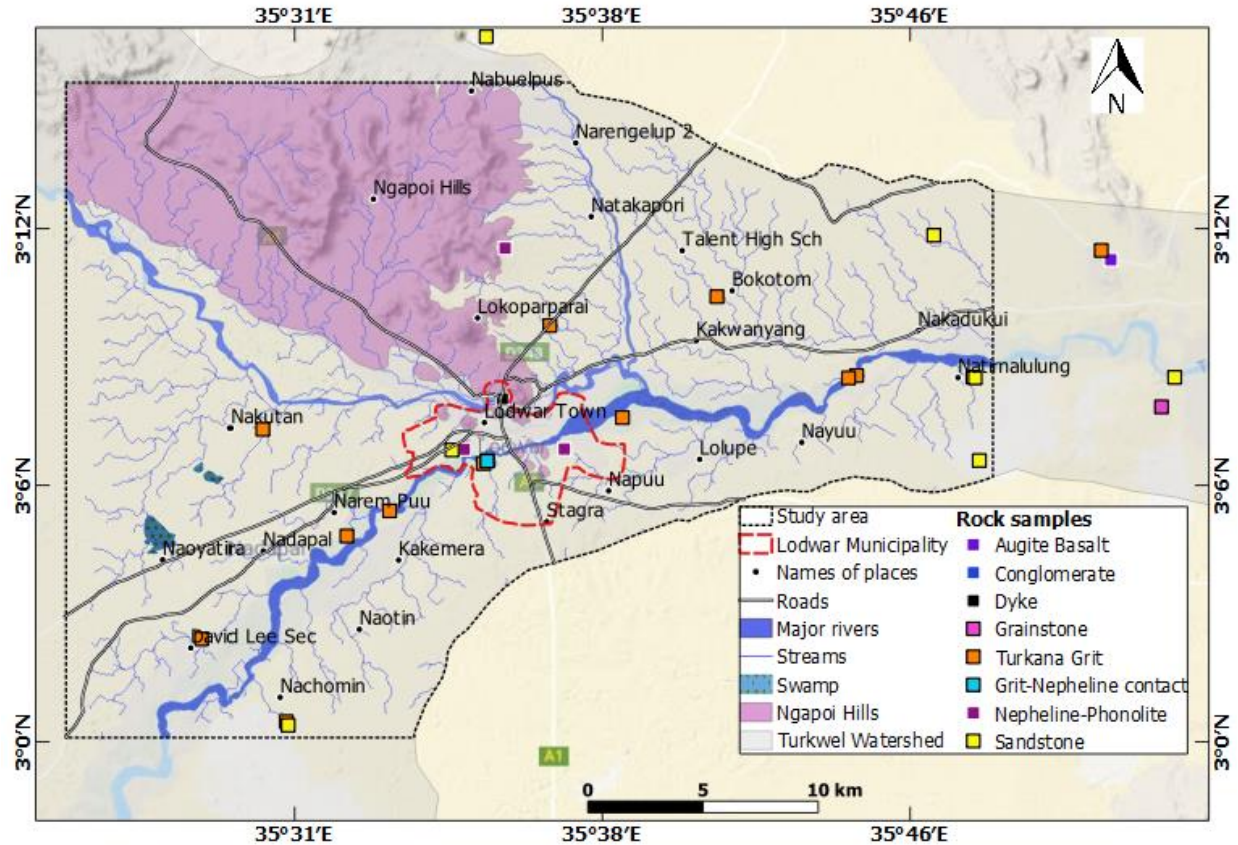


Figure 3.9: Location of rock samples collected during the geological mapping

(b) Drone Mapping

Recent technological developments in unmanned aerial systems (UAS), together with unmanned aerial vehicles (UAV) and data processing technologies, have resulted in extensive application of these techniques in a variety of fields (Török *et al.*, 2020). A number of studies have utilised drones in geoscience studies (Dandar *et al.*, 2018; Hawkins, 2016; Rocca, 2017; Török *et al.*, 2020). The purpose of drone mapping in Lodwar town was to obtain a high-resolution digital terrain model for extracting urban stream lineament. Owing to the low elevations within Lodwar (average 465 m asl), the SRTM-based DEM would not be accurate for the identification of point and non-point pollution sources.

Drone mapping was conducted within three days between 21 and 23rd February 2019, where a total of 2039 geo-tagged images were collected using a Mavic 2 Pro drone model. The camera model used was LID-20c with a focal length of 10 mm. The selected flight height was 500 m above ground level, and the drone was set at its maximum speed of 15 m/s to minimize distortion by the sandstorm in the area. The selected frontal overlap was 75%, while the side overlap was set at

70% to achieve an overall image overlap $> 70\%$ for photogrammetric analysis. In flat terrains, increasing the flight height improves the accuracy of the images. The ground sampling distance (GSD) achieved was 9 cm. The higher resolution of $< 5\text{cm}$ was not possible in the selected site due to flat terrain and strong winds mostly loaded with dust. The image pixel obtained was 5472 (width) by 3648 (height) with a horizontal and vertical resolution of 72 dpi. The images were captured along the flight paths (Figure 3.10) and in a grid-pattern (Figure 3.11).



Figure 3.10: Flight paths for the drone during the flight mission in Lodwar town overlaid on the ESRI satellite imagery

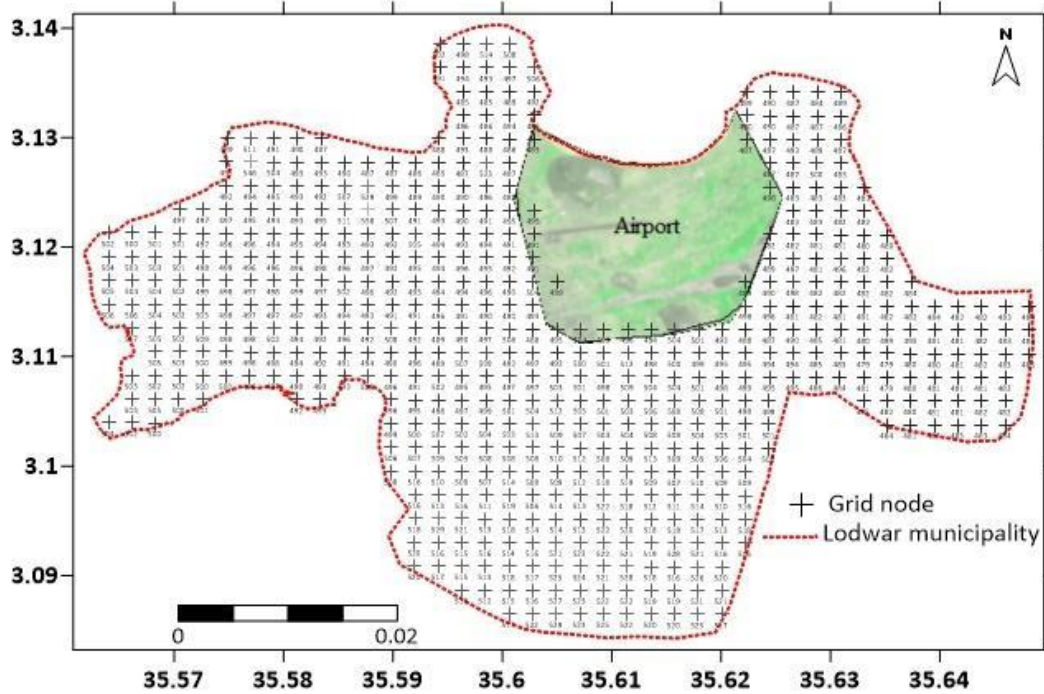


Figure 3.11: Grid pattern for the image collection points within the boundary of Lodwar town

(c) Vertical electrical sounding

A total of 26 vertical electrical soundings (VES) survey were carried out within the Lodwar Alluvial Aquifer System to unveil the nature of subsurface geology and to determine the approximate depth of the aquifer units. The Schlumberger Configuration was used, which involved passing a current through two electrodes (A and B) to the ground and calculating the potential difference (V) between the M and N potentials (Figure 3.12). The VES locations within the LAAS (Figure 3.14) were selected based on a number of factors; the spatial distribution of groundwater abstraction points, availability of sufficient space for the spread of AB line, and types of overlying geological formations. The current electrode (AB/2) spacing varied from 1 to 200 m, and the potential electrode (MN/2) spacing varied from 0.5 to 10 m (Table 3.4). Data were acquired using PASI 16 GL-N model geophysical equipment. The apparent resistance values were calculated by multiplying the resistance product by the terametre and the geometric factor, a parameter that depends on the potential and current electrode spacing. On the log-log graph, the apparent resistivity values are plotted against the half-current spacing. They were created led by the general pattern of field curves. Field data were interpreted using IPI2WIN software while the distribution

of geoelectric layers in the study area was plotted using Golden Software Surfer Version 16. Figure 3.12 shows the arrangement of the current and potential electrodes during the fieldwork.

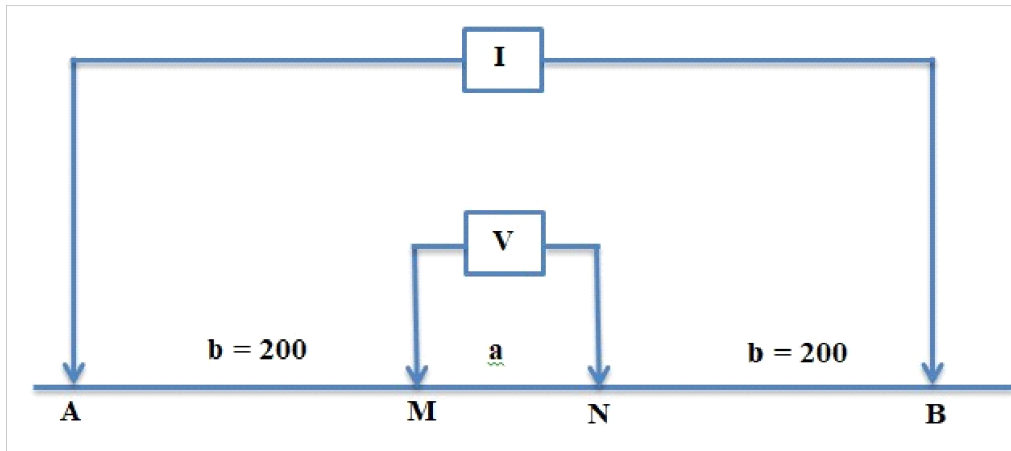


Figure 3.12: Schlumberger array configuration used in the study area

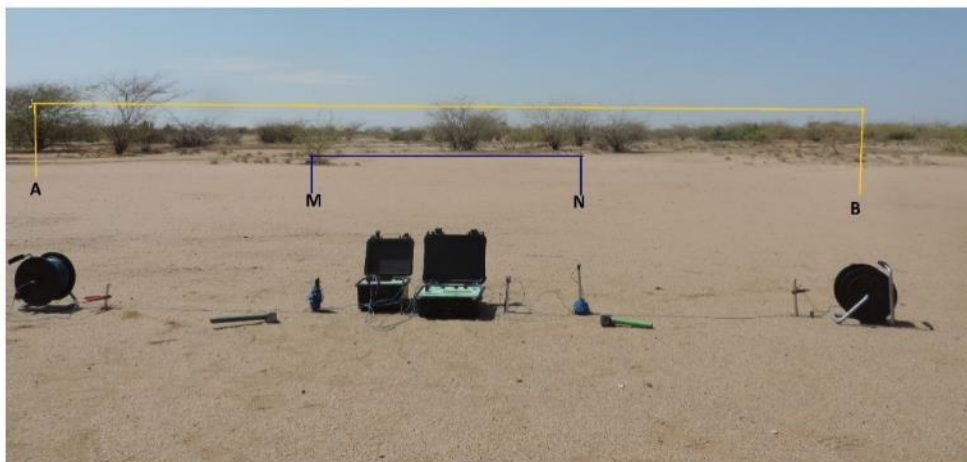


Figure 3.13: Image showing Schlumberger array configuration used during the fieldwork for the vertical electrical soundings

Table 3.4: VES orientation;(east (E), west (W), north (N), south (S), probing depth (m), elevation (m asl), and length of the AB line at each sounding location of the vertical electrical sounding (VES)

VES	Date	Elev.	Direction	AB	VES	Date	Elev.	Direction	AB
VES 1	17/02/2019	474	E_W	50	VES 15	04/03/2019	501	NE-SW	200
VES 2_3	18/02/2019	479	E_W	200	VES 16	04/03/2019	492	NE-SW	200
VES 4	18/02/2019	472	NE_SW	200	VES 17	05/03/2019	506	E-W	200
VES 5	19/02/2019	467	EW	200	VES 18	05/03/2019	506	E-W	200
VES 6	19/02/2019	476	NE_SW	200	VES 19	06/03/2019	518	E-W	200
VES 7	20/02/2019	474	NE_SW	200	VES 20	06/03/2019	502	E-W	200
VES 8	25/02/2019	470	NE_SW	200	VES 21	07/03/2019	466	E-W	200
VES 9	25/02/2019	485	E_W	200	VES 22	07/03/2019	462	E_W	200
VES 10	26/02/2019	482	E_W	200	VES 23	08/03/2019	534	E-W	200
VES 11	27/02/2019	466	E-W	200	VES 24	08/03/2019	513	E_W	200
VES 12	27/02/2019	457	E-W	200	VES 25	08/03/2019	495	E_W	200
VES 13	03/03/2019	492	N-S	200	VES 26	09/03/2019	471	E_W	200
VES 14	03/03/2019	494	NE-SW	200	VES 27	09/03/2019	469	E_W	200

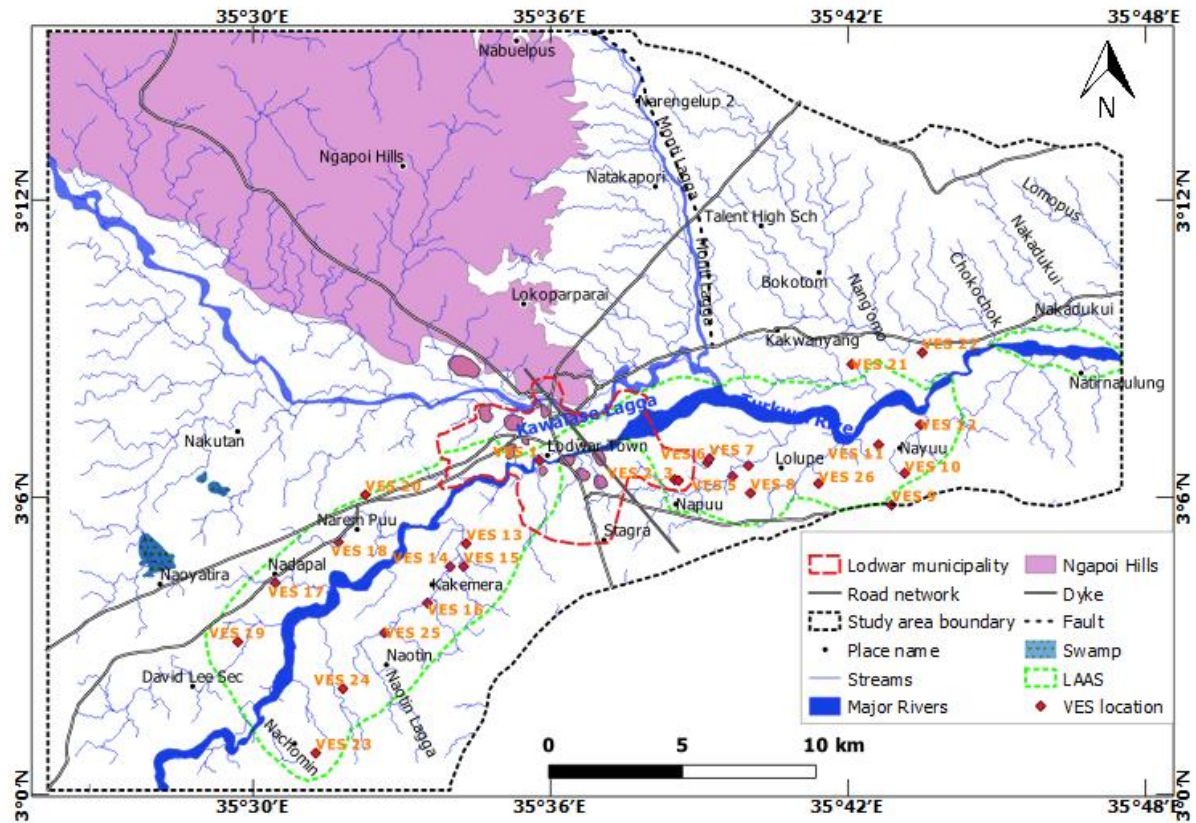


Figure 3.14: VES Locations within the Lodwar Alluvial Aquifer System

3.4.1.3 Laboratory analyses

a) Petrography

Twelve thin sections for selected rock samples were prepared at the Department of Mines and Geology, Kenya. The rock samples and the respective sample codes included; nepheline-phonolite (1650), igneous intrusions (1656 and 3845), conglomerate (3857), sandstone (1659, 3833 and 3858), Augite basalt (1651), Turkana grits (1656 and 3831) and the quartzo-feldspathic gneiss (3843 and 3844). The thin polished sections were prepared using laboratory techniques described by Grundmann and Scholz (2015). The petrographic light microscope was used for mineral identification based on colour, form and other optical properties while observing the thin sections under plane polarised light (PPL) and crossed polarised light (XPL) (Mugerwa, 2015).

b) X-Ray Fluorescence Spectrometry (XRF)

A total of 54 rock samples were analysed for major and minor trace elements at the International Council for Research in Agroforestry (ICRAF) lab using X-ray fluorescence technology. Each rock sample was assigned a specific sample code ranging from 1648-1678 to 3820-3858 for reconnaissance and detailed fieldworks, respectively. All rock samples were first crushed by the Department of Mines and Geology, Kenya, before being submitted to the ICRAF laboratory for XRF analysis. Tracer 5i and vacuum technology were used in quantitative analysis of lighter elements in rock samples using the XRF technique. The TRACER 5i is flexible with various applications and incorporates a Silicon Drift Detector (SDD), that offers high-speed data acquisition and light element sensitivity (Chacha, 2014a). The analytical procedures and quality control were in accordance with Chacha (2014). The data acquired was filtered using R Knime, and Shiny App and the filtered data in parts per million (ppm) was then uploaded into the database for analysis.

c) Atomic Absorption Spectroscopy (AAS)

The determination of major elements in rock samples was done using atomic absorption spectroscopy (AAS) at the Department of Mines and Geology, Kenya. All the 69 rock samples obtained during the reconnaissance and during the detailed fieldwork were coded (1647-3858) and submitted to Mines and Geology labs for analysis. The compounds analysed in the whole rock analysis include; SiO₂, Al₂O₃, CaO, MgO, Na₂O, K₂O, TiO₂, MnO, Fe₂O, and LOI. The concentrations of these elements are reported as a percentage (%), where the sum should be 100%.

However, acceptable totals lie between 98.5 to 101 wt.% (Alhawdar, 2014). The samples were first crushed to 4µm particle size, and about 0.1 g of the crushed rock sample and 0.6 g of LiBO₂ was used to make reagents for analysis. The determination of major rock oxides; silicon (SiO₂), aluminium (Al₂O₃), calcium (CaO), iron (Fe₂O₃), sodium Na₂O magnesium (MgO), potassium (K₂O), titanium (TiO₂) and manganese (MnO) were carried out using lithium metaborate fusion procedure designed for analysis of silicates and carbonates (Butler and Kokot, 1971). In this method, the rock samples are decomposed using lithium metaborate fusion (Butler and Kokot, 1971). Three reagents were used during the analysis; concentrated hydrochloric acid, lanthanum solution, 5% (w/v) - prepared Standard Conditions for La and Lithium metaborate (LiBO₂). The three reagents help in digestion and extraction of major elements (Belt, 1964; Potts, 1987; Suvardhan *et al.*, 2003) and to remove chemical interferences (Butler and Kokot, 1971). The detection limit for most elements is 0.1ppm (Belt, 1964). Replicate analyses determined the precision and accuracy of this method through actual separate digestions and subsequent quantification. The nitrous oxide-acetylene flame prevented inter-element interferences.

Each element weight was calculated as follows;

$$Element (wt \%) = \frac{(No. \ of \ grams \ in \ solution * (d.f) * 0.02)}{weight \ of \ the \ sample} \quad Equation \ 3-5$$

where d.f. = dilution factor

3.4.1.4 Data analysis

a) Vertical electrical sounding

The field data were interpreted using IPI2WIN software. All the 26 vertical electrical soundings field data were entered into an excel spreadsheet and later imported to the IPI2WIN software interface. At the initial opening of the data file, a graph is displayed without the resistivity cross-section (Kurniawan, 2009). The best-fitting two-layered model is selected as recommended by IPI2WIN software. The software automatically will suggest a best-fitting model for the initial interpretation of the input sounding points data (Gurugnanam *et al.*, 2009). Model editing entails changing the number of layers by splitting or joining them (to add or remove a layer) and changing the properties of the layers. The fitting error (Error = 1.92 % to 3.69) expresses the degree of uncertainty in the computed model parameters and the goodness of fit in the curve fitting algorithm

(Kurniawan, 2009). Several inversions are used to reproduce the resistivity of different layers and the corresponding thickness until the model parameters of all the VES curves are completely resolved with the fitting error (Kurniawan, 2009). The resistivity layer, log resistivity graph, resistivity depth table, and pseudo-cross-section are the results of sounding data analysis using IP2Win software, and they can all be exported in preferred file formats. The benefit of IPI2Win software is that it uses 2D cross-sections (many subsurface layers) to identify the targeted aquifer. The only shortcoming in the IP2Win software is a bug that occurs frequently when analyzing data and can be fixed by restarting the software.

b) Drone image processing

Drone-acquired images are processed using photogrammetry techniques. Several photogrammetric software exists; Burnham (2019) has evaluated the various software based on their market price, quality of products and nature of projects. Pix4D software was selected due to its robust capability to process huge number of images and the high quality of outputs (Burnham, 2019). The 2039 drone acquired images were processed using PiX4D photogrammetric software that uses Structure-from-Motion (SfM) algorithms. The SfM is a photogrammetric technique that can generate 3-dimensional (3-D) information from 2-dimensional photos. The process involves the identification of key points such as rock outcrops, trees, and fractures between overlapping images and utilizes triangulation calculations to determine the 3-D location for the set of data points (point clouds). Each point within the point cloud has unique coordinates (latitude, longitude, and elevation) that allow for post GIS analysis and interpretation. The outputs from the drone-acquired images include high-resolution orthomosaics (geometrically corrected for distortions), a high-resolution digital terrain model, and a textured 3-D mesh. The workflow and outputs of image processing using the Pix4D software are shown in Figure 3.15.

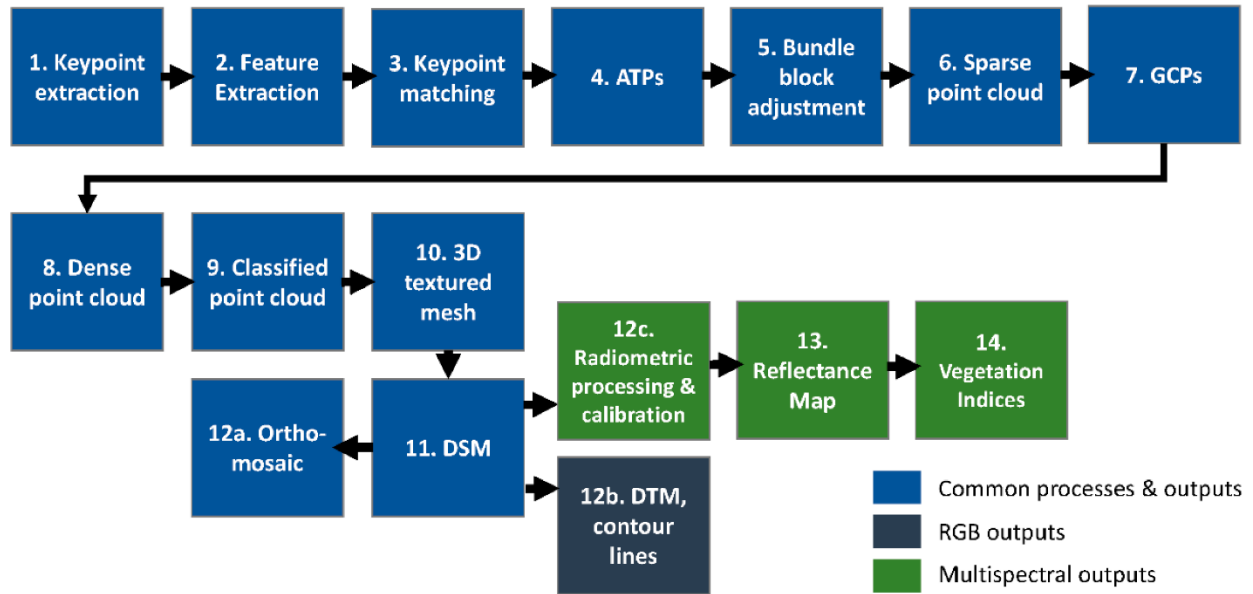


Figure 3.15: Workflow for processing drone-acquired images using Pix4D photogrammetric software (Hawkins, 2016)

c) Determination of aquifer characteristics

The aquifer characteristics determined are outlined below.

(i) Porosity

Porosity is expressed as;

$$Pososity (n) = \frac{V_v}{V} \quad \text{Equation 3-6}$$

Where V_v is the volume of voids in a porous medium, while V is the total volume of the porous medium

Generally, consolidated materials have lower porosities than unconsolidated materials – gravels, sands, and silts with angular and rounded particles have lower porosities as compared to clay. Besides, the poorly sorted sub-surface materials have lower porosities than well-sorted sub-surface deposits.

(ii) Specific yield

The specific yield (S_y) expressed as;

$$S_y = \frac{V_d}{V} \quad \text{Equation 3-7}$$

Where, V_d is the volume of water drained by gravity, and V is the total volume of the porous medium. Porosity can be linked to specific yield by;

$$n = S_y + S_r \quad \text{Equation 3-8}$$

Where n = porosity, S_y = specific yield and S_r = specific retention

Specific yield is dimensionless and often depends on the grain size, distribution and shape of pores, subsurface compaction, and duration of drainage. Due to compaction processes, the value of S_y decreases with depth. Typical porosity values and specific yield for different geological materials are given in Table 6 (Brassington, 2010).

Table 3.5: Representative values of porosity and specific yield for different geological materials (Brassington, 2010)

No	Type of Geological Material	Porosity (%)	Specific Yield (%)
1	Medium Gravel	32.00	24.00
2	Fine Gravel	34.00	25.00
3	Coarse Sand	39.00	27.00
4	Medium Sand	39.00	28.00
5	Fine Sand	43.00	23.00
6	Silt	46.00	8.00
7	Clay	42.00	3.00
8	Fine-grained Sandstone	33.00	21.00
9	Medium-grained Sandstone	37.00	27.00
10	Limestone	30.00	14.00
11	Dune Sand	45.00	38.00
12	Loess	49.00	18.00
13	Peat	92.00	44.00
14	Schist	38.00	26.00
15	Siltstone	35.00	12.00
16	Till (mainly Sand)	31.00	16.00
17	Till (mainly Silt)	34.00	6.00
18	Tuff	41.00	21.00

(iii) Storage coefficient and specific storage

Storage coefficient is a dimensionless property of an aquifer is expressed as;

$$S = S_s + b \quad \text{Equation 3-9}$$

Where S_s = specific storage and b = thickness of the aquifer material.

The specific storage is a dimension of $[L^{-1}]$ and is expressed as;

$$S_s = \rho_w g (\alpha + n\beta) = \gamma_w (\alpha + n\beta) \quad \text{Equation 3-10}$$

Where ρ_w denotes the density of water; α denotes compressibility of the aquifer material and (is equal to $\frac{1}{E_s}$, Wherein E_s is the bulk modulus of elasticity of aquifer skeleton); β = compressibility of water and (is equal to $1/K_w$, wherein K_w is the bulk modulus of elasticity of water), n = porosity of the aquifer material, and γ_w refers to the unit weight of water. Therefore, the specific storage is the most crucial aquifer parameter depending on the type of aquifer material, the amount of water contained in the aquifer, and the overburden stress. The value of K_w is $2.1 \times 10^9 \text{ N/m}^2$, while the E_s values for selected geological materials are shown in Table 3.4 (Raghunath, 2007).

Since the storage coefficient (S) of an aquifer is a function of aquifer thickness and is different for every location. The storage coefficient (S) of an aquifer can be expressed as;

$$S = \gamma_w (\alpha + n\beta) \times b \quad \text{Equation 3-11}$$

The study of Mook (2000) determined the values of S for confined and unconfined aquifers. The value of S in the confined aquifer ranged from 5×10^{-5} to 5×10^{-3} indicating substantial pressure changes over extensive areas required for sufficient yields (Mook, 2000). The storage coefficient (S) of unconfined aquifers, on the other hand, was equal to the effective porosity because most of the groundwater is released by a declining unconfined (free) water table because of gravitational drainage. S ranges from 0.15 to 0.25 in unconfined aquifers of alluvial sediments, which is much higher than in confined aquifers (Mook, 2000).

(iv) Transmissivity (T)

Transmissivity of an aquifer is expressed as;

$$T = Kb \text{ (m}^2\text{/day)} \quad \text{Equation 3-12}$$

Where T = transmissivity, K = hydraulic conductivity, b = saturated aquifer thickness

(v) Hydraulic Conductivity

In Darcy's law, hydraulic conductivity (K) acts as a constant of proportionality relating the specific discharge of a porous medium under hydraulic gradient expressed as;

$$v = -Ki \quad \text{Equation 3-13}$$

Where v = specific discharge, K = hydraulic conductivity and i = is hydraulic gradient.

Table 3.6: Typical values of hydraulic conductivity in various geological materials

No.	Materials	Hydraulic Conductivity (m/s)	
		Min	Ma x
1	Fine Sand	2.0×10^{-7}	2.0×10^{-4}
2	Medium Sand	9.0×10^{-7}	5.0×10^{-4}
3	Coarse Sand	9.0×10^{-7}	6.0×10^{-3}
4	Sand; Clean; Good Aquifer	1.0×10^{-5}	1.0×10^{-2}
5	Sand/Gravelly Sand; Poorly Graded; Little to No Fines	2.5×10^{-5}	5.3×10^{-4}
6	Sand/Gravelly Sand; Well Graded; Little to No Fines	1.0×10^{-8}	1.0×10^{-6}
7	Silty Sand	1.0×10^{-8}	5.0×10^{-6}
8	Clayey Sand	5.5×10^{-9}	5.5×10^{-6}
9	Alluvial Gravel/Sand	4.0×10^{-4}	4.0×10^{-3}
10	Sand/Gravel; Uniform	4.0×10^{-3}	4.0×10^{-1}
11	Sand/Gravel; Well Graded; No fines	4.0×10^{-5}	4.0×10^{-3}
12	Gravel	3.0×10^{-4}	3.0×10^{-2}
13	Silty Gravel/Silty Sandy Gravel	5.0×10^{-8}	5.0×10^{-6}
14	Silt; Compacted	7.0×10^{-10}	7.0×10^{-8}
15	Clay	1.0×10^{-11}	4.7×10^{-9}
16	Limestone / Dolomite	1.0×10^{-9}	6.0×10^{-6}
17	Sandstone	3.0×10^{-10}	6.0×10^{-6}
18	Siltstone	1.0×10^{-11}	1.4×10^{-8}
19	Anhydrite	4.0×10^{-13}	2.0×10^{-8}
20	Permeable Basalt	4.0×10^{-7}	2.0×10^{-2}
21	Igneous/Metamorphic Rock; Fractured	8.0×10^{-9}	3.0×10^{-4}
22	Basalt	2.0×10^{-11}	4.2×10^{-7}
23	Igneous/Metamorphic Rock; Unfractured	3.0×10^{-14}	2.0×10^{-10}

3.4.2 *Hydrogeochemistry and Aquifer Susceptibility to Pollution*

Methods described herein are for investigation of the hydrogeochemistry of the LAAS and its susceptibility to pollution. Each method and the fieldwork procedures are presented, and the analytical rationale is provided in Appendix 3-2

3.4.2.1 *Desktop studies*

Secondary data on water quality were very limited. Available data was collected from Water Resources Authority (WRA) for the period 2015 and 2017 for five boreholes (LOWASCO Bh, Nakwameki Bh, Kakemera Bh, Napuu Church, and Napuu Mission) and one Turkwel River sample. The datasets contained the following parameters: electrical conductivity, pH, total suspended solutes, turbidity, total dissolved solids, total hardness, total alkalinity (EC), iron (Fe^{2+}), manganese (Mn^{2+}), magnesium (Mg^{2+}), calcium (Ca^{2+}), fluoride, chloride (Cl^-), sulphate (SO_4^{2-}), Nitrite (NO_2^-) and nitrate (NO_3^-). From the desk study review, it was clear that understanding of water quality and hydrogeochemistry of the LAAS required a detailed water sampling framework that included water sampling from every possible groundwater source as well as seasonal water quality monitoring of selected wells.

3.4.2.2 *Fieldwork*

Seasonal water sampling was carried out in the study area as follows; in the dry season of February 2018 water samples collected included; seven samples of the Turkwel River, ten borehole samples and two handpump samples. May 2018 was the wet season in the area, and extensive water point mapping and groundwater sampling were conducted. As a result, a total of 137 groundwater sources were established in the region (53 boreholes, 84 handpumps). Of these, only 94 water points (53 handpumps and 41 boreholes) were sampled, an equivalent of 68.61 per cent. The rest 47 (31 Hps and 16 Bhs), were not sampled because they were either dry, vandalized, or were non-operational at the time of the survey. In the subsequent dry season, February 2019, a total of 58 groundwater samples (27 boreholes and 31 handpumps) of the previous 94 set were collected. Figure 15 shows the location of the surface water and groundwater samples (Figure 3.16). Duplicate samples were collected from each sampling site for cation and anion determinations, respectively, as well as for isotope analysis. As sampling containers, clean polythene 500 mL bottles with air-tight caps were used, and each bottle was cleaned with deionized water before sampling. To preserve the cation samples, three drops of analytical grade % nitric acid were used.

Before being placed in a cool box for transport to Nairobi, the bottles were labeled and refrigerated at 4 °C in the laboratory. The pH, Electrical conductivity, and temperature were measured in the field using hand-held Combo Tester HI98129 for all the water samples. EC was measured in the groundwater samples and expressed in milliSiemens per centimetre ($\mu\text{S}/\text{cm}$).

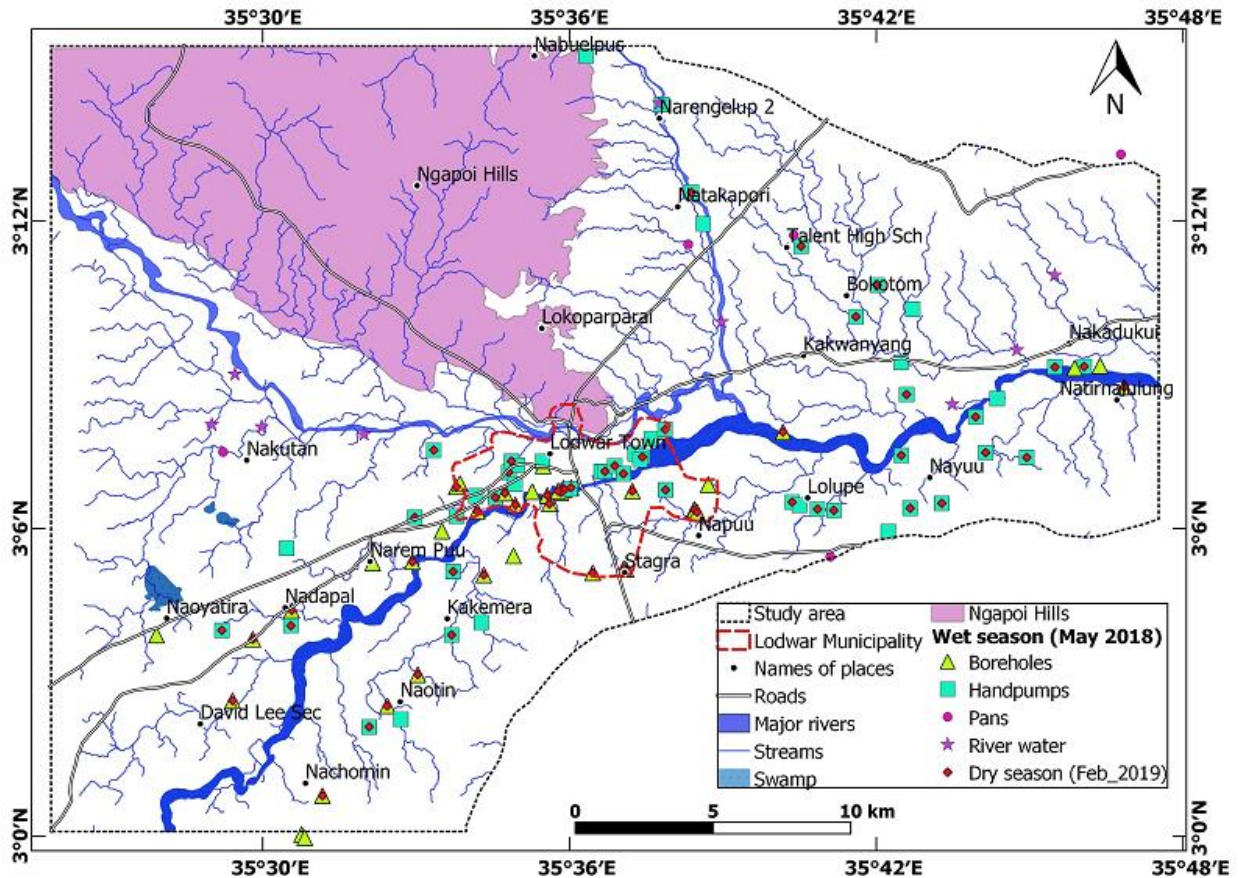


Figure 3.16: Surface water and groundwater sources in the mid-Turkwel River watershed

3.4.2.3 Laboratory analysis of water samples

All the samples were submitted to the Water Resources Authority Central Lab for full chemical analyses. The laboratory analyses were based on standard analytical procedures (APHA, 1985). The measured parameters include; pH, turbidity, total hardness, total alkalinity, EC, Ca, Mg, Na, K, Fe, Mn, Cl, F, NO_3 , NO_2 , HCO_3 , SO_4 , and CO_3 . The standard laboratory tests for the various parameters are discussed below.

Turbidity was determined using a turbidimeter MRC model in nephelometric turbidity units (NTU), where 5 NTU is the guideline value established by both WHO (2011) and KEBS (2014). Hardness was determined using the titrimetric method that measures the calcium and magnesium

ions, and the results were expressed in CaCO_3/l . The guideline value provided by WHO for total hardness in natural portable water is 500 mg/L, while that of KEBS is 600 mg/L. The WHO guideline value of 500 mg/L was used for drinking water evaluation since it is lower than that of KEBS. Total alkalinity was measured using the titrimetric method. The guideline value of 500 mg/L established by both WHO (2011) and KEBS (2014) was used to evaluate the total alkalinity in groundwater.

The major cations analysed were sodium, potassium, calcium, magnesium, iron, and manganese, using standard analytical procedures based on APHA (1995). Sodium and potassium were determined using the Jenway PFP7 photometer standard flame photometric method. The results were expressed in mg/L, and the guideline values of 200 mg/L (sodium) and 50 mg/L (potassium) were used to evaluate their concentrations in groundwater. Calcium and magnesium were determined using titrimetric methods, where the calculation method was used to determine magnesium concentration. The results were expressed in mg/L, and a guideline value of 100 mg/L established by WHO (2011) for calcium and magnesium was used to evaluate the drinking water quality. In this case, the guideline value of 150 mg/L defined by KEBS (2014) for calcium was ignored. The iron was determined using a colorimetric method, while the manganese was determined using the Jenway Calorimeter 6051 and the Phenanthroline Perusulfate method. The persulfate method is the most used colorimetric method for measuring manganese because the use of mercuric ion controls interference from a constrained chloride ion concentration. The measurements were in milligrams per litre, with a guideline value of 0.3 mg/L for Fe^{2+} and 0.1 mg/L for Mn^{2+} used for drinking water evaluation.

Chloride was measured using the argentometric method, and this method is often used in relatively clear waters and when 0.15 to 10 mg of Cl^- is present in the portion titrated. Fluoride was determined using the ion-selective electrode method using a Jenway 3345 model using Ion Meter. The results for both chloride and fluoride were expressed in mg/L. The WHO and KEBS have established guideline values of 250 mg/L for Cl^- and 1.5 mg/L for F^- and were used to evaluate the drinking water quality. Nitrate was determined using the UV spectrophotometric method by utilizing UVmini 1240 Shimadzu spectrophotometer. Nitrite was, on the other hand, determined using the colorimetric method using the Jenway Calorimeter 6051 model. The results for both nitrate and nitrite were expressed as mg/L ($\text{NO}_3\text{-N}$) and mg/L ($\text{NO}_2\text{-N}$), respectively. The WHO and KEBS guideline value for NO_3^- in drinking water is 10 mg/L ($\text{NO}_3\text{-N}$). The WHO guideline

value for NO_2^- is 0.1 mg/L ($\text{NO}_2\text{-N}$) while that of KEBS is 0.003 mg/L ($\text{NO}_2\text{-N}$). For nitrite, the WHO (2011) guideline value was used for drinking water evaluation since it is also used by the United States Environmental Protection Agency (EPA, 2018). Sulphate was determined using the turbidimetric method, and the results were expressed in mg/L while the free carbon dioxide was measured using the trimetric method, and the results were also expressed in mg/L. The WHO (2011) guideline value for SO_4^{2-} is 450 mg/L while that of KEBS (2014) is 400 mg/L, and the KEBS value was used for drinking water evaluation. No guideline value has been provided for free carbon dioxide.

3.4.2.4 Data analysis

a) Data validation

Validation of the chemical data obtained from the Central Laboratory of the Water Resources Authority was carried out by calculating the charge balance of all surface water and groundwater samples. Charge balance determination involved four key stages, where all the calculations were carried out in an Excel spreadsheet.

Step 1: The concentration of each cation and anions were divided by their respective atomic masses and molecular masses to obtain the milli-equivalents. The cations tested were Ca^{2+} , Mg^{2+} , Na^+ , K^+ , Fe^{2+} , and Mn^{2+} , while the anions were HCO_3^- , CO_3 , SO_4^{2-} , Cl^- , F^- , NO_2^- and NO_3^- .

The atomic masses and oxidation states used for cations and anions are shown in Table 3.7.

Table 3.7: Atomic masses and oxidation states of cations and anions tested

cations	Atomic mass	oxidation state	Anions	Molecular mass	Oxidation state
Ca	40.00	2	HCO_3	61.02	-1
Mg	24.30	2	CO_3	60.00	-2
Na	23.00	1	SO_4	96.00	-2
K	39.00	1	Cl	35.50	-1
Fe	55.80	2	F	19.00	-1
Mn	54.90	2	NO_3	62.00	-1

Step 2: The mEq calculation was determined for cations and anions by multiplying the result in step 1 above with the respective valence electrons or the oxidation state.

Step 3: Total cations and total anions were determined in Excel by obtaining the sum of cations and anions from step 2 above.

Step 4: The overall charge balance was determined using the equation:

$$\text{Charge balance} = \frac{(\Sigma\text{cations}-\Sigma\text{anions})}{(\Sigma\text{cations}+\Sigma\text{anions})} * 100 \quad \text{Equation 3-14}$$

Generally, accepted limits of experimental error are a charge balance of $\pm 5\%$ (Huh *et al.*, 1998), and the excess charge is attributed to unanalysed organic acid anions or the analysed cations and anions present in the water sample. According to Huh *et al.* (1998), the causes of charge imbalance include: laboratory error, missed sampling procedure, use of unfiltered water samples and the number of parameters measured. Unfiltered water samples may contain particulate matter that dissolves into the sample when an acid preservative is added. Following the charge balance determination, the chemical data were then used to evaluate the drinking water quality, seasonal water quality variation, identification of hydrochemical facies, and determining the aquifer hydrogeochemistry.

b) Determination of drinking water quality

Field and Laboratory results for all physico-chemical parameters were compared against the guideline values provided by WHO (2011) and KEBS (2014). Based on WHO (2011), each country should use its own standards for drinking water following public health policies and practices. In this study, KEBS guideline values were used whenever the value was similar or lower than that of the WHO, whereas the guideline values of the WHO (2011) were applied in case of higher KEBS values (2014) like in the case of calcium.

c) Water quality index determination

Samples were assessed for 13 physicochemical parameters that included pH, EC, Ca^{2+} , Mg^{2+} , Na^+ , K^+ , Fe^{2+} , Mn^{2+} , HCO_3^- , SO_4^{2-} , Cl^- , F^- , and NO_3^- to assess the suitability of groundwater for drinking and determine the degree of aquifer contamination. The water quality index was determined using Equation 3-10 above for the Weight Arithmetic water quality index (WQI). Rating weights (w_i) ranging from one to five were assigned to the selected parameters based on their overall influence on water quality (Ravikumar *et al.*, 2013; Kumari *et al.*, 2014; Boah *et al.*, 2015). Table 3.8 below shows the rating weights and unit weights assigned to each parameter to calculate the water quality index. Water quality index results of the study are then expressed in terms of excellent quality (0-

25), good quality (26-50), poor quality (51-75), very poor quality (76-100), unsuitable for drinking (WQI > 100). A spatial map was then plotted using Surfer software from the resultant water quality indices to yield water quality index map for the study area.

Table 3.8: The rating weights (w_i) and unit weight (W_i) assigned to the water quality parameters

Parameter	WHO/KEBS	Rating (w_i)	Unit weight (W_i)
pH	8.5	4	0.098
EC	1500	4	0.098
Ca	100	2	0.049
Mg	100	2	0.049
Na	200	3	0.073
K	50	1	0.024
Fe	0.3	3	0.073
Mn	0.1	5	0.122
HCO ₃	500	3	0.073
SO ₄	400	3	0.073
Cl	250	3	0.073
F	1.5	5	0.122
NO ₃	10	3	0.073
n=13		$\sum w_i = 41$	$\sum W_i = 1.001$

The primary goal of water quality monitoring is to determine suitability for a specific use. The water quality index (WQI) is a mathematical tool used to convert large amounts of water quality data into a single number that represents the level of water quality (Ravikumar *et al.*, 2013; Sharma and Chhipa, 2016). Generating WQI in a specific area is a critical step in land use planning and sustainable water resource management (Kumar and James, 2013; Stambuk-Giljanovic, 1999; Yidana *et al.*, 2010). The water quality index is widely regarded as the most effective tool for communicating water quality trends to the public and policymakers (Kumari *et al.*, 2014). A water quality index condenses large amounts of water quality data into simple terms such as excellent, suitable, or unsuitable for drinking (Boah *et al.*, 2015). The weighted arithmetic index method was used to calculate the water quality index (WQI), which reflects the influence of water quality parameters on overall water quality (Ravikumar *et al.*, 2015).

The WQI is calculated as follows;

$$WQI = \frac{\sum_{i=1}^n qiwi}{\sum_{i=1}^n wi} \quad \text{Equation 3-15}$$

Where,

q_i = quality rating of each water quality parameter

w_i = unit weight if each water quality parameter.

In order to calculate the WQI, each of the 15 selected parameters was assigned weights (w_i) ranging from 1-5 based on their relative importance in overall drinking water quality (Boah *et al.*, 2015; Sharma and Chhipa, 2016; Javadi *et al.*, 2017; Faye *et al.*, 2019). Secondly, the relative weight (W_i) of each parameter was calculated using the equation;

$$W_i = \frac{w_i}{\sum_{i=1}^n w_i} \quad \text{Equation 3-16}$$

where,

W_i = relative weight

w_i = weight of each parameter and

n = is the number of parameters

Thirdly, the quality rating q_i was obtained by dividing the observed concentration of parameter in each sample by the respective standard based on KEBS guidelines using the equation:

$$q_i = \left(\frac{C_i}{S_i} \right) * 100 \quad \text{Equation 3-17}$$

Where,

q_i = quality rating

C_i = observed concentration of each parameter

S_i = KEBS drinking water standard for each physico-chemical parameter

For calculating the WQI, the water quality sub-index (SI) was first determined for each chemical parameter by:

$$SI = w_i * q_i \quad \text{Equation 3-18}$$

Finally, the WQI was determined as follows;

$$WQI = \sum SI_{1-n} \quad \text{Equation 3-19}$$

The water samples were then rated based WQI calculation (Richards, 1954; Boah *et al.*, 2015; Sharma and Chhipa, 2016) in Table 3.9.

Table 3.9: Water quality rating based on WQI

WQI	Water Quality Rating
0-25	Excellent
26-50	Good
51-75	Poor
76-100	Very poor
>100	Unsuitable for drinking

d) Spatial maps

Spatial maps for physico-chemical parameters were prepared for the study area using Golden Software Surfer V16, where the Kriging method was applied for gridding. When estimating values in unknown areas, kriging is a geostatistical interpolation technique that takes both distance and degree of variation between known data points into account (Wackernagel, 2013) and thus, considered the most accurate gridding method for most datasets.

e) Determination of hydrochemical facies

There are numerous graphical methods for representing water chemistry and hydrochemical facies (Giménez-Forcada, 2010). Triangle diagrams depict concentrations of major cations and anions as a percentage meq/L of total anions and cations, with a point representing different chemical compositions assigned to different positions in each triangle (Ghoraba and Khan, 2013; Glover *et al.*, 2012). The majority of the hydrochemical studies use piper trilinear diagrams (Glover *et al.*, 2012; Kumar, 2013; Lokhande and Mujawar, 2016; Ravikumar *et al.*, 2015) to represent the groundwater facies. The Piper diagram's limitation is that a single point not only represents unique facies, but the point also takes on the corresponding interpretation (Giménez-Forcada, 2010).

According to Giménez-Forcada (2010), the representation of two ions in the same field of the Piper diagram implies a similar behaviour of both water types and reinforces the value of a parameter in the interpretation of a process.

The hydrochemical facies of the groundwater and surface water samples were determined using Piper trilinear diagram (Kumar, 2013). The sample plots fall in different areas in these diagrams, characterising the different facies (Afzali *et al.*, 2015; Glover *et al.*, 2012). The anions and cations are expressed in Meq/L in the Piper plot. Anions are plotted in the left triangle, while cations are plotted as a single plot in the right triangle. The tri-linear diagram's central diamond-shaped area is a projection of these two plots (Ghaffar *et al.*, 2017) (Ghaffar *et al.*, 2017). Groundwater charts can more effectively express similarities and differences in groundwater samples because similar qualities of samples are plotted together to form groups (Abdelshafy *et al.*, 2019).

f) Rock-water interactions

(i) Mineral saturation indices

The geochemical modelling tools used to calculate saturation indices of water include WATEQF, SOLMNEQ, and PHREEQC (Haile-Meskale, 2017). This study used the PHREEQC tool to evaluate the groundwater of the area. The saturation indexes were determined on the groundwater samples of the study area utilizing the PHREEQC – hydrogeochemical equilibrium model for windows (Haile-Meskale, 2017).

The mineral saturation index helps to determine the equilibrium state of water for a mineral phase using analytical data (Aghazadeh *et al.*, 2017; Garrels and Berner, 1983). Changes in the saturation state are used to identify the geochemical reactions controlling the water chemistry and to differentiate between different stages of hydrochemical evolution (Aghazadeh *et al.*, 2017; Al-Ruwaih, 2017). The saturation index (SI) is given by (Garrels and Mackenzie 1967);

$$SI = \text{Log} \frac{IAP}{KT} \quad \text{Equation 3-20}$$

Where IAP indicates the ion activity product of the dissociated chemical species in solution, and KT denotes the chemical's equilibrium solubility product at the sample temperature (Garrels and Mackenzie 1967).

As saturation indices, positive and negative saturation indices can be obtained (Zaheeruddin and Khurshid, 2004). Positive SI indicates that the groundwater is oversaturated for a specific mineral, unable to dissolve more of the mineral, whereas negative SI indicates that the groundwater is under-saturated for a specific mineral (Aghazadeh et al., 2017; Al-Ruwaih, 2017). SI values close to zero indicate that groundwater and the mineral are in equilibrium. Groundwater discharged from an aquifer containing a sufficient amount of the mineral with sufficient resident time to reach equilibrium results in zero index values (Aghazadeh et al., 2017).

(ii) Principal component analysis (PCA) and Cluster hierarchical analysis (HCA)

Multivariate statistical techniques are widely used to evaluate groundwater chemistry and to determine prevailing aquifer processes (Dash *et al.*, 2018; Abdullahi *et al.*, 2014; Islam *et al.*, 2017). Principal Component Analysis (PCA) and Hierarchical Cluster Analysis (HCA) are the most used statistical methods for determining the most important contributing parameters that decide the geochemistry of groundwater samples (Li *et al.*, 2018). PCA is useful for identifying correlated variables as well as the process and grouping of types of water quality (Mrklas *et al.*, 2006; Wu *et al.*, 2015). HCA, on the other hand, groups similar observations together to reveal different chemical characteristics of the various groups of groundwater samples (Dash *et al.*, 2018; Abdullahi *et al.*, 2014; Islam *et al.*, 2017). Statistical Package for Social Sciences (SPSS) and Microsoft Excel Add-in, XLSTAT, are the widely used software for PCA and HCA analytical tools (Dash *et al.*, 2018; Douglas, 2015; Abdullahi *et al.*, 2014).

Both PCA and HCA were applied to the 94 groundwater samples from boreholes (41), and handpumps (53) collected in the wet season (May 2018), and 58 samples collected in the dry season. The physico-chemical parameters for all samples were; pH, EC, TDS, Ca, Mg, Na, K, Fe, Mn, HCO₃, CO₃, SO₄, Cl, F, NO₃. PCA and HCA were performed on groundwater samples using group average clustering and Euclidean distance methods based on dissimilarities (Islam *et al.*, 2017; Ravikumar and Somashekar, 2015). The extraction methods of varimax rotation and Keiser normalization were applied in the PCA to interpret the geochemical data (Ravikumar and Somashekar, 2015) and the resultant Principal Components (PCs) with eigenvalues >1 was retained (Cattell and Jaspers 1967 Ravikumar and Somashekar, 2015; Islam *et al.*, 2017). In the case of HCA, Ward's linkage clustering method was used for distance computing (Glover *et al.*, 2012; Li *et al.*, 2018), which is considered more accurate than, complete linkage, single linkage,

and average linkage methods (Li *et al.*, 2018). Ward's method employs the nearest-neighbour chain algorithm to determine the best merging cluster pair that produces the most distinct signature for hydrogeochemical clusters in water samples (Li *et al.*, 2018). Using discriminant function analysis, the significance of seasonal variations in water chemistry was determined.

g) Identification of point and non-point pollution sources

Point sources of pollution refer to the discharge of contaminants into the groundwater through a pipe, ditch, discrete fissure, tunnels, concentrated animal feed, and municipal wastewater (Abdullahi *et al.*, 2014; Islam *et al.*, 2017) while nonpoint sources may result from agricultural chemicals (fertilizers and pesticides) through surface runoff, precipitation, atmospheric deposition, seepage, drainage, or hydrological modification (Islam *et al.*, 2017). Sound management of non-point sources of pollution groundwater requires a thorough scientific understanding of these sources and the linkages between nonpoint sources and groundwater discharges to users or affected well and streams (Lathamani *et al.*, 2015). The likely point sources within the study area include; on-site septic systems, municipal wastes, and industrial chemicals, while the potential non-point sources may include upstream use of agricultural chemicals. The concentration of nitrates and sulphates in groundwater are used to indicate point and non-point pollution sources, respectively (Bruthans *et al.*, 2019; Gardner and Vogel, 2005; Miljević *et al.*, 2012).

To identify the point and non-point pollution sources, the water quality index map of the area was also overlaid on the DEM to evaluate the potential areas of point pollution sources. The drone-acquired digital terrain model (DEM), with a resolution of 1.26 m for the Lodwar municipality, was used to extract the stream lineament within the municipal boundary. It was also used to determine possible dispersal routes of non-point sources facilitated by stream channels. Heat maps of SO₄ and NO₃ in boreholes and handpumps were overlaid on DEM for the Lodwar municipality to identify whether they originated from the point or non-point sources and to establish the extent of anthropogenic pollution. Boreholes and handpumps located on one or more streams are likely to bear non-point source pollution while those located away from stream lineament are polluted by point sources (Barilari *et al.*, 2020).

3.4.3 *Rainfall-Surface Water-Groundwater Interactions and Groundwater Recharge*

3.4.3.1 *Desktop studies*

Two boreholes with short-term groundwater monitoring data, LOWASCO Bh 9 (December 2017 to September 2018) and Napuu Bh (December 2017 to April 2018) were available to apply the water table fluctuation method. A literature review was carried out of rainfall-surface water-groundwater interactions and recharges, with particular attention paid to alluvial and volcano-sedimentary systems analogous to reports of governmental organizations such as the county government of Turkana, National Drought Management Authority (NDMA) that report on drought events and climate trends were also reviewed. Fieldwork

Ninety-one groundwater samples (handpumps = 53 and boreholes =38), eight scoop hole samples from major laggas (Nakutan, Kawalase, Monti, Nakadukui and Chokchok), four Turkwel River samples and one from Kawalase River, two Lake Turkana samples (at Eliye springs and Turkwel delta); five water pan samples (four within the study area and one from the Kerio watershed), one spring sample and a rain sample were collected. The Turkwel River samples, the lake samples, and the spring sample were collected in February 2018. The water samples collected in May 2018 included all the 91 groundwater samples, the rain samples, scoop hole samples, water pans samples, and Kawalase river samples. All the samples were preserved at 4°C acid and later transported to a commercial laboratory, Elemtex Limited (UK), for analysis. Table 3.10 shows the types and number of samples collected, while Figure 3.17 shows the distribution of surface water and groundwater samples in the study area.

Table 3.10: Samples submitted for stable isotope analysis at Elemtex lab, United Kingdom

No	Sample type	Number of samples tested for ¹⁸O	Number of samples tested for ²H	Number of samples tested for ³H
1	Rain	1	1	1
2	Turkwel River	5	5	1
3	Kawalase River	1	1	0
4	Scoop Holes	4	4	0
5	Water pans	5	5	0
6	Handpumps	52	52	26
7	Boreholes	38	38	13
8	Spring	1	1	0
9	Lake	2	2	2
Total		110	110	43

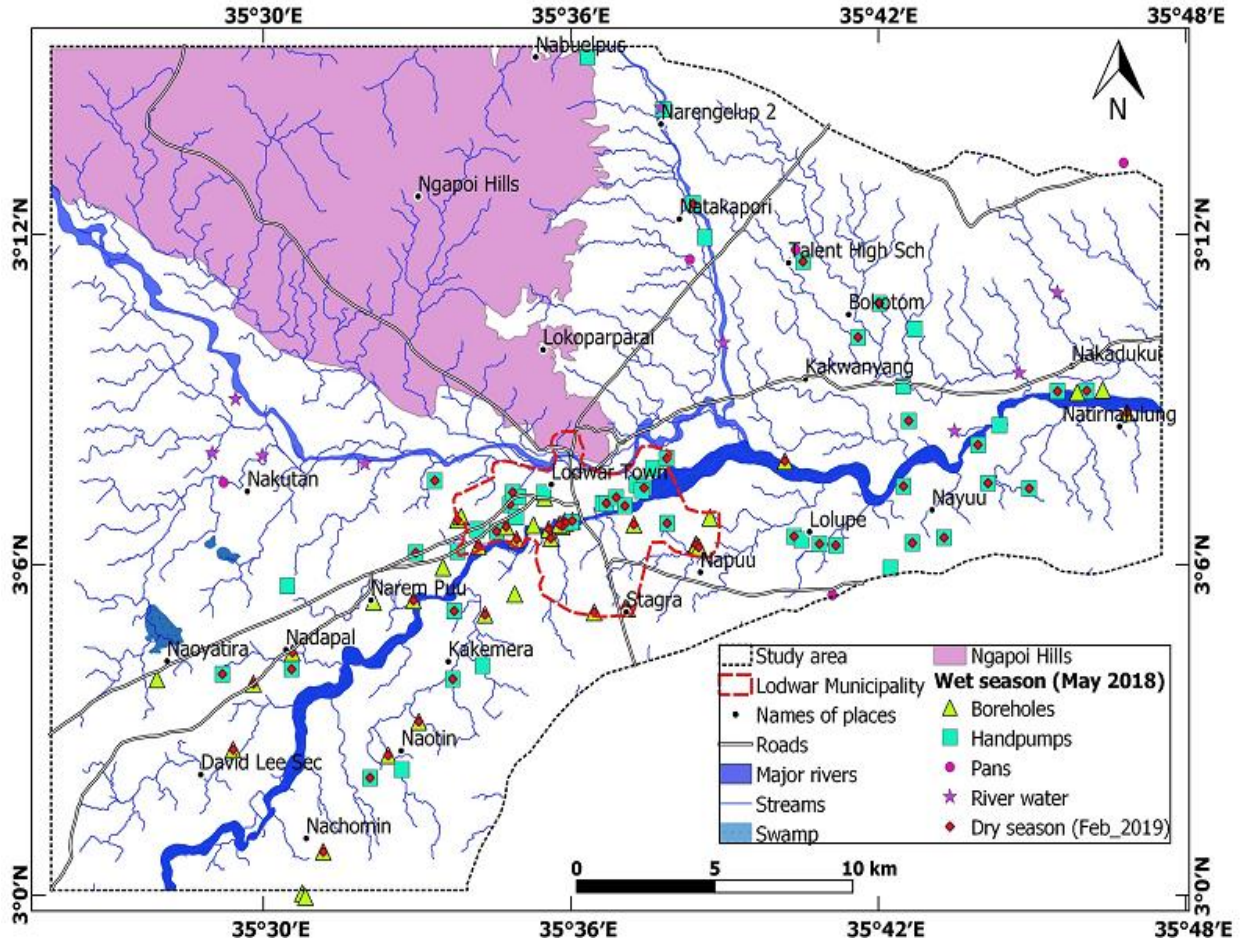


Figure 3.17: Distribution of surface water and groundwater isotope samples within the mid-Turkwel watershed

3.4.3.2 Laboratory analyses

a) Oxygen and Deuterium Measurements

The measurement of hydrogen (^2H) and oxygen (^{18}O) isotope ratios in water samples was done using an isotope ratio mass spectrometer (IRMS) combined with a high-temperature conversion elemental analyser (TC/EA) operated in continuous flow (CF) mode. The isothermal chromatography, which is part of TC/EA, separates the reaction gasses and these gasses are admitted to the IRMS via the ConFlo IV universal interface, where oxygen and hydrogen gases are converted to CO and H₂ respectively (Yeh and Lee, 2018). The ConFlo IV allows for automatic sample gas dilution and generation of reference gas pulses, enabling for the individual referencing of each sample gas peak (Carter and Barwick, 2011; Yeh and Lee, 2018) (Figure 3.18).

Standard CO₂ with known $\delta^{18}\text{O}$ values were reacted with the water samples during pre-treatment for two hours to achieve an equilibrium. Excess water was removed by freezing and purification, where the CO₂ produced was collected in a glass tube. The IRMS was utilized to evaluate the isotopic oxygen compositions of water samples that had attained equilibrium with oxygen in the CO₂. The hydrogen was extracted using zinc granules to produce H₂, where 200 mL of zinc granules were weighed, and a capillary tube was then used to remove 4 μL of the water sample. Both the zinc granules and the water sample were sealed in a 6.35 mm vacuum Pyrex specimen and placed in a 1400 °C oven for 30 minutes to allow for the water sample to completely react with zinc to produce H₂ by reduction process (Carter and Barwick, 2011). The specimen tube was then placed in the IRMS equipment to quantify the hydrogen isotopic composition. For quality control, five samples were injected at a time, and the normalization followed the requirements of FIRMS IRMS guide v2 (Carter and Barwick, 2011). The isotope ratios were expressed as $\delta^2\text{H}$ and $\delta^{18}\text{O}$ values relative to the Vienna Standard Mean Ocean Water (VSMOW) reference materials where $\delta\text{D} = 0 \text{ ‰}$ and $\delta^{18}\text{O} = 0 \text{ ‰}$ (Carter and Barwick, 2011). In this study, the analytical reproducibility was ± 0.1 for the oxygen and ± 1.0 for deuterium.

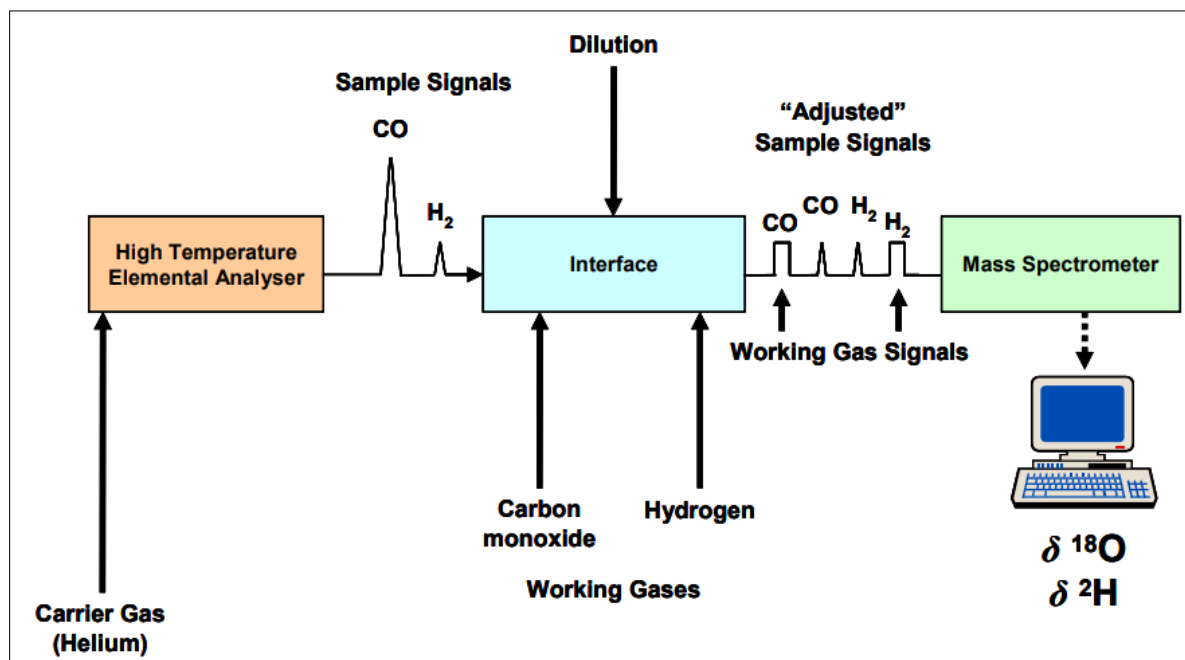


Figure 3.18: Simple schematic diagram of TC/EA-IRMS for determination of $\delta^2\text{H}$ and $\delta^{18}\text{O}$

b) Tritium measurement

Tritium analysis was carried for 43 water samples consisting of 26 handpumps, 13 boreholes, two lake samples, and one sample each for rainfall and Turkwel river samples. Tritium was measured by a liquid scintillation counter (LSC) (Motzer, 2007) by counting β^- decay events. A 10 ml sample of distilled and electrolytically enriched water was mixed with the scintillation compound, which emits a photon when struck by a β^- particle. Using Spectrometer 1220 Quantulus equipment, photomultiplier tubes in the scintillation counter convert photons to electrical pulses that are counted over 90-minute intervals of six cycles (Moore, 2011). The count obtained was compared to calibrated standards and blanks to calculate the results. Increased precision was obtained by electrolytic enrichment of ^3H in water prior to counting. Direct liquid scintillation counting carries an accuracy of ± 8 TU, but with enrichment and LSC, this is improved to ± 0.8 TU (Singh *et al.*, 2016). Propane synthesis was carried out to improve the analytical precision to ± 0.1 TU (Moore, 2011).

3.4.3.3 Data analysis

a) Recharge estimation using ^2H and ^{18}O isotopes

The oxygen and hydrogen isotopic compositions of precipitation and groundwater can be used to assess groundwater recharge mechanisms (Adomako *et al.*, 2010; Yeh *et al.*, 2014). In this study, the isotopes for the groundwater samples were also compared to that of the surface water in the area. The Global Network of Isotopes in Precipitation (GNIP) provides long term d-excess data across the globe, which is used to characterize the evolution of water through the hydrologic cycle (Bershaw *et al.*, 2018). The GNIP data were download from <https://nucleus.iaea.org>, three GNIP monitoring stations within the proximity of the study area; Moyale, Kericho, and Soroti (Uganda). Kericho station had a total of 19 observations, Soroti had 14, and Moyale station had only four observations. Kericho and Soroti GNIP stations are in high altitude regions while the Moyale station is in a low altitude region, thus, exhibiting varying isotopic compositions in the rainfall.

The Global Meteoric Water Line (GMWL) was produced for each of the three stations using the equation $\delta\text{D} = 8 * \delta^{18}\text{O} + 10$ (Craig, 1961). The Local Meteoric Water Lines (LMWL) for each station was plotted based on the relationship between isotopic compositions of hydrogen and oxygen in precipitation (Oiro *et al.*, 2018). The GMWL based on Crag's model and the trend line

analysis of the LMWL was used as the reference for the stable groundwater isotopes of the study area. By associating the analysed stable isotopes with the derived relationships from the GMWL and LMWL equations, it is possible to understand the processes affecting isotopic compositions during precipitation and recharge. A linear trend line of the $\delta^{18}\text{O}$ and $\delta^2\text{H}$ can be extended to intercept the meteoric water line (MWL), and the point of interception indicates the amount of monthly rainfall required before recharge occurs (Xu and Beekman, 2003). In the MWL, the slope represents the ratio between temperature and $\delta^2\text{H}$ and $\delta^{18}\text{O}$ when condensation occurs, while the value of the intercept (d-excess) is based on the evaporative conditions in the water source origin (Yeh *et al.*, 2014). Spatial maps with the distribution of $\delta^{18}\text{O}$ and $\delta^2\text{H}$ isotopes for the surface water and groundwater samples were generated to determine potential groundwater recharge zones.

b) Recharge estimation using water table fluctuation method (WTF)

Although the water table fluctuation method is recommended for small areas with limited groundwater data, the available water table measurements in the study area were too scarce for successful application in the study area. For successful utilization of the water table fluctuation (WTF) method, there is a need to ensure that the observed water table fluctuations are a result of recharge rather than changes in atmospheric pressure, anthropogenic effects, or entrapped air (Hussein and Broder 2014). The recharge is calculated by: -

$$R (t_{1-}) = s_y * \Delta H(t_{1-}) \quad \text{Equation 3-21}$$

Where $R (t_1)$ (measured in cm) is the recharge between times t_0 and t_1 , S_y (dimensionless) is the specific yield, while $\Delta H (t_1)$ is the peak water level rise for the period (cm). The S_y is calculated by subtracting the porosity (n) from the specific retention (S_r) (Brears and Post, 2014).

$$s_y = n - s_r \quad \text{Equation 3-22}$$

The major limitation of the WTF method is that the inflow and outflow to/from groundwater, as well as the specific capacity, are usually unknown (Xu and Beekman, 2003; Brears and Post, 2014). Besides, long term time-series for rainfall and groundwater monitoring are required.

c) Age of groundwater

The age of groundwater was estimated qualitatively by comparing tritium levels in water samples against the recharge period outline by (Clark and Fritz, 1997). The qualitative approach indicates whether the groundwater; was recharged before the 1950s (< 0.8TU), is a mixture of sub-modern and modern water (0.8 to 4 TU), comprise modern water recharged <5 to 10 years (5 to 15 TU) was recharged in 1990s to <1990s (15 to 30 TU) (Atwood, 2013; Zhao *et al.*, 2018), recharged in the 1960s to 1970s (> 30 TU) or recharged in the 1950s to 1960s (>50 TU).

The quantitative age of groundwater was also calculated using the equation;

$${}^3H_t = {}^3H_0 \ln e^{-\lambda t} \quad \text{Equation 3-23}$$

Where 3H_t is the measured tritium after decay, 3H_0 is the initial tritium value usually 1 TU before the 1950s, λ is the decay constant for tritium given by $\ln 2$ divided by half-life $t_{1/2}$. Using tritium's half-life, $t_{1/2} = 12.43$. Thus, the above equation can be rephrased as:

$$t = -17.77 * \ln \frac{{}^3H_t}{{}^3H_0} \quad \text{Equation 3-24}$$

Where t is the age of groundwater in years

3.4.4 Development of aquifer conceptual model

A conceptual model of the aquifer geometry is the representation of the hydrogeological units and the flow characteristics of a groundwater system. The primary objective of developing a conceptual aquifer model is to simplify the field problem and organize the associated groundwater datasets so that the system can be more easily be understood (Anderson and Woessner, 1992). The development of an aquifer model requires data inputs such as transmissivity, conductivity, storativity, and specific yield of the individual aquifer unit. Due to a lack of drill core data within the selected area, electrical resistivity data (VES), digital terrain model, and assessment of depth and yields of the wells, hydrogeochemistry and isotope data were used to determine the geometry of the LAAS. This study was focused on the shallow aquifer and the vertical electrical soundings interpretation provided information about the depth and thickness of the aquifer at some specific points. The digital terrain model was used to delineate the surface topography of the aquifer, while the depth data obtained from the secondary data was used to prepare a depth-to-aquifer contour

map. A combination of methods; hydrogeology, aquifer geochemistry and knowledge of surface water-groundwater interactions were used to depict the geometry and to develop its conceptual model.

CHAPTER FOUR: RESULTS AND DISCUSSION

4.1 Introduction

This chapter consists of four parts; section 4.1 outlines the layout of the chapter, while section 4.2 presents the results obtained from desk studies, field data collection and laboratory results and analyses for all the research techniques used for each of the three specific objectives, section 4.3 comprises the discussion, and section 4.4 provides a summary of the chapter. Section 4.2 is further divided as follows; section 4.2.1 presents results for geological field mapping, petrography, rock geochemistry, borehole data analysis and geophysics; section 4.2.2 provide results for water quality, hydrogeochemistry and vulnerability to pollution, section 4.2.3 gives the results for water table fluctuation and isotope analysis, while section 4.2.4 presents the conceptual aquifer model for the Lodwar Alluvial aquifer System (LAAS).

4.2 Results

4.2.1 Hydrogeological *characteristics of the LAAS*

4.2.1.1 *Geological field mapping*

(a) Surface Geology

The surface geology of the study area comprises; Basement System rocks (quartzo-feldspathic gneiss), sedimentary rocks (Turkana grits, sandstones, and Quaternary to Holocene sediments), Paleogene and Neogene volcanics (augite basalts and nepheline-phonolites) and recent alluvial deposits (Figure 4.1).

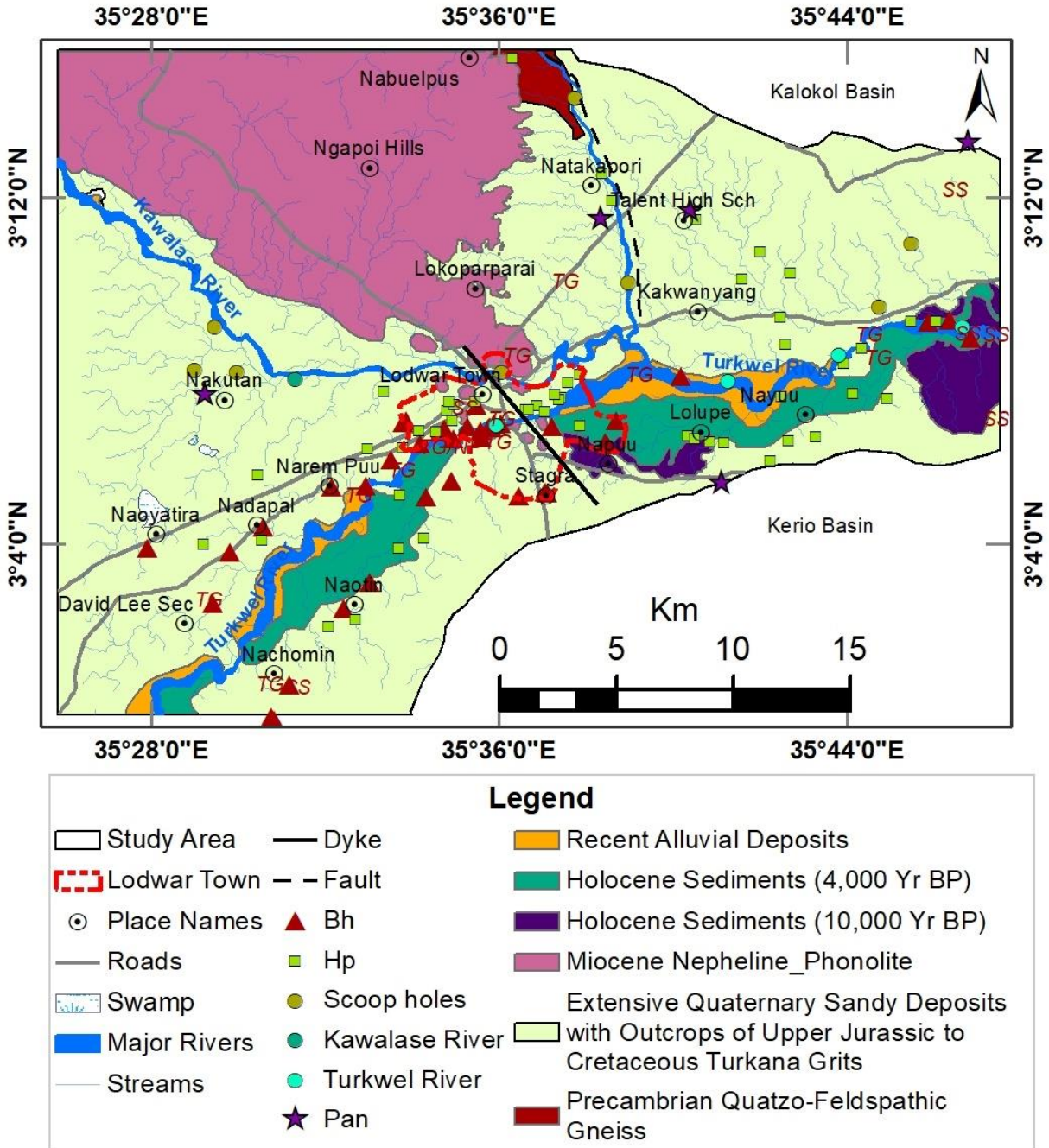


Figure 4.1: Geological map of the area showing the distribution groundwater abstraction sources in Lodwar town and its environs

(i) Precambrian Quartzo-feldspathic Gneiss

The Precambrian quartzo-feldspathic gneiss is the oldest geological formation the study area and is exposed in the north-eastern section of Ngapoi Hills (Figure 4.4). Its exposure is limited by the convergence of basaltic rocks and the Turkana grits in the area that resulted in high deformation.

The immense folding and faulting of the quartzo-feldspathic gneiss made it challenging to measure its dip angles accurately and strike directions. However, the general dip direction of this formation was determined to be NW-SE. The quartzo-feldspathic gneisses were highly fractured, resulting in fragmentation, transportation and deposition of quartzite boulders and feldspars minerals in the Monti lagga to the Katapakori areas. The exposed thickness on this formation along the Monti lagga is 3 m. Intrusions in these rocks were observed and caused the deformation and mineral alterations.

(ii) Upper Jurassic to Cretaceous Turkana grits

The Turkana grits are mainly coarse-grained, sandstone-derived basement deposited on a dissected basement topography by aggrading river systems. The outcrops of this formation were observed at a few locations within the extensive Quaternary sands cover. The 'Turkana Grits' are covered by Palaeogene volcanic rocks (35 Ma), which are thought to be the earliest evidence of plume-related volcanism inside the East African Rift System (Agyemang *et al.*, 2019). The grits encountered had current and fluting features indicating their deposition in a deltaic environment with flood washings (Rhemtulla, 1970). Around Nawaitorong areas, the Turkana grit is cemented by calcite (Figure 4.2a). North-east of the municipality of Lodwar, on the eastern slope of the Ngapoi Hills, the exposed grits consist of light grey-brown sandy clay covered by pebbly grit (Figure 4.2b) while at Lorengelup areas, the Turkana grits overlie the Basement System. The Turkana grits at Naotin is intercalated with a sandstone unit (Figure 4.2c) with graded bedding features (Figure 4.2d). Extensive Quaternary sands derived from the Basement System rocks and wind-blown sands cover the Turkana grits (Olago, 2018). The observed current features suggest localized sediment input by alluvial fans (Agyemang *et al.*, 2019). In most parts of the study area, this formation was covered by the Quaternary sands and ranged from 0.3 to 1.0 meters where it was exposed.



Figure 4.2: Exposures of Turkana Grit (a) calcite-cemented grit at Naiwaitorong area, (b) an exposure of the Turkana grit formation, (c) grits at Naotin intercalated with a sandstone unit, and (d) grit showing graded bedding (Field Photo May, 2018)

(iii) Palaeogene volcanic rocks

The Paleogene and Neogene volcanics in the study area are mainly nephelinites and phonolites (nepheline-phonolites) that comprise the Ngapoi Hills and the volcanic cones that form ridges within Lodwar Municipality. South of the Ngapoi Hills, the nepheline-phonolites overlie the Turkana grits (Walsh, and Dodson, 1969) and contain patches of pebbles derived from the grits. These rocks were observed to rest directly on the Turkana grits around Lodwar town and overlie basaltic rocks at Nabuelpus area. Augite basalts were observed to occur in patches North of Ngapoi Hills and were not mapped as a geological unit within the study area. The outcrops observed within Lodwar town range from 1.0 to 4.5 m thickness. However, cone-shaped hills > 20 m comprises this formation.

(iv) Holocene sediments

The Holocene sediments cover the southern bank of the Turkwel River with thicknesses ranging from 2 to 7.5 m (Figure 4.3a, b), and they extended into the Napuu and Nayuu areas which are between 5 and 8 km away from the river. The intermittent exposures of the Holocene sediments and Turkana grits suggest that they have been deposited on former synclines. Besides, the existence of folding features in the area is likely evidenced by widening and thinning of the Turkwel River, where the soft Holocene sediments are exposed in the broad sections while the hard Turkana grits occur in the constricted sections of the river banks. These sediments bear erosional features as observed at Nayuu areas (Figure 4.3c, d), and form undulating landforms. Particle sizes ranged from fine sand to medium gravel, and graded bedding was commonly observed.



Figure 4.3: Exposed Holocene sediments illustrating thick deposits and erosional features at Napuu-Nayuu areas, Turkana county

(v) Alluvial deposits

The alluvial deposits are considered the youngest geological formation in the study area and are of recent age. They comprise fine sands, silts, clay, and gravels broken down from weathered volcanic rocks and wind-blown sands. The thickness of the alluvial deposits within the Turkwel and Kawalase rivers and Monti lagga ranged from 0.3 m to 1.5 m. In particular, the alluvial deposits in the Turkwel River are extensive, especially to the east of the municipality of Lodwar. A thin layer of alluvial deposits (<1 m thick) is found within the Kawalase River. However, these deposits were found to be thicker at the confluence of the Kawalase River and the Monti lagga.

(b) Geological structures

Volcanic dykes and erosional surfaces were the major geological structures and features identified in the study area. According to Hughes (1933), the Turkana grits are punctuated by dykes from volcanic activity between Lodwar and Lokitaung areas. In the study area, a dolerite dyke dissecting Lodwar town with a 45° NW trend was mapped for the first time. The dyke is exposed within the Turkana grits at Kawalase lagga next to the drift road crossing. A dyke with similar orientation and mineralogical composition was encountered in the northern part of the area near the Nabuelpus area. These dolerite dykes appear to follow the NW-SE trending plane of weakness and have been eroded more than the host Turkana Grits, forming linear trenches as observed by Rhemtulla (1970). At Nabulon area next to the Turkwel River, a contact zone between the nepheline-phonolites and the Turkana grits, with a 35 NE trend, was identified. A thin layer of conglomerate rock capped the Turkana grit.

4.2.1.2 Remote sensing - Digital Terrain Model

(a) Satellite Imagery - STRM-based digital terrain model

The STRM of the study area indicated that the altitude ranges from 440 to 920 m above sea level. High elevations are around the Ngapoi Hills ranging from 560 to 920 m asl. The Turkwel River basin in the study area lies at altitudes < 520 m asl while the Kawalase occurs at altitudes ranging between 470 to 530 m asl (Figure 4.4).

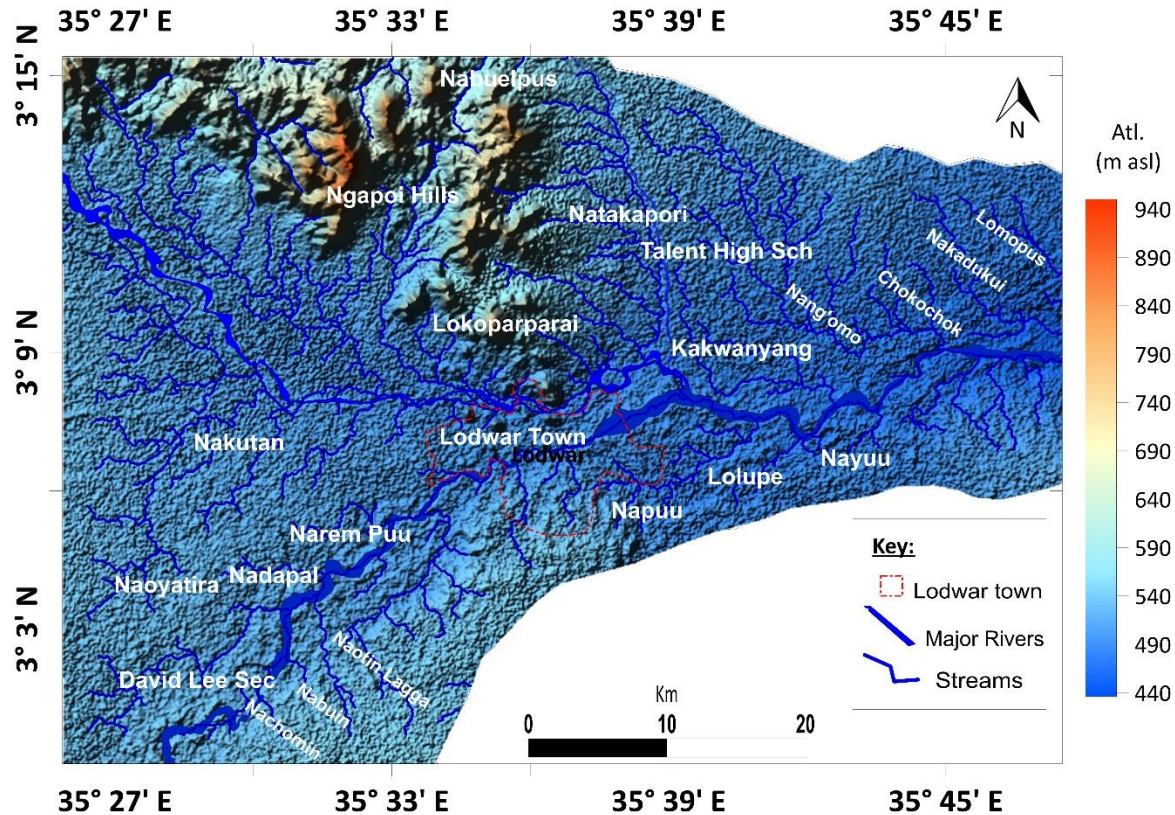


Figure 4.4: STRM of the study area within the Turkwel River watershed

(b) Stream lineament analysis

The STRM of the study area was used to delineate the watershed and to automatically generate the stream network in the study area using a cell threshold of 700. The pre-digitized layers of the Turkwel and Kawalase rivers were uploaded onto the watershed map to extract the river pour-points and intersections (Figure 4.5). The results showed that the Kawalase River has multiple streams flowing between 470 and 530 m asl on a fairly flat surface. It has also been found that all the streams that contribute to the Monti lagga are situated in the western part of this river, forming parallel drainage systems. The streams occur between linear series of escarpments that form parallel, elongate landforms due to resistant Miocene volcanics outcropping east of Ngapoi Hills. According to Boulton and Whittaker (2009) straight rivers fed by parallel streams flowing in the same directions are typically located in a fault line. This phenomenon deduce that the Monti Lagga is flowing on a fault. The streams which enter the Turkwel River directly within the study area drain elevation areas ranging from 440 to 520 m asl. The remaining streams that drain the eastern and northeastern parts occur at altitudes <500 m asl.

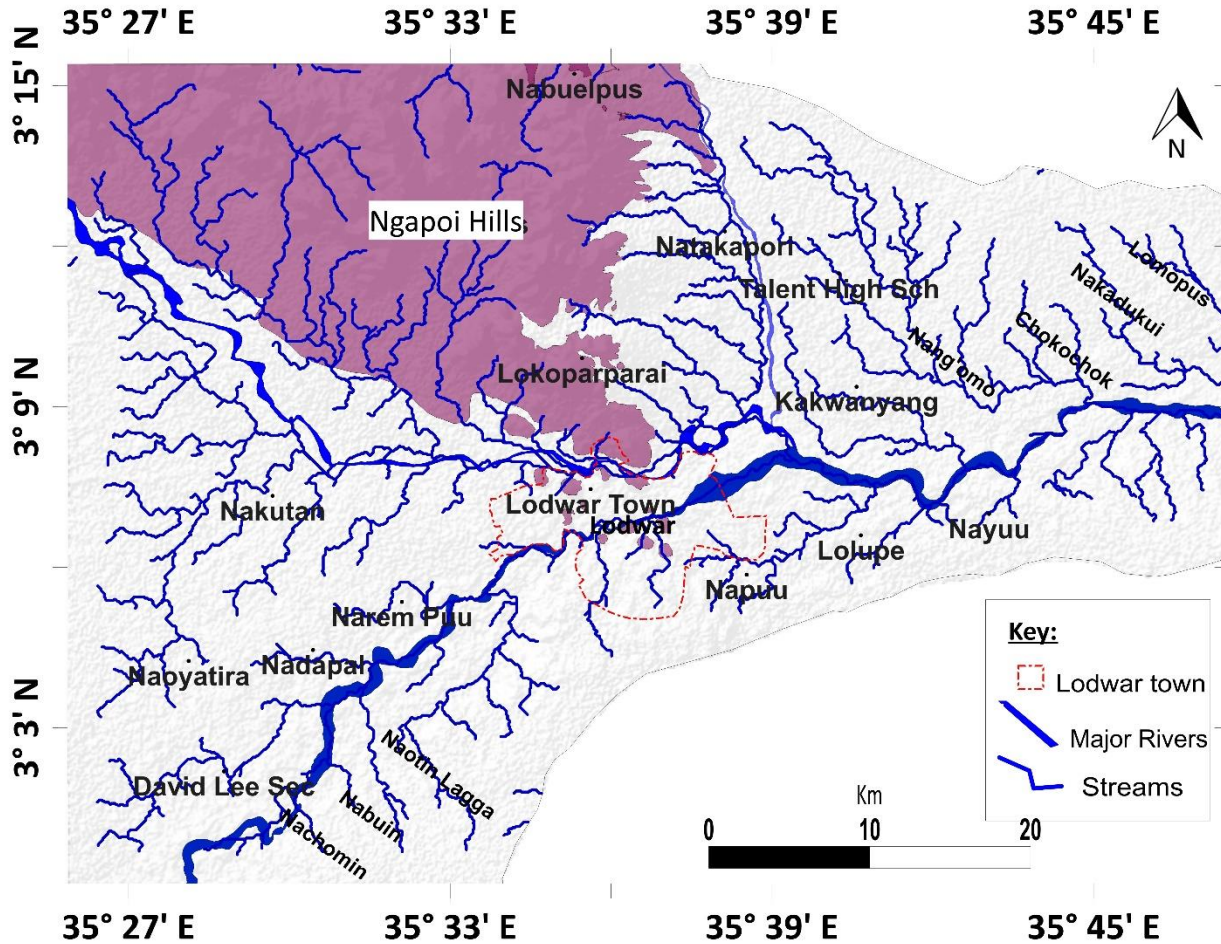


Figure 4.5: Drainage lineaments map of the area extracted from the STRM-based DEM

(c) Analysis of drone-acquired images

(i) Drone-based digital terrain model (DEM)

The analysis of drone acquired images provided a high-resolution digital terrain model of Lodwar town showing elevations ranging from 460 to 598 m asl with the Lodwar Hill recording the highest elevations (Figure 4.6). Generally, Kanamkemer area has high elevations between <460 and 560 m asl while the Nawaitorong, Napuu and some parts of California and Napetet areas recorded low elevations of < 480 m asl. The DEM revealed the cone-like volcanic features in Lodwar town as well as the outline of the Turkwel River. Lodwar airport's lack of drone images is a significant limitation to the analysis using drone mapping.

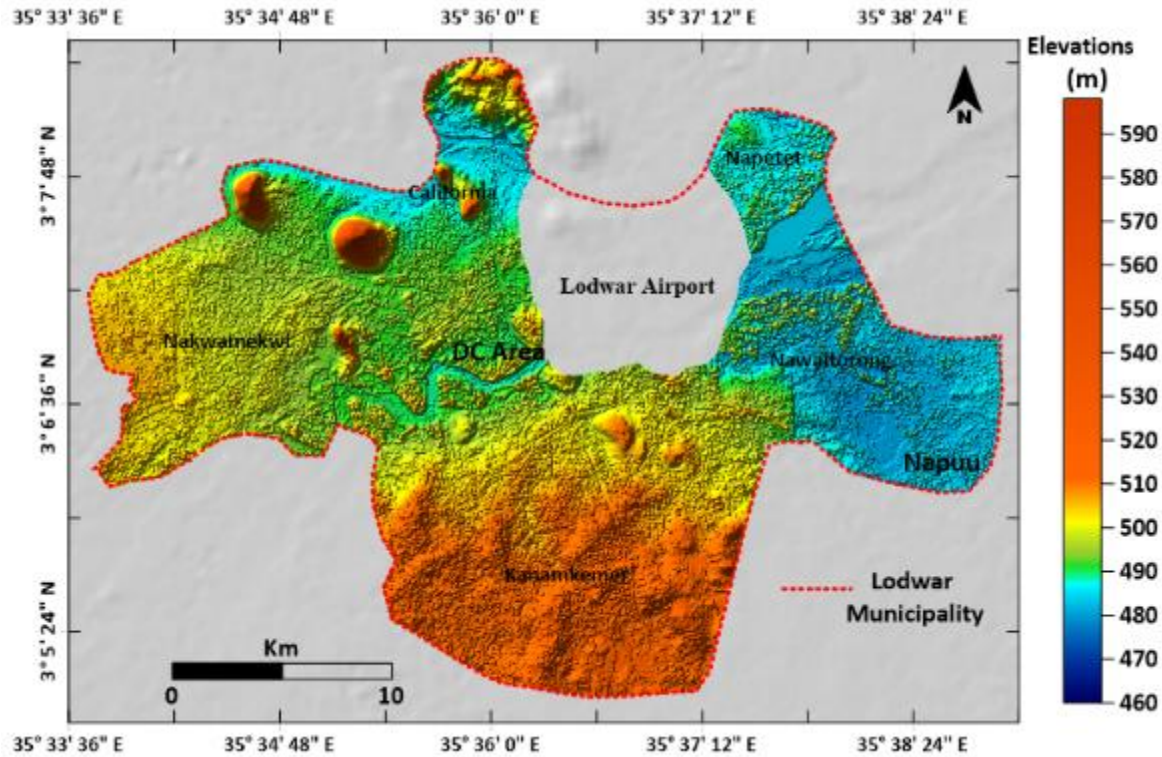


Figure 4.6: Digital terrain model of Lodwar town produced from drone-acquired images that excluding the airport section

(ii) Contour map

The contour map was used to depict elevations above sea level, revealing the shape of the landforms in Lodwar town. The five-meter spacing contour map (Figure 4.7) revealed that the floodplains are located at elevations < 465 m and comprise mainly the Turkwel River basin, Nawaitorong, and Napuu areas, and consist primarily the alluvial deposits. Holocene sediments cover the areas with elevations ranging from between 465 and 495 m asl while the Quaternary wind-blown sandy deposits occur within 495 to 510 m asl. Turkana grits outcrops in areas occur at elevations ranging between 515 to 520 m asl while the volcanic rocks occupy areas with altitudes > 525 m asl.

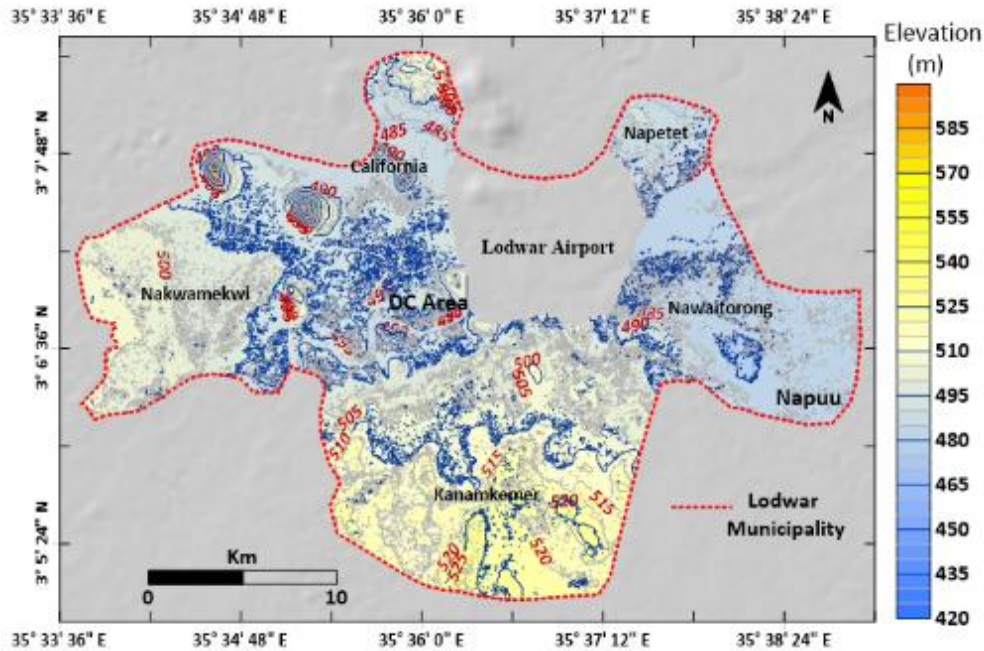


Figure 4.7: Five-meter contour map of Lodwar town obtained from the drone-acquired images

(iii) Comparison of drone-based and STRM based DEM

Drone-based and STRM based DEM were analysed and compared within Lodwar town (Figure 4.8). The designated Survey of Kenya (SOK) datum point of Lodwar town located at 3° 07' N and 35° 36' E is 477 m and was used to determine the accuracy of the heights of the two digital elevation models at the same point. The drone-based and STRM based slope angles were also compared (Table 4.1).

Table 4.1: Comparison of STRM-based and drone-based digital elevation models and slope angle maps

Remote sensing product	Drone-based DEM	STRM-based DEM
(i) Digital terrain model	<ul style="list-style-type: none"> - Min and Max elevation (460 and 598 m asl) - Elevation at datum point = 476 m - Close accuracy (-1m) from the SOK datum 	<ul style="list-style-type: none"> - Min and Max elevation (480 and 595 m asl) - Elevation at datum point (492 m) - Wide gap (+12 m) from the SOK datum point
(ii) Slope angle map	<ul style="list-style-type: none"> - Drone (0.00 to 72.20°) (average = 7.87°) - Slope angles reveal deep sediment erosion and rock exposures along Turkwel and Kawalase rivers 	<ul style="list-style-type: none"> - STRM: 0.00 to 33.02° (average = .2.87°) - Erosional features along Turkwel and Kawalase Rivers not visible

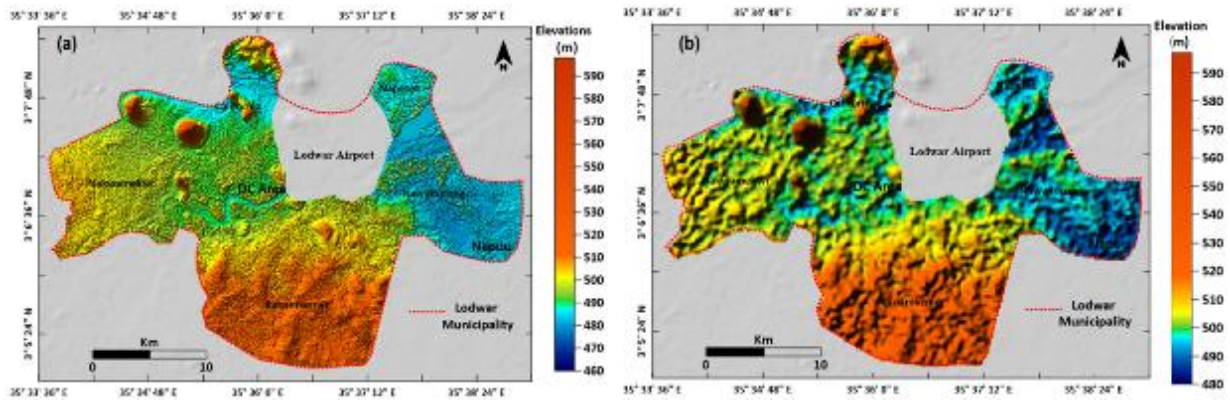


Figure 4.8: Comparison between (a) drone-based DEM and (b) STRM-based DEM for Lodwar town

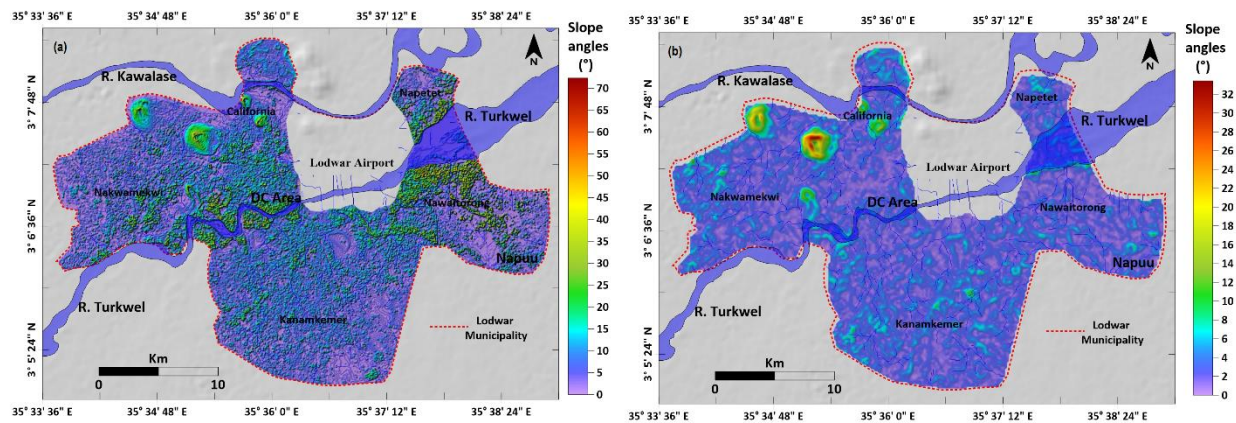


Figure 4.9: Comparisons between (a) UAV drone-based slope angle map and (b) STRM-based slope angle map

(iv) High-resolution orthomosaic

The orthomosaic obtained from the drone mapping has a vertical resolution of 0.5 m and is useful in identifying ground features such as residential areas, rock outcrops, river and stream channels as well as demarcating geological boundaries. The grey areas were due to poor lighting conditions from sandstorm occurrences at the time of mapping (Figure 4.10). Thus, it can also be used in mapping/monitoring short-lived events.

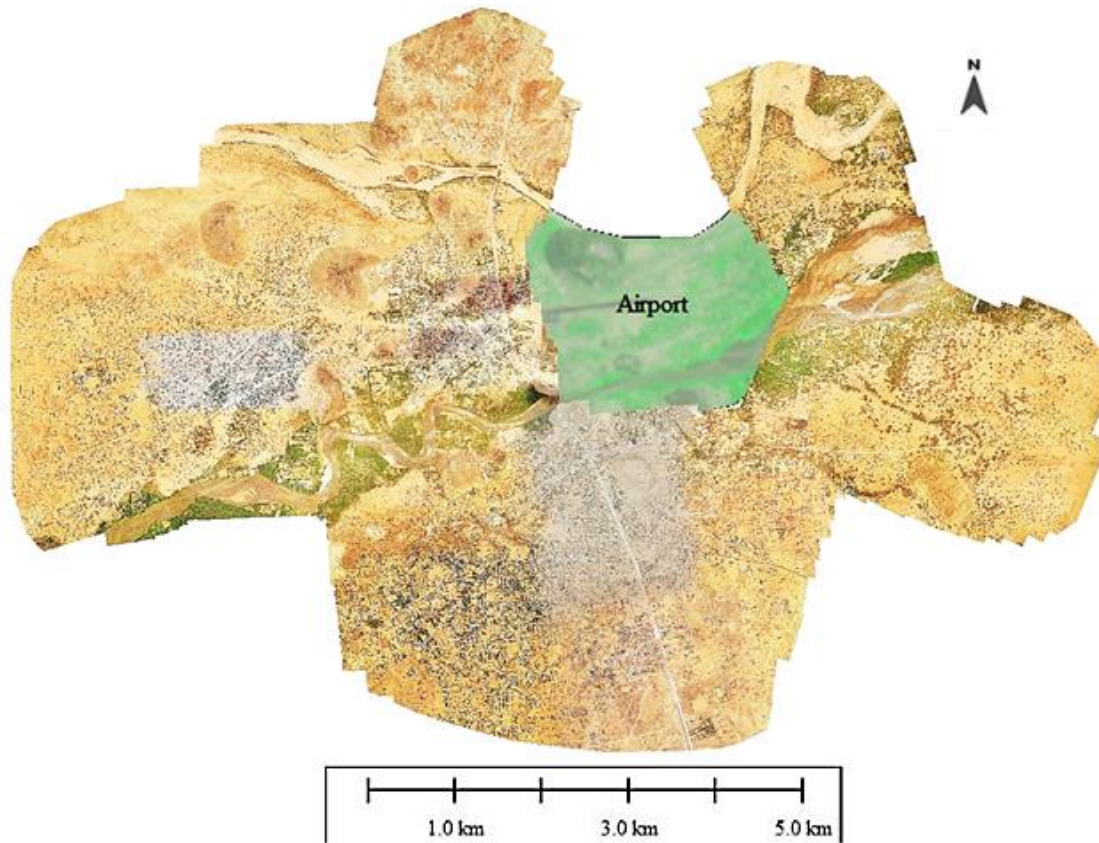


Figure 4.10: Orthomosaic image obtained from the processing of the drone-acquired images. The Mapping exercise did not cover Lodwar airport which is demarcated as a no-fly zone for drones

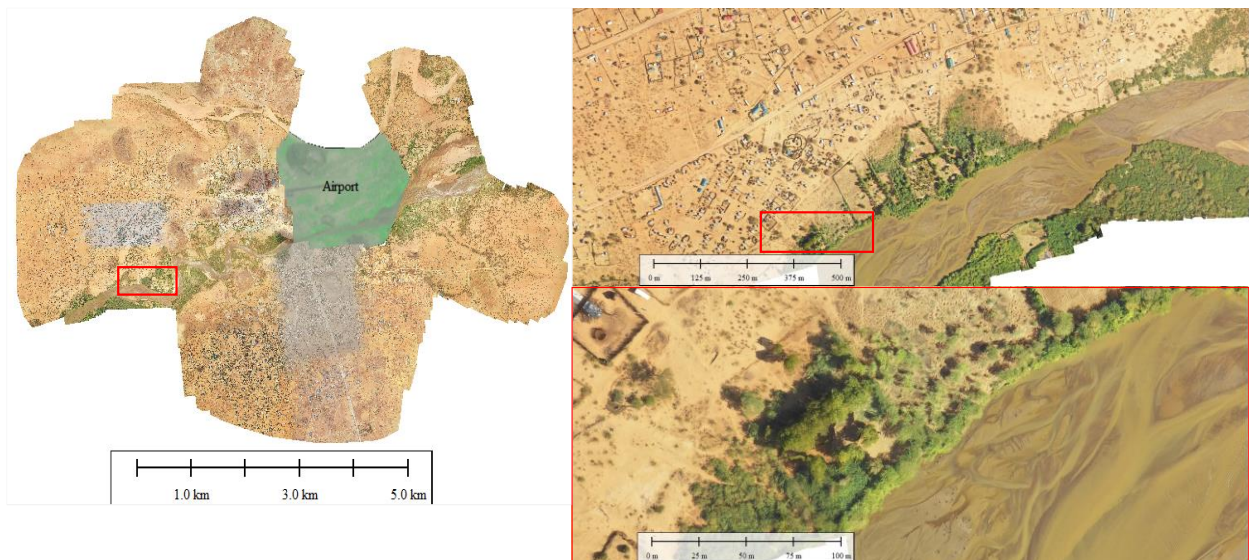


Figure 4.11: Zooming inside the red rectangle within the orthomosaic image

(v) Textured 3D model

The texture 3D models acquired from processing drone-acquired images are used for urban planning, population monitoring, and preparation of water supply networks and simulation. The 3D model is an interactive map that allows you to rotate in 360° for viewing and studying ground-based objects (Figure 4.11).

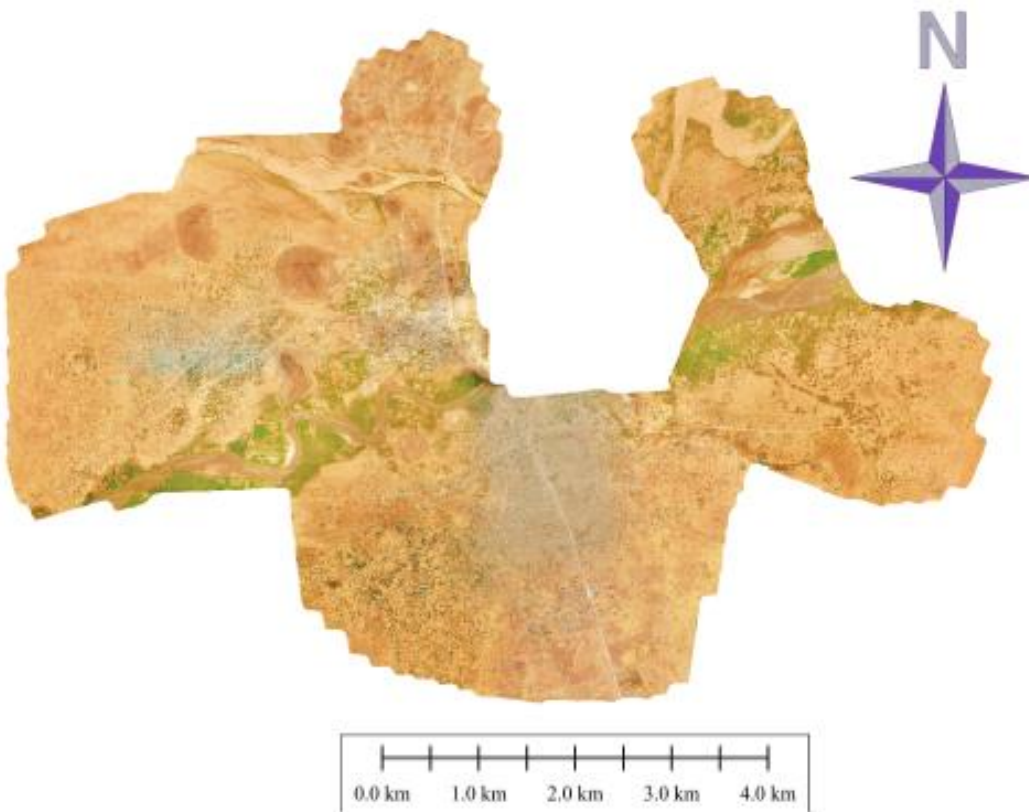


Figure 4.12: Textured 3D model for Lodwar municipality excluding the airport area (original model too large to be included in the report)

4.2.1.3 Rock sample collection and analysis

(i) Field description

The field specimens for quartzo-feldspathic gneiss, Turkana grits, Holocene sediments, sandstone, conglomerate, grainstone, nepheline-phonolites, augite basalts, dolerites and alluvial deposits are described in Appendixes 4-1 to 4-6.

a. Precambrian quartzo-feldspathic gneiss

The hand specimens of the quartzo-feldspathic gneiss were light-grey with granoblastic texture and alternating mineral banding of felsic and mafic minerals (Appendix 4-1). Quartz and feldspars are the dominant minerals. Iron and manganese nodules were observed in specimen 384.

(i) Upper Jurassic to Cretaceous Turkana Grits

Turkana grits exhibited different physical characteristics at different locations within the study area based on grain size, degree of consolidation and presence of capping calcareous material (Table 4.3). The hand specimens ranged from fine-grained to medium-grained to gravelly Turkana grits, where the fine-grained grit was mostly consolidated while either semi-consolidated or unconsolidated were the coarse-grained ones (Appendix 4-2).

(ii) Holocene sediments

Holocene sediments were collected between Napuu and Lolupe, east of Lodwar, at Natir and at Turkwel River bank in the Kakwanyang area. Their texture generally ranged from coarse-grained-medium-grained to fine-grained with distinct beddings that ranged from 0.50 m thick to 1.50 m. Calcite and quartz were present in all Holocene sediments with a thin clay layer at Kakwanyang area (Appendix 4-3).

(iii) Sandstone

Sandstone exposures were identified at Nadapal, Nakwamekwi, Turkwel River at Natir and east of Natir, Nachomin and Nabuelpus areas. Like in the case of the Turkana grit, the fine-grained sandstone was consolidated while the loosely consolidated type was calcite-cemented. Micaceous sandstone comprised clay with gravel-sized clasts (Appendix 4-4).

(iv) Conglomerate and grainstone

Grainstone was encountered at Natir and ranged from fine-grained-to-medium-grained, consisted of clast-sized quartz pebbles (Appendix 4-5). The conglomerate, on the other hand, graded from finer-grained sediments to silty grains with coarsening upward sand fragments cemented by calcium carbonate.

(v) Volcanic rocks

Specimens of volcanic rocks included augite basalt (1648), nepheline-phonolite (1650, 1653 and 1674), dolerite dykes (1656 and 3845) described in Appendix 4-6. The nepheline-phonolite specimens were well-polished, unweathered with fine-to medium-grained texture with prism-

shaped nepheline crystals, plagioclase feldspars, magnetite, and haematite. The dolerite dyke in Turkana grits consisted of plagioclase and pyroxene minerals with inclusions of the grits indicating the Turkana grits are older (Appendix 4-6).

a) Alluvial deposits

Alluvial deposits consisted of white to brown sandy deposits with dark-coloured organic matter and graded bedding structures. There was no reaction of HCl with feldspars, biotite and mica grains were observed. The deposits mainly consisted of sands, silts, clay and gravel.

b) Petrographic analysis

The rock samples were assigned specific codes ranging from 1650 to 3858 for analysis. These codes are indicated below in brackets. The rock samples petrographically analysed included; nepheline-phonolite (1650), dolerite dykes (1656 and 3845), conglomerate (3857), sandstone (1659, 3833 and 3858), Turkana grits (1656 and 3831) and the quartzo-feldspathic gneiss (3843 and 3844).

(i) Nepheline-phonolite

The nepheline-phonolite (sample number 1650) had anhedral prismatic nepheline crystals (Figure 4.13). The crystals are anhedral, assuming the hexagonal crystal symmetry and altered in parts to sodalite and turbid anorthoclase feldspar. The fine-grained groundmass of green aegirine-augite, anorthoclase, and nepheline contains euhedral haematite grains. Cataclastic deformation (a later, lower-temperature phase of strain localisation in plutonic rocks) of plagioclase was observed under PPL and XPL, forming deformation bands that correlated with the shear strain. The hematite grains appeared to be larger in the deformation zone. In a thin fragment, rare nepheline microphenocrysts, partially modified to sodalite, and turbid anorthoclase feldspar are also present in the fine-grained groundmass.

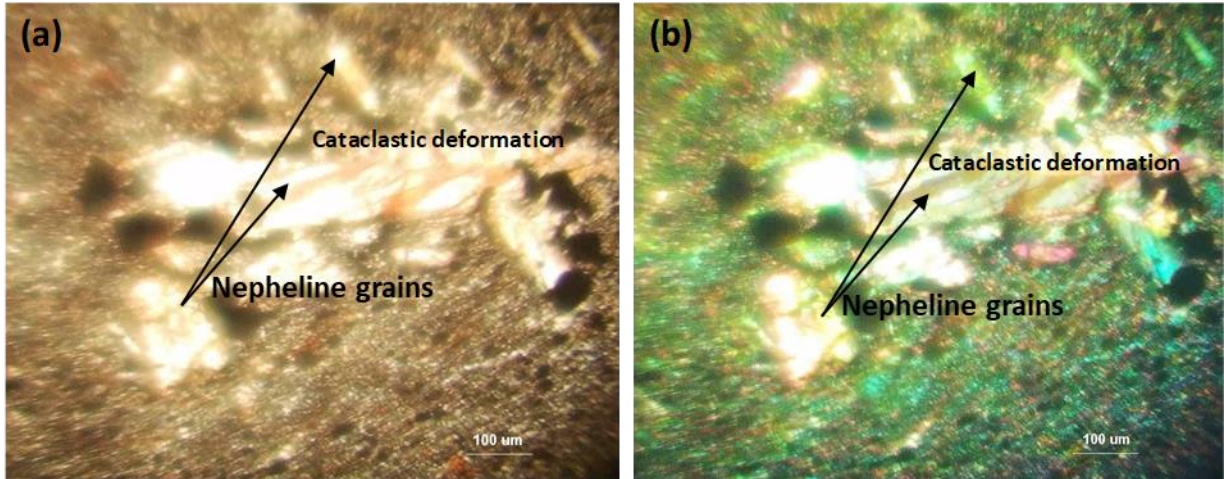


Figure 4.13: Microphotograph of the nepheline-phonolite (sample 1650) observed under (a) PPL and (b) XPL showing the prismatic nepheline crystals and euhedral hematite grains, with cataclastic deformation of plagioclase was observed in the thin section

(ii) Dolerite

Dolerite is a dark-grey to black intrusive rock with fine to medium-grained groundmass and was identified occurring as a dyke in the Turkana grits. Instead of a thin section preparation, a thick section ($> 30\mu$) was achieved in the slice preparation and has been used for fluid or melt inclusion and melt inclusion analysis (Grundmann and Scholz, 2015). However, Figure 4.14 shows fracturing in PPL and with no fluid inclusion entrapment observed. Possible twinning of minerals can be observed in XPL (Figure 4.14b), however, a confirmation in thin section ($< 30\mu$) is required). In thin sections, most dolerites show numerous colourless grains of quartz and feldspars, where the feldspars assumed prismatic habit (Shekhar *et al.*, 2018). Primary minerals identified include plagioclase, pyroxene, and amphiboles, where the plagioclase crystals are acicular, and the pyroxene grains are subhedral with chloritised outlines while the secondary minerals included chlorite and quartz (Mugerwa, 2015).

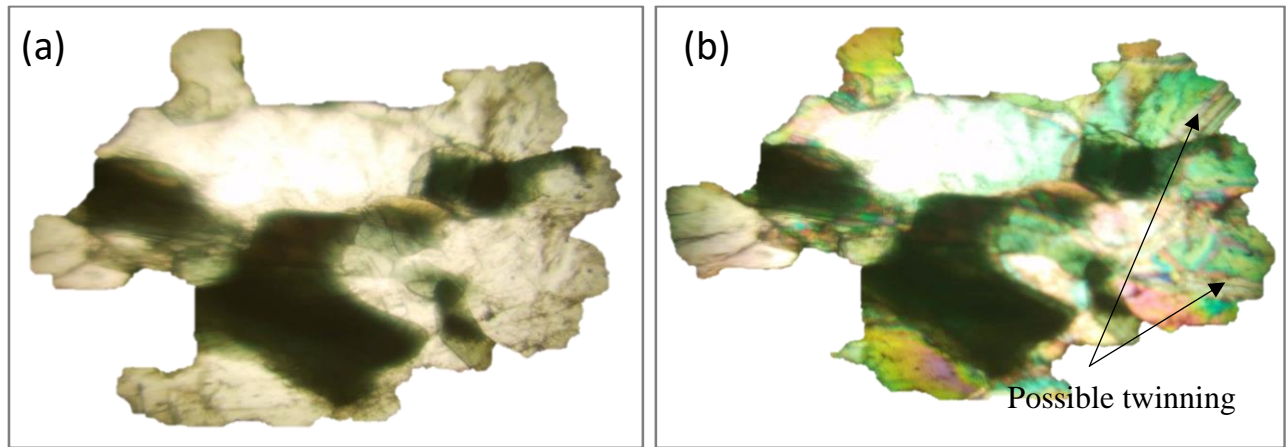


Figure 4.14: Microphotograph of the dolerite dyke rock within the Turkana grits shows fracturing in PPL and with no fluid inclusion entrapment observed, in XPL, possible twinning of is observed. However, this can be further evaluated in a slice < 30 μ

(iii) Conglomerate

Specimen 3857 of conglomerate capping the Turkana grit at its contact zone with the nepheline phonolite revealed angular quartz and feldspar fragments cemented by clay and some calcite. Colourless sub-rounded quartz minerals are observed in both in XPL (a) and PPL (b), and prismatic nepheline crystals were present in the rock sample (Figure 4.15). With angular altered volcanic rock fragments, there is poorly defined sedimentary banding. There are also altered biotite grains, which indicate alkalic or acidic volcanism. The conglomerate is cemented with coarse-grained sparry calcite cement which fills the clasts in cracks as well. The feldspars present are andesite and deep brown sodic amphibole like that described by Muia (2015) and Walsh and Dodson (1969).

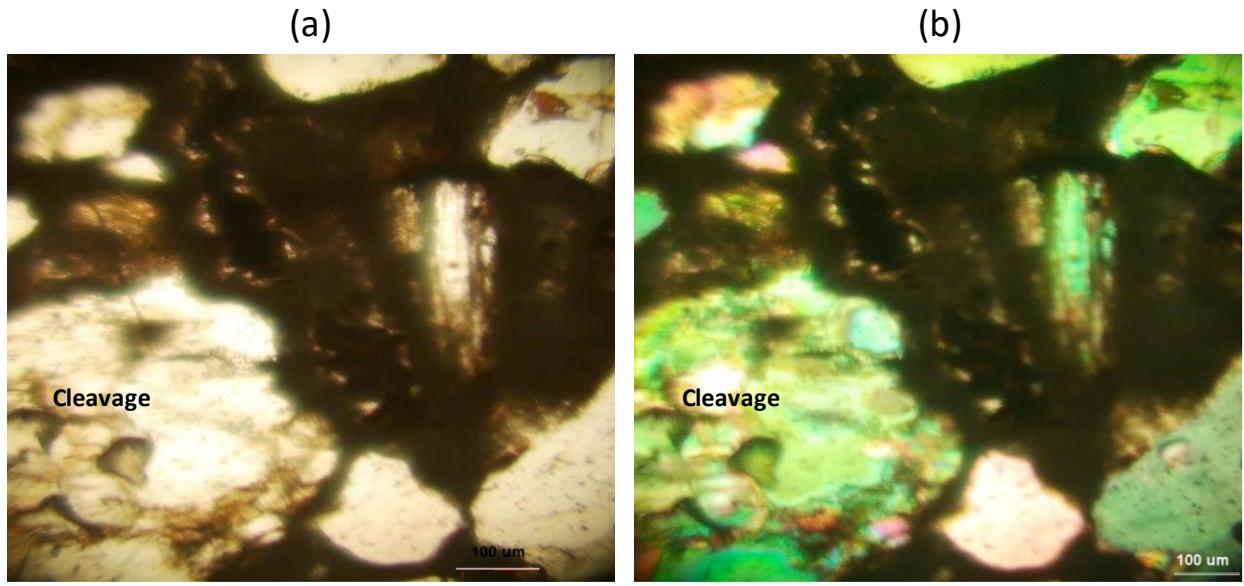


Figure 4.15: Microphotograph of the conglomerate sample (3857) under (a) PPL and (b) XPL showing sub-rounded quartz grains and prismatic nepheline crystal with distinct cleavages

(iv) Sandstone

Three sandstone samples (1659, 3833, and 3858) have medium-sized grains (Figure 4.16 a and b) comprised of quartz, feldspars, and biotite. The fine-grained compact sandstone sample (Figure 4.19 c and d) show dominant feldspar grains under XPL (d). What appears to be fluid inclusion features had diameters ranging from less than 20.00 μm to 130.47 μm is observed in in Figure 4.6 c and d. indicating that temperatures $>100\text{ }^{\circ}\text{C}$ were not reached during the burial history of the sandstone. The same may represent bubbles trapped in the slice during the thin-section preparation. The sandstone was highly fractured with some of the microfractures filled with brown minerals, possibly iron and oxyhydroxides. The poorly sorted sand and gravels in the coarse-grained sandstone and existence of fractures in the fine-grained counterpart suggest high permeability of sandstone in the study area. The coarse-grained sandstone (Figure 4.16 e and f) comprised mainly of sub-rounded to well-rounded quartz pebbles cemented by calcite and carbonate. Cryptocrystalline chert, micro micaceous mudstone, siltstone and stretched quartz grains dominate the mineral framework. Fewer feldspars grains were present in the coarse-grained sandstone as compared to those present in the fine-grained specimens.

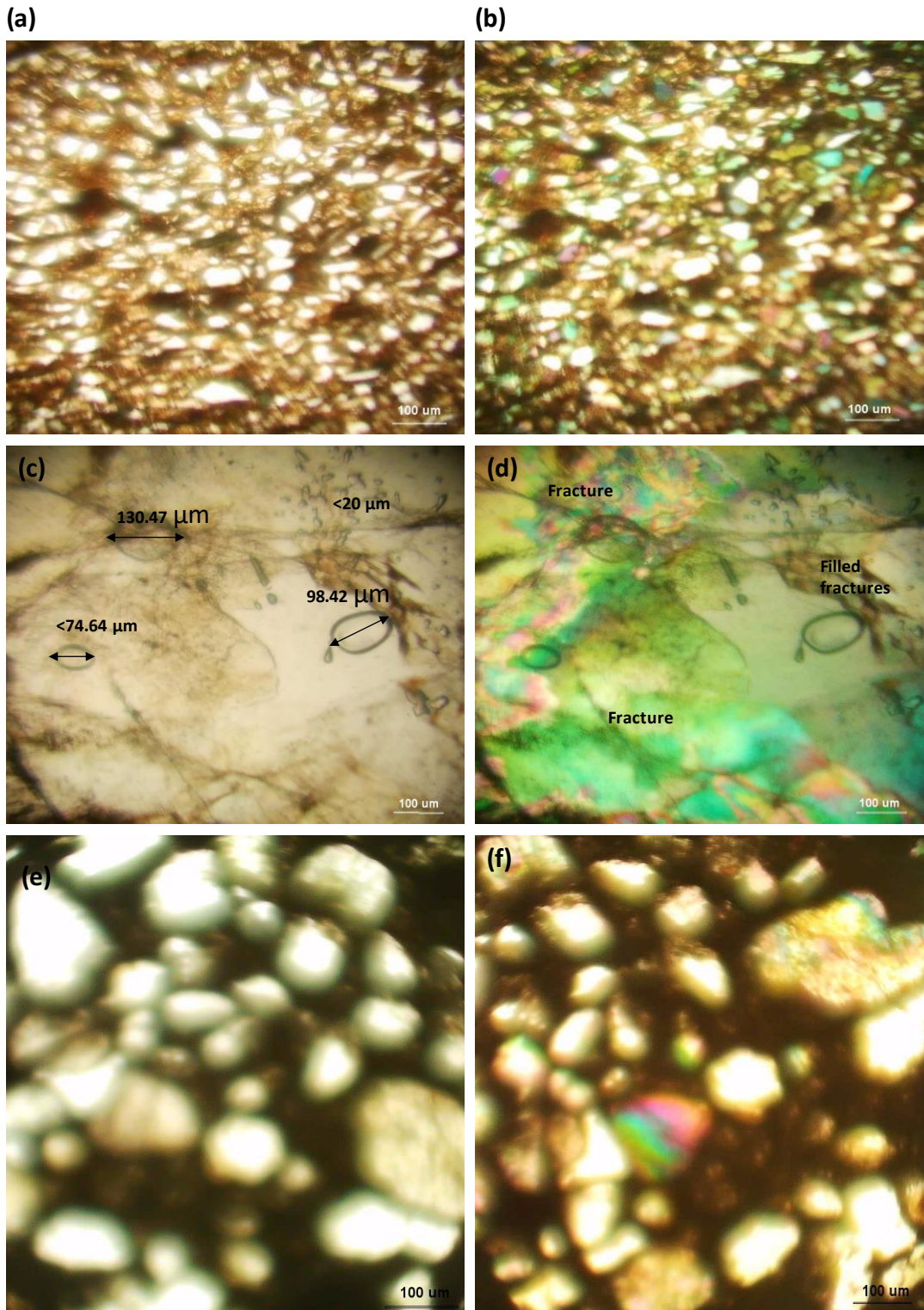


Figure 4.16: Microphotographs for the medium-grained gravelly sandstone (sample 1659) under (a) PPL and (b) XPL, compact altered sandstone shown in PPL (b) and XPL (c); coarse-grained gravelly-sandstone (sample 3858) shown in PPL (e) and XPL (f)

(v) Turkana grits

The Turkana grit samples (1656 and 3831) predominantly consists of fine to coarse arkosic sandstone suggesting fluvial deposition and comprised mainly quartz and feldspars (25-40%), cemented by calcite. The yellow crystals observed under PPL were regarded as staurolite, and green are hornblende minerals. The Turkana grit in contact with the dolerite dyke (Figure 4.17 a and b) had zoning features and altered minerals caused by contact metasomatism. The quartz and feldspars are anhedral-shaped and are poorly sorted within the calcite matrix with grains ranging from 0.25 to 1.00 mm (Figure 4.17 c and d).

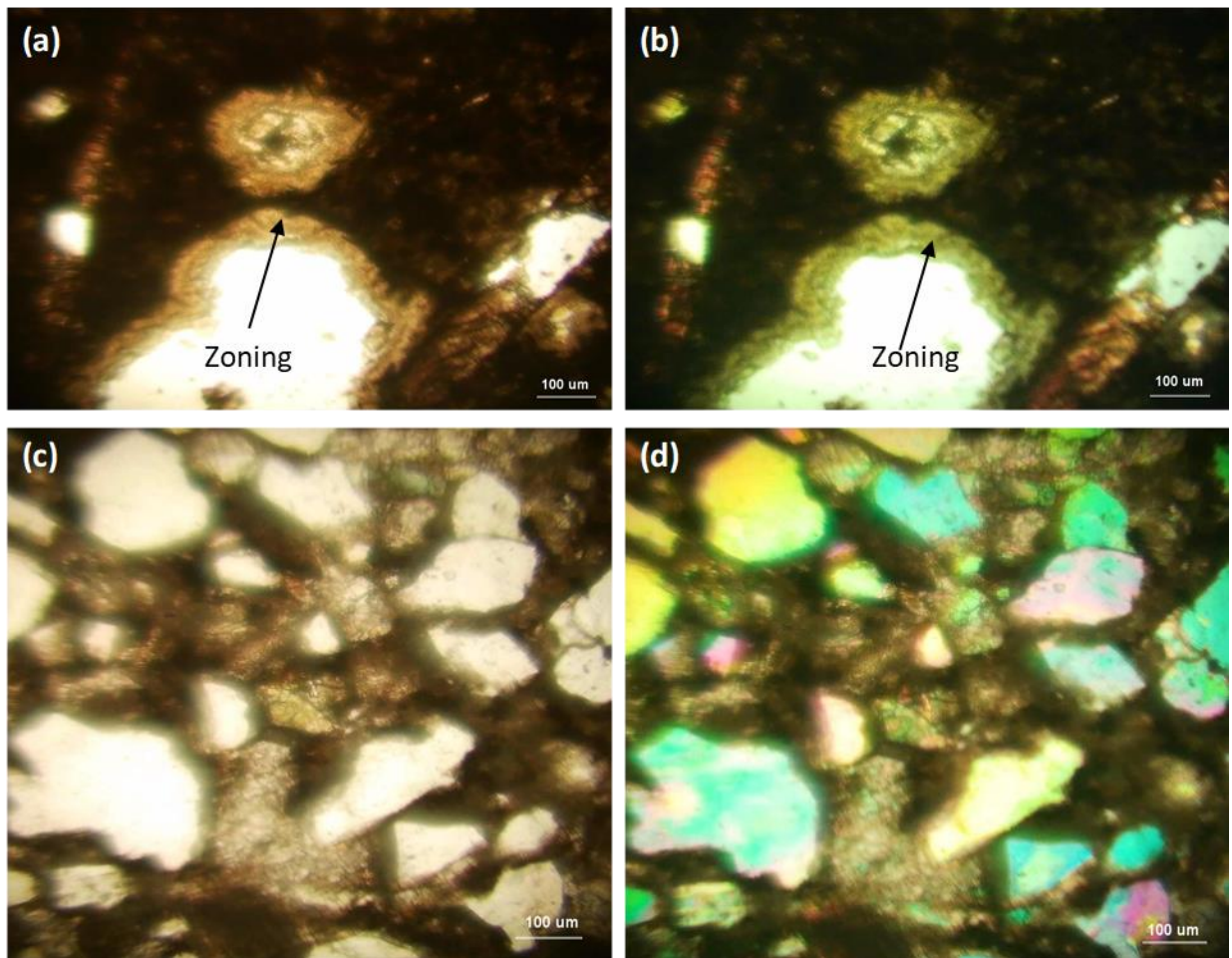


Figure 4.17: Microphotographs of the Turkana grit samples showing zoning features (a and b) calcite-cemented matrix on quartz and feldspars minerals (b and c)

(vi) Quartzo-feldspathic gneiss

Two samples of the quartzo-feldspathic gneiss collected at the same location indicate different mineralogical characteristics. Sample 3343 (Figure 4.18 a and b) was attached to the igneous intrusion and showed highly deformed minerals caused by high-grade metamorphism. Quartz and feldspars are the dominant minerals observed in sample 3344 (Figure 4.18 c and d), and biotite comprises 5% of the mineralogy occurring as an accessory mineral. The feldspars present include altered orthoclase, microcline, and plagioclase. The majority of the orthoclase grains have been converted to small flakes of sericite while the initial biotite grain has reacted to oxides, orthopyroxene, and (inferred) melt during contact metamorphism. The partly replaced biotite grains are surrounded by relict plagioclase in sieve texture with spaces filled with quartz and feldspars.

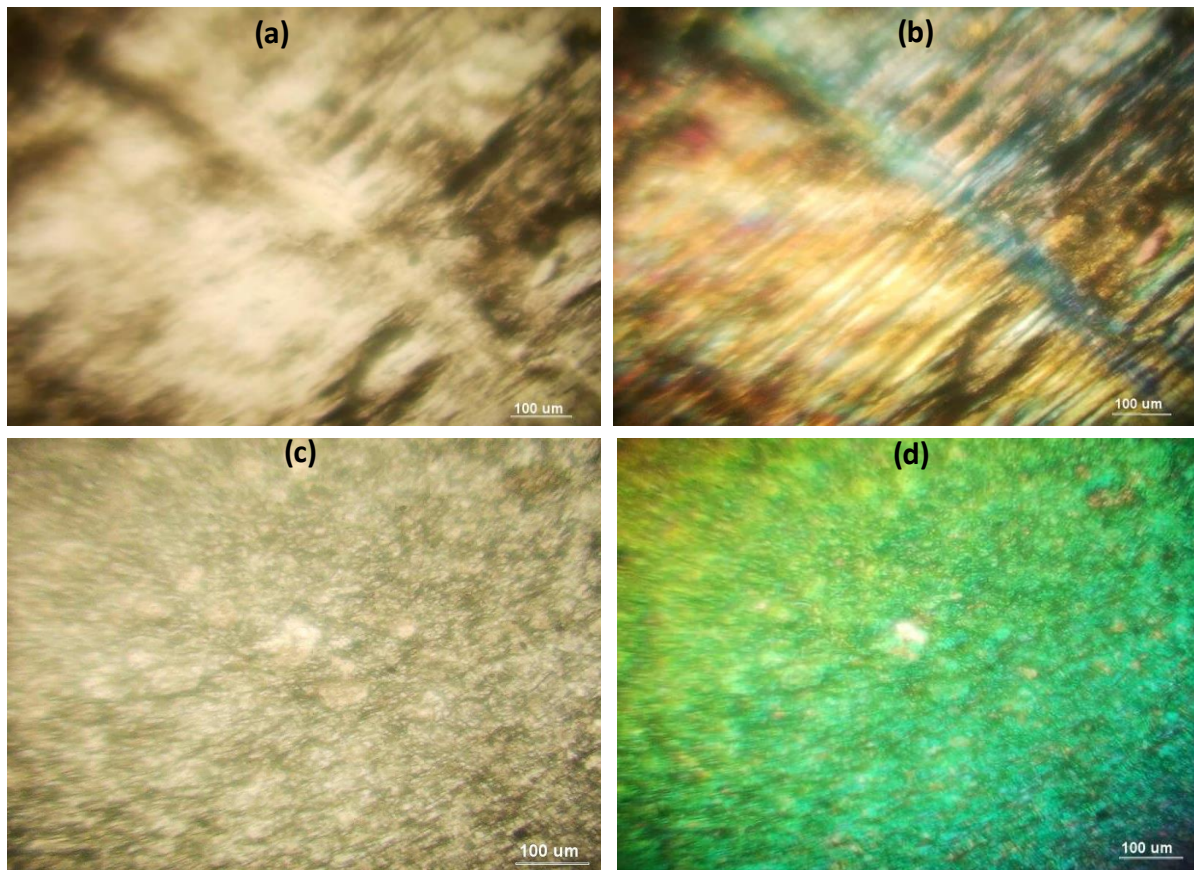


Figure 4.18: Microphotographs of the quartzo-feldspathic gneiss adjacent to the dolerite intrusion showing highly deformed surfaces (a and b) and fine-grained surface of quartz and feldspars further away from the intrusion (c and d)

4.2.1.4 Geochemistry of rock samples

The geochemistry of the rock samples has been described based on the results of the major elements and the concentration of trace metals and trace elements using XRF. The major elements were expressed as oxides of SiO₂, Al₂O₃, CaO, MgO, Na₂O, K₂O, TiO₂, MnO, Fe₂O, and LOI (Appendix 4-7 and Appendix 4-8). The sum of the concentration of each oxide ranged from 97.80 to 99.99 %. The trace elements comprised Cr, Co, Ni, Cu, Zn, As, Se, Mo, and Pb and are expressed as a percentage (Appendix 4-9).

(i) Metamorphic rocks

In the three rock samples (3841, 3843 and 3846) of the quartzo-feldspathic gneiss, silica (SiO₂) ranged between 52.83 to 53.71 wt % and was the most abundant oxide. The abundance of Al₂O₃ (18.20 to 19.95 wt %) indicates the presence of aluminosilicates and clay minerals such as kaolinite as a result of weathering processes. As in the case of most metamorphic gneisses, all the specimens of the quartzo-feldspathic gneiss had high K₂O content with K₂O/Na₂O ratios exceeding 1 (1.62, 1.19, 1.10), indicating high-temperature recrystallization. The rock samples are poor in ferromagnesian elements - MnO (0.25 wt %), TiO₂ (0.19 wt %) and MgO (0.09 wt%). Their An-Ab-Or normative classification plot in the granite field (Figure 4.19 a), as a result of low CaO content (2.15 wt %) (Irvine and Baragar, 1971). AFM classification of the rock samples (Figure 4.22) indicate they are calc-alkaline (Figure 4.19 b).

The major elements present include Ca (8.60 %), Fe (3.90%), Mg (2.42%), Al (2.30%), K (0.22%), Mn (0.15%) and P and S (0.04%) each. The lack of Na in all the rocks samples suggests that the quartzo-feldspathic gneiss is rich in anorthite, a characteristic of the granulite facies of metamorphic rocks. In terms of trace elements, Co, As, Se, Mo and Pb were not detected in all the rock samples. Zn was 0.01% in all the samples as well as that of Ti in sample 3841 and 3843. Cr was 0.01% in sample 3841 and 0.08% in sample 3843 and 3846 suggesting they are more enriched in pyroxenes and mica than sample 3841. Cu was only present in sample 3841 (0.03%) (Table 4.2).

Table 4.2: Results for the major oxides, major elements and trace metals in the quartzo-feldspathic gneiss (three rock samples, see Appendix 4-7 to 4-9 for detailed results per sample)

Major element oxides										
Rock sample	SiO ₂	Al ₂ O ₃	CaO	MgO	Na ₂ O	K ₂ O	TiO ₂	MnO	Fe ₂ O ₃	LOI
3841-18	53.71	18.2	1.52	1.07	4.03	6.52	0.19	0.27	3.92	9.63
3843-18	52.83	19.95	2.15	0.01	4.93	5.87	0.18	0.25	4.31	8.66
3846-18	53.21	19.89	2.49	0.09	5.01	5.5	0.23	0.24	4.49	8.84
Average	53.25	19.35	2.05	0.39	4.66	5.96	0.20	0.25	4.24	9.04
Major elements										
	Na	Mg	Al	P	S	K	Ca	Mn	Fe	
3841-18	nd	1.96	1.71	0.03	0.07	0.37	12.63	0.07	1.12	
3843-18	nd	2.89	1.82	0.05	nd	0.17	5.34	0.18	4.26	
3846-18	nd	2.42	3.38	0.03	0.01	0.14	7.82	0.20	6.32	
Average		2.42	2.30	0.04	0.04	0.22	8.60	0.15	3.90	
Trace elements										
	Ti	Cr	Co	Ni	Cu	Zn	As	Se	Mo	Pb
3841-18	0.01	0.01	nd	0.00	0.03	0.01	nd	nd	nd	nd
3843-18	0.01	0.08	0.00	0.02	nd	0.01	nd	nd	nd	nd
3846-18	nd	0.08	0.00	0.01	nd	0.01	nd	0.00	nd	nd
Average	0.01	0.06	0.00	0.01	0.03	0.01	nd	0.00	nd	nd

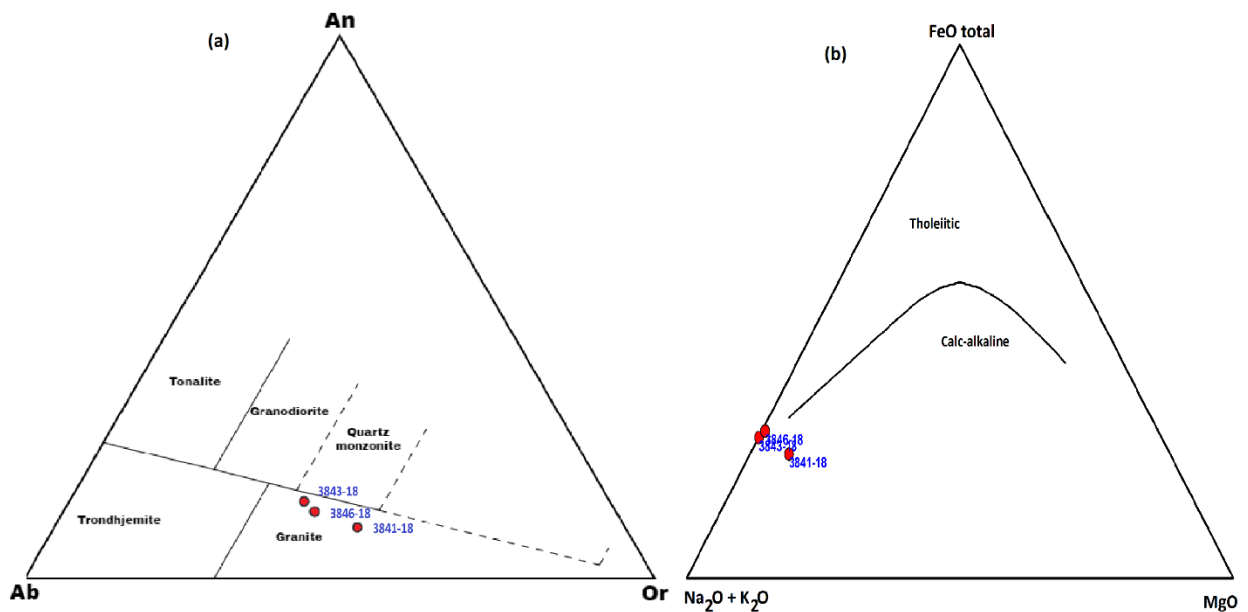


Figure 4.19: (a) An-Ab-Or normative classification based on O'Connor (1965) and (b) AFM diagram for the quartzo-feldspathic gneiss showing high Na₂O and K₂O content (after Irvine and Baragar, 1971)

(ii) Sedimentary rocks

(a) Turkana grits

A total of eighteen rock samples of the Turkana grits were analysed for major elements while 11 of these samples were analysed for major and trace elements. The results of the major elements represented complex geochemistry among the different rock specimens (Figure 4.20). Generally, the chemical and mineralogical compositions of the sediments and sedimentary rocks are extremely diverse due to the varied origin of sediments and resulting end-members. Application of the K means clustering algorithm revealed four unique clusters of the Turkana grits in the study area (Table 4.3). Table 4.4 shows the class centroids for each cluster based on the compositions of the major elements in the rock samples, while Table 4.5 present the description of their chemical compositions.

Table 4.3: Description of the different clusters of the Turkana grits based K Means Clustering Algorithm

Turkana grit Clusters	Description
Cluster 1: Fine-grained Turkana grits	Cluster 1 had seven members (1646, 1649, 1651, 1654, 1655, 3835 and, 3839) and represented specimens of the Turkana grits collected within Lodwar town and at Nakutan area.
Cluster 2: Gravelly Turkana grits	Two rock samples comprised Cluster 2 (1652 and 3848) and were collected north-east of Lodwar town at Kakwanyang and to the east of Talent High school.
Cluster 3: Semi-consolidated sandy Turkana grits	Cluster 3 comprised six rock samples of the Turkana grits (1671, 1672, 1673, 3831, 3836, and 3838) that occurred adjacent to the Holocene sediments. The rock specimens were mainly sandy and semi-consolidated and often capped by a highly consolidated gravelly layer.
Cluster 4: Consolidated Turkana grits	Cluster 4 comprised three rock samples of the Turkana grits (3830, 3849 and 3856) recorded at Nachomin, Nakadukui and Natirnalulung areas. Like Cluster 2 samples, these members were observed at isolated locations and often capped by calcareous material.

Table 4.4: Class centroids for each cluster based on the compositions of the major elements in the rock samples

Class	SiO ₂	Al ₂ O ₃	CaO	MgO	Na ₂ O	K ₂ O	TiO ₂	MnO	Fe ₂ O ₃	LOI
1	53.86	8.53	13.58	4.82	0.77	2.06	0.59	0.45	2.83	11.76
2	51.03	4.12	33.57	3.54	0.39	0.63	0.21	0.14	1.49	4.35
3	65.60	11.00	5.03	1.57	0.14	1.92	0.53	0.17	3.43	10.24
4	28.81	3.94	28.03	5.07	0.27	0.76	0.20	0.35	2.06	29.88

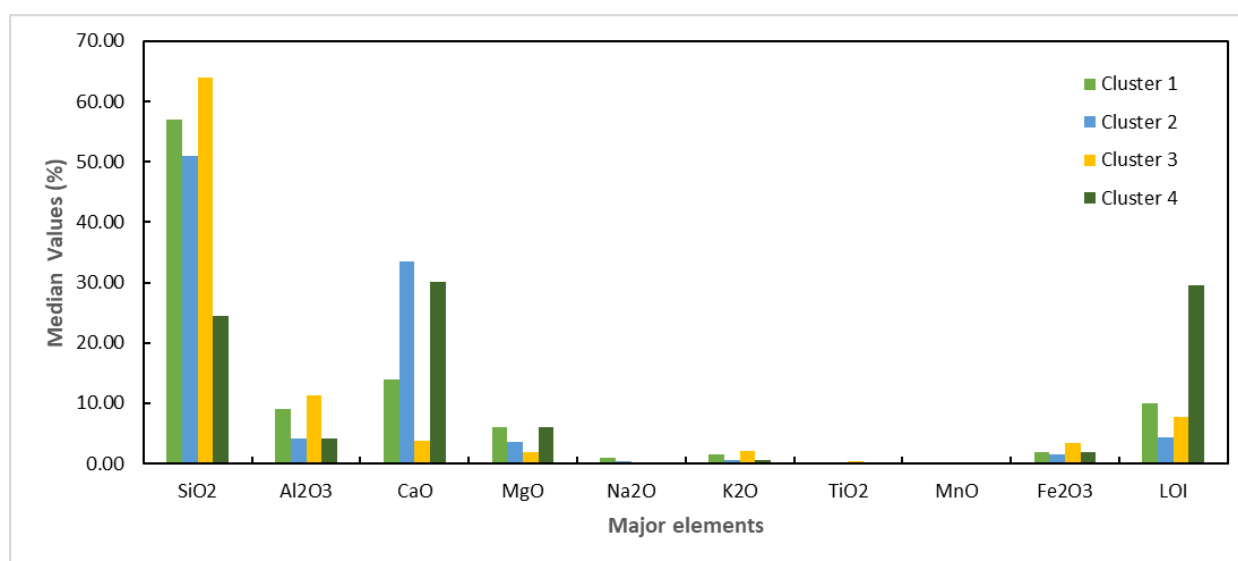


Figure 4.20: Variations of the chemical compositions of the major elements among the clusters of Turkana grits

Table 4.5: Description of the major oxides, major and trace elements of the four clusters of the Turkana grits

Cluster	Major Oxides	Major elements	Trace elements
Cluster 1: Fine-grained Turkana grits	<ul style="list-style-type: none"> - Characterised by high MgO, Na₂O, K₂O and MnO. - SiO₂ ranged from 45.70 to 60.48 %, CaO (7.80 -18.24%), - LOI (7.88-17.37%), Al₂O₃ (3.89 - 16.40%), MgO (0.02 - 9.21%), Fe₂O₃ (1.32 - 7.90%), - K₂O (0.98 - 4.03%), TiO₂ (0.09 - 2.40%), and the least composition was Na₂O (0.02 - 1.98%). 	<ul style="list-style-type: none"> - Ca, Al, and Fe are the most abundant major elements with median values of 8.83%, 2.80 % and Fe 2.42 % respectively - K, Mg, Mn, Na had median concentrations <0.50%. 	<ul style="list-style-type: none"> - Ti, Cr, Co, Ni, Cu, Zn, Se and Mo had median values <0.01% while As, and Pb was not within detectable limits in this cluster
Cluster 2: Gravelly Turkana grits	<ul style="list-style-type: none"> - Characterised by very high CaO (30.14 - 37.00%) and low Fe₂O₃ (1.17 -1.81%) - SiO₂ (48.36 – 53.70%), Al₂O₃ (4.03-4.21%) was also relatively lower than that of Clusters 1 and 3 	<ul style="list-style-type: none"> - Like in cluster 1, Ca (9.08%), Al (2.62%), and Fe (2.22%) were the most abundant major elements - Mg was 0.74% P, S, and K were < 0.05% while Na was not detected in specimens of this cluster. 	<ul style="list-style-type: none"> - Cu, As, and Pb were below detectable limits while Ti was 0.07%. - Cr, Ni, Co, Zn, Se and Mo was <0.01%
Cluster 3: Semi-consolidated sandy Turkana grits	<ul style="list-style-type: none"> - Highest compositions of SiO₂ (60.80 – 71.06 %), Al₂O₃ (4.81-15.87%), K₂O (0.94 – 2.51%), TiO (0.32 – 0.89%), Fe₂O₃ (2.49 – 4.90%), CaO (2.76 – 9.80), with the lowest levels of MgO (0.03 – 3.02 %), and Na₂O (0.09 – 0.21%) than in Clusters 1, 2 and 4. 	<ul style="list-style-type: none"> - Ca (9.08%), Al (2.62%), and Fe (2.22%) were most abundant than the rest of the trace elements. - Mg was 0.74%, while P, S, and K were below 0.05%. Na was not detected like cluster 2 	<ul style="list-style-type: none"> - Ti was 0.05% - As, Se and Pb were below detectable limits in this cluster. - The rest of the elements (Ti, Cr, Co, Ni, Cu, Zn, and Mo were <0.01%
Cluster 4: Consolidated Turkana grits	<ul style="list-style-type: none"> - High concentration of CaO (15.80 – 38.15 %) after cluster 2 and - Highest moisture and volatile materials (25.87 - 34.27%) and MgO (0.05 – 9.15%), and the least SiO₂ (<40.09%) content among all the four clusters. 	<ul style="list-style-type: none"> - Major elements showed the highest Ca concentration of the four clusters (17.08%) - Al was 1.78%, Fe 1.53% and Mg 0.70%, - K, P and S were below 0.05% 	<ul style="list-style-type: none"> - Concentration of all trace elements was <0.02%

Table 4.6: Descriptive statistics for the major elements (Cluster 1 to 4) for the different groups of Turkana grits samples (SD – standard deviation)

(a) Cluster 1: Descriptive statistics for the Cluster 1 Turkana grits samples (wt. %)										
Statistic	SiO ₂	Al ₂ O ₃	CaO	MgO	Na ₂ O	K ₂ O	TiO ₂	MnO	Fe ₂ O ₃	LOI
Minimum	45.70	3.89	7.80	0.02	0.02	0.98	0.14	0.09	1.32	7.88
Maximum	60.48	16.40	18.24	9.21	1.98	4.03	2.40	2.01	7.90	17.37
Range	14.78	12.51	10.44	9.19	1.96	3.05	2.26	1.92	6.58	9.49
Median	56.92	9.12	14.01	6.10	0.87	1.51	0.17	0.19	1.95	9.89
Mean	53.86	8.53	13.58	4.82	0.77	2.06	0.59	0.45	2.83	11.76
Variance	43.48	19.51	12.38	14.78	0.58	1.21	0.69	0.48	5.53	15.44
SD	6.59	4.42	3.52	3.84	0.76	1.10	0.83	0.69	2.35	3.93

(b) Cluster 2: Descriptive statistics for the gravelly Turkana grits (wt. %)										
Statistic	SiO ₂	Al ₂ O ₃	CaO	MgO	Na ₂ O	K ₂ O	TiO ₂	MnO	Fe ₂ O ₃	LOI
Minimum	48.36	4.03	30.14	1.06	0.20	0.61	0.19	0.13	1.17	1.88
Maximum	53.70	4.21	37.00	6.01	0.58	0.65	0.23	0.15	1.81	6.81
Range	5.34	0.18	6.86	4.95	0.38	0.04	0.04	0.02	0.64	4.93
Median	51.03	4.12	33.57	3.54	0.39	0.63	0.21	0.14	1.49	4.35
Mean	51.03	4.12	33.57	3.54	0.39	0.63	0.21	0.14	1.49	4.35
Variance	14.26	0.02	23.53	12.25	0.07	0.00	0.00	0.00	0.20	12.15
SD	3.78	0.13	4.85	3.50	0.27	0.03	0.03	0.01	0.45	3.49

(c) Cluster 3: Descriptive statistics for the Semi-consolidated sandy Turkana grits (wt. %)										
Statistic	SiO ₂	Al ₂ O ₃	CaO	MgO	Na ₂ O	K ₂ O	TiO ₂	MnO	Fe ₂ O ₃	LOI
Minimum	60.80	4.81	2.76	0.03	0.09	0.94	0.32	0.08	2.40	5.47
Maximum	71.06	15.87	9.80	3.02	0.21	2.51	0.89	0.32	4.90	24.91
Range	10.26	11.06	7.04	2.99	0.12	1.57	0.57	0.24	2.50	19.44
Median	64.05	11.29	3.73	1.92	0.13	2.06	0.46	0.11	3.31	7.77
Mean	65.60	11.00	5.03	1.57	0.14	1.92	0.53	0.17	3.43	10.24
Variance	19.29	12.78	8.11	1.59	0.00	0.28	0.04	0.01	0.81	53.83
SD	4.39	3.57	2.85	1.26	0.04	0.53	0.21	0.12	0.90	7.34

(d) Cluster 4: Descriptive statistics for the consolidated Turkana grits (wt. %)										
Statistic	SiO ₂	Al ₂ O ₃	CaO	MgO	Na ₂ O	K ₂ O	TiO ₂	MnO	Fe ₂ O ₃	LOI
Minimum	21.83	3.41	15.80	0.05	0.03	0.54	0.18	0.15	1.65	25.87
Maximum	40.09	4.21	38.15	9.15	0.57	1.12	0.23	0.71	2.73	34.27
Range	18.26	0.80	22.35	9.10	0.54	0.58	0.05	0.56	1.08	8.40
Median	24.51	4.20	30.14	6.01	0.20	0.61	0.19	0.19	1.81	29.49
Mean	28.81	3.94	28.03	5.07	0.27	0.76	0.20	0.35	2.06	29.88
Variance	97.22	0.21	128.22	21.37	0.08	0.10	0.00	0.10	0.34	17.75
SD	9.86	0.46	11.32	4.62	0.28	0.32	0.03	0.31	0.58	4.21

(b) Holocene sediments

The geochemistry of the Holocene sediments is based on specimens collected along with selected profiles in the east of Lodwar town, between Napuu and Lolupe, Turkwel River at Kakwanyang and Natirnalulung area.

East of Lodwar town

Holocene sediments east of Lodwar town showed relatively high silica content (57.97 - 69.67 wt %) with the top layer (3824) having low SiO₂ than the bottom bed (3825) based on median values. The top layer was also richer in Al₂O₃ (16.52 %), Fe₂O₃ (7.97 wt %) and LOI (11.26 wt %) against that of the bottom layer; Al₂O₃ (11.89 wt %), Fe₂O₃ (3.14 wt %), and 4.10% LOI content. Like in all the samples of the Holocene sediments in the study area, Na was not present in the sediment samples (3824 and 3825). Al (4.17 wt %), Fe (4.03 wt %), Ca (3.21 wt %), and Mg (1.01 wt %) were the most abundant major elements, indicating metamorphic origin. In terms of trace elements, Ti, Cr, Cu and Zn occurred in the two specimens of the Holocene sediments east of Lodwar town with higher concentrations observed in the upper layer (3824) than in sample 3825 (Table 4.7). Co, Ni and Mo had concentrations < 0.00 wt % while As, Se and Pb were not detected.

Table 4.7: Results and summary statistics for the major oxides, major and trace elements of the Holocene sediments East of Lodwar town

Major element oxides (wt %)										
Description	SiO ₂	Al ₂ O ₃	CaO	MgO	Na ₂ O	K ₂ O	TiO ₂	MnO	Fe ₂ O ₃	LOI
3824-(A)	57.97	16.52	2.06	1.37	0.14	1.39	0.94	0.12	7.97	11.26
3825-(B)	69.97	11.89	5.34	1.97	0.09	2.02	0.43	0.08	3.14	4.10
Average	63.97	14.21	3.70	1.67	0.12	1.71	0.69	0.10	5.56	7.68
Major elements (wt %)										
Description	Na	Mg	Al	P	S	K	Ca	Mn	Fe	
3824-(A)	nd	1.18	5.32	0.04	0.18	0.69	1.49	0.09	5.67	
3825-(B)	nd	0.84	3.01	0.05	0.00	0.26	4.93	0.07	2.40	
Average	nd	1.01	4.17	0.05	0.09	0.47	3.21	0.08	4.03	
Trace elements (wt %)										
Description	Ti	Cr	Co	Ni	Cu	Zn	As	Se	Mo	Pb
3824-(A)	0.13	0.01	0.00	0.00	0.01	0.02	nd	nd	0.00	nd
3825-(B)	0.05	0.01	0.00	0.00	nd	0.01	nd	nd	0.00	nd
Average	0.09	0.01	0.00	0.00	0.01	0.02	nd	nd	0.00	nd

Napuu/ Lolupe area

Holocene sediments between Napuu and Lolupe areas exhibited four distinct layers; layer A, a compact light-coloured fine-grained sediment (3820), layer B, dark-coloured sediment (3821), layer C, slightly light-coloured bed (3822) and a bottom layer (D) consisting of a fine-grained sandy layer (3823). SiO_2 was observed to decrease from layer A to C (66.90 to 51.80 wt %) and a significant increase to 80.85 wt % in layer D. There was an alternating decrease and increase in Al_2O_3 content from top to bottom (Table 4.9) a characteristic observed in the compositions of CaO and K_2O . Layer B (7.70%) and C (7.71%) had relatively similar Fe_2O_3 content that was higher than in layer A (3.78%) and D (1.11%). Of all the four layers (A, B, C and D), only the bottom layer D (3823) had Na, with a concentration of 0.11 wt %. Like in the case of Holocene sediments East of Lodwar, Al (4.23 wt %), Fe (3.91 wt %), Ca (2.19 wt %), and Mg (0.47 wt %) are the most abundant major elements, though with slightly lower Fe, Ca and Mg content than at east of Lodwar. The occurrence of trace elements was like at East of Lodwar town (Ti, Cr, Cu and Zn) with increasing concentrations of Ti from the bottom (3823) to the top (3920) layer (Table 4.8).

Table 4.8: Results and summary statistics for the major oxides, major and trace elements of the Holocene sediments at Napuu/Lolupe area

Major element oxides (wt %)										
Lab No.	SiO ₂	Al ₂ O ₃	CaO	MgO	Na ₂ O	K ₂ O	TiO ₂	MnO	Fe ₂ O ₃	LOI
3820 (A)	66.90	16.05	2.74	1.50	0.15	2.43	0.76	0.10	3.78	5.50
3821 (B)	55.10	14.70	2.55	1.47	0.10	1.87	1.34	0.19	7.70	14.16
3822 (C)	51.80	16.42	2.62	0.11	0.17	1.84	1.24	0.20	7.71	17.09
3823 (D)	80.85	10.92	2.61	0.12	0.12	1.68	0.14	0.17	1.11	2.07
Minimum	51.80	10.92	2.55	0.11	0.10	1.68	0.14	0.10	1.11	2.07
Maximum	80.85	16.42	2.74	1.50	0.17	2.43	1.34	0.20	7.71	17.09
Median	61.00	15.38	2.62	0.80	0.14	1.86	1.00	0.18	5.74	9.83
SD	13.16	2.51	0.08	0.79	0.03	0.33	0.55	0.05	3.23	7.08
Major elements (wt %)										
	Na	Mg	Al	P	S	K	Ca	Mn	Fe	
3820 (A)	nd	0.64	3.76	0.07	0.01	0.39	2.51	0.09	3.03	
3821 (B)	nd	0.73	4.87	0.07	0.00	0.64	1.88	0.14	5.16	
3822 (C)	nd	0.69	4.69	0.06	nd	0.62	1.88	0.14	4.80	
3823 (D)	0.11	0.09	1.72	0.03	0.01	0.11	2.50	0.03	1.23	
Minimum	0.11	0.09	1.72	0.03	0.00	0.11	1.88	0.03	1.23	
Maximum	0.11	0.73	4.87	0.07	0.01	0.64	2.51	0.14	5.16	
Median	n/a	0.67	4.23	0.07	0.01	0.50	2.19	0.12	3.91	
SD	n/a	0.30	1.44	0.02	0.00	0.25	0.36	0.05	1.80	
Trace elements (wt %)										
	Ti	Cr	Co	Ni	Cu	Zn	As	Se	Mo	Pb
3820 (A)	0.14	0.01	0.00	0.00	0.00	0.01	nd	nd	0.00	nd
3821 (B)	0.19	0.01	0.00	0.00	0.00	0.02	nd	nd	0.00	nd
3822 (C)	0.19	0.01	0.00	0.00	0.00	0.02	nd	nd	0.00	nd
3823 (D)	0.02	0.01	nd	0.00	0.00	0.01	nd	nd	0.00	nd

Holocene sediments at Turkwel River bank near Kakwanyang area

The thick layer of Holocene sediments found at the Turkwel River near Kakwanyang consisted of four distinct layers A, B, C and D represented by sample codes 3852 to 3855. SiO₂ (46.07-48.79 %) was comparatively lower than the Holocene sediment in Lodwar and between Napuu and Lolupe areas. Al₂O₃ decreased from the top (18.80 %) to the bottom (9.87 %) of the deposit, while CaO showed the reverse (Figure 4.26). Fe₂O₃ were comparatively higher than in Lolupe and Napuu and decreased from Layer B (15.97 %) to the bottom layer (D) (3.90 %). Similar characteristic was observed for the occurrence of K₂O and Na₂O and minor elements (Ca, Al and Fe) (Table 4.9). Na was detectable in the Holocene sediments at Turkwel River bank near Kakwanyang up to 0.19 wt %. Although Al, Fe, Mg, and Ca are the most abundant major elements like at East of Lodwar,

Napuu and Lolupe areas, Ca concentrations were relatively higher (11.34 %) suggesting increased carbonate content and low composition of clay minerals. The occurrence of trace elements was <0.02 wt % in all the samples (3852 to 3855).

Table 4.9: Results and summary statistics for the major oxides, major and trace elements of the Holocene sediments at Turkwel River bank near Kakwanyang area

Major oxides (wt %)										
Description	SiO ₂	Al ₂ O ₃	CaO	MgO	Na ₂ O	K ₂ O	TiO ₂	MnO	Fe ₂ O ₃	LOI
3852 (A)	48.79	18.90	1.25	1.93	1.30	3.24	1.20	0.14	9.53	13.16
3853 (B)	43.69	18.70	1.01	0.08	1.96	3.41	1.41	0.17	13.15	15.97
3854 (C)	46.51	13.95	8.15	3.05	0.99	2.41	0.14	0.15	6.51	16.72
3855 (D)	46.07	9.87	19.50	2.87	0.87	1.57	0.75	0.60	3.90	12.91
Minimum	43.69	9.87	1.01	0.08	0.87	1.57	0.14	0.14	3.90	12.91
Maximum	48.79	18.90	19.50	3.05	1.96	3.41	1.41	0.60	13.15	16.72
Median	46.29	16.33	4.70	2.40	1.15	2.83	0.98	0.16	8.02	14.57
SD	2.09	4.31	8.67	1.36	0.49	0.85	0.56	0.22	3.98	1.94
Major elements (wt %)										
Description	Na	Mg	Al	P	S	K	Ca	Mn	Fe	
3852 (A)	0.00	1.80	4.23	0.06	0.06	0.36	5.22	0.12	3.96	
3853 (B)	nd	0.75	1.79	0.09	0.07	0.26	14.79	0.71	2.29	
3854 (C)	0.00	4.53	2.06	0.03	0.08	0.12	13.32	0.13	1.17	
3855 (D)	0.19	0.37	1.31	0.08	0.02	0.40	9.36	0.26	1.84	
Minimum	0.00	0.37	1.31	0.03	0.02	0.12	5.22	0.12	1.17	
Maximum	0.19	4.53	4.23	0.09	0.08	0.40	14.79	0.71	3.96	
Median	0.00	1.28	1.93	0.07	0.06	0.31	11.34	0.19	2.06	
SD	0.11	1.88	1.29	0.03	0.02	0.13	4.30	0.28	1.19	
Trace elements (wt %)										
Description	Ti	Cr	Co	Ni	Cu	Zn	As	Se	Mo	Pb
3852 (A)	0.10	0.01	0.00	0.00	0.02	0.02	nd	nd	0.00	nd
3853 (B)	0.10	0.01	0.00	0.00	0.00	0.01	nd	nd	0.00	nd
3854 (C)	0.01	0.01	nd	0.00	nd	0.01	nd	nd	0.00	nd
3855 (D)	0.01	0.01	0.00	0.00	0.00	0.01	nd	nd	0.00	nd

Holocene sediments at Natir

The three samples of Holocene sediments at Natir consisted of the upper layer A (3829), the middle layer B (3827) and the lower layer C (3826). Significant variations in SiO₂ content were observed, with Layer A at 68.97 wt %, Layer B at 12.89 % and Layer C at 24.91 wt %. Different patterns

were found in the Al₂O₃ material, where the first layer had the most composition (10.21 %), followed by the bottom layer (4.89wt %) and then middle layer B (2.01 wt %). Similar characteristics have been observed for K₂O, TiO₂ and Fe₂O₃. Layer B was determined to have elevated CaO, LOI and Ca levels relative to Layer A (3829) and C (3826) (Table 4.10). Al, Fe, Mg, and Ca are the most abundant major elements but with the highest Ca compositions (18.98 %) as compared to at Lodwar, Napuu, Lolupe and at Turkwel River near Kakwanyang. Al, Fe and Mg contents are observed to generally decrease with increasing levels of Ca as you move eastwards from Lodwar town. The occurrence of trace elements was generally low (< 0.02 wt %) except for Layer A (3829) that had levels of 0.06 wt % of Ti.

Table 4.10: Results and summary statistics for the Major oxides, major and trace elements of the Holocene sediments at Natir

Major element oxides (wt %)										
Description	SiO ₂	Al ₂ O ₃	CaO	MgO	Na ₂ O	K ₂ O	TiO ₂	MnO	Fe ₂ O ₃	LOI
3829 (A)	68.97	10.21	1.82	2.67	0.05	1.81	0.62	0.09	4.73	8.48
3827 (B)	12.89	2.01	45.78	0.07	0.04	0.06	0.14	0.52	1.99	36.31
3826 (C)	24.91	4.89	27.15	7.01	0.08	0.72	0.27	0.30	2.14	32.00
Minimum	12.89	2.01	1.82	0.07	0.04	0.06	0.14	0.09	1.99	8.48
Maximum	68.97	10.21	45.78	7.01	0.08	1.81	0.62	0.52	4.73	36.31
Median	24.91	4.89	27.15	2.67	0.05	0.72	0.27	0.30	2.14	32.00
SD	29.53	4.16	22.06	3.51	0.02	0.88	0.25	0.22	1.54	14.98
Major elements (wt %)										
Description	Na	Mg	Al	P	S	K	Ca	Mn	Fe	
3829 (A)	nd	1.36	4.04	0.02	nd	0.27	1.25	0.05	3.32	
3827 (B)	nd	0.34	1.13	nd	0.02	0.07	25.23	0.87	0.88	
3826 (C)	0.00	2.83	1.62	0.03	0.02	0.09	18.98	0.23	1.18	
Minimum	0.00	0.34	1.13	0.02	0.02	0.07	1.25	0.05	0.88	
Maximum	0.00	2.83	4.04	0.03	0.02	0.27	25.23	0.87	3.32	
Median	n/a	1.36	1.62	0.03	0.02	0.09	18.98	0.23	1.18	
SD	n/a	1.25	1.56	0.00	0.00	0.11	12.44	0.43	1.33	
Trace elements (wt %)										
Description	Ti	Cr	Co	Ni	Cu	Zn	As	Se	Mo	Pb
3829 (A)	0.06	0.01	0.00	0.00	0.00	0.01	nd	nd	0.00	nd
3827 (B)	nd	0.01	nd	0.02	nd	0.01	nd	0.00	0.00	nd
3826 (C)	0.02	0.00	nd	0.00	nd	0.01	nd	nd	0.00	nd

Sources of Holocene sediments

The $\text{SiO}_2 / \text{Al}_2\text{O}_3$ ratio is used to determine the maturity of sedimentary rocks, as well as the presence of quartz in comparison to clay minerals and feldspar (Cullers, 1994). Values of $\text{SiO}_2/\text{Al}_2\text{O}_3$ ratio >5.0 indicate the progressive maturity of the sediments (Shekhar *et al.*, 2018). The Holocene sediments in the study area have moderate (2.3 to 4.7) to high values (5.1 to 7.4) indicating a low degree of clay (Table 4.11), suggesting that samples in Natir and those underlying Napuu and Lolupe are mature. The sediments at Turkwel River at Kakwanyang have an average ratio of 3.9, suggesting they are immature and are derived from mixed sources (Obasi, 2015). Mature Holocene sediments in the study area may represent the 10,000 yr BP sedimentation while the immature samples of Holocene sediments with medium to moderate $\text{SiO}_2/\text{Al}_2\text{O}_3$ ratio represent the 4,000 yr BP deposits. The $\text{K}_2\text{O} / \text{Al}_2\text{O}_3$ ratio is slightly diverse for clay minerals and feldspars and is used as a pointer of the source composition of pelitic sedimentary rocks. Pelitic sedimentary rocks with a $\text{K}_2\text{O} / \text{Al}_2\text{O}_3$ ratio of > 0.5 indicate a significant concentration of alkali feldspar relative to other minerals in the original rock, while those with a $\text{K}_2\text{O} / \text{Al}_2\text{O}_3$ ratio of < 0.4 indicate that pelitic sedimentary rocks are recycled (Cox *et al.*, 1995). In all the samples of the Holocene sediments of the study area, the ratio of $\text{K}_2\text{O} / \text{Al}_2\text{O}_3$ was ≤ 0.2 ; therefore, they are derived from older pelitic sedimentary rocks. The spatial variability of the chemistry of the Holocene sediments suggests varied sediment sources of igneous, sedimentary, and metamorphic origin to a large extent.

Table 4.11: Ratio of SiO_2 / Al_2O_3 showing the maturity of Holocene sediments in the study area while the ratio of K_2O / Al_2O_3 indicating the pelitic origin of the sediments

No.	Description	Lab No.	SiO_2 / Al_2O_3	K_2O / Al_2O_3
1	East of Lodwar	3824 (A)	3.5	0.1
2	East of Lodwar	3825 (B)	5.9	0.2
3	Napuu/Lolupe	3820 (A)	4.2	0.2
4	Napuu/Lolupe	3821 (B)	3.7	0.1
5	Napuu/Lolupe	3822 (C)	3.2	0.1
6	Napuu/Lolupe	3823 (D)	7.4	0.2
7	Turkwel River at Kakwanyang	3852 (A)	2.6	0.2
8	Turkwel River at Kakwanyang	3853 (B)	2.3	0.2
9	Turkwel River at Kakwanyang	3854 (C)	3.3	0.2
10	Turkwel River at Kakwanyang	3855 (D)	4.7	0.2
11	Natir	3829 (A)	6.8	0.2
12	Natir	3827 (B)	6.4	0.0
13	Natir	3826 (C)	5.1	0.1

(c) Sandstone

Fine-grained consolidated sandstone and coarse-grained unconsolidated sandstone displayed variations in the composition's major chemical oxides. The coarse-grained sandstone is rich in SiO_2 , Al_2O_3 , MgO , Na_2O , K_2O , TiO_2 , and Fe_2O_3 . The fine-grained sandstone, on the other hand, had higher CaO and LOI as compared to the coarse-grained counterpart. Ca (15.43%), Al (1.50 wt %), Fe (0.98 wt %) and Mg (0.75 wt %) are the major elements in the fine-grained sandstone. Higher relative concentrations of Al (2.68 wt %) and Mg (1.09 wt %) are observed in the coarse-grained sandstone, indicating more elevated amounts of silicate minerals than the carbonate counterparts. Generally, the sandstone in the study area has low compositions (<0.05%) of trace elements, Ti , Cr , Mn , Co , Ni , Cu , Zn , As , Se , Mo and Pb , suggesting possible leaching and dispersion processes (Table 4.12).

Table 4.12: Results and summary statistics for the major oxides in the (a) fine-grained sandstone and (b) coarse-grained sandstone in the study area

(a) Major oxides - fine-grained sandstone (wt. %)										
Lab No.	SiO ₂	Al ₂ O ₃	CaO	MgO	Na ₂ O	K ₂ O	TiO ₂	MnO	Fe ₂ O ₃	LOI
1645	40.01	7.70	25.15	1.81	0.89	1.13	0.40	0.31	3.40	18.19
1659	47.61	9.03	24.42	0.04	0.37	1.32	0.50	0.38	6.15	10.11
1668	49.40	5.87	18.61	4.13	0.65	1.12	0.30	0.12	1.90	17.49
1669	52.60	5.15	24.91	4.70	0.53	0.84	0.19	0.07	1.60	9.25
3832	47.84	5.92	25.01	0.02	0.06	1.32	0.17	0.50	1.50	17.20
3833	48.09	5.32	24.91	0.03	0.13	1.51	0.16	0.18	1.18	18.47
3850	30.91	6.51	27.90	0.10	0.21	1.35	0.64	1.21	8.53	22.59
3858	40.01	7.50	26.20	0.05	0.87	1.09	0.41	0.32	3.61	18.86
Minimum	30.91	5.15	18.61	0.02	0.06	0.84	0.16	0.07	1.18	9.25
Maximum	52.60	9.03	27.90	4.70	0.89	1.51	0.64	1.21	8.53	22.59
Median	47.73	6.22	24.96	0.08	0.45	1.23	0.35	0.32	2.65	17.84
SD	7.05	1.35	2.67	1.99	0.32	0.21	0.17	0.36	2.62	4.54
(b) major oxides - coarse-grained sandstone (wt. %)										
	SiO ₂	Al ₂ O ₃	CaO	MgO	Na ₂ O	K ₂ O	TiO ₂	MnO	Fe ₂ O ₃	LOI
1658	55.80	13.41	7.60	3.15	1.55	2.61	0.92	0.13	5.15	9.08
1670	64.02	11.87	4.87	4.31	0.72	1.51	0.70	0.06	3.92	8.01
1675	62.07	10.92	10.91	0.02	1.86	2.14	0.42	0.17	2.40	8.99
1676	72.00	10.93	4.60	1.41	0.80	2.30	0.39	0.09	2.40	5.06
1678	65.10	13.69	1.72	2.82	0.49	1.95	0.64	0.09	4.05	9.44
3842	26.67	12.31	8.05	21.01	5.04	6.31	0.17	0.05	0.92	19.03
3847	57.50	20.15	8.59	6.79	0.12	0.43	0.13	0.09	5.47	0.46
Minimum	26.67	10.92	1.72	0.02	0.12	0.43	0.13	0.05	0.92	0.46
Maximum	72.00	20.15	10.91	21.01	5.04	6.31	0.92	0.17	5.47	19.03
Median	62.07	12.31	7.60	3.15	0.80	2.14	0.42	0.09	3.92	8.99
SD	14.63	3.20	3.07	7.11	1.67	1.84	0.29	0.04	1.64	5.61

Table 4.13: Results and summary statistics for the major elements in the (a) fine-grained sandstone and (b) coarse-grained sandstone in the study area

(a) Major elements - fine-grained sandstone (wt. %)									
Sample	Na	Mg	Al	P	S	K	Ca	Mn	Fe
3832	0.19	0.24	0.95	0.04	0.03	0.22	19.13	0.22	0.99
3833	0.22	0.24	0.94	0.03	0.04	0.21	18.21	0.22	0.97
3850	nd	1.26	5.89	0.07	0.02	0.88	0.62	0.09	6.88
3858	0.00	3.91	2.04	0.05	0.02	0.12	12.65	0.11	0.97
Minimum	0.00	0.24	0.94	0.03	0.02	0.12	0.62	0.09	0.97
Maximum	0.22	3.91	5.89	0.07	0.04	0.88	19.13	0.22	6.88
Median	0.19	0.75	1.50	0.04	0.03	0.22	15.43	0.17	0.98
SD	0.12	1.74	2.34	0.02	0.01	0.35	8.52	0.07	2.95
(b) major elements - coarse-grained sandstone (wt. %)									
1675	nd	1.09	2.68	0.04	0.03	0.15	11.09	0.15	1.70
1676	nd	1.07	2.63	0.06	0.01	0.22	7.74	0.11	1.91
1678	nd	1.09	4.37	0.03	nd	0.30	1.18	0.05	3.68
3842-18	0.27	0.29	4.73	0.03	0.01	0.74	1.37	0.19	3.41
3847-18	0.00	2.67	1.49	0.01	0.08	0.07	19.70	0.15	0.97
Minimum	0.00	0.29	1.49	0.01	0.01	0.07	1.18	0.05	0.97
Maximum	0.27	2.67	4.73	0.06	0.08	0.74	19.70	0.19	3.68
Median	0.13	1.09	2.68	0.03	0.02	0.22	7.74	0.15	1.91
SD	0.19	0.87	1.34	0.01	0.03	0.26	7.69	0.05	1.16

Classification of sandstone

Sandstones are classified using bivariate diagram plots based on the chemical compositions of their three major oxide groups: silica and alumina, alkali oxide, and iron oxide plus magnesia. Sandstone classification (Figure 4.21) showed that the sandstone formation comprises five distinct groups; Fe-sand, Fe-shale, wacke, litharenite, and arkose. The majority of the coarse sandstone falls within the wacke category while the fine-grained sandstone comprised mainly the litharenite and wacke categories.

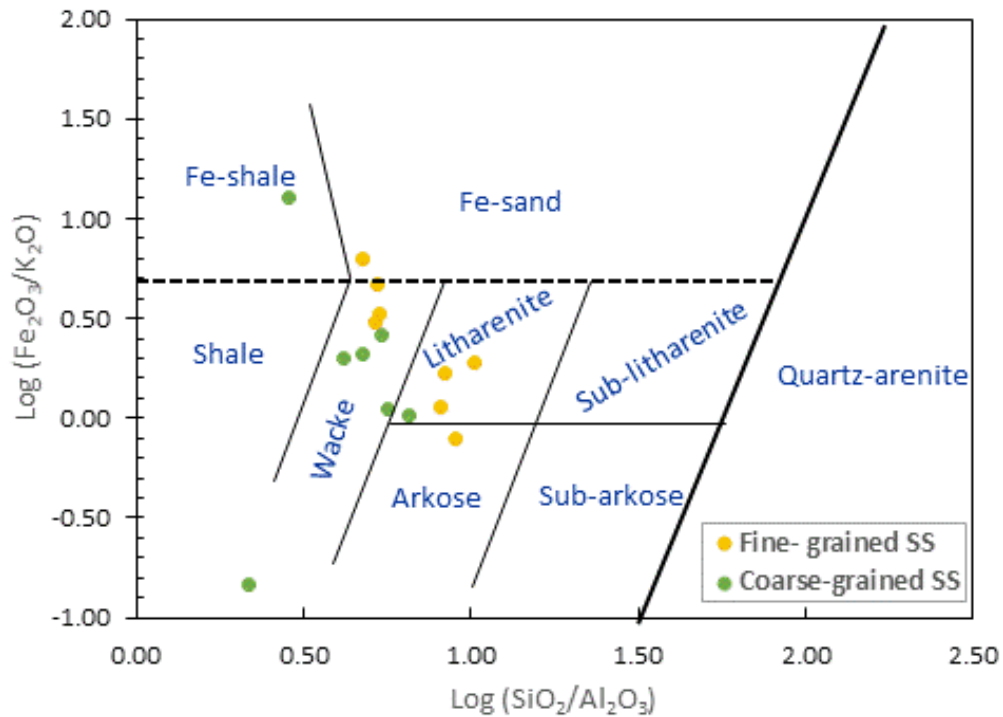


Figure 4.21: Sandstone classification diagram after Herron (1988)

(d) Conglomerate – Specimens 1677 and 3857

The mineralogical compositions of two specimens of conglomerate collected at Lodwar town (1677) and Natir area (3857) were as follows; SiO₂ ranged was 60.07% for sample 1677 and 71.60% for sample 3857. There was no significant variation in Al₂O₃ (1677 = 9.72 and 3857 (9.15%) and that of Fe₂O₃ (1677=2.03 % and 3857 = 2.51%) (Figure 4.22). The conglomerate at Natir had higher CaO (12.15%) as compared to that at Lodwar town (4.99 %). Similarly, LOI (8.68%), K₂O (3.52%), Na₂O (1.7%), and MnO (0.70%) were also higher in this formation. In terms of minor elements, Ca was relatively higher (14.86%) for the conglomerate at Natir than in Lodwar town (2.63%) and is believed to be derived from the underlying Turkana grits. Mg (2.20%) was also observed to be higher in sample 3857 than in specimen 1677 (1.08). Al, Fe, and Ti were observed to be slightly higher in specimen 1677 than in specimen 3857, while there were no significant variations in P, S, K, Cr, Ni, Cu, Zn and Mo with concentrations <0.05%.

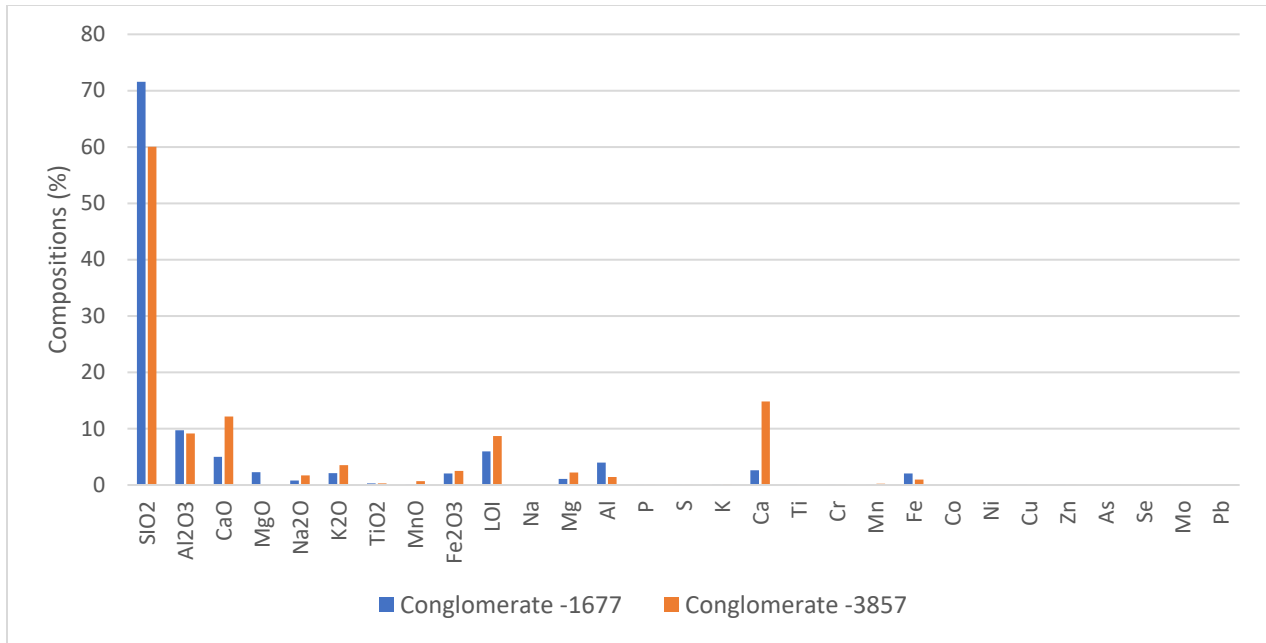


Figure 4.22: Variations of major and trace elements in the conglomerate at Lodwar town (1677) and Natir area (3857)

(e) Grainstone

Generally, slight variations were observed in the compositions of major elements in Grainstone except for CaO that was relatively higher (23.00 %) in the fine-grained sample (1657). The coarse-grained grainstone had higher levels of SiO₂ (64.30%), Al₂O₃ (8.30%), MgO (5.19%), K₂O (2.19%), and Na₂O (0.73%) than in medium-grained grainstone; SiO₂ (58.07%), Al₂O₃ (5.80 %), MgO (0.02%), K₂O (1.06%), and Na₂O (0.20%) (Figure 4.23). Occurrence of minor elements in the medium-grained grainstone was as follows; Ca =17.18%, Al = 1.37%, Fe = 1.22%, Mg = 0.43%, Mn =0.41% and K = 14%. The compositions of Na, P, S, Cr, Ni, Zn, Se and Mo ranged from <0.01 to 0.05% while Ti, Cu, As and Pb were not detected limits in the rock samples.

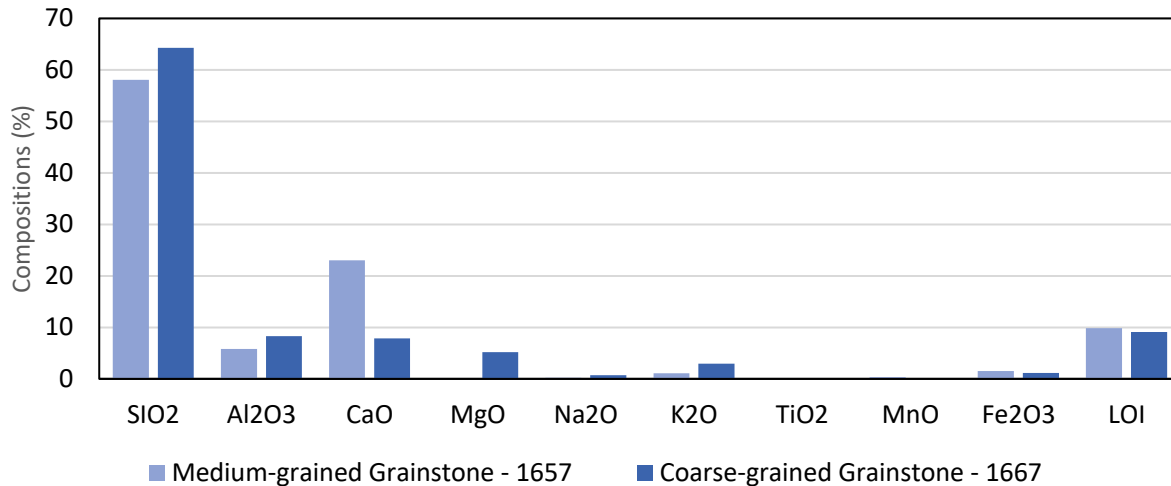


Figure 4.23: Variations in compositions of major elements in Grainstone samples

(iii) Volcanic rocks

(a) Nepheline-phonolites

SiO₂ in the nepheline-phonolite ranged from 48.24 to 54.81 % with the specimen that formed a contact with the Turkana grit (1653) having the highest silica content. The nepheline-phonolite at contact zone also had the highest compositions of Al₂O₃ (15.31 %), CaO (8.20 %) and K₂O (2.50 %). Slight variations in the Fe₂O₃ content were observed with values ranging from 9.61 to 10.08%. The rock samples also had low Na₂O (0.90 -1.28 %) and MnO (0.16 - 0.70 %) compositions as compared to the rest of the oxides (Figure 4.24). The occurrence of the minor and trace elements was determined for specimen 1650 of the nepheline-phonolite and the Turkana grit sample at contact zone (1653). As a result, S, As, and Pb were not detected while Mg was determined to be 1.37% at the contact zone. Fe (3.62-6.01 %), Al (3.87 - 5.46 %), and Ca (1.69 - 6.80 %) were the most abundant minor elements, followed by K (0.52 -0.87 %), Ti (0.10- 0.71 %), P (0.08 - 0.33 %) and Mn (0.13 - 0.20%). Concentrations <0.01 to 0.02% were observed in Na, Cr, Co, Ni, Cu, Zn, Se and Mo.

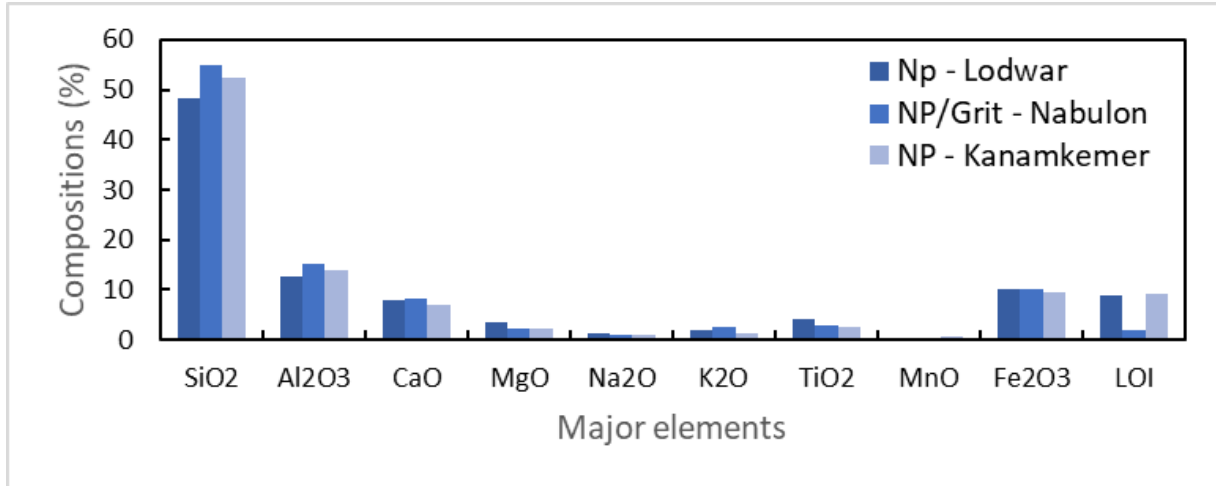


Figure 4.24: Distribution of the major elements in the rock samples of the nepheline-phonolite at Lodwar town, grit contact and at Kanamkemer

(b) Augite basalts

The analysis of the distribution of the major elements in the augite basalt was as follows; SiO₂ (53.79 %), Al₂O₃ (18.00%), moisture and volatile materials (9.22%), Fe₂O₃ (6.08%), CaO (5.69%), Fe (5.08%), Ca (4.99%), Al (4.70%), MgO (3.22%), K₂O (2.06%), Mg (1.26%), and TiO₂ (1.09%). Fe (5.09%), Ca (4.99%), Al (4.70%), and Mg (1.26%) had significant concentrations of the minor elements while K, P, and Mn were ranged from 0.17 to 0.48%. All the trace elements were 0.26% in the augite basalt (Figure 4.25).

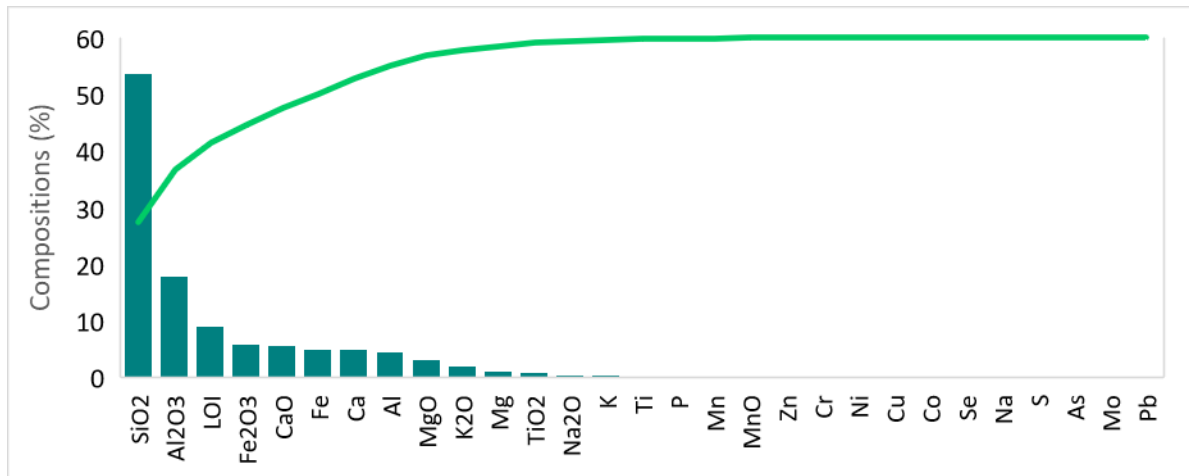


Figure 4.25: Occurrence of major and trace elements in the augite basalt with a cumulative frequency curve showing their distribution

(c) Dolerite dyke

Variations in the compositions of the major elements for two igneous intrusions; dolerite dyke (1656) in the Turkana grits and that in the quartzo-feldspathic gneiss were observed. The dolerite in the basement system had higher levels of SiO₂ (74.09 %) and MgO (7.31 %) than for that in the Turkana grits (SiO₂ = 50.59% and MgO = 1.71%). Similar compositions of CaO were observed; specimen 1656 (4.70%) and 3845 (4.99%) while the compositions of Al₂O₃, K₂O, TiO₂, Fe₂O₃ and LOI were higher in the dolerite in the Turkana grits (Figure 4.26). Minor and trace elements were not measured in the dolerite within the Turkana grits.

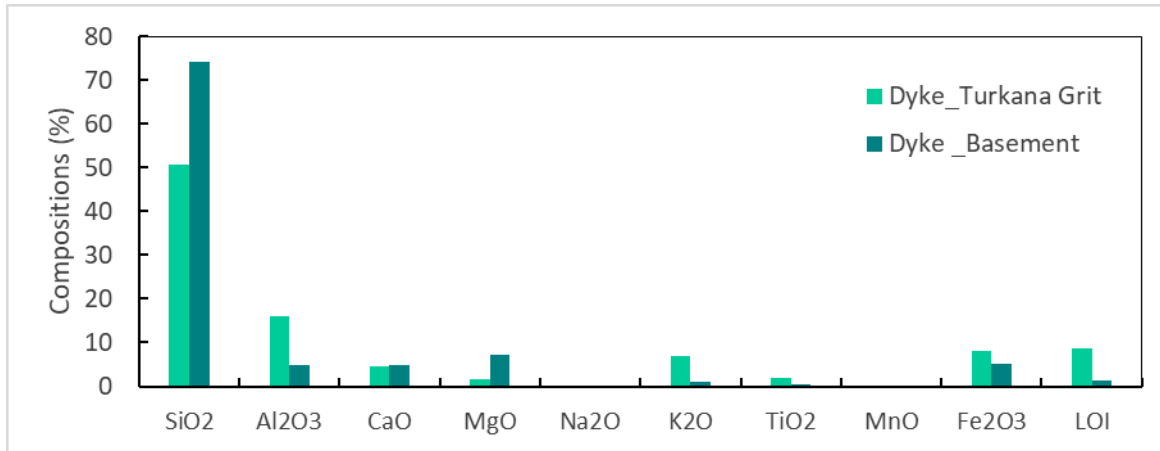


Figure 4.26: Compositions of major elements in the dolerite dyke in the Turkana grits and in the Basement system

Classification of Volcanic rocks

The TAS classification diagram (Figure 4.30) revealed that the nepheline phonolite at Lodwar town and that forming contact with the Turkana grits belonged to basaltic-andesite group while augite basalt and the nepheline phonolite at Kanamkemer area were identified to be volcanic andesite. The intrusive rock was identified to be a dolerite of distinct volcanic origins; the dolerite dyke in the Turkana grit was determined to be basaltic trachyandesite in nature while the intrusion in the basement system identified to be dacite rock grading into rhyolite. The AFM classification of the volcanic rocks in the study area based after Irvine and Baragar (1971) showed that augite basalt and dolerite in the Turkana grit being calc-alkaline while the nepheline-phonolite, and the dolerite in the Basement system as tholeiitic in nature Figure 4.33.

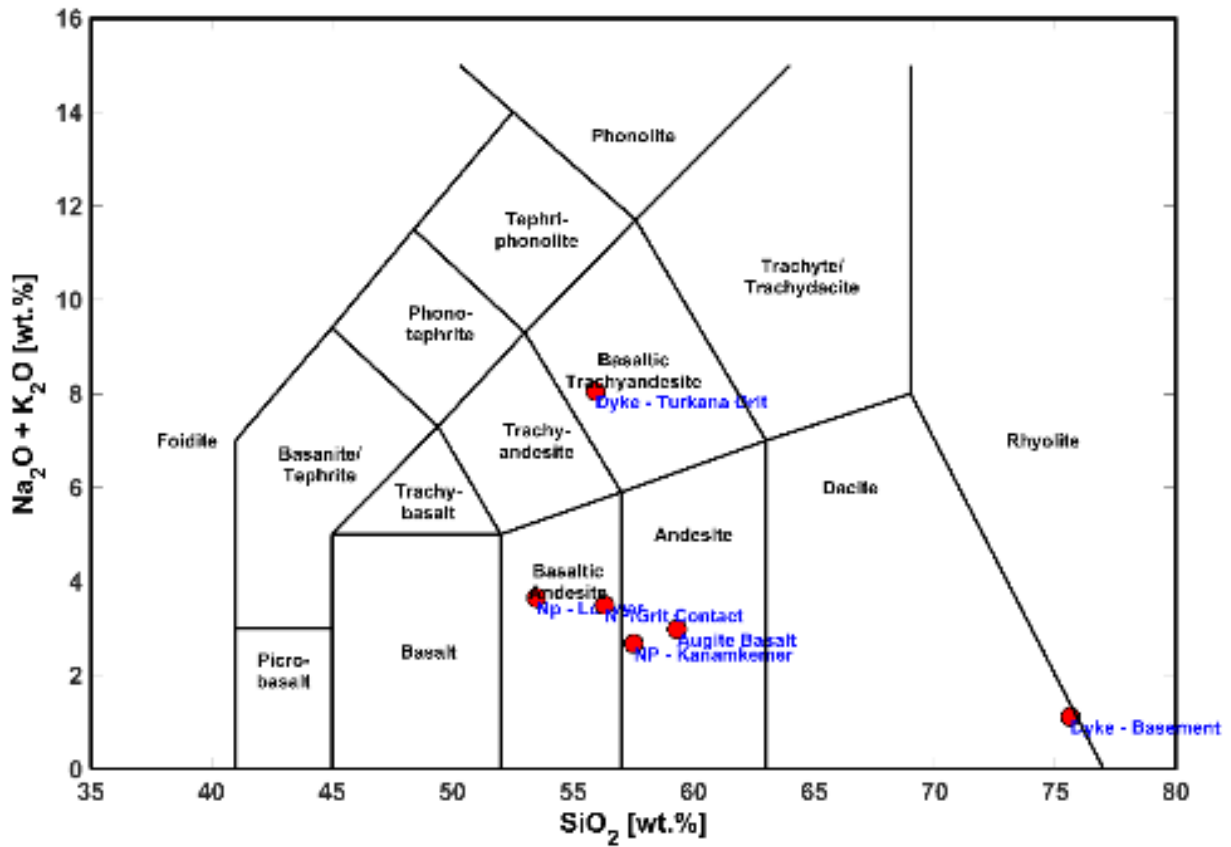


Figure 4.27: TAS classification diagram for the volcanic rocks

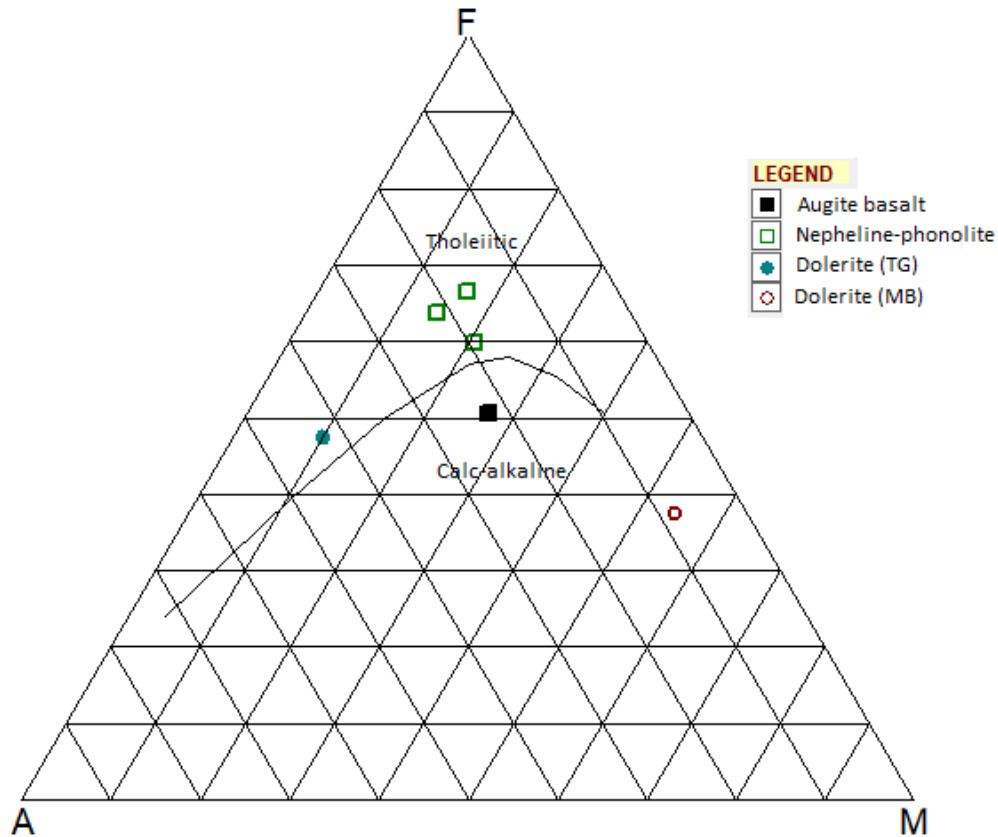


Figure 4.28: AFM classification diagram After Irvine et al., 1971 showing augite basalt and dolerite in the Turkana grit being cacl-alkaline while the nepheline-phonolite, and the dolerite in the Basement system as tholeiitic in nature

4.2.1.5 Results of the Geophysical Survey

The results of the 26 vertical electrical soundings (VES) carried out in Sections A-D of the LAAS aquifer are presented. Table 4.16 and Table 4.17 provide the field VES results, where VES 2 was disregarded due to poor potential contact during the geophysical survey. A graph of apparent resistivity (Ωm) against electrode spacing (m) was prepared for each of the VES points using IP2WIN inversion software. The graph shows the number of layers (N), apparent resistivity value (ρ), the thickness of the layer (h) and depth bgl (d).

LAAS Section A

Section A consists of the aquifer section west of the Lodwar municipality and north of the Turkwel River, where four VES measurements were carried out (VES 17, 18, 19 and 20) with AB/2 of 200 m and five geoelectric layers were displayed (Appendix 4-12). The first layer had resistivity values

ranging from 24.40 to 100.00 Ohm-m and up to 3.75 m bgl while the second layer had resistivity ranging between 136.00 to 183.00 Ohm-m to a depth of 12 m. The resistivity of the third layer ranged from 17.00 to 28.70 Ohm-m at depths between 22.50 to 60.00 m, followed by a fourth layer with low resistivity values of 3.95 to 13.00 Ohm-m at a depth of 25.00 – 160.00 m. The fifth (bottom) layer had resistivity <10.00 Ohm-m at a depth >163.00 m, these readings were carried out shortly after the long rains in May 2018 and, thus, the low resistivity values of the first top layer and the second layer regarded as unsaturated sands. The third and the fourth layer are likely to be saturated with fresh water while the resistivity of the fifth layer (< 10 Ohm-m) reflect saline groundwater or clay. Pseudo-cross-section (Figure 4.29) shows resistivity distribution of the sub-surface strata across VES 20, 18, and VES 19. The VES 20 was conducted in the area adjacent to Turkana grits formation, and thus the huge disparity with VES 19, 18 and 17.

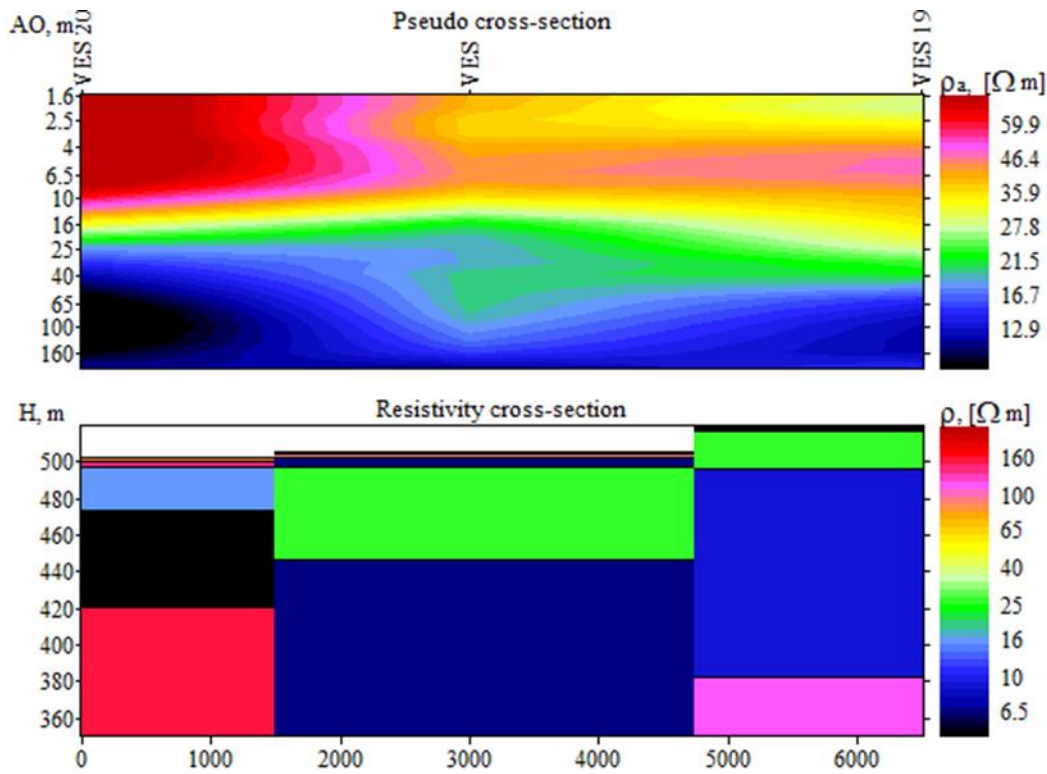


Figure 4.29: Pseudo-cross-section and resistivity cross-section between VES 18, 19 and 20 where VES 17 was omitted from the pseudo section since it was not in the straight path with the three selected points

LAAS Section B

Section B of the LAAS system covers the area west of the municipality of Lodwar and the south of the Turkwel River, stretching from Kakemera to Nachomin areas where seven resistivity measurements were performed (VES 13, 14, 15, 16, 23, 24 and 25). The results of the geophysical survey indicated that four geoelectric layers underlie this section of the aquifer (Appendix 4-13). Disparities were observed in the resistivity values of the top layer in this area up to a depth of 3.50 m; VES 16 and 23 had the lowest resistivity value of 17.70 and 23.20 Ohm-m attributed to the wet top surface at the time of the survey. Moderate resistivity values between 53.00 to 86.40 Ohm-m were recorded at VES 13, 15 and 24. Highest resistivity values (average = 256.60 Ohm-m) were recorded at VES 14 and 25. The second layer had moderate resistivity values ranging from 29.8 to 39.8 Ohm-m at a depth of 4.30 at VES 16 and VES 23 and up to a depth of 16.00 m at VES 24. This layer was not identified in VES 13 and 15, which were carried out in the adjacent Turkana grits. The third layer had resistivity ranging between 17.00 and 79.40 Ohm-m and occurred at varying depths, between 5.50 to 35.00 m to the east and between 6.50 to 100.00 m to the west of the area., and can be associated with fresh groundwater in this section. The fourth layer had resistivity 10 Ohm-m and interpreted to be an aquiclude (clay layer). Pseudo-sections were prepared for VES 13, 15, 16, 23, and 24 to show the sub-surface resistivity distribution of rocks in the area (Figure 4 30).

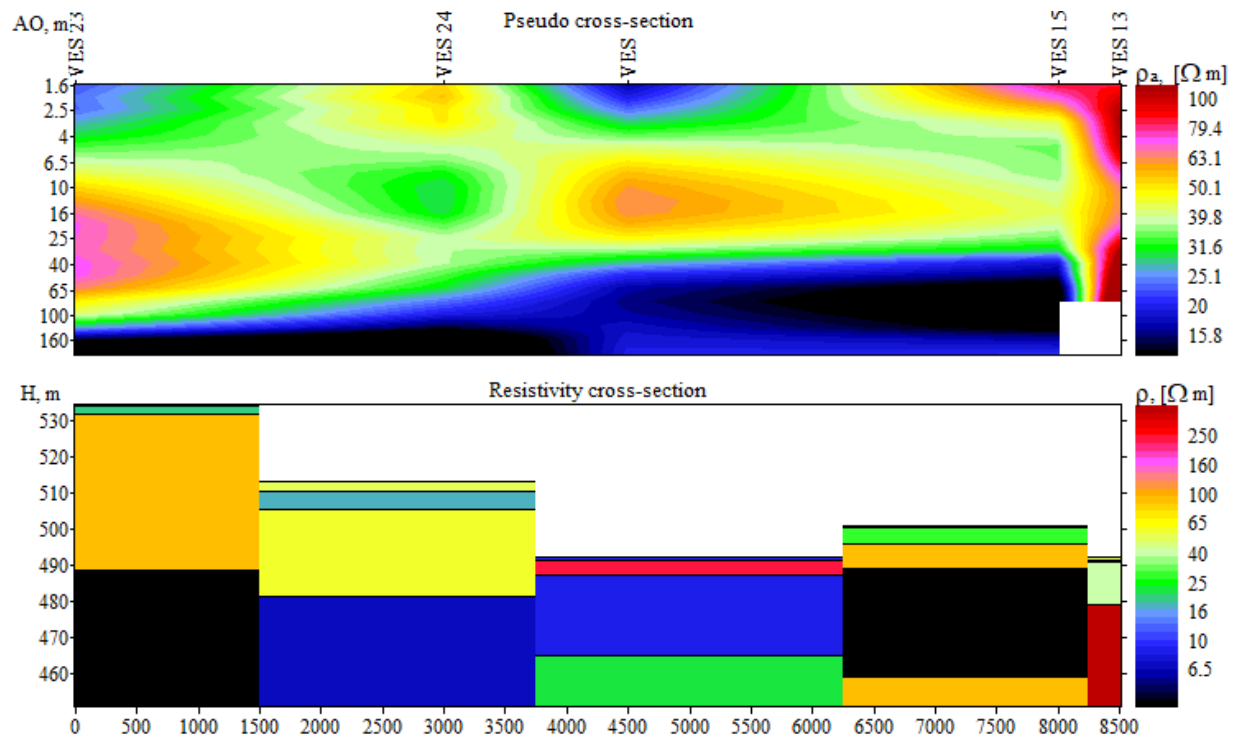


Figure 4.30: Pseudo-cross-section and resistivity cross-section between Kakemera (east) and Nachomin (west) areas (VES 13, 15,16, 24, and 23)

LAAS Section C

Section C of the LAAS covered East of Lodwar municipality and north of the Turkwel River, including Kakwanyang and Nang’omo areas. Only two vertical electrical soundings were carried out in this section (VES 21 and 22) due to thick vegetation cover. Three layers were identified in this section of the aquifer, where VES 21 had generally higher resistivities than VES 22. The first layer had resistivity values between 62.69 and 140.00 Ohm-m, while the second layer had moderate resistivity values from 36.10 to 56.30 Ohm-m up to a depth of 16 m. Below this layer are resistivity values between 12.00 to 27.77 Ohm-m up to a depth > 100 m reflecting resistivities of a saturated formation. A low resistivity layer of < 10 Ohm-m is believed to underlie this site based on the observed trends of resistivity (Figure 4.31).

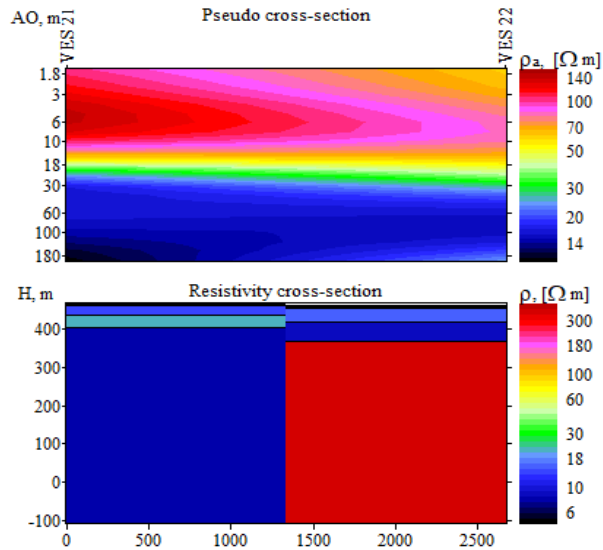


Figure 4.31: Pseudo-cross-section and resistivity cross-section of VES 21 and VEs 22 between Kakwanyang and Nang'omo areas

LAAS Section D

Section D of the LAAS covers the area East of Lodwar municipality and south of Turkwel River, including Napuu, Lolupe, and Nayuu areas. A total of 13 vertical electrical soundings were carried out within a thin section (VES 1, VES 3 to VES 12, VES 26 and VES 27). More electrical soundings were considered in this area than in other parts of the LAAS due to the large area and increased groundwater abstraction observed (See Figure 3.4). The VES results in this section revealed three distinct groups of electrical resistivities;

- 1) Group 1 comprised low to moderate resistivity values (VES 9, 10, 11, 12, and 26) and were located in the Holocene sediments at Lolupe and Nayuu areas. The top layer had average resistivity values between 50.00 and 130.00 Ohm-m to a depth of 2.50 m of 62.32. The second layer had medium resistivity values between 150.00 and 480.00 Ω m while the third layer consisted of relatively lower resistivity values than the second layer (18.00 and 35.00 Ω m) from depths ranging from 40 to 100 m and may be hosting fresh groundwater between Lolupe and Nayuu areas. Resistivity values $< 10.00 \Omega$ m underlie the area and may be clayey materials or saline groundwater.

- 2) Group 2 comprised VES 1, 3,4, 6 and 7 and were located in the Holocene sediments adjacent to the Turkana grits in Lodwar (VES 1) and between Napuu and Lolupe areas (VES 3, 4, 6 and 7). These VES points are characterised by medium to high resistivity values (300 to 1070 Ohm-m) in the upper layer, 90 to 140 Ohm-m in the second layer and while the third layer comprised resistivity values ranging from 25 to 65 Ohm-m from 40 to 160 m, which is considered deeper than between Lolupe and Nayuu areas (group 2). The fourth layer comprise resistivity values $< 10 \Omega \text{ m}$ representing that of clay layer or saline groundwater.
- 3) Group 3 comprised VES 5, 8 and 27 located in the Turkana grits and were characterised by extremely high resistivity values (1260 to 3825.00 Ohm-m) in the upper layers and very low resistivity values in the bottom layer ($< 10 \text{ Ohm-m}$). The middle layers had relatively high values between 200 to 800 Ohm (second layer) followed by a third layer with resistivity values from < 10.00 and 70.00 Ohm-m . The Turkana grit is highly consolidated and thus the high resistivities observed in this formation. The low resistivity values recorded in this formation is associated with saline groundwater.

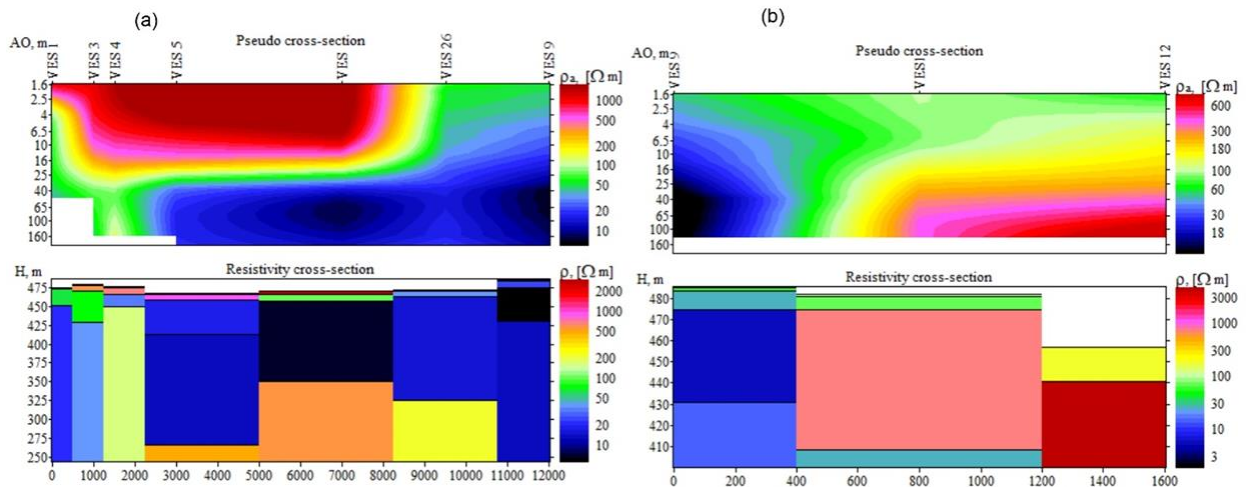


Figure 4.32: Pseudo-cross-section from west to east of Section D of the LAAS (a) and from south to north (b) toward the Turkwel River

(i) Aquifer geometry and storage capacity

The aquifer geometry and storage of the Lodwar Alluvial Aquifer System was assessed based on the aquifer properties described from the secondary data of the boreholes in section 4.2.1.1 (porosity, aquifer thickness, and aquifer depth) and calculated areas of each part of the aquifer as indicated in Table 4.15. Electrical resistivity values in the investigated area for Layer 1 (ρ^1) to Layer 4 (ρ^4) were plotted in Surfer Software to evaluate their variation in LAAS (Figure 4.33). The Lodwar Alluvial Aquifer System covers an area of 104.93 km² east and west of the Lodwar Municipality. The average depth to the aquifer as well as the aquifer thicknesses varied within the aquifer sections (A, B, C, D), based on drilled depth information, in addition to the different resistivity values (Figure 4.34). The total estimated aquifer storage was 1.3 Billion Cubic Meter (BCM).

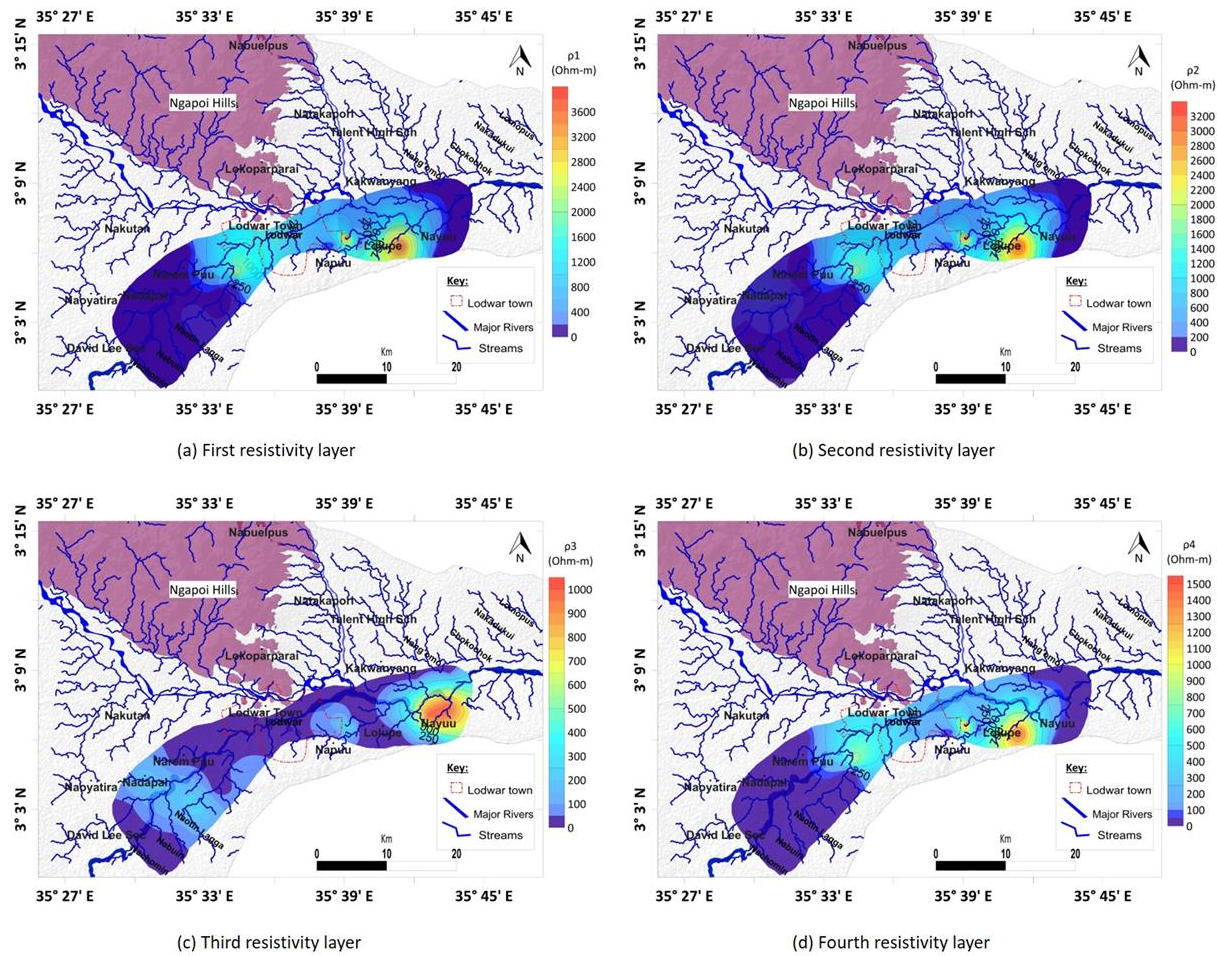


Figure 4.33: Variations in electrical resistivities values with depth (ρ_1 to ρ_4) based on the 26 VES locations

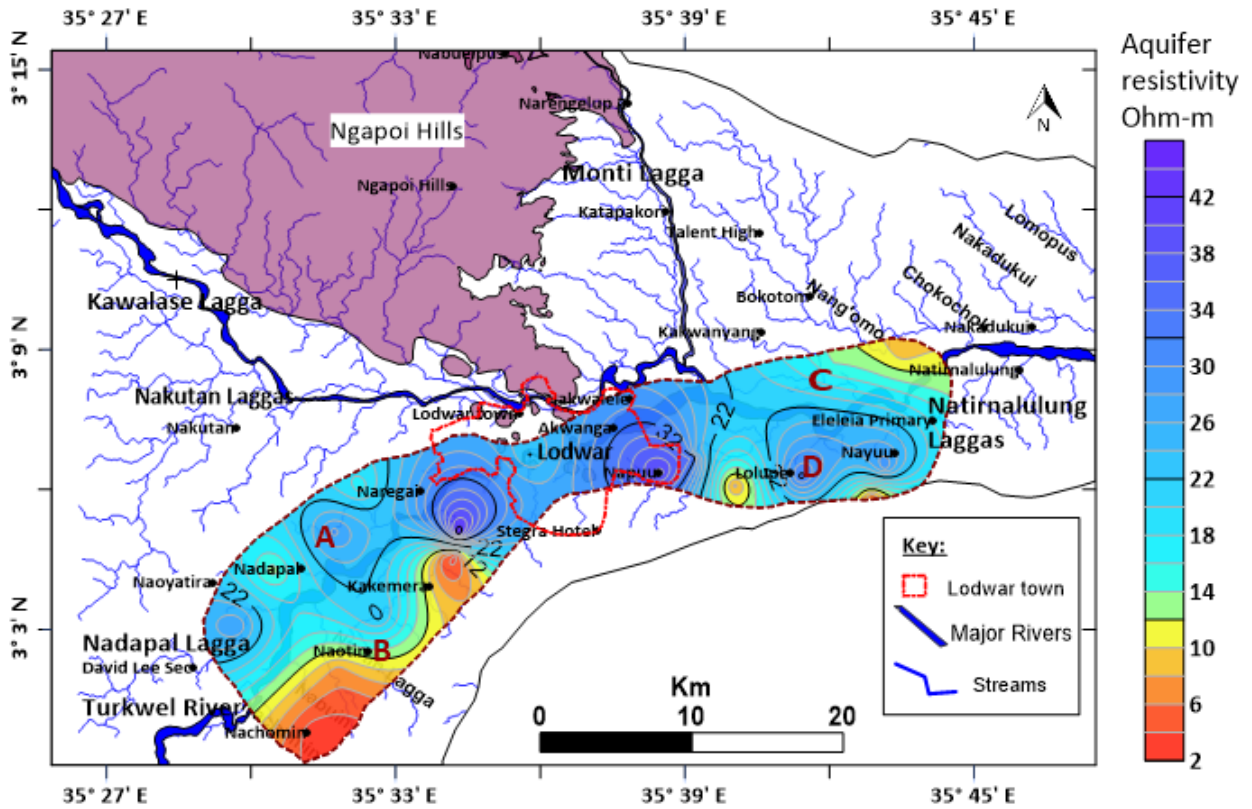


Figure 4.34: Resistivity values of the inferred aquifer layer in the study area showing values <10 Ohm-m indicating possible saline groundwater

Table 4.14: Calculated aquifer properties based on geological mapping, secondary data and geophysics covering the proposed aquifer sections

Aquifer Section	Section A	Section B	Section C	Section D	Section E	Section F	Total
Area (m ²)	23,687,141	32,662,565	10,245,935	35,106,056	1,678,132	1,550,128	
Area covered by the aquifer (Km ²)	23.69	32.66	10.25	35.11	1.68	1.55	104.93
Average Porosity	0.20	0.17	0.22	0.25	0.20	0.17	
Average aquifer Depth (m)	37.50	40.00	30.00	87.50	27.50	32.50	
Approximated aquifer Storage (m ³)	180,022,272	222,105,442	67,623,171	772,333,232	9,397,539	8,696,218	1,260,177,874
Average aquifer thickness = b	12	25	15	45	8	10	

4.2.1.6 Aquifer Characteristics of the LAAS

A total of 71 georeferenced data points was obtained and analysed (see section 3.4.1.1). In this dataset, all the 71 wells have drilled depth information, 52 have static water levels (swl) and water rest levels (wrl), 50 have tested yield data, while 47 have elevation data. Majority of the boreholes are distributed along the Turkwel River and are mainly concentrated within Lodwar Municipality (Figure 4.35). These wells have not been classified as either boreholes or handpumps since the information was missing.

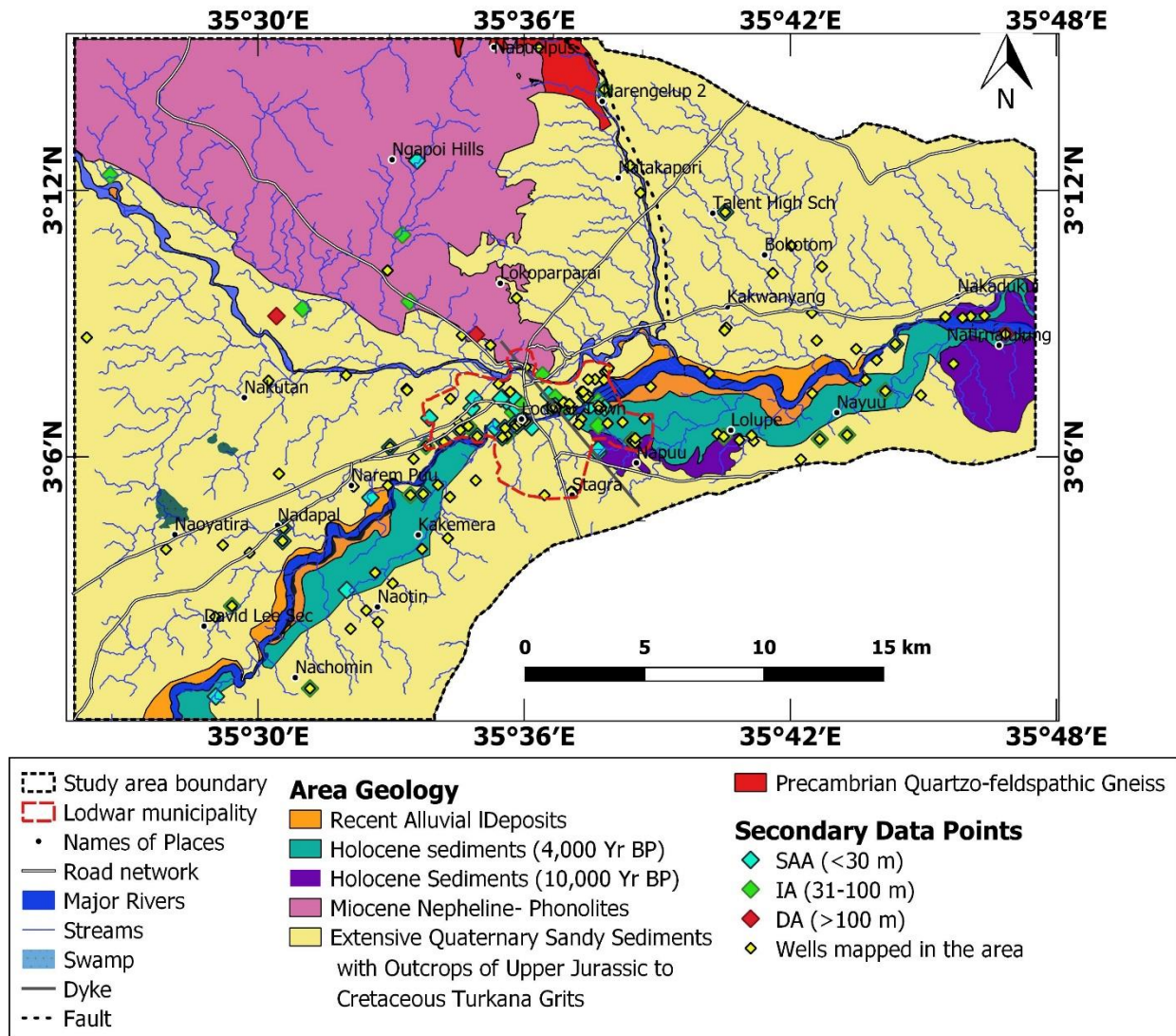


Figure 4.35: Distribution of secondary data points in the study area with depth information - the majority of shallow boreholes are along the Turkwel River and are mainly concentrated within Lodwar town

(i) Aquifer depth

The drilled depth of boreholes ranged between 5.6 and 121.0 m below ground level. Boreholes with a depth between 5.6 and 30.0 m are in the shallow aquifer (44), 31.0 to 100.0 m deep are in the intermediate aquifer (23), while boreholes with depth > 100.0 m (four) are considered to be in the deep aquifer (cf. Olago 2018). Thus, the majority of the wells (62%) tap the shallow aquifer while the rest tap either the intermediate aquifer (32%) or the deep aquifer (6%). From Figure 4 -

14 above, it can be noted that the shallow boreholes are within the riparian zones of the Turkwel River while deeper wells are located outwards.

(ii) Aquifer yield

Of the 71 boreholes in the study area obtained from the Water Resources Authority database, 51 had tested yield information as follows; 36 in the SA, 11 in the IA and three in the deep aquifer. The yields of boreholes in the shallow aquifer (<30.0 m deep) ranged from 1.02 – 77.00 m³/h, 0.30 – 27.00 m³/h in the intermediate aquifer and between 45.00 to 100.00 m³/h in the deep aquifer. The average yields of the wells in the shallow and intermediate aquifers were 16.87 m³/h and 8.28 m³/h, respectively. The yields of the three wells in the deep aquifer are as follows: Napuu Bh, 100.00 m³/h; Natir Bh, 8.00 m³/h and; borehole C5167, 4.5 m³/h.

(iii) Static water levels (swl) and water rest levels (wrl)

The water rest levels ranged between 1.0 and 22.0 m bgl in the shallow aquifer, 2.4 to 77.0 m in the IA and between 3.5 to 62.0 m in the deep aquifer. The static water levels, on the other hand, ranged from 0.7 to 17.0 m in the shallow aquifer, 1.1 to 19.1 m in the intermediate aquifer and 1.2 to 54.7 m in the deep aquifer. Thus, the piezometric surface is nearer to the surface in the shallow aquifer, followed by the intermediate aquifer and then the deep aquifer.

(iv) Porosity and specific yield

Most studies regard the porosity of alluvium, which is a mixture of sand and gravel to be between 0.20 to 0.35 (Chilton and Seiler, 2006; Foster and Chilton, 2003; Okiongbo and Soronnadi-Ononiwu, 2004). An average value of 0.27 was taken to represent the porosity of the shallow alluvial aquifer, representing the porosity of both sand and gravel in the aquifer. The porosity of the Turkana Grit Shallow Aquifer, intermediate aquifer and that of the deep aquifer was estimated based on (Malvić *et al.*, 2005), taking into account the different porosity of geological materials (Table 4.15).

Table 4.15: Minimum and maximum porosity values of various geological materials based on Todd, 1980

Aquifer type	Formation	Min	Max
SAA	Sand and gravel	0.20	0.35
TGSA	Clayey gravels, clayey sandy gravels	0.17	0.27
IA	Fine medium sand	0.29	0.46
DA	Silty or sandy clay	0.20	0.64

(v) Hydraulic conductivity

The aquifer material of the Lodwar Alluvial Aquifer System comprises of fine-medium sand with hydraulic conductivity ranging between 2.0×10^{-7} m/sand 5.0×10^{-4} m/s. Thus, the average hydraulic conductivity of the aquifer would be 1.14×10^{-5} m/s and equivalent of 1.22 m/day.

(vi) Transmissivity

Transmissivity of the boreholes in the study was calculated using Equation 3-12 for 44 boreholes and handpumps with data on yield, static water level (swl) and water rest levels (wrl), where yield is divided by drawdown, and the result is multiplied by the hydraulic conductivity. The hydraulic conductivity used in the calculation was 1.22 m/day. The transmissivity of boreholes in the shallow aquifer ranged from 2.99 and 2166.72 m²/day in the shallow aquifer, 0.31 to 608.12 m²/day in the intermediate aquifer, and 10.98 to 1273.04 m²/day in the deep aquifer. Average transmissivity values indicate that the deep aquifer in Napuu has a high groundwater potential (1316.11 m²/day), followed by the shallow aquifer (440.00 m²/day) and then the intermediate aquifer (115.18 m²/day). It is important to note that majority of the boreholes in the study area have been drilled in the shallow aquifer (Figure 4.36).

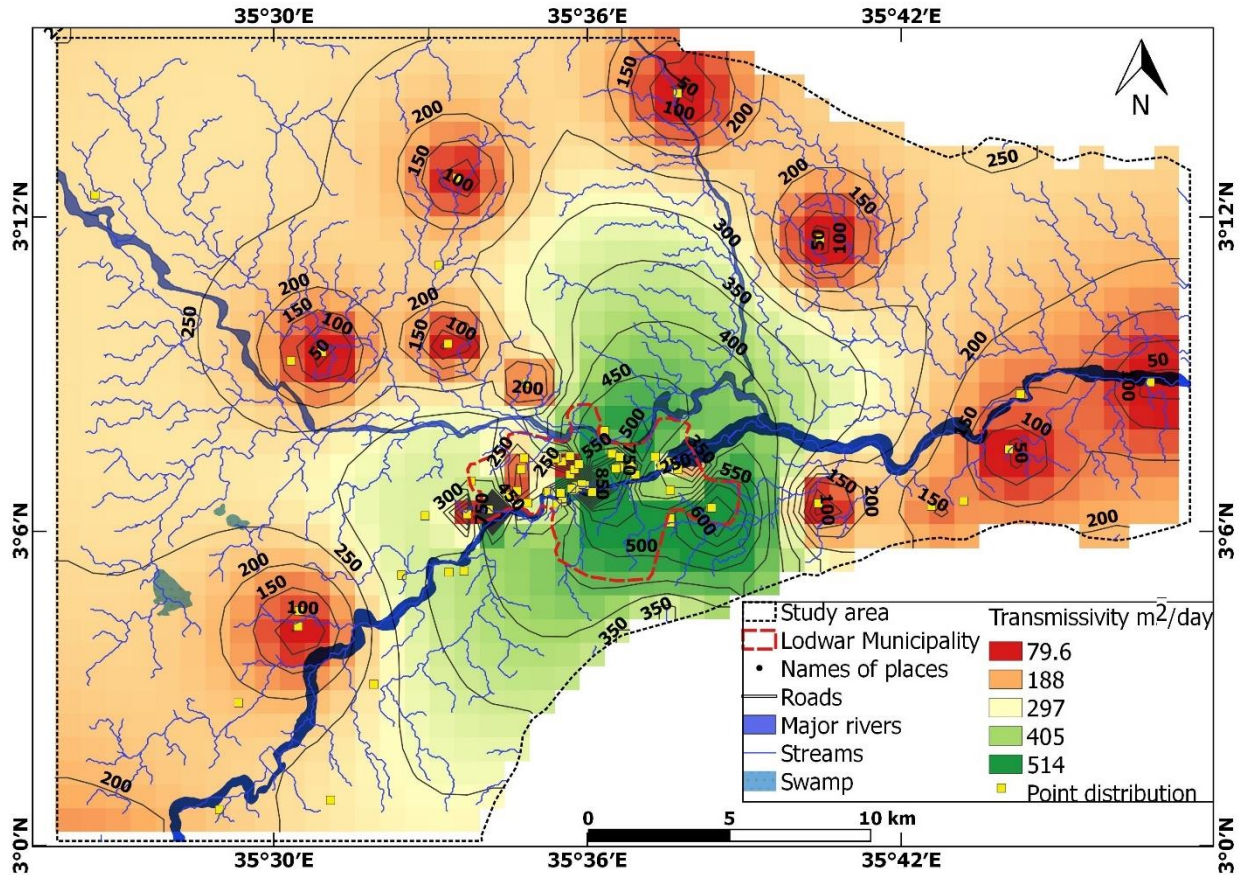


Figure 4.36: Spatial distribution of transmissivity values in the study area based on secondary data obtained from the WRA database

(vii) Groundwater flow

Groundwater flow in an aquifer is governed by changes in gravity and hydraulic head. The topography of an area determines the general direction of groundwater flow. In the study area, the trend shown by the stream lineament is northwest to south-east north of Turkwel River and the south-west to north-east south of Turkwel River. The surface run-off in the areas originates in from the higher elevation volcanic and metamorphic terrains and passes through the Turkana grits into the alluvial zones of the Turkwel River. Piezometric data of 52 boreholes and handpumps in the study area were plotted in Surfer Software to determine the general groundwater flow direction. The results revealed that the groundwater movement followed the general trend of the surface water in the area with localized flow systems occurring in the southern portion of the river (Figure 4.37). Kuria (2013) has linked localized flow systems to a low local recharge.

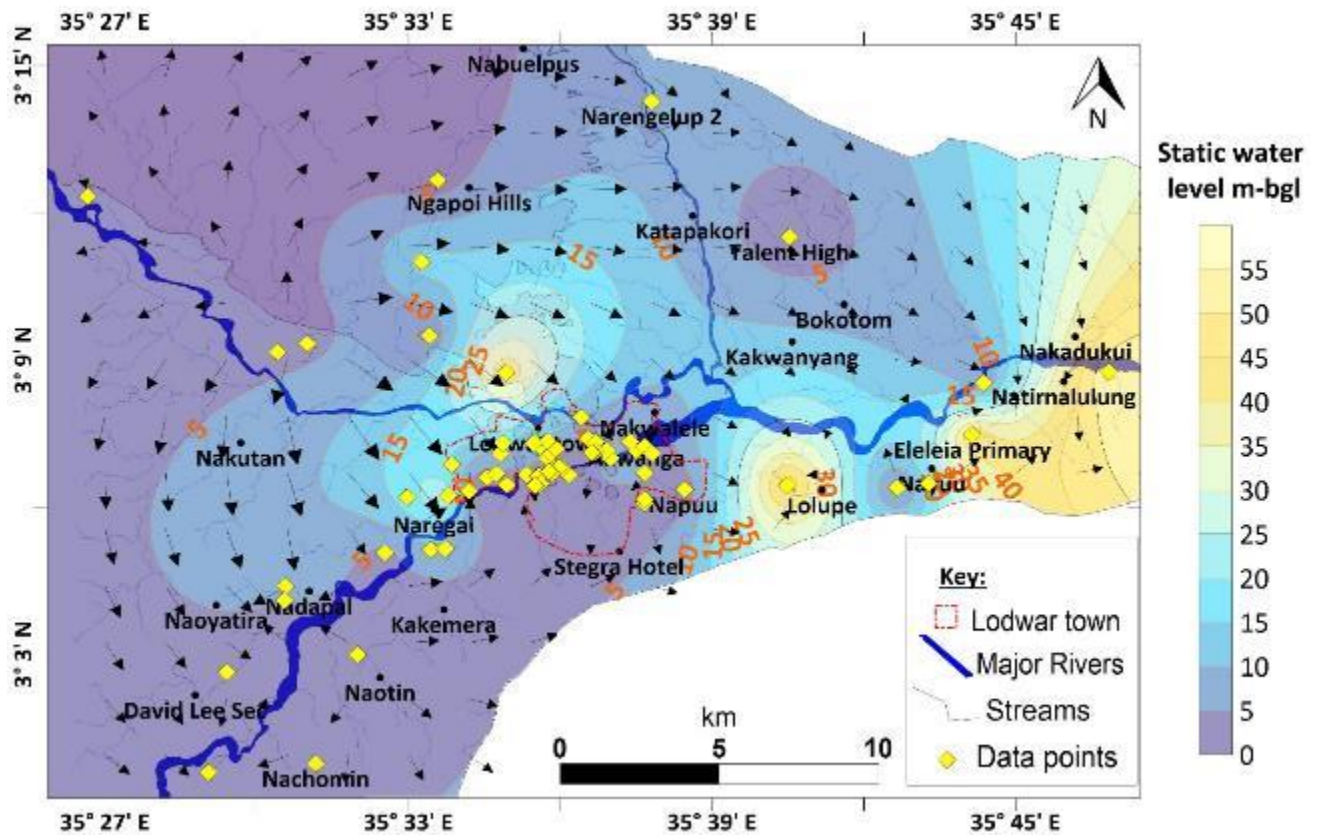


Figure 4.37: Piezometric surface map of the study area determined from static water levels

4.2.2 Hydrogeochemistry and Water Quality

To characterise the aquifer hydrogeochemistry and its susceptibility to pollution borehole depth information acquired from the secondary data was used. However, information on the drilled depth of each handpump and borehole was not fully available. Drilled depth data was available for only 28 of the 53 observed handpumps (depth ranging between 5 – 45 m), with one recorded outlier at 75 m; 17 of these had depth less than 30 m below ground level, and therefore fall in the shallow aquifer category (cf. Olago, 2018)—similarly, 22 of 41 observed boreholes, including all nine LOWASCO production boreholes. The depth of these boreholes ranged from 17 to 110 m. Of these, ten had depth between 17 and 30 m and were categorised as shallow alluvial aquifer (SAA), including seven LOWASCO boreholes. Likewise, another set of ten boreholes had depth between 31 to 100 m and was in the intermediate aquifer (IA) while the remaining two had depth greater than 100 m and are in the deep aquifer (DA) (cf. Olago 2018). In general, the number of sampled sites without drilled depth information was 44 (25 handpumps and 19 boreholes) and have been referred to in this study as “depth unknown” (DU). Of the 94 groundwater samples collected in

the wet season of May 2018, 58 were resampled in February 2019 dry season, where only 16 handpumps and 18 boreholes had drilled depth information. With this regard, groundwater chemistry in the LAAS has been evaluated in SAA, IA, DA and DU. Shallow aquifer located outside the riparian zones of the Turkwel River has been identified as Turkana Grit Shallow Aquifer (TGSA).

4.2.2.1 Physico-chemical properties

a) Turkwel River

The electrical conductivity (EC) of the Turkwel River had a small range of between 200.0 and 420.0 $\mu\text{S} / \text{cm}$, with a median value of 209.36.0 $\mu\text{S} / \text{cm}$ (Table 4.16). The pH of the Turkwel River samples was slightly alkaline, varying from 7.5 to 8.0; slightly less alkaline waters are noted to the east of the Turkwel and Kawalase rivers confluence (Figure 2-1). The river water was quite warm, with temperatures ranging from 30.6 °C to 36.1 °C, and was slightly cooler than the average high temperature (about 38 °C) observed in the region during the sampling period. No clearly discernible characteristics are observed in concentrations of cations from upstream to downstream, except for Na, which rises considerably east of the confluence of the Turkwel and Kawalase rivers (Figure 2-1). Relatively higher content of Fe and Mn occurred in all samples of the Turkwel River except for sample 2437 where Mn was <0.01 mg/L, but with the highest level of Fe (2.76 mg/L). No sulphate and nitrites were detected, while nitrate, chloride, and bicarbonate concentrations are generally low.

Table 4.16: Physico-chemical results for samples collected in the dry season of February 2018 for the Turkwel River shaded fields are values that exceed guideline values for drinking water, and 'nd' refers to not detected. The samples were arranged (left to right) from upstream to downstream

Sample Code	2434	2435	2437	2438	2439	2440	2441	Min	Max	Median
EC	210	380	220	200	420	200	210	200	420	210.00
pH	8.65	7.70	8.82	9.11	8.92	8.73	9.53	7.70	9.53	8.82
Temp.	33.4	33.7	36.1	32.6	30.6	31.7	34.0	30.6	36.1	33.4
Turb.	311	228	154	549	96	834	521	96	834	311
Ca	25.60	25.60	26.40	25.60	24.00	26.40	24.80	24.00	26.40	25.60
Mg	6.33	7.79	5.36	7.79	8.76	7.30	7.30	5.36	8.76	7.30
Na	2.10	2.00	7.70	2.00	2.80	2.20	6.00	2.00	7.70	2.20
K	5.1	4.6	5.4	4.7	4.3	4.4	5.3	4.3	5.4	4.7
Fe	2.06	2.37	2.76	2.7	1.66	2.46	2.13	1.66	2.76	2.37
Mn	0.16	0.16	<0.01	0.16	0.12	0.16	0.2	0.12	0.2	0.16
HCO ₃	96.63	96.83	101.97	99.25	116.19	121.23	121.61	96.63	121.61	101.97
SO ₄	nd	nd	nd	nd	nd	nd	nd	N/A	N/A	N/A
Cl	2	10	5	4	1	1	5	1	10	4
NO ₃	0.32	<0.01	0.37	0.86	0.17	<0.01	0.25	0.17	0.86	0.32
NO ₂	nd	nd	nd	nd	nd	nd	nd	N/A	N/A	N/A

b) Groundwater – seasonal variations

(a) *Shallow Aquifers*

(i) Shallow alluvial aquifer (SAA)

The range of EC values in the shallow alluvial aquifer differed significantly between the dry and wet seasons; the minimum EC values were roughly comparable (195-207 S / cm for the dry seasons versus 210 S / cm for the wet season), but the EC maximum was three times higher in the wet season than in any of the dry seasons (1857 μ S / cm versus 630-632 μ S / cm) (Table 17). Likewise, although the pH level in the dry seasons was 7.60 to 8.22, in the wet season in the wet season, it was higher, from 7.65 to 8.91. Besides, the maximum turbidity values in the wet season also show a two- and five-fold increase as compared to each of the two dry seasons. Groundwater temperatures ranged from 28.1 to 35.7°C.

The groundwater can be classified as non-saline in terms of chemistry except for the Napuu 1 borehole that was mildly saline in the dry season of February 2018, the only time it was tested. With respect to the median concentrations of the cations in the SAA, Ca concentration is consistent over the two-dry, and one wet season, Mg and K were depleted in the dry season in February 2019 compared to the dry season in February 2018 and the wet season in May 2018, and Na is significantly depleted in the wet season relative to the two dry seasons. For the anions, the season in February 2018 has the highest concentrations for HCO₃, SO₄ and Cl and the lowest concentrations in the wet season in May 2018 while F concentrations are comparable in all three seasons. The nitrate concentrations are generally low; February 2018 (0.03-0.68 mg N/L); May 2018 (0.02-0.54 mg N/L); and February 2019 (0.02-0.19). Ca (very low, Kakemera Primary handpump – wet season May 2018), Na (high, BH7 – dry season February 2019), K (high, KFS handpump – wet season May 2018) and SO₄ (very high, BH7 – dry season February 2019; high, Napuu 1, dry season February 2018) are noted as major site-specific anomalies.

Table 4.17: Physico-chemical parameters results during the February 2018 dry season for the SAA and IA (2452 and 2460); (the shaded values exceed the drinking water guidelines of KEBS (2014) and WHO (2011))

No	Sample ID	Code	EC	pH	Temp	Turbidity	Ca	Mg	Na	K	Fe	Mn	HCO ₃	SO ₄	Cl	F	NO ₃	NO ₂
	Units		μS/cm		°C	NTU	Mg/L	Mg/L	Mg/L	Mg/L	Mg/L	Mg/L	Mg/L	Mg/L	Mg/L	Mg/L	Mg/L	MgN/L
1	Bh 1A	2455	209	7.90	28.90	1.06	26.40	6.33	3.00	4.60	0.03	0.01	118.62	1.82	3.00	0.46	0.03	nd
2	Bh 1B	2454	220	7.60	28.10	0.17	28.00	7.31	2.00	4.40	0.17	0.01	123.95	3.41	2.00	0.47	nd	nd
3	Bh 2C	2453	262	8.00	29.50	0.42	33.60	7.31	5.20	4.10	0.07	0.50	125.62	1.78	4.00	0.50	nd	nd
4	Bh 3	2448	233	7.80	29.30	0.91	28.00	10.20	2.60	4.30	0.03	0.01	123.66	2.22	2.00	0.41	nd	nd
5	Bh 5	2449	265	7.60	29.80	0.69	32.00	8.28	5.50	4.60	0.03	0.01	138.53	nd	5.00	0.44	nd	nd
6	Bh 6	2444	561	8.20	34.20	0.36	20.80	1.31	100.00	4.00	0.03	0.01	230.58	19.00	28.00	0.45	0.16	0.02
7	Bh 6	2450	257	7.70	29.20	1.59	36.80	7.31	2.40	4.60	0.03	0.01	126.25	2.63	4.00	0.43	nd	Nd
8	Bh 7	2445	207	7.90	28.80	1.01	25.60	5.85	5.00	4.00	0.10	0.01	99.25	2.69	2.00	0.39	0.20	Nd
9	Napuu 1	2451	1256	8.00	32.70	1.02	47.20	22.90	190.00	5.10	0.07	0.01	422.76	109.00	114.00	0.99	0.68	Nd
10	Napuu 4	2452	503	8.10	32.60	0.94	23.20	7.79	72.00	3.90	0.03	0.01	260.24	6.80	18.00	1.29	0.20	Nd
11	Nayuu Hp	2460	596	8.60	35.70	2.06	1.60	2.43	130.00	1.30	0.07	0.01	253.41	10.70	19.00	1.26	2.34	Nd
12	Lolupe Hp	2456	630	8.00	33.40	2.00	25.60	22.40	70.00	4.20	0.90	0.01	321.30	13.50	12.00	0.75	nd	Nd

Table 4.18: Physicochemical parameters for the SAA in the wet season (shaded fields indicate values that exceed the guidelines for drinking water)

No	sample ID	Code	EC	pH	Temp	Turbidity	Ca	Mg	Na	K	Fe	Mn	HCO ₃	SO ₄	Cl	F	NO ₃	NO ₂
	Units		µS/cm		°C	NTU	Mg/L	Mg/L	Mg/L	Mg/L	Mg/L	Mg/L	Mg/L	Mg/L	Mg/L	Mg/L	Mg/L	MgN/L
1	Akibululu Hp	3344	306	8.50	31.40	2.65	29.60	8.28	20.00	3.80	0.10	0.40	170.00	0.03	8.00	0.79	0.12	0.07
2	Bh 1A	3381	260	8.91	28.90	5.94	36.80	6.82	3.00	4.70	0.03	0.04	126.80	2.07	13.00	0.31	0.30	nd
3	Bh 1B	3380	240	8.64	29.80	0.03	26.40	7.79	4.00	4.90	0.03	<0.01	124.10	6.49	6.00	0.32	0.36	nd
4	Bh 2C	3382	310	8.21	30.40	3.30	34.40	9.25	8.00	4.30	0.07	0.50	156.10	2.70	12.00	0.31	0.15	nd
5	Bh 3	3383	240	8.45	30.00	0.43	28.00	8.76	3.00	4.70	>0.01	<0.01	121.50	2.73	6.00	0.29	0.06	nd
6	Bh 5	3387	270	8.32	29.90	1.87	33.60	7.79	3.00	4.70	0.03	0.08	160.50	2.00	5.00	0.32	>0.01	nd
7	Bh 7	3384	210	8.56	29.90	0.54	25.60	8.28	3.00	4.20	0.03	0.14	111.80	2.28	5.00	0.29	>0.01	nd
8	Bh 9	3388	260	8.35	28.70	0.66	29.60	11.68	3.00	4.50	0.03	<0.01	133.40	4.83	5.00	0.27	0.09	nd
9	Kakemera Pri Hp	3300	528	8.67	32.90	5.30	3.20	9.23	99.00	1.10	0.07	<0.01	259.40	9.15	12.00	0.93	0.21	nd
10	KFS Hp	3390	424	7.92	28.70	10.53	30.40	14.11	27.00	14.00	0.17	0.50	216.70	23.85	12.00	0.60	0.08	nd
11	Locher A Akalale Hp	3346	297	8.51	31.10	1.85	16.80	5.35	37.00	2.60	0.07	0.10	145.00	6.40	8.00	0.74	0.17	nd
12	Lodwar Mixed Pri 1	3355	353	7.84	30.30	8.05	29.60	6.82	32.00	2.90	0.03	0.20	180.40	2.77	8.00	1.68	0.04	0.02
13	Lodwar Mixed Pri 2	3356	332	7.65	31.80	1.23	34.40	8.77	18.00	3.70	0.03	0.60	159.80	4.22	11.00	1.08	0.07	nd
14	Lokipetot Bh	3329	380	8.32	29.00	5.15	24.80	16.05	29.00	4.30	>0.01	<0.01	218.70	6.36	1.00	0.56	0.14	nd
15	Lolupe 3 Hp	3360	594	8.05	34.40	1.41	27.20	11.68	80.00	4.30	>0.01	<0.01	341.60	7.37	12.00	0.81	0.04	nd
16	Nabulon water well	3365	236	8.36	31.30	0.29	28.00	4.88	10.00	4.40	0.07	<0.01	116.80	2.65	7.00	0.53	>0.01	nd
17	Nadapal Hp	3313	324	7.84	31.00	7.09	29.60	15.57	8.70	3.20	0.07	0.60	173.90	2.38	1.00	1.18	0.02	nd
18	Nakwalele Hp 2	3338	632	8.70	32.60	5.28	24.80	8.28	98.00	4.20	0.07	0.04	281.90	19.92	36.00	0.99	0.13	nd
19	Nakwamekwi Pri Bh	3307	270	8.33	29.70	5.12	26.40	12.16	6.00	3.50	0.03	<0.01	145.50	3.44	3.00	0.57	>0.01	nd
20	Naregai Bh	3312	350	8.35	32.80	4.51	20.80	18.96	20.00	5.70	0.07	<0.01	191.60	10.15	3.00	0.93	>0.01	nd
21	Nasenyanait Hp 2	3351	320	8.23	32.00	1.78	32.00	14.60	6.40	4.10	0.07	0.06	171.50	5.80	3.00	0.66	0.16	nd
22	Natotol	3354	271	8.18	30.20	6.05	28.00	9.74	9.00	4.10	0.17	0.60	138.00	1.03	2.00	0.63	0.54	nd

Table 4.19: Physico-chemical parameters for the SAA in the dry season (February 2019 - shaded values exceed the KEBS and WHO guidelines for drinking water)

No.	Sample ID	Code	EC	pH	Turbidity	Ca	Mg	Na	K	Fe	Mn	HCO ₃	SO ₄	Cl	F	NO ₃	NO ₂
	Units		µS/cm		°C	NTU	Mg/L	Mg/L	Mg/L	Mg/L	Mg/L	Mg/L	Mg/L	Mg/L	Mg/L	Mg/L	Mg/L
1	Akibululu Hp	2256	360	7.95	1.20	33.60	5.85	32.00	2.70	0.07	0.60	195.89	3.70	9.00	0.51	0.11	nd
2	Bh 1A	2225	195	8.13	0.58	27.20	2.93	6.10	3.10	0.10	nd	103.52	1.10	15.00	0.44	0.02	nd
3	Bh 1B	2226	224	8.09	0.10	33.60	2.94	6.60	1.10	0.07	nd	125.33	2.26	nd	0.45	nd	nd
4	Bh 2C	2227	241	8.13	4.92	40.80	0.51	6.90	1.00	0.13	0.60	146.85	1.55	4.00	0.57	0.05	nd
5	Bh 3	2263	228	8.00	0.49	32.00	4.39	6.00	2.00	0.07	nd	86.97	5.19	25.00	0.34	0.13	nd
6	Bh 5	2224	249	8.15	NIL	33.60	5.37	7.40	1.90	0.07	nd	120.30	3.83	5.00	0.52	nd	nd
7	Bh 7	2269	1857	8.04	0.41	44.00	0.03	375.00	3.20	0.10	0.12	205.15	721.00	5.00	0.33	0.04	nd
8	Bh 9	2223	309	8.10	0.22	31.20	2.45	30.00	2.80	0.07	nd	139.76	5.88	29.00	0.50	0.03	nd
9	Kakwanyang Dispensary Bh	2258	280	8.08	0.85	33.60	3.91	17.00	3.10	0.10	nd	156.71	4.39	2.00	0.41	0.19	nd
10	Lodwar Mixed Pri 1	2249	403	8.18	0.36	39.20	5.37	40.00	1.40	0.07	nd	218.72	3.84	8.00	1.62	0.10	nd
11	Lolupe 3 Hp	2214	496	8.20	1.26	31.20	1.96	75.00	2.40	0.03	nd	283.42	5.87	4.00	1.16	nd	nd
12	Nadapal Hp	2233	392	8.15	0.68	18.40	8.76	50.00	1.10	0.07	1.20	218.94	2.16	14.00	1.18	0.07	nd
13	Nakwamekwi Pri Bh	2237	239	8.22	0.06	33.60	6.34	3.00	2.30	0.07	nd	144.00	1.02	1.00	0.56	0.02	nd
14	Naregai Bh	2264	387	8.11	0.80	25.60	16.05	30.00	4.10	0.07	nd	183.08	10.60	3.00	0.22	nd	nd
15	Nasenyanait Hp 2	2251	256	8.15	0.40	40.00	1.48	8.20	3.10	0.07	nd	144.36	6.62	nd	0.63	0.07	nd

(ii) Turkana Grit Shallow Aquifer (TGSA)

Data are available for the TGSA for one dry season (February 2019) and one wet season (May 2018) (Table 4.20). There were few handpumps targeting this aquifer, presumably as a result of its moderately saline water. There are no significant variations between the dry and wet seasons in the EC, except for the Bokotom hand pump. In general, however, the EC range for the shallow groundwater of the Turkana grit was marginally lower in the wet season (3410 to 6840 $\mu\text{S}/\text{cm}$) compared to the dry season (5170 to 8260 $\mu\text{S}/\text{cm}$). As in the case of the shallow alluvial aquifer, whereas the minimum pH values were more or less the same (8.35 versus 8.40), the maximum pH for this aquifer was markedly higher in the wet season (9.28) than in the dry season (8.68), and the maximum turbidity difference between the dry seasons (7.64 NTU) and the wet seasons (20.86 NTU) was about three-fold. Temperature, recorded only in the wet season, ranged from 33.1 to 36.9 °C, suggesting that the TGSA is warmer overall than the shallow alluvial aquifer.

The concentrations of Na, Cl and HCO_3 are much higher as compared to the shallow alluvial aquifer, and in most instances, the concentrations of all three parameters exceed 1000 mg/L each. Also notable are: (i) the amounts of Ca in TGSA are lower than in SAA; and (ii) the concentrations of SO_4 , F, and NO_3 are far higher than in SAA. Contrasts between the dry and wet seasons in TGSA relate to (i) higher median concentrations of Mg, SO_4 , F and NO_3 in the wet as compared to the dry season, except for the Loyo Primary handpump where the reverse is observed, and (ii) relatively lower median values of Cl in the wet season (685.00 mg/L) as compared to the dry season (830.50 mg/L). However, comparison of Cl concentrations for individual wells between the wet and dry seasons showed a reverse trend for some wells.

Table 4.20: Physico-chemical parameters for the TGSA during the wet and dry seasons (shaded values exceed the KEBS (2014) and WHO (2011) guidelines for drinking water)

Turkana Grit Shallow Aquifer (TGSA)- Dry season (February 2019)																		
No	Sample ID	Code	EC	pH	Temp.	Turb.	Ca	Mg	Na	K	Fe	Mn	HCO ₃	SO ₄	Cl	F	NO ₃	NO ₂
	Units		μS/cm		°C	NTU	Mg/L	Mg/L	Mg/L	Mg/L	Mg/L	Mg/L	Mg/L	Mg/L	Mg/L	Mg/L	Mg/L	MgN/L
1	Talent High Sch Hp	2252	5600	8.56	nm	7.64	3.20	1.46	1280.00	1.20	0.27	nd	941.73	350.00	1120.00	9.60	7.81	nd
2	Bokotom Hp	2253	8260	8.40	nm	1.24	8.00	17.98	1850.00	3.10	0.07	nd	492.68	268.00	2395.00	2.19	3.27	nd
3	Loyo Pri Hp	2266	5170	8.68	nm	1.38	4.80	0.49	1182.00	2.70	0.10	nd	1769.51	351.60	446.00	17.24	5.03	nd
4	Trumpet of Hope Ministries	2267	5570	8.82	nm	0.86	0.80	0.49	1280.00	2.30	0.10	nd	1773.54	388.00	541.00	12.28	7.82	nd
Turkana Grit Shallow Aquifer (TGSA)- Wet season (May 2018)																		
	Sample ID	Code	EC	pH	Temp.	Turb.	Ca	Mg	Na	K	Fe	Mn	HCO ₃	SO ₄	Cl	F	NO ₃	NO ₂
5	Talent High Sch Hp	3331	6370	9.06	35.70	12.70	4.80	2.92	1453.00	2.60	0.27	nd	1407.19	426.00	1020.00	10.41	19.81	nd
1	Namuthia Hp	3333	3410	9.12	36.00	20.86	4.00	2.92	770.00	1.50	0.67	nd	828.27	207.03	525.00	3.09	7.15	nd
3	Bokotom Hp	3334	6840	8.35	36.90	4.26	12.00	18.04	2020.00	2.90	nd	nd	492.38	610.00	2390.00	2.22	4.76	nd
6	Trumpet of Hope Ministries	3394	5340	9.28	35.40	6.74	<1.00	0.49	1226.00	2.70	0.17	nd	1333.31	608.06	500.00	15.31	33.64	nd
2	Al Noor Community	3396	6270	8.62	33.10	1.10	9.60	13.60	1400.00	5.10	0.10	nd	1215.15	934.60	780.00	18.74	1.34	nd
4	Loyo Pri Hp	3399	5190	8.79	33.50	4.56	2.40	1.95	1190.00	3.70	0.03	nd	1602.75	324.71	590.00	18.67	7.92	nd

(iii) Intermediate Aquifer (IA)

Data for this aquifer is available for the two dry and one wet season but for the first dry season of February 2018 are limited to only two samples. Based on the EC, the groundwater is mainly non-saline in the intermediate aquifer, but there are some slightly saline pockets. Compared to the SAA, although in both dry and wet seasons the minimum EC values were similar, the EC average was higher in the wet season, but not considerably higher than in the SAA. The pH range was wider in the wet season (7.61-9.76) than in the dry season (8.10-8.67). Furthermore, similar to the SAA and TGSA, the average turbidity in the wet season was far higher than in the dry season, and a seven-fold increase is observed in this aquifer for the maximum turbidity values in the wet season compared to the dry season. The groundwater temperature range is 31.3 to 36.0 ° C, broadly comparable to the TGSA.

The median concentration values of Ca, Mg, K, HCO₃, SO₄ and Cl in this aquifer are higher in the wet season compared to the dry season, and much more so particularly for Mg and SO₄. More generally, the concentration ranges for the measured cations and anions in the wet season are wider and more variable in the wet than in the dry season.

Table 4.21: Results for the intermediate aquifer physico-chemical parameters in the wet season (the shaded fields are values that exceed guideline values for drinking water of KEBS (2014) and WHO (2011))

No	Sample ID	Code	EC	pH	Temp	Turbidity	Ca	Mg	Na	K	Fe	Mn	HCO ₃	SO ₄	Cl	F	NO ₃	NO ₂
	Units		µS/cm		°C	NTU	Mg/L	Mg/L	Mg/L	Mg/L	Mg/L	Mg/L	Mg/L	Mg/L	Mg/L	Mg/L	Mg/L	MgN/L
1	Bh 6	3389	590	8.33	32.9	0.75	20	14.6	76	4.4	0.03	0.04	281	25	25	0.35	0.3	nd
2	Chokochok Pry	3341	929	7.77	33.4	3.77	32	42.3	93	4.7	nd	0.6	327	20.9	118	0.84	0.14	0.07
3	Chukultom Hp	3386	888	9.28	35.3	2.03	1.6	7.77	186	2.6	0.03	nd	337	47.1	93	0.67	0.17	0.04
4	Comboni Girls	3398	1220	9.58	33.6	0.16	nd	1.46	272	1.6	0.03	nd	383	73.7	140	1.41	0.57	0.05
5	Eleleia Pri Hp	3364	1557	9.59	35.7	1.44	4	12.2	330	1.1	0.1	nd	812	29.9	25	4.58	0.37	nd
6	Kakemera Chr	3302	1308	7.61	35	6	42.4	24.8	203	2.7	0.07	nd	758	15.7	24	1.25	0.2	nd
7	Kochoda Hp	3391	850	9.76	33.9	2.17	nd	3.89	187	1.2	0.1	nd	437	22.2	15	1.62	0.15	nd
8	Limyounsim Bh	3309	1673	7.93	34.7	4.72	56	13.2	227	6.4	0.07	nd	701	41.2	44	1.43	1.08	nd
9	Loporkou- Eleleai Hp	3366	914	9.52	35.3	1.3	nd	2.43	205	1.3	0.07	nd	383	36.5	57	1.64	3.45	nd
10	Nachomin Bh	3306	1060	8.48	36	4.15	6.4	4.86	188	1.5	0.03	nd	498	23.1	3	2.24	0.54	nd
11	Nadapal Supply	3314	750	7.76	32.6	4.65	20.8	35.5	86	3.2	0.1	0.12	446	12.3	13	0.95	nd	nd
12	Nagis Bakhita	3317	520	7.98	33.5	4.08	24.8	22.9	53	2.6	0.07	nd	296	12.2	20	0.14	nd	nd
13	Nakwamekwi	3310	805	9.33	34.5	5.1	nd	5.34	174	1.4	0.07	nd	394	31.1	26	0.95	0.66	nd
14	Napuu 2	3373	370	8.9	32	1.01	15.2	8.27	44	3.6	0.07	nd	199	5.13	4	0.77	1.17	nd
15	Napuu	3374	520	8.52	32	0.48	24	10.2	63	4.3	0.07	nd	264	14.4	2	0.81	0.37	nd
16	Nareng'elup 2	3323	1040	7.86	33.8	49.28	45.6	73.9	45	0.2	0.5	nd	512	41.6	22	2.01	3.71	0.23
17	Natot Pri Bh	3357	370	8.68	31.3	1.18	25.6	12.7	33	3	0.03	nd	208	6.53	4	1.55	nd	nd
18	Nauren Puu	3392	600	8.2	34	0.2	16	9.73	91	4.2	0.03	nd	335	9.55	16	0.86	0.07	nd
19	Nayuu Hp 4	3368	820	8.56	34.5	2.32	8.8	6.81	164	2.9	0.2	nd	384	32.5	61	0.48	2.1	nd
20	Nayuu Hp Resample	3363	650	9.3	35.4	1.17	0.8	1.94	144	1.4	0.1	nd	317	20.5	21	0.97	2.44	nd

Table 4.22: Results for the intermediate aquifer measured water quality parameters of February 2019 (the shaded values exceed the drinking water guidelines of KEBS (2014) and WHO (2011))

No	Sample ID	Sample ID	EC	pH	Turbidity	Ca	Mg	Na	K	Fe	Mn	HCO ₃	SO ₄	Cl	F	NO ₃	NO ₂
			µS/cm		NTU	Mg/L	Mg/L	Mg/L	Mg/L	Mg/L	Mg/L	Mg/L	Mg/L	Mg/L	Mg/L	MgN/L	MgN/L
1	Chukultom Hp	2228	736	8.56	nd	7.2	0.98	160	1.1	0.07	nd	283	35	62	1.56	0.13	nd
2	Eleleia Pri Hp	2216	906	8.67	0.49	nd	0.97	206	0.2	0.03	nd	396	32.1	50	2.15	3.07	nd
3	Kakemera Church	2222	1182	8.18	7.12	39.2	22.4	180	0.9	0.23	nd	661	11.3	538	1.75	0.15	nd
4	Nachomin Bh	2217	1025	8.41	0.33	9.6	1.95	220	1.7	0.1	nd	547	22.8	15	2.85	0.29	nd
5	Nadapal Supply bh	2234	510	8.29	0.1	16.8	8.27	80	1.5	0.07	0.2	275	7.49	10	1.14	0.02	nd
6	Nakwamekwi Hp	2230	678	8.63	nd	4	0.97	150	0.4	0.04	nd	302	26.3	29	1.05	0.63	nd
7	Napuu 2	2246	420	8.24	0.55	22.4	2.93	65	2.4	0.07	nd	240	1.15	3	0.88	0.76	nd
8	Napuu 4 Resample	2245	614	8.23	nd	24.8	8.76	100	2.3	0.03	nd	312	16.9	21	0.71	0.17	nd
9	Nareng'elup 2	2261	1051	8.11	4.49	21.6	31.6	160	2.8	0.27	nd	624	24.7	nd	0.77	1.71	nd
10	Natot Pri Bh	2244	375	8.36	0.66	26.4	11.7	35	1.9	0.03	nd	203	7.31	4	1.72	<0.01	nd
11	Nauren Puu	2235	545	8.24	nd	18.4	8.76	86.3	1.8	0.07	nd	285	9.08	14	1.54	nd	nd
12	Nayuu Hp	2211	607	8.55	0.59	4.8	nd	135	0.7	0.1	nd	309	19.6	14	1.23	2.14	nd
13	Nayuu HP4	2212	813	8.41	0.45	15.2	1.47	170	1.2	0.2	nd	338	33.9	55	0.69	1.79	nd

(iii) Deep Aquifer

There are no marked differences in the physico-chemical parameters for each of the two deep borehole sites in the wet-dry season, suggesting recharge occurs over time scales longer than the seasonal cycles. The Natir borehole is non-saline while the Napuu 1 borehole is slightly saline, but the two have fairly similar pH, temperature, and turbidity values, as well as concentrations of Ca, K, and Fe (Table 4.23). The concentrations of Ca in the DA are similar throughout the seasons compared to the SAA, and IA. During dry season generally, the concentrations of Mg and Na in Napuu 1 Bh are similar to those of the IA while in Natir Bh are in the range of observed values in the SAA in the dry season.

Table 4.23: Water quality parameters for the deep aquifer during the dry and wet seasons (highlighted values exceed the KEBS (2014) and WHO (2011) guideline value for drinking water)

Sample ID	Napuu 1			Natirnalulung Bh (Natir)	
Sample Code	2451			2210	
Parameters	Feb-18	May-18	Feb-19	May-18	Feb-19
EC	1256	1250	1392	320	273
pH	8.00	8.30	8.12	8.63	7.95
Temperature	32.70	33.00	N	32.00	N
Turbidity	1.02	1.06	0.15	1.46	1.37
Ca	47.20	22.40	36.00	36.00	33.60
Mg	22.87	25.28	24.32	7.80	5.85
Na	190.00	203.00	230.00	11.50	11.20
K	5.10	5.70	3.10	4.80	3.00
Fe	0.07	0.03	0.07	0.03	0.07
Mn	0.01	nd	nd	nd	nd
HCO ₃	422.76	495.27	553.88	145.67	125.76
SO ₄	109.00	69.08	81.40	8.41	6.29
Cl	114.00	111.00	110.00	19.00	13.00
F	0.99	0.83	0.95	0.42	0.50
NO ₃	0.68	0.71	0.42	0.15	4.69
NO ₂	nd	nd	nd	nd	nd

Seasonal variation of groundwater chemistry

(i) Physical parameters

Seasonal variations of major cations and anions are given in Figure 4.38. Figure 4.38a shows a decreasing trend of EC in aquifers in the wet season, with the TGSA recording the highest EC values. Figure 4.38b shows slightly alkaline pH in the wet season than in the dry season across the aquifers. The SAA is observed to be cooler than the TGSA, IA and the DA. High

turbidity is observed in the TGSA in wet and dry seasons while turbidity in the SAA, IA and DA is observed to be relatively higher in the wet season (Figure 4.38c).

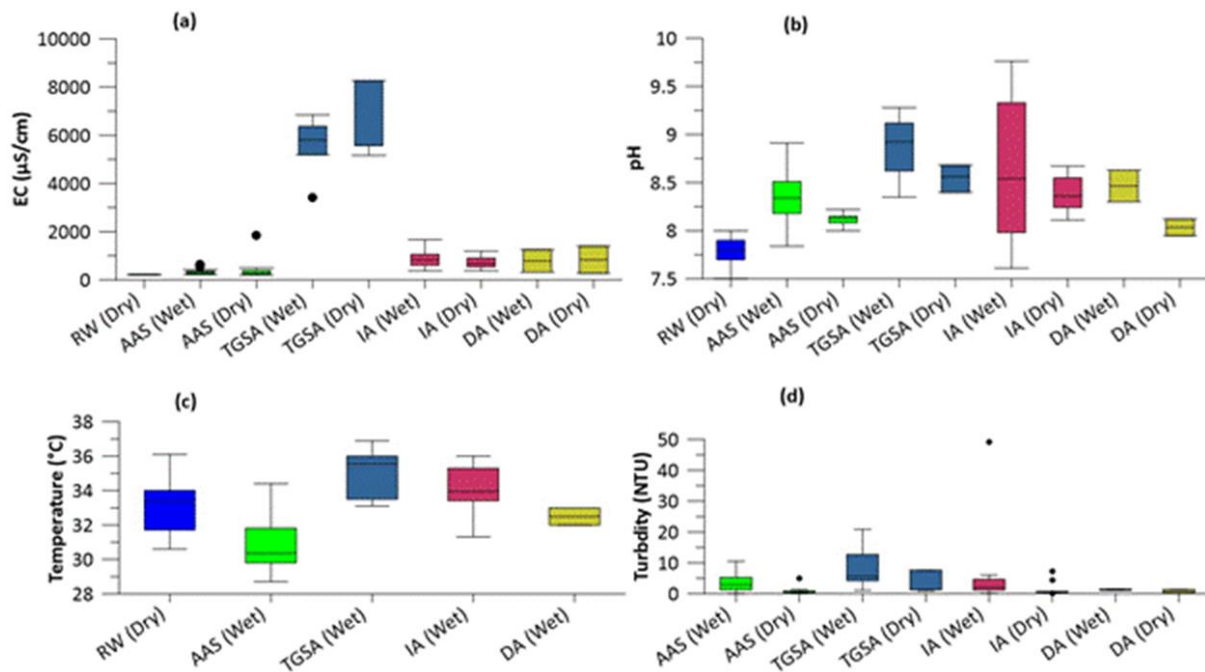


Figure 4.38: Seasonal variations in the physico-chemical parameters in the river warer (RW), shallow alluvial aquifer (SAA) intermediate aquifer (IA), Turkana Grit Shallow Aquifer (TGSA) and the deep aquifer (DA)

(ii) Major cations

Na^+ concentration was observed to be higher in the dry season as compared to in the wet season in shallow and deep aquifers, where the Turkana grit shallow aquifer had the highest concentrations of Na^+ during the wet and dry seasons (Figure 4.39a). The intermediate aquifer had higher Na^+ in the wet season compared to in the dry season. Ca^{2+} concentration was higher in the SAA and in the DA in the dry season but higher in the TGSA and in the IA in the wet season (Figure 4.39b). Mg^{2+} was generally higher in the wet season across all the groundwater samples where significantly higher concentrations were observed in the Turkana grit shallow aquifer (Figure 4.39c). The K^+ was also higher across all the aquifers in the wet season (Figure 4.39d). The Fe^{2+} of the river water was relatively higher than the shallow and intermediate aquifers, which had higher increased concentrations of Fe^{2+} in the wet season due to existence of oxidising an environment (Figure 4.3e)

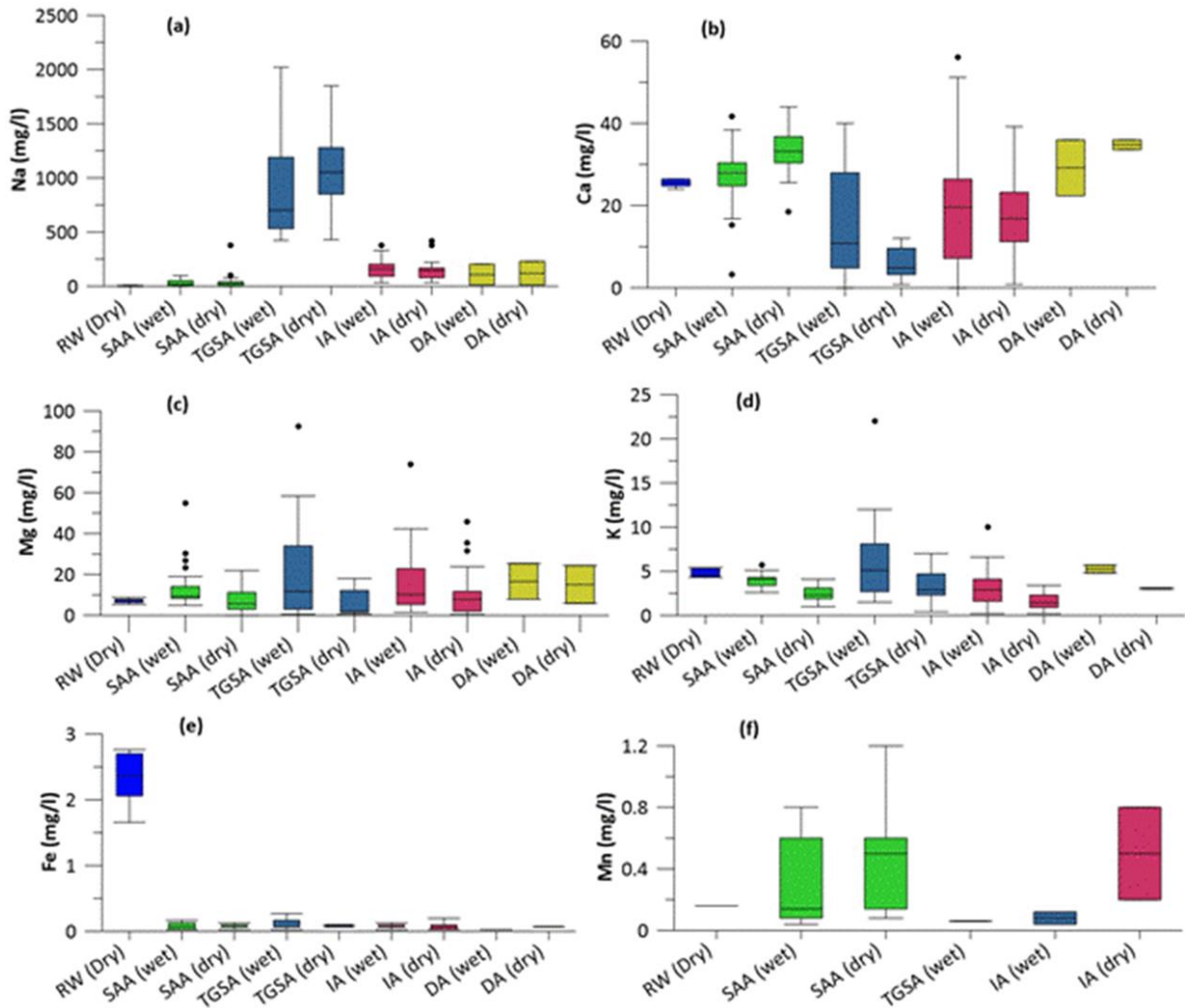


Figure 4.39: Seasonal variations in the major cations in the river water (RW), shallow alluvial aquifer (SAA) intermediate aquifer (IA), Turkana Grit Shallow Aquifer (TGSA) and the deep aquifer (DA)

(iii) Major anions

The concentrations of HCO_3^- increased across all the aquifers in the wet season with the Turkana Grit shallow aquifer having concentrations > 492 mg/L during the wet and dry seasons (Figure 4.40a). Precipitation of mineral phases such as calcite in the dry season may result in decreased concentration of HCO_3^- in groundwater in the dry season. The Cl^- in the shallow alluvial aquifer slightly increased in the wet season (median = 6.50 mg/L) compared to a median value of 4.0 in the dry season. Turkana grit aquifer had high Cl^- levels with a median value of 685.0 mg/L in the wet season and a median value of 830.50 mg/L in the dry season. Dilution of chloride salts was observed in this aquifer in the wet season. The Cl^- concentration in the intermediate aquifer was 18.20 during the wet and dry season (Figure 4.40b).

The SO_4^{2-} concentrations in the shallow and intermediate aquifer were observed to increase in the wet season (Figure 4.40c). However, their levels did not exceed the acceptability values for drinking water. Significantly high SO_4^{2-} concentration was observed in the TGSA in the wet season (median = 517.0 mg/L) and in the dry season (median = 350.8 mg/L). The SO_4^{2-} in the deep aquifer increased in the dry season possible from rock dissolution. NO_3^- concentration increased in all the aquifers in the wet season with the TGSA having the highest concentrations in dry and wet seasons (Figure 4.40d). Generally, F^- concentrations increased in the dry season in all the aquifers (Figure 4.40e). NO_2^- was detected in few samples of the shallow alluvial aquifer and the intermediate aquifer in the wet season with concentrations higher than the guideline value of 0.1 mg/L in the wet season (Figure 4.40f).

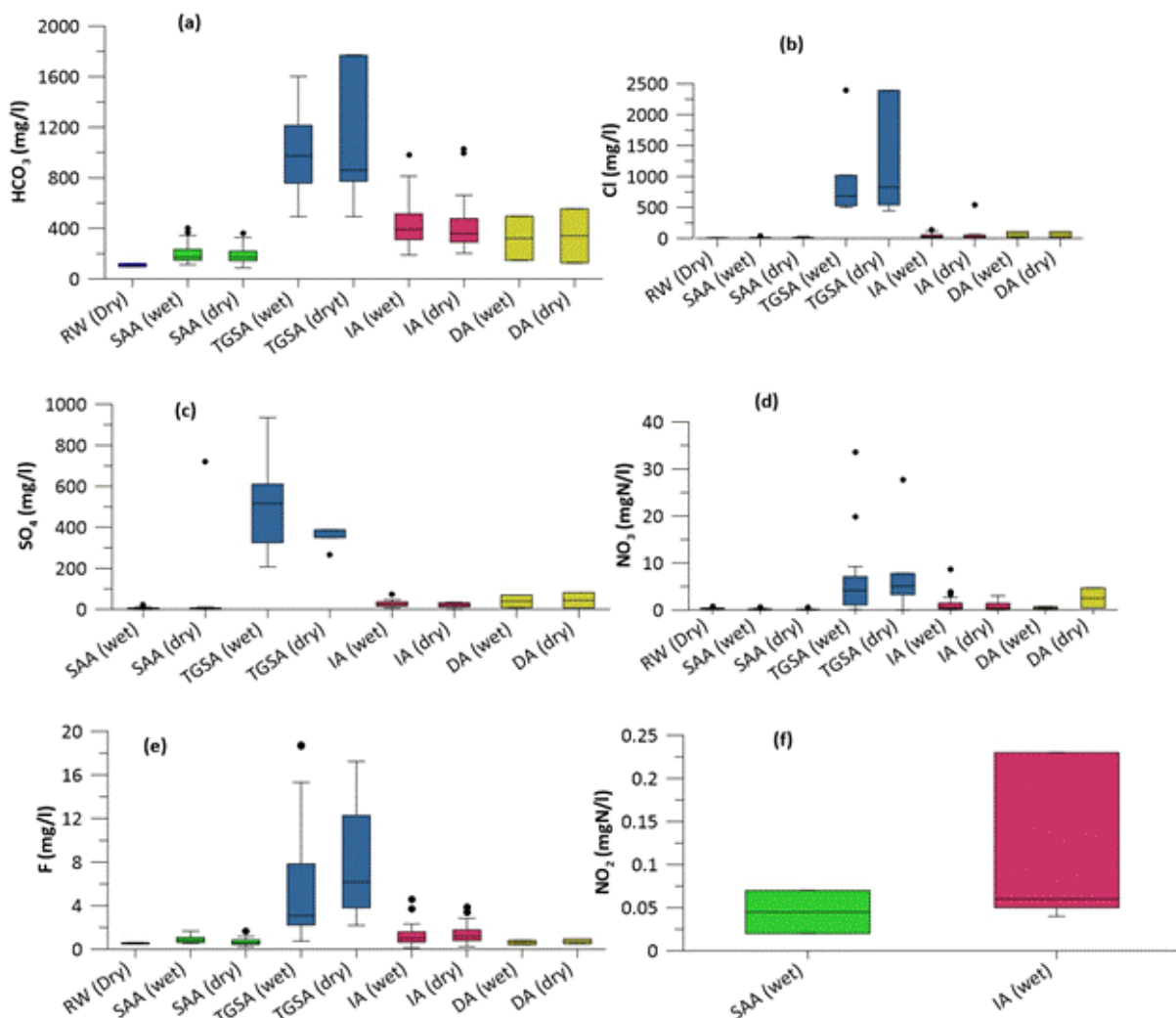


Figure 4.40: Seasonal variations in the major anions in the river water (RW), shallow alluvial aquifer (SAA) intermediate aquifer (IA), Turkana Grit Shallow Aquifer (TGSA) and the deep aquifer (DA)

c) Groundwater – spatial variations

Spatial changes in the physicochemical properties (EC, pH, and temperature) of the LAAS indicated a variety of interesting characteristics (Figure 4.41). The lowest EC values are in wells along the profile of the Turkwel River, in alluvial sediments of the Holocene epoch, and where there are and ephemeral and seasonal feeder streams. The Turkana grits and the Miocene nepheline-phonolites are correlated with the highest EC values, though their outcrops are sometimes obscured by Quaternary deposits. The lowest groundwater pH (acidic waters) and temperature are recorded next to the Turkwel River and its corresponding tributaries, while the alkaline waters is associated with groundwater in the Turkana grits and the nepheline phonolite zones. Higher turbidity in the wet season within both of the shallow aquifers and in the intermediate aquifer is attributed to the remobilisation of clay and silt minerals by recharge water. Another notable characteristic was the progression of rising Na^+ and Cl^- concentrations from the shallow alluvial aquifer, through the intermediate aquifer to the Turkana Grit and vice versa for Ca^{2+} and Mg^{2+} .

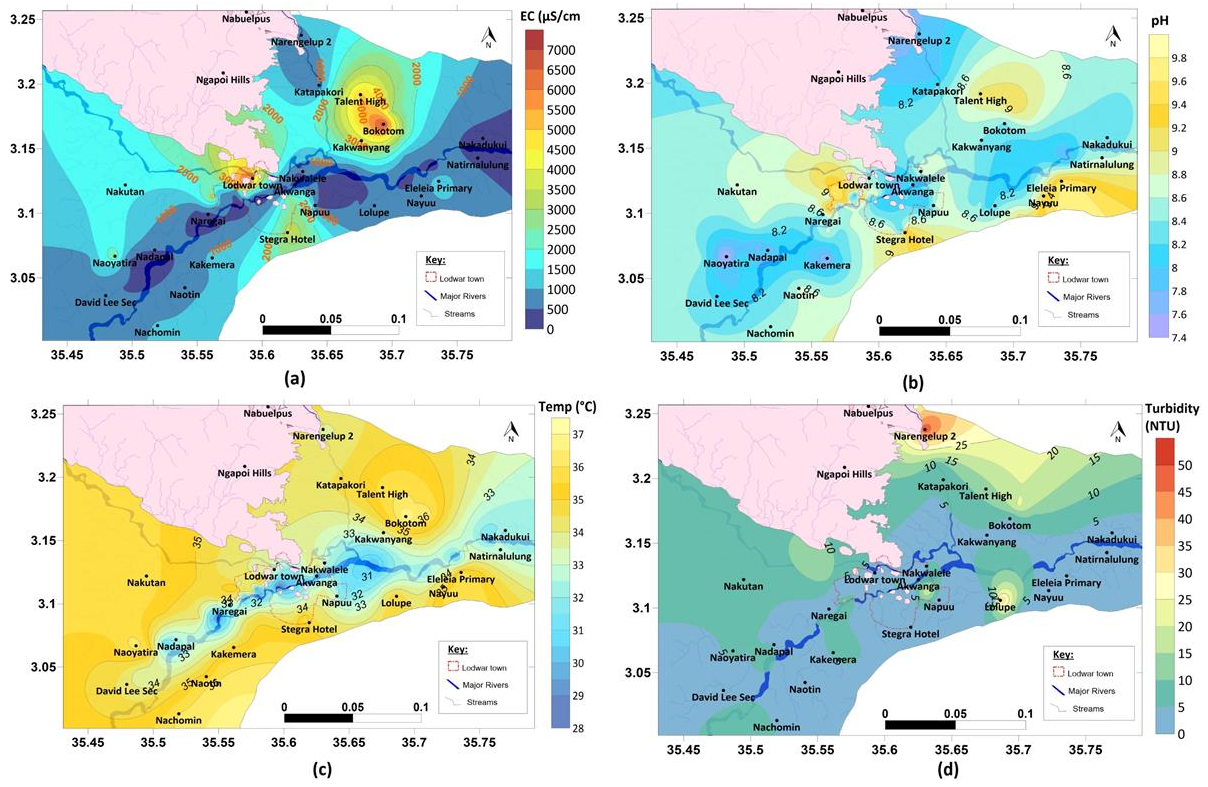


Figure 4.41: Spatial variation of the physicochemical parameters (EC, PH, temperature and turbidity) for the river water (RW), shallow alluvial aquifer (SAA) intermediate aquifer (IA), Turkana Grit Shallow Aquifer (TGSA) and the deep aquifer (DA)

4.2.2.2 Hydrochemical facies

Four water types were identified from the study area's surface water and groundwater samples using the Piper diagram (Figure 4.42a): Na-HCO₃, Ca-HCO₃, Na-Cl, and Mg-HCO₃. All of the surface water samples are Ca-HCO₃ water. The Ca-HCO₃ water type dominates the shallow alluvial aquifer (59%) followed by the Na-HCO₃ water type (29%), and four samples had Mg-HCO₃ water type (12%). The Na-HCO₃ water type of the shallow alluvial aquifer is observed at Lolupe, Nakwalele, and Kakemera areas within the Holocene sediments. The TGSA at its contact with the Holocene sediments has Na-HCO₃ water type, while within the grit formation proper it is 44% Na-Cl water type. The intermediate aquifer is almost entirely Na-HCO₃ water type (95%) except for Katapakori and Narengelup handpumps that belong to the Mg-HCO₃ water type (12%). Mg-HCO₃ water type occurs in isolated areas such as Akwanga, Nakadukui, and Naregai. The Napuu and Natirnalulung boreholes of the deep aquifer belong to Na-HCO₃ and Ca-HCO₃, respectively.

The hydrochemical facies varies seasonally, for example, 55% of the dry season Na-HCO₃ water type transitions to Ca-HCO₃ in the wet season due to mixing with recharge waters (Figure 4.42b). Seven observations were made from sixteen groundwater samples that showed changes in water facies between wet and dry season (Table 4.24):

- (i) Na-HCO₃ type water of the dry season becomes recharged with Ca-HCO₃ type water (3307, 3313, 3362 and 3367) and Mg-HCO₃ type water (3312 and 3322) in the wet season;
- (ii) Some of the recharge water reaches the intermediate aquifer in the dry season (February 2019) changing the water type from Na-HCO₃ to Ca-HCO₃ (3299, 3310, 3346) and to Mg-HCO₃ type (3321, 3361, and 3371);
- (iii) Some of the fresh groundwater becomes saline in the dry season (3302), indicating seasonal aquifer mineralization;
- (iv) Increased sulphate concentration in the dry season (3384) is linked to dissolution of gypsum (calcium sulphate);
- (v) Mg-HCO₃ water type of the wet season may be altered to Ca-HCO₃ water type in the dry season (3323 and 3343); and
- (vi) Na-Cl water type does not change seasonally (3331, 3334, and 3400).

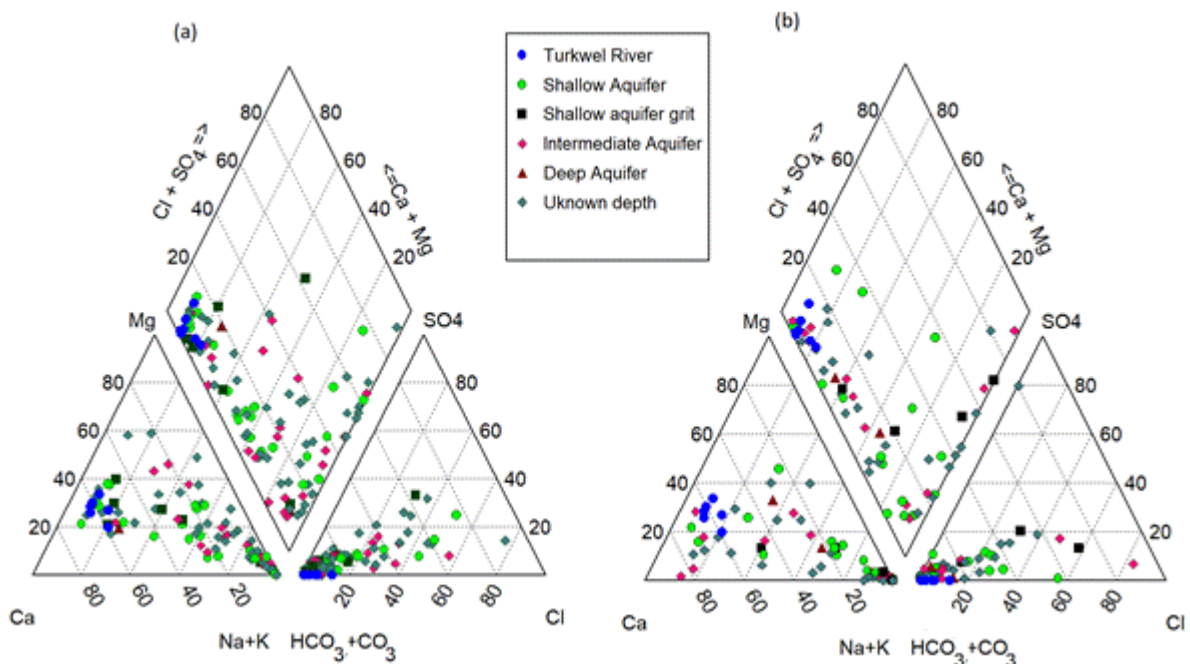


Figure 4.42: Groundwater and surface water piper diagram (a) in the wet season and in (b) the dry season

Table 4.24: Groundwater samples with variations in hydrochemical facies between the wet and the dry season

S/No	Sample Code	May 2018 (Wet Season)	February 2019 (Dry season)
1	3299	Na-HCO ₃	Ca-HCO ₃
2	3302	Na-HCO ₃	Na-Cl
3	3307	Ca-HCO ₃	Na-HCO ₃
4	3310	Na-HCO ₃	Ca-HCO ₃
5	3312	Mg-HCO ₃	Na-HCO ₃
6	3313	Ca-HCO ₃	Na-HCO ₃
7	3321	Na-HCO ₃	Mg-HCO ₃
8	3322	Mg-HCO ₃	Na-HCO ₃
9	3323	Mg-HCO ₃	Ca-HCO ₃
10	3343	Mg-HCO ₃	Ca-HCO ₃
11	3346	Na-HCO ₃	Ca-HCO ₃
12	3361	Na-HCO ₃	Mg-HCO ₃
13	3362	Ca-HCO ₃	Na-HCO ₃
14	3367	Ca-HCO ₃	Na-HCO ₃
15	3371	Na-HCO ₃	Mg-HCO ₃
16	3384	Ca-HCO ₃	Na-SO ₄

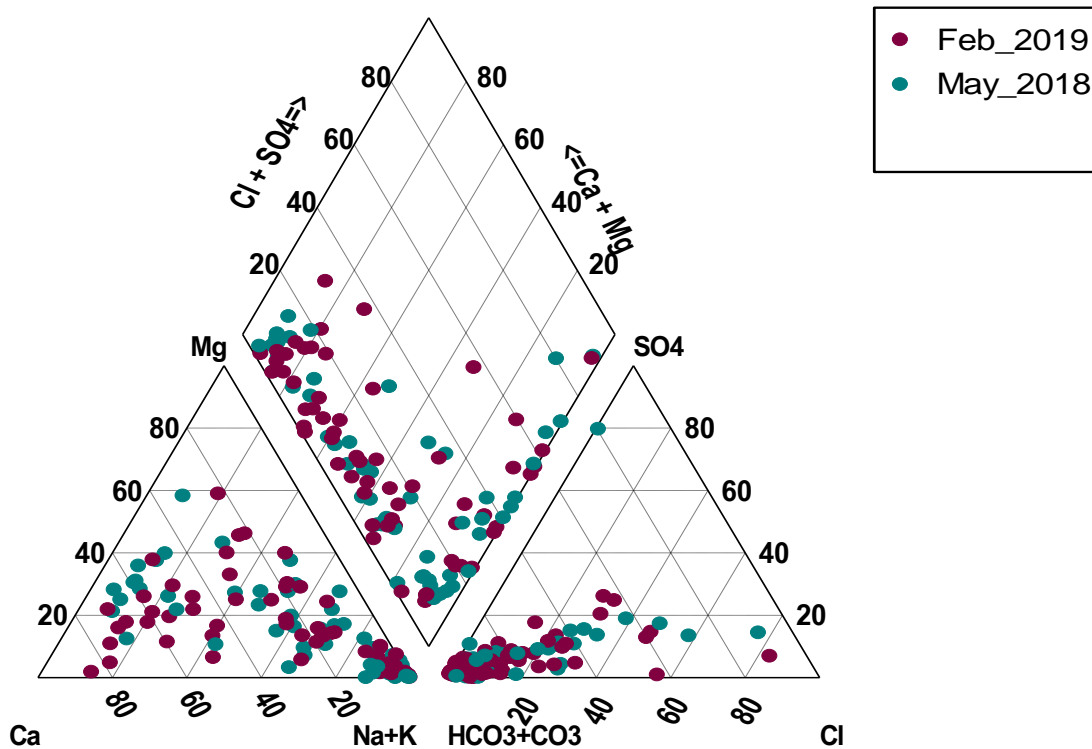


Figure 4.43: Changes in 58 groundwater samples collected in the wet season (May 2018) and in the dry season (February 2019) in the hydrochemical facies

4.2.2.3 Groundwater quality Index (GWQI) and its seasonal variations

The groundwater quality indices (Figure 4.44, 45-; Table 4.25) for both the wet and dry seasons were evaluated based on the ratings given in Table 3.13 (section 3.42). The results revealed that the SAA is characterised by excellent (WQI = 0-25) to good (WQI = 26-50) quality water during the wet and dry seasons except for seven samples in the wet season; two with poor water quality (WQI = 51-75) and five with very poor water quality (WQI = 76-100). In the dry season, one sample of the SAA had poor water quality while two samples had very poor water quality index. The TGSA groundwater had a water quality index > 200 in both seasons and is considered unsuitable for drinking. The intermediate aquifer is characterised by good groundwater quality in the wet and dry seasons except for water sources adjacent to the Turkana grit that had poor drinking water quality (WQI = 51-75). The deep aquifer also had good drinking water quality. In the wet season, the majority of the boreholes and handpumps with unknown depth had good drinking water quality (22 samples), poor water quality (seven), very poor water quality (six), and unfit for drinking (nine). The water quality index of these boreholes and handpumps (DU category) ranged between excellent quality in the dry season (13 samples), good water quality (two), poor water quality (three), and very poor water quality

(six). Generally, the WQI of groundwater in the study area was observed to improve in the dry season (Table 4.25), suggesting possible flushing of pollutants and mineral dissolution in the aquifers in the wet season. Excellent groundwater quality means that none of the assessed parameters exceeded the KEBS (2014) and WHO (2011) drinking water guidelines, whereas poor water quality means that one or more parameters exceeded the guideline. It was also found that water samples with WQI greater than 100 had more than five chemical parameters in excess of the guideline values.

Table 4.25: Water quality index (a) in the wet season and (b) in the dry season for the SAA, IA, TGS and the DA, and for the boreholes and handpumps with an unknown depth

(a) WQI wet season								
WQI Range	Type of water	SAA	TGSA	IA	DA	Depth Unknown	Total Samples	% Samples
<25	Excellent	6	Nil	1	Nil	Nil	7	7.4%
26-50	Good	9	Nil	11	2	22	44	46.8%
51-75	Poor	2	Nil	6	Nil	7	15	16.0%
76-100	Very poor	5	Nil	1	Nil	6	12	12.8%
>100	Unfit for drinking	Nil	6	1	Nil	9	16	17.0%
Total		22	6	20	2	44	94	100.0%
(b) WQI dry season								
WQI Range	Type of water	SAA	TGSA	IA	DA	Depth Unknown	Total Samples	% Samples
<25	Excellent	9	Nil	Nil	Nil	13	22	37.9%
26-50	Good	2	Nil	9	2	2	15	25.9%
51-75	Poor	1	Nil	4	Nil	3	8	13.8%
76-100	Very poor	2	Nil	Nil	Nil	6	8	13.8%
>100	Unfit for drinking	1	4	Nil	Nil	Nil	5	8.6%
Total		15	4	13	2	24	58	100.0%

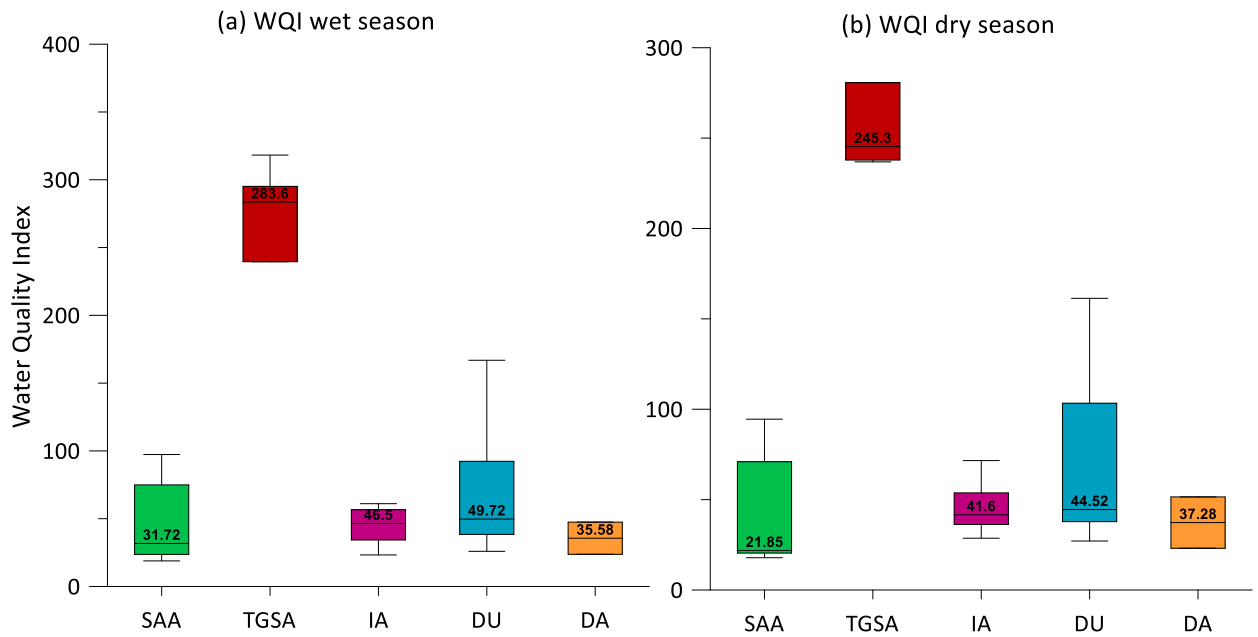


Figure 4.44: Variations in the water quality index values during the (a) wet season and in the (b) dry season showing improved water quality in all the aquifers in the dry season

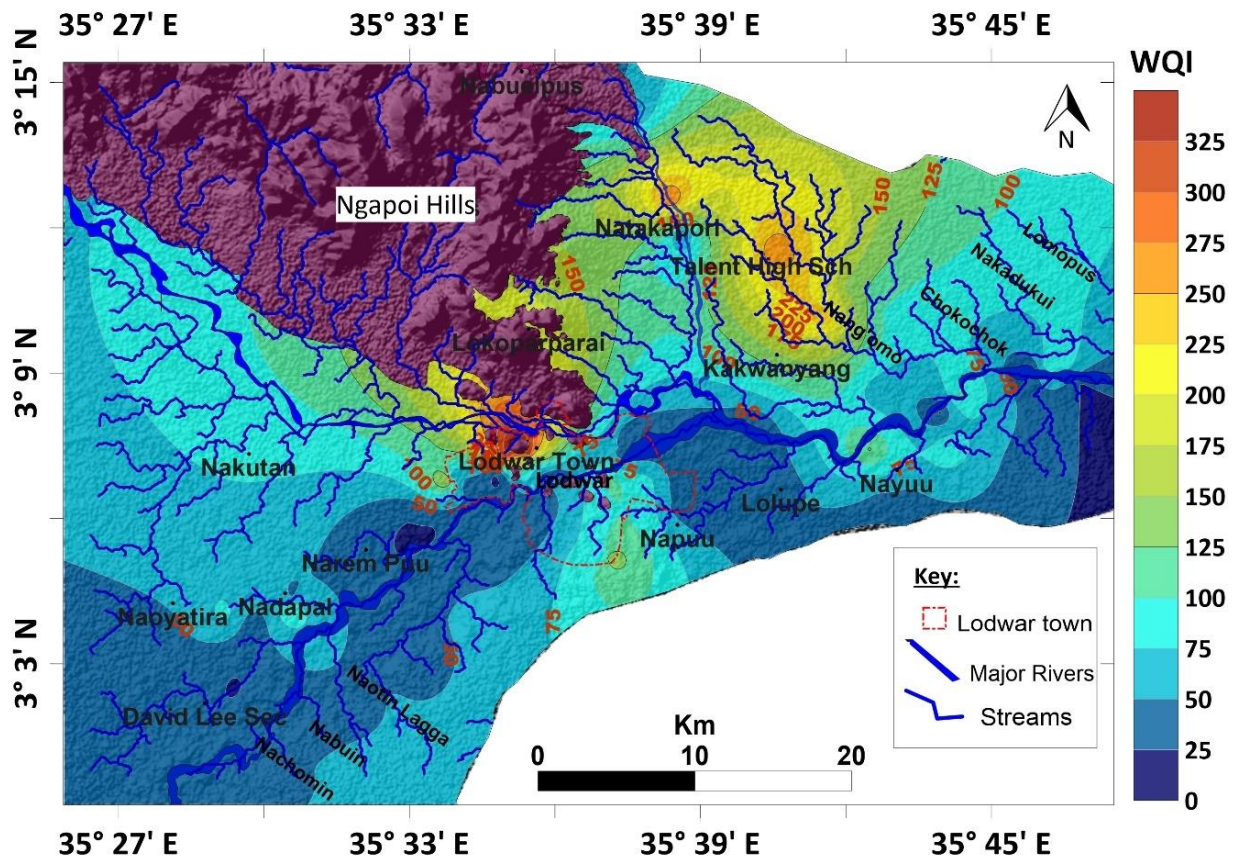


Figure 4.45 WQI map for the study area based on the 94 groundwater samples of the wet season

4.2.2.4 Determination of processes affecting groundwater quality by a multivariate statistical approach

PCA and HCA were carried out on the sample's shallow alluvial aquifer, Turkana grit shallow aquifer and on samples of the intermediate aquifer during the wet and dry seasons except for the deep aquifer whose samples were insufficient for application of statistical techniques.

1) Principal Component analysis

(a) Shallow alluvial aquifer

The PC1 and PC2 for shallow alluvial aquifer contributed 33.0% and 20.2 % respectively of the total variance in the wet season while the PC 1 and PC 2 in the dry season contributed 28.8% and 19.0%, respectively. Most of the chemical parameters loaded positively on PC 1 and PC 2 during the wet (Figure 4.46a) and majority loaded negatively on PC 1 and PC 2. In the dry season, there was an enrichment of PC 1 variables in the groundwater leading to the addition of K, Fe and Mn. The positive factors of PC1 in the wet season for the shallow alluvial aquifer reflected changing ionic strength on the concentrations of EC, Na, Mg and HCO_3^- as a result of dilution by recharge water.

(b) Turkana grits shallow aquifer

In the wet season, the PC1 and PC2 for Turkana grit shallow aquifer contributed 49.8% and 25.8 % respectively of the total variance while the PC 1 and PC 2 in the dry season contributed 68.7% and 17.9% respectively. pH, HCO_3^- , F, and NO_3^- were loaded positively on PC 1 and PC 2 in the wet season (Figure 4.46c) and in the dry seasons (Figure 4.46d), where only NO_3^- became negatively loaded in the dry season. EC, Ca^{2+} , Mg^{2+} , Na^+ and Cl^- were loaded negatively on PC 1 in both seasons. The positive factors of PC1 in the wet season reflect chemical concentrations controlled mainly by pH (EC, Na, Mg, HCO_3^- , SO_4 , Cl and NO_3). The negative variables of PC 1 in this aquifer were Ca, Fe and Mn in the dry season with the enrichment in the dry season leading to the addition of K, Mg and F.

(c) Intermediate aquifer

In the wet season, the PC1 and PC2 for intermediate aquifer contributed 30.2% and 23.6 % respectively of the total variance while the PC 1 and PC 2 in the dry season contributed 33.8% and 32.8% respectively. PC 1 during the wet and dry seasons was negatively loaded for most chemical parameters, while PC 2 was positively loaded for most chemical parameters in both seasons (Figure 4.46e, f). As in the case of the SAA, the positive factor loadings of PC1 in the

intermediate aquifer reflects changing ionic strength as a result of dilution by recharge water. However, pH influences the positive chemical variables of PC1 in this aquifer and subsequent addition of Fe to this PC. The negative members of PC 1 were Ca, K, Mn and NO₃ reflecting leaching of these ions from the soil zone. In the dry season, the reverse role of pH was observed, and mineral enrichment leads to the addition of Ca and K to the positive factor loadings of PC 1. Ion exchange processes reflected by positive variables of PC 2 in the wet season involved Ca and Mg carbonates leading to low pH, and this characteristic was reversed in the dry season. The negative factor loadings in the wet season were Na, K and Cl reflecting salt dissolution influencing changes in pH while the negative factor loadings in the dry season included Ca, Mg, K and Mn indicating carbonate precipitation.

(d) Depth unknown

In the wet season, the PC 1 and PC 2 for the groundwater samples with unknown depths contributed 39.7% and 19.7% of the total variability respectively. In the dry season, the PC 1 and PC 2 for these samples contributed 57.0% and 11.9% of the total variance. Majority of the chemical parameters were positively loaded on PC 1 and PC 2 in the wet season (Figure 4.46g) and in the dry season (Figure 4.46h). Positive PC1 factors for these samples in the wet season represented dilution by recharge water and subsequent enrichment of EC, Na, K, Cl, and F in this PC in the dry season. In the dry season, the positive factors of PC 2 indicated rock-water interaction influenced by pH changes and leaching of Ca, Mg, K and Fe from the soil zone as indicated by the negative variables of PC 2.

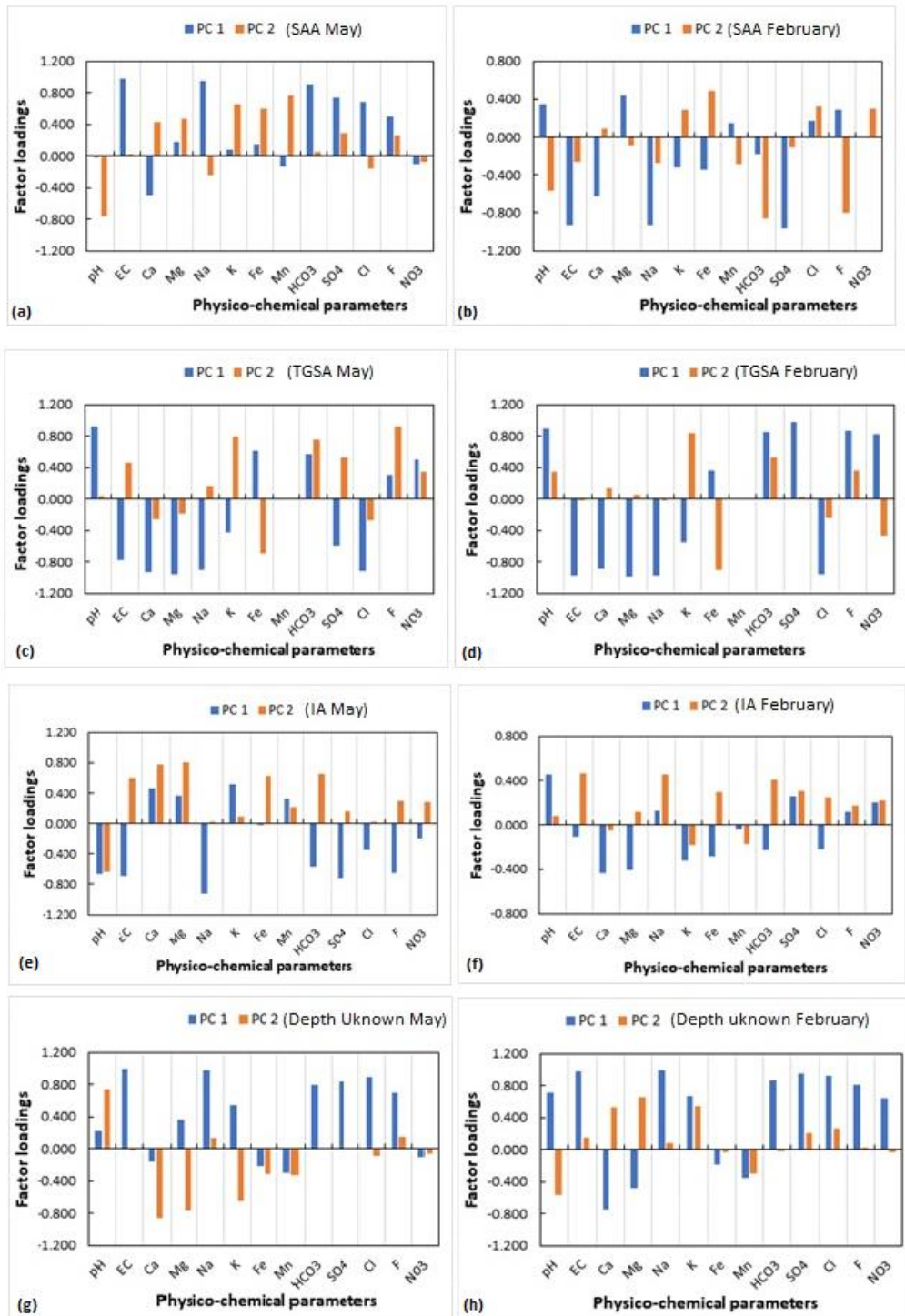


Figure 4.46: Factor loadings for PC 1 and PC 2 during (a) wet season and during (b) dry season for the SAA; TGSA (c) wet season and during (d) dry season; IA during (e) wet season and during (f) dry season and for the wells without the drilled depth information (g) wet season and during (h) dry season

2) Hierarchical Cluster Analysis

The HCA was carried out for groundwater samples of the study area using the Microsoft Excel add-in module XLSTAT 2019 utilizing group average clustering and euclidean distance methods based on dissimilarities. Based on HCA, the groundwater samples of the study area can be classified under two major groups; Group 1 (bicarbonate) and Group 2 (Sodium chloride) water. The degree of mineralisation controlled by EC, Na, SO₄ and Cl determines the varied clusters in each group. In the wet season (Figure 4.47a), Cluster 1 (C1) of Group 1 consisted all samples (22) of the SAA, eight samples of the IA, two samples of the deep aquifer and 32 samples with an unknown depth. Cluster 2 (C2) on the other hand, indicated increased mineralisation from Cluster 1 (C1) with only two samples of the intermediate aquifer while the rest had unknown depth value. Cluster 3 (C3) represented moderately to highly mineralised groundwater as a result of mixing between the groundwater of the Holocene sediments and that of the Turkana grit. In the dry season (Figure 4.47b) C1 of Group 1 consisted two sub-groups; Ca-HCO₃ water of the shallow alluvial aquifer and the Na-HCO₃ water of the intermediate aquifer, with each sub-group incorporating samples with an unknown depth. Cluster 2 (C2) of Group 1 represented moderately mineralised groundwater in the transition zone between the Holocene sediments and the Turkana grits. Clusters C3 and C4 are members of Group 2 representing highly mineralised groundwater of the Turkana grit shallow aquifer with C4 being the Bokotom Hp which was more mineralised due to excess Na and Cl concentrations.

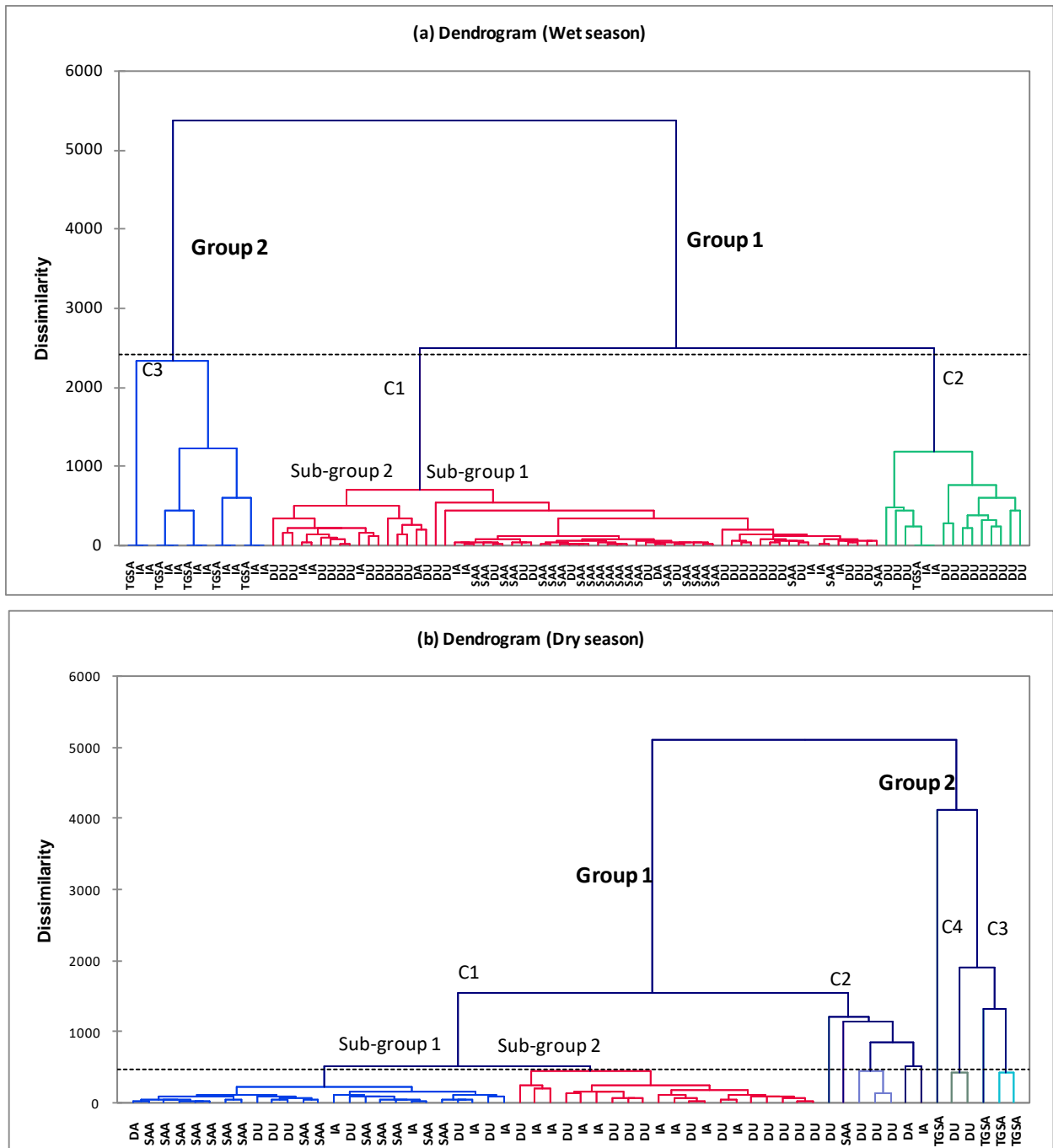


Figure 4.47: Dendrogram (a) in the wet season and (b) in the dry season for groundwater samples, showing three main clusters in the wet season and four main groups in the dry season, based on aquifer mineralization levels

3) Mineral saturation indices

The SI of the minerals in the SAA were undersaturated in the wet season while aragonite, calcite, dolomite and manganese compounds showed saturation in the dry season (Figure 4.48a). In the wet season, the mineral SI was undersaturated except for the manganese

compounds and saturated in the dry season with respect to aragonite, calcite, dolomite and hausmannite (Figure 4.48b). Apart from aragonite, calcite, dolomite and manganese compounds, the SI of the rest of the minerals were undersaturated in the intermediate aquifer during the wet and dry seasons (Figure 4.48c). The SI of the minerals in the deep aquifer was undersaturated during the wet and dry seasons except for aragonite, calcite and dolomite (Figure 4.48d). The SI of the minerals for the wells with unknown depth was undersaturated in the wet season and saturated for aragonite, calcite, dolomite and manganese compounds in the dry season (Figure 4.48e).

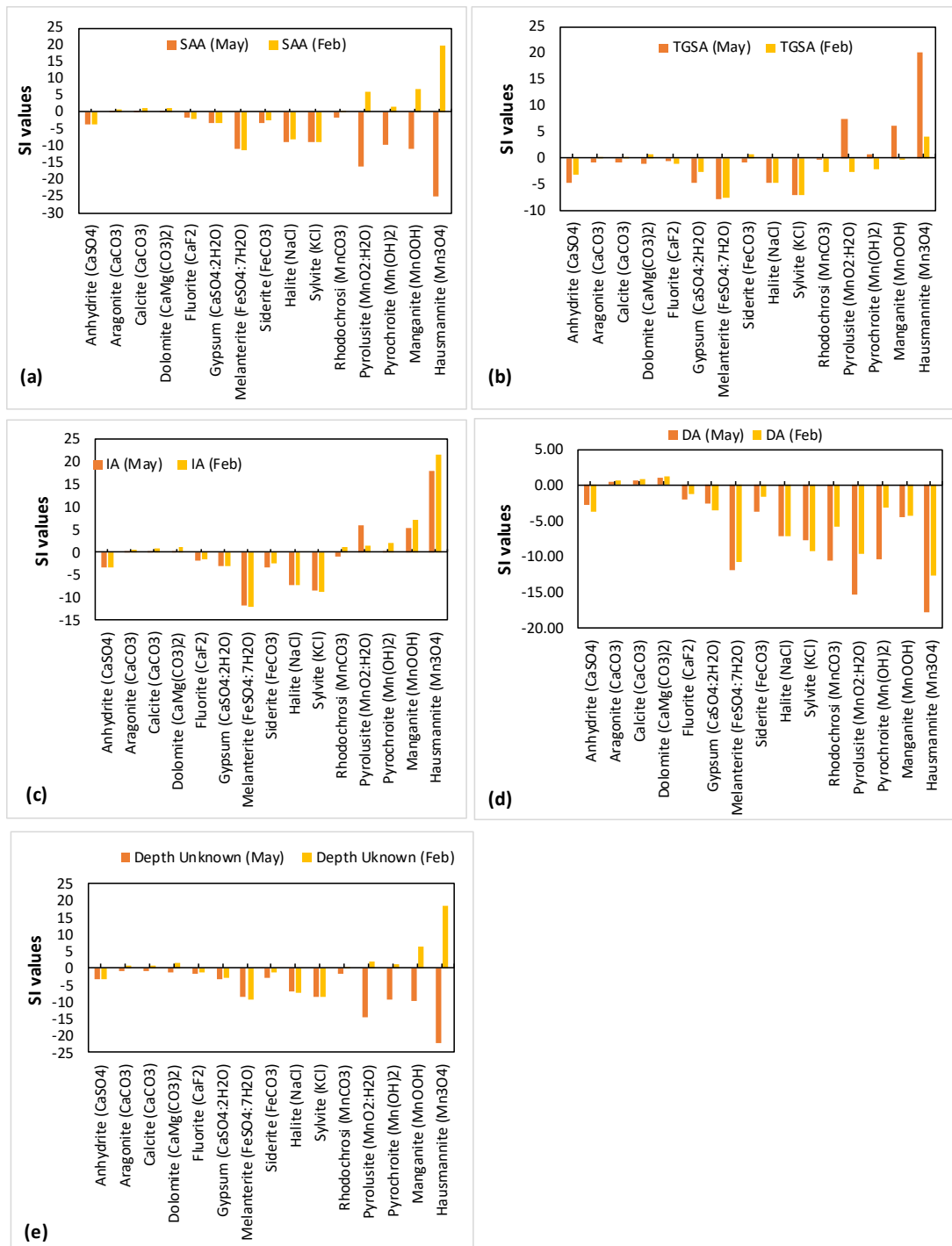


Figure 4.48: Saturation indices of minerals in the wet season (May) and in the February - dry season for (a) SAA; (b) TGSA; (c) IA; (d) DA and wells without drilled depth information

4.2.2.5 *Rock-water interactions in the LAAS*

a) General aspects

The results presented in the sections above allow for investigation of the primary rock-water interactions in the LAAS both generally and also in relation to the four different aquifer sub-systems. The TGSA had the greatest Na^+ concentrations followed by those with unknown depths, then the intermediate aquifer and lastly those in the shallow alluvial aquifer. All the groundwater and the surface water of the study region demonstrated a linear relationship with a slope similar to -1 during the wet and dry seasons. Thus, this plot reveals that Na^+ , Ca^{2+} and Mg^{2+} participate in ion change processes where dissolved Ca^{2+} and Mg^{2+} are exchanged with adsorbed Na^+ in the aquifer matrix. Figure 4.12 suggests that ion exchange is a major hydrochemical process indicated by the slope, which is close to -1 (Fisher and Mullican, 1997). The hierarchical cluster analysis (Figure 4.10) revealed that the groundwater of the study area belongs to three major clusters in the wet season and four major clusters in the dry season based on levels of mineralization in the aquifer systems. The relationship between Na^+ and Cl^- ions in the groundwater formed similar clusters observed in the HCA results. The minerals determined by the PHREEQC from the groundwater of the study area during the dry and the wet seasons included; anhydrite, aragonite, calcite, dolomite, fluorite, gypsum, melanterite, siderite, halite, sylvite, rhodochrosite, pyrolusite, pyrochroite, manganite, and hausmannite mineral phases.

b) Contrasts in the LAAS Sub-systems

(i) Variations in Na^+ and Cl^- ions

The Na^+/Cl^- ratios of the shallow alluvial aquifer in the wet season were less or equal to 1.0 for 31.8% of the samples while the rest had ratios greater than one (Figure 4.49). In the dry season, only two boreholes; Bh 1A and Bh 3 had Na^+/Cl^- ratios <1.0 while the rest (86.7%) had ratios >1 . All Turkana grit shallow aquifer samples had Na^+/Cl^- ratios greater than 1.0 in the wet seasons (Figure 4.49a) and dry (Figure 4.49b), except for the Bokotom Hp, the ration of which was equivalent to one in both seasons. All the groundwater samples of the intermediate aquifer during the wet and dry seasons had Na^+/Cl^- ratios more significant than one except for Chokocho Pri Hp that had a molar ratio of 1.2 in the wet season (Figure 4.49a) and that of Kakamera Church Hp whose ratio was 0.5. The progression in Na^+ concentration suggests that many of the Bh/Hp with unknown depth are in the transition areas between the Holocene sediments and the grit areas. The Na^+/Cl^- ratio for the wet season was 2.83 compared to that of

the dry season, which was 2.75, indicating that some of the Na^+ are remobilized into solution. Deep aquifer (DA) – Natirnalung Bh of the deep aquifer had Na^+/Cl^- a ratio of 0.9 in the wet season and 1.3 in the dry season while that of Napuu 1 Bh was 2.8 in the wet season and 3.2 in the dry season (Figure 4.49). Wells with Unknown depth – Only two of the boreholes and handpumps with no depth records had Na^+/Cl^- ratios less or equal to one in the wet season; Nakadukui Bh (0.80) and Nasenyanait Hp (1.3) (Figure 4.49). In the dry season, only Nakoporor Hp had a Na^+/Cl^- ratio of 0.7.

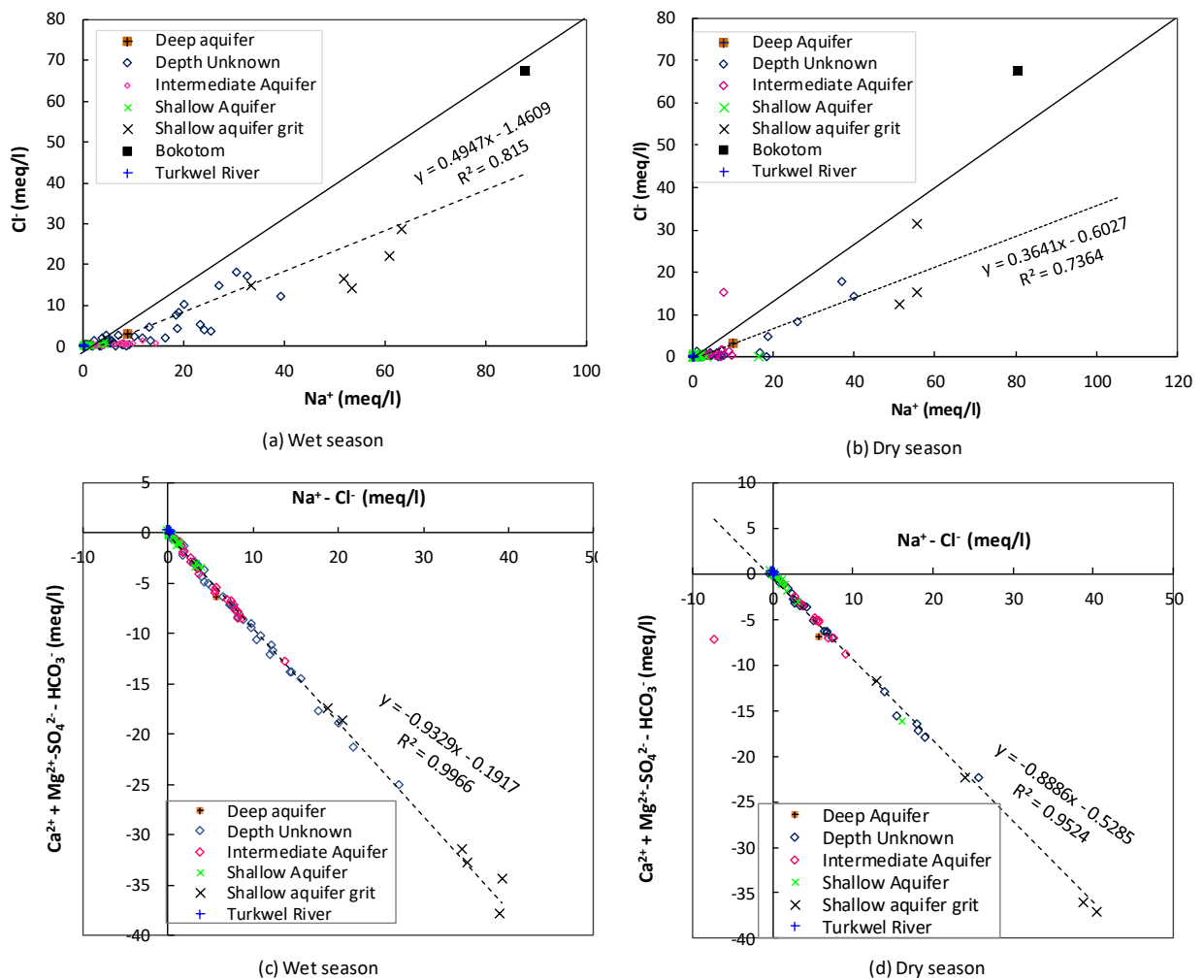


Figure 4.49: Plots for Na^+/Cl^- in groundwater in the (a) wet season and (b) dry season and for the relationship between $[\text{Ca}^{2+} + \text{Mg}^{2+} - \text{SO}_4^{2-} - \text{HCO}_3^-]$ and $[\text{Na}^+ - \text{Cl}^-]$ (c) and (d) in the surface water, shallow alluvial aquifer (SAA), intermediate aquifer (IA), Turkana grit shallow aquifer (TGSA) and the deep aquifer (DA) (Fisher and Mullican, 1997)

(ii) Hydrogeochemical process in aquifers

Dilution by recharge water occurs both in the SAA and IA related to changing ionic strength in dry and wet seasons based on common behaviour of factor loadings on PC 1. The undersaturation and saturation of aragonite, calcite and dolomite in the SAA controls the factor loadings on PC 1 and PC 2 during the wet and dry seasons. While the saturation of these minerals control PC1 and PC 2 of the IA. Other processes in this aquifer include; Ion exchange processes reflected by positive variables of PC 2, leaching of ions (Ca, K, Mn and NO₃) soil zone, dissolution and carbonate precipitation motivated by reserves role of pH in the wet and dry seasons, respectively. HCA revealed Natir Bh of the deep aquifer exhibits similar characteristics with the SAA while that of Napuu Bh reflects the behaviour of the intermediate aquifer. The positive factor loadings of PC 1 for wells with unknown depth are related to an undersaturation of aragonite, calcite, dolomite and manganese compounds. Dilution by recharge water, mineral dissolution and ion exchange were identified to the dominant processes for these wells based on factor loadings of PC 1 and PC 2. Rock water interaction in the wet season and increased mineral enrichment in the dry season from weathering and release of Na, Ca, Mg, K, Mn, in the aquifer medium to the groundwater are the major processes in the TGSA.

The groundwater of the SAA belonged to Cluster 1 (C1) sub-group 1, characterized by low mineralization during the wet and dry season, as shown by the HCA (Figure 4.47). The HCA revealed that two factors influence the groundwater chemistry of the intermediate aquifer in the wet and dry seasons; (1) the proximity to the Turkwel river (Cluster C1) and (2) proximity to the Turkana grits formation (C2 and C3) (Figure 4.47). The groundwater chemistry of the TGSA is displayed as a unique system disconnected from the SAA, IA and the DA. The HCA revealed highly mineralized groundwater in the TGSA belonging to Cluster 3 (C3) during the wet and dry season with Bokotom Hp forming Cluster 4 (C4) in the dry season, owing to its excess Na⁺ and Cl⁻ ions. The HCA of the samples during the wet and dry seasons revealed that the majority of the boreholes and handpumps with unknown drilled depth (32) belonged to the shallow alluvial aquifer (Cluster 1), 12 in the intermediate aquifer while only two were in the Turkana grit formation.

4.2.2.6 *Aquifer vulnerability to pollution from point and diffuse sources; anthropogenic pollution (results)*

(a) *Nitrate loading in river water*

Nitrate loading in the Turkwel River was evaluated for the seven water samples collected in the dry season of February 2018; two upstream samples (SW/006 and SW001), three within the Lodwar Municipality ((SW/002, SW/007, and SW/005), and two samples (SW/004 and SW/008) were located downstream (Figure 3.16). Samples located inside the municipal boundary showed elevated NO_3 levels Figure 4.50).

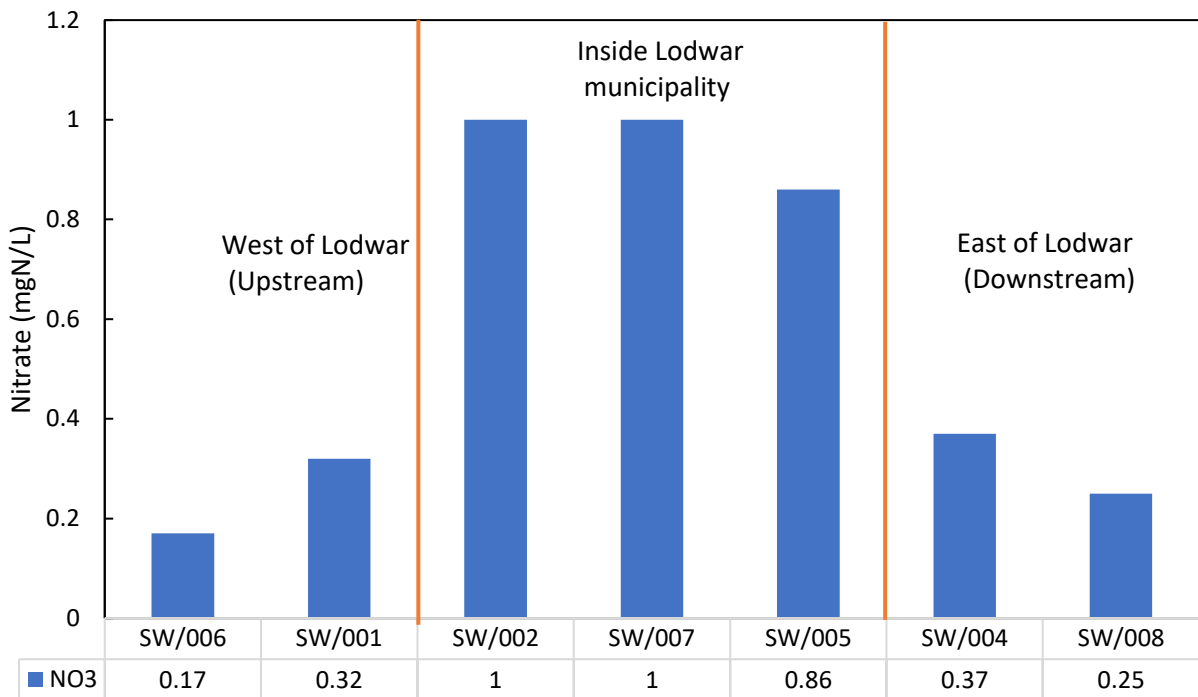


Figure 4.50: Nitrate levels across the Turkwel river samples indicating elevated levels for the samples within the Lodwar Municipal boundary in the dry season of February 2018.

(b) *Vulnerability of municipal groundwater sources to pollution*

NO_3 in 25 groundwater sources within the Lodwar municipality boundary showed increased concentrations in the wet season. Although these concentrations were generally below the guideline value of drinking water, institutional groundwater sources showed values approaching the guideline values in the wet and dry season (Table 4.26). Generally, increased NO_3 concentrations were observed within the shallow alluvial aquifer than in the intermediate aquifer and may be linked to leaching of NO_3 ions from domestic wastewater (point sources) and surface runoff (non-point sources).

To establish the water sources exposed to either point and non-point pollution sources, the high-resolution DEM acquired from the drone mapping was used to extract the drainage lineaments of the Lodwar municipality. The NO₃ concentrations within the municipality boundary were used to generate heatmaps based on natural breaks algorithm for identification of point and non-point source pollution. The distribution of NO₃ in groundwater of Lodwar town is in the range of 0.01 to 0.37 mg N/L for most wells in the wet season and between 0.01 and 0.29 mg N/L in the dry season (Figure 4.51). No significant variations are observed in the spatial distribution in the dry season apart from sample 3376 opposite Stegra Hotel that was higher in the dry season. The Stegra Hotel boreholes are located in a major stream in the area. It is interesting to note that all wells with elevated nitrate levels (> 0.29 mg / L in the dry season and 0.37 mg / L in the wet season) are located on or adjacent to streams in the region. This indicates that surface runoff is a driving factor for groundwater pollution in Lodwar town in the wet season (non-point sources); otherwise, they are associated with point-source pollution.

Table 4.26: Institutional groundwater supply sources with NO₃ levels >5.0 mg/L in the wet and dry seasons

Sample ID	Lab Code	NO ₃ Wet season (mgN/L)	NO ₃ Dry season (mgN/L)
Loyo Pri Hp (at Nakwamekwi)	3399	7.92	5.03
Opposite Stegra Bh	3376	9.25	27.65
Stegra Hotel Bh	3377	5.52	5.24
Trumpet of Hope Ministries (at Nakwamekwi)	3394	33.64	7.82

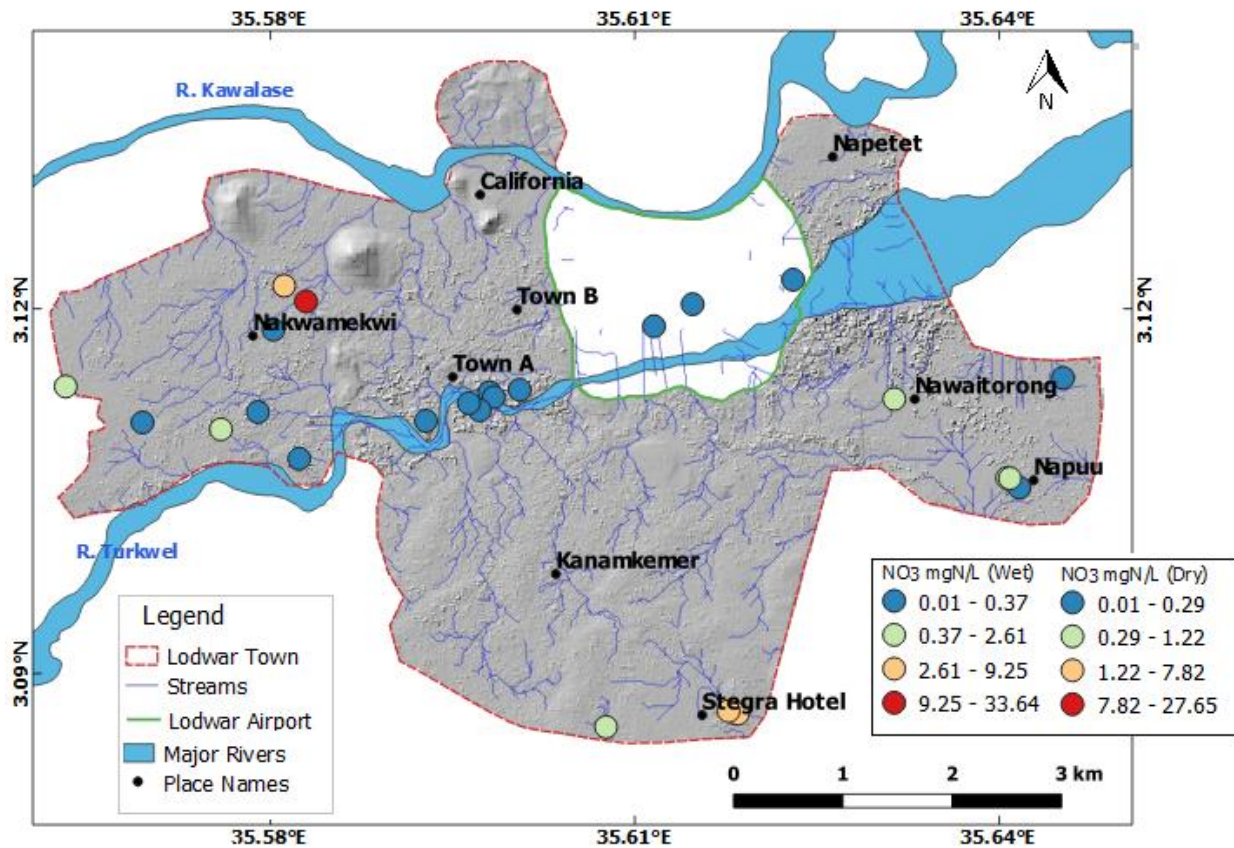


Figure 4.51: Heat map for NO₃ within Lodwar Municipal boundary indicating areas of elevated concentrations across the Lodwar municipality

The groundwater of Lodwar Alluvial Aquifer System (SAA, IA and DA) is generally uncontaminated (Tanui *et al.*, 2020). However, increasing NO₃ concentrations in these sub-systems in the wet season indicate their vulnerability to pollution. On-site sanitation is widely practised in Lodwar town owing to lack of functional sewerage network and proper disposal of municipal waste (Olago, 2018; Hirpa *et al.*, 2018). In the wet season, pollutants are likely to be flushed into the aquifers, especially the shallow alluvial aquifer by surface runoff. Upstream human activities such the proposed 10, 000 Ha of irrigated land (Oera, 2015) pose a human-induced pollution risk to an already vulnerable system to climate variability (Hirpa *et al.*, 2018).

4.2.3 *Rainfall-Surface Water-Groundwater Interactions and Groundwater Recharge*

This section presents the results of the stable isotopes of oxygen-18 (^{18}O) deuterium (^2H) and tritium (^3H) for the surface water (Turkwel river, Kawalase river, Monti river water pans, and scoop holes), groundwater (boreholes and handpumps), Eliye spring, rainwater, and Lake Turkana samples. This section also establishes the rainfall-surface water-groundwater interaction and recharge characteristics.

4.2.3.1 *Oxygen, deuterium and tritium isotope results*

(1) Rainfall and surface water

(a) Rainfall

The $\delta^{18}\text{O}$ of the rain sample was -1.33‰ while the $\delta^2\text{H}$ was $+7.4\text{‰}$ while the tritium content was 1.7 TU.

(b) River water

Turkwel River (4) and Kawalase lagga (2) were analysed for oxygen-18 and deuterium (Appendix 4-16). The Turkwel River samples had fairly uniform isotope compositions of $\delta^{18}\text{O}$ ($+0.06$ to $+0.90\text{‰}$) and $\delta^2\text{H}$ ($+6.5$ to $+9.8\text{‰}$). One sample of the flowing water of Kawalase River showed $\delta^{18}\text{O}$ compositions of $+0.25\text{‰}$ and $+2.6\text{‰}$ for $\delta^2\text{H}$, indicating a slight $\delta^{18}\text{O}$ ($+0.19 \text{‰}$) enrichment as compared to that of Turkwel River. The Turkwel River was more enriched in deuterium ($+4.5 \text{‰}$) than the Kawalase River. Tritium was measured for one sample of the Turkwel River within Lodwar town and was found to be 2.1 TU.

(c) Water pans

Oxygen-18 and deuterium were measured for four water pans within the Turkwel River basin (Monti, Nakutan, Namuthia, and Nakariong'ora) and one (Kerio water pan) at its border with the Kerio River basin. The isotope composition of water pans in the Turkwel River basin was -4.40 to -2.52‰ for $\delta^{18}\text{O}$ and -10.7 to -7.6‰ for $\delta^2\text{H}$. The $\delta^{18}\text{O}$ of the Kerio water pan was $+0.19 \text{‰}$ and $+5.8\text{‰}$ for $\delta^2\text{H}$. The Kerio water pan was more enriched in both $\delta^{18}\text{O}$ and $\delta^2\text{H}$ as compared to that of the water pans in the Turkwel River basin.

(d) Scoop holes and spring samples

The $\delta^{18}\text{O}$ for the scoop holes ranged from -3.95 to -1.43‰ with a median value of -2.42‰ while the $\delta^2\text{H}$ ranged from -23.7 to 2.4‰ with a median value of (-9.7‰) . The $\delta^{18}\text{O}$ for the

Eliye Spring sample collected on its outlet was -2.51‰ and -7.4‰ for $\delta^2\text{H}$. Tritium was not measured for both the scoop holes and Eliye Spring samples.

(e) Lake Turkana

Isotopic compositions of the Lake Turkana at the shoreline of the Eliye Spring area was 5.41‰ for $\delta^{18}\text{O}$ and $+41.3\text{‰}$ for $\delta^2\text{H}$, while at the Turkwel River delta, $\delta^{18}\text{O}$ was $+6.60$ and 42.4‰ for $\delta^2\text{H}$. Tritium levels of Lake Turkana at Turkwel delta were 1.8 TU and 1.7 TU for the sample on its shores at the Eliye spring, indicating mixing with river water, leading to Tritium enrichment at the delta region.

Figure 4.52 shows the isotope signatures of $\delta^{18}\text{O}$ and $\delta^2\text{H}$ in various types of water samples from the study area. A comparison of the composition of hydrogen and oxygen isotopes between rainwater and Turkwel river water showed that the composition of river water $\delta^{18}\text{O}$ and $\delta^2\text{H}$ isotopes does not correspond to that of local rainfall. The river water has more enriched $\delta^{18}\text{O}$ and $\delta^2\text{H}$ isotopes than that of the rainfall, suggesting effects of evaporation in the Turkwel River.

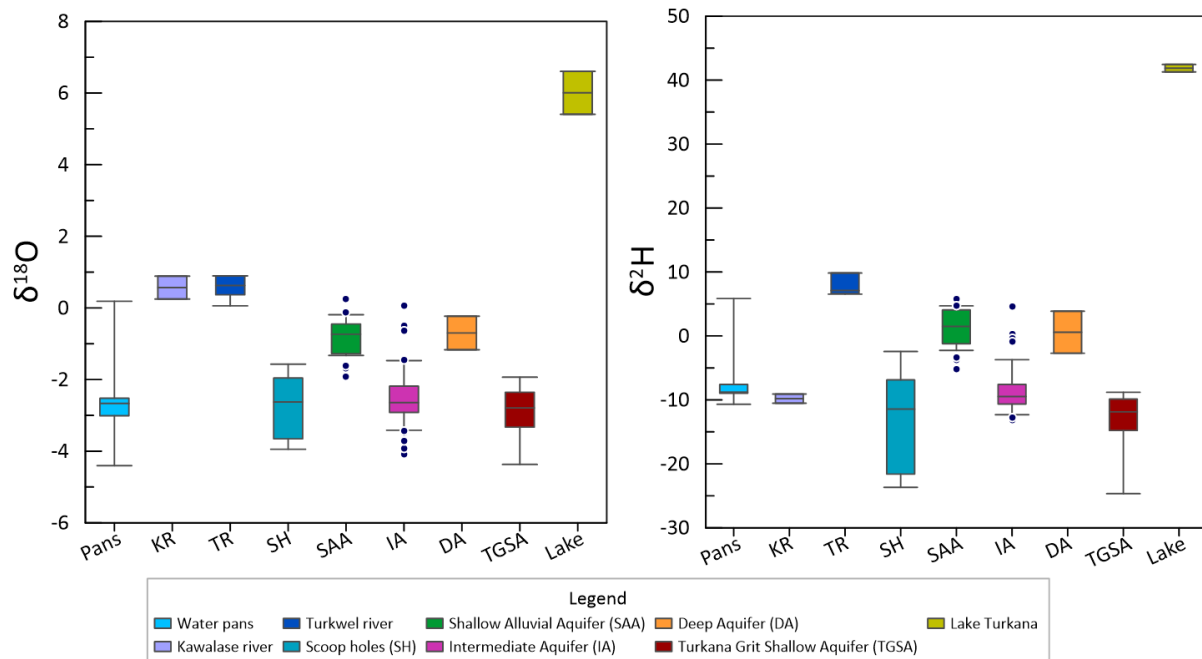


Figure 4.52: Isotope signatures of (a) $\delta^{18}\text{O}$ and (b) $\delta^2\text{H}$ in river water (KR and TR), water pans, scoop holes (SH), spring and lake samples, as well as groundwater samples from the shallow alluvial aquifer (SAA), intermediate aquifer (IA), Turkana grit shallow aquifer (TGSA) and the deep aquifer (DA)

Table 4.27: Descriptive statistics for $\delta^{18}\text{O}$ and $\delta^2\text{H}$ in rainfall and surface water in the Lodwar and its environs (n/a for median and standard deviation values represent one sample available for analysis)

Description	Minimum	Maximum	Median	SD
Descriptive statistics for oxygen-18 (‰)				
Rain	-1.33	-1.33	n/a	n/a
Turkwel River (TR)	+0.06	+0.90	+0.63	0.41
Kawalase River (KW)	+0.25	+0.25	n/a	n/a
Water pans (Pans)	-4.40	+0.19	-2.67	1.67
Scoop holes (SH)	-3.95	-1.43	-2.42	0.95
Eliye Spring	-2.51	-2.51	n/a	n/a
Lake Turkana (LT)	+5.41	+6.60	+6.01	+0.85
Descriptive statistics for deuterium (‰)				
Rain	+7.4	+7.4	n/a	n/a
Turkwel River (TR)	+6.5	+9.8	+7.1	1.5
Kawalase River (KW)	+2.6	+2.6	n/a	n/a
Water pans (Pans)	-33.9	+0.9	-15.9	13.0
Scoop holes (SH)	-23.7	-2.4	-9.7	7.7
Eliye Spring	-7.4	-7.4	n/a	n/a
Lake Turkana (LT)	+41.3	+42.4	+41.9	0.8

(2) Groundwater

(a) Shallow alluvial aquifer

A total of 22 groundwater samples (twelve handpumps and ten boreholes) in the shallow alluvial aquifer system showed that the $\delta^{18}\text{O}$ ranged between -2.92 and +0.25‰ with a median value of +0.68 ‰. The $\delta^2\text{H}$ in this aquifer ranged from -13.1 to +5.8 ‰, with a median value of +2.35 ‰ (Appendix 4-17). Tritium was measured for ten wells (seven handpumps and three boreholes) in the SAA, and all the samples revealed detectable levels of tritium. The values ranged between 1.1 and 2.2 TU, with an average TU value of 1.6 TU.

(b) Turkana Grit Shallow Aquifer

Six (6) handpump samples in this aquifer have a $\delta^{18}\text{O}$ range from -3.33 to -1.93‰ with a median value of -2.53 ‰ (Appendix 4-17)), while the $\delta^2\text{H}$ ranges from -14.78 to -8.81 ‰ with a median value of -10.55 ‰. Generally, this aquifer has more depleted isotope ratios than in

the shallow alluvial aquifer. Tritium was <0.8 TU in all the four groundwater samples of the Turkana Grit Shallow aquifer.

(c) Intermediate aquifer

A total of 20 groundwater samples from ten handpumps and ten boreholes were analysed for oxygen-18 (^{18}O) deuterium (^2H) in the intermediate aquifer (Appendix 4-17). The $\delta^{18}\text{O}$ ranged from -3.92 to 0.07 ‰ with a median value of -2.55 ‰. The $\delta^2\text{H}$ ranged between -11.30 to -4.54 ‰ with a median value of -7.79 ‰. Groundwater samples of this aquifer adjacent to the Turkwel River were more enriched in both ^{18}O and ^2H isotopes than those further away. Of the 20 groundwater samples of the IA, tritium was determined on seven samples, where four showed tritium values <0.8 TU. Tritium in the remaining three groundwater samples ranged from 1.0 to 1.9 TU (Kakemera Church Hp = 1.0 TU, Chokochok Primary Hp = 1.9 TU, and Napuu 4 Bh = 1.5 TU).

(d) Deep aquifer

The results of the isotope compositions for the samples of the deep aquifer are given in Appendix 4-17). The $\delta^{18}\text{O}$ for the Natirnalulung Bh (depth = 102) was +.23‰, and the $\delta^2\text{H}$ was +3.87‰. The $\delta^{18}\text{O}$ of Napuu 1 (depth = 100) was -1.17‰ while the $\delta^2\text{H}$ was +1.0‰. The Natirnalulung borehole is more enriched in $\delta^2\text{H}$ than in the $\delta^{18}\text{O}$ counterpart, while the Napuu 1 Bh is more enriched in $\delta^{18}\text{O}$. Napuu 1 borehole has more depleted isotope ratios as compared to that of the Natirnalulung Bh. The tritium for Natirnalulung Bh (Natir) was 2.1 TU, while that of Napuu 1 was 1.0 TU.

(e) Depth unknown

Of the 44 boreholes and handpumps with unknown depth, the isotope compositions of oxygen-18 and deuterium were determined for 41 samples (25 handpumps and 16 boreholes) (Appendix 4-17). The $\delta^{18}\text{O}$ ranged from -4.37 to -0.12 ‰ with a median value of -2.39 ‰. The $\delta^2\text{H}$ ranged between -24.7 to +5.9 ‰ with a median value of -9.0 ‰. Generally, these samples showed more $\delta^2\text{H}$ as compared to the $\delta^{18}\text{O}$ content. Tritium measurement for sixteen groundwater samples (four boreholes and twelve handpumps) of wells with unknown depth revealed values <0.8 TU for nine samples (four boreholes and five handpumps) and values ranging between 1.2 and 1.8 TU for the rest seven handpumps samples.

Table 4.28: Descriptive statistics Results for oxygen-18, ^2H and ^3H groundwater samples in the SAA, TGSA, IA, DA, and for wells with unknown depth (DU)

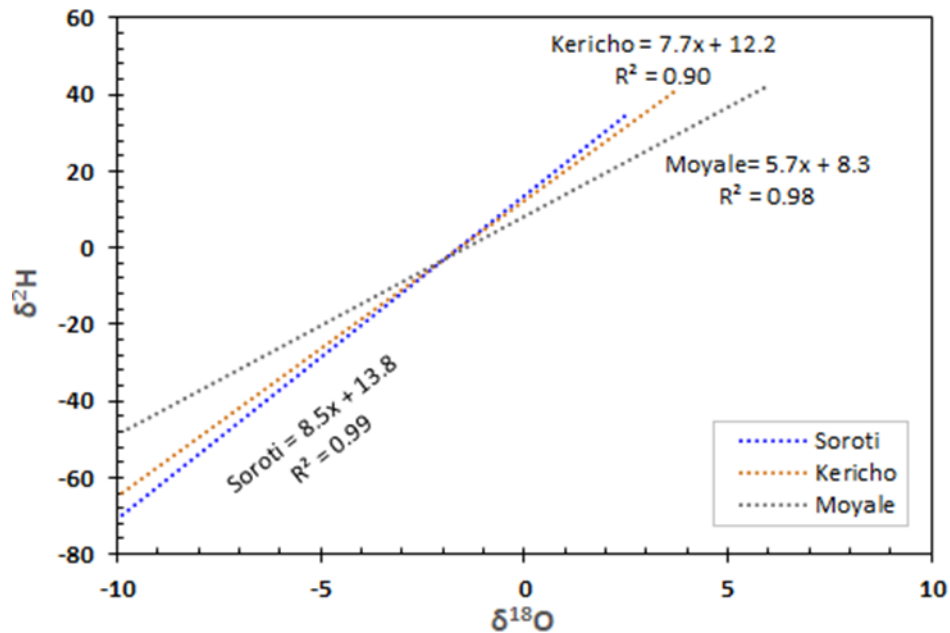
Description	Minimum	Maximum	Median	SD
Oxygen-18 ($\delta^{18}\text{O}$ ‰)				
SAA	-2.92	0.25	-0.68	0.88
TGSA	-3.33	-1.93	-2.53	0.50
IA	-3.92	+0.07	-2.55	0.97
DA	-1.17	-0.23	-0.70	0.66
DU	-4.37	-0.12	-2.39	1.08
Deuterium ($\delta^2\text{H}$ ‰)				
SAA	-13.1	+5.8	+2.3	5.4
TGSA	-14.8	-8.8	-10.5	2.2
IA	-11.3	+4.5	-7.8	4.4
DA	-2.7	+3.9	+0.6	4.6
DU	-24.7	+5.9	-9.0	6.3
Tritium (TU)				
SAA	1.1	2.2	1.6	0.3
TGSA	<0.8	n/a	n/a	n/a
IA	1.0	1.9	1.5	0.5
DA	1.0	2.1	1.6	0.8
DU	1.2	1.8	1.5	0.2

4.2.3.2 Isotopic ratios of oxygen-18 and deuterium

a) Selection of the linear regression model

The Global Mean Meteoric Water Line (GMWL) for three GNIP stations, Kericho, Soroti, and Moyale, is given by equation $\delta\text{D} = 8.0 \text{ }^{18}\text{O} + 10$ (Craig, 1996). The significance and data source for GMWL and LMWL is described in section 3.43. Regression statistics were tested to determine the best regression model for the three GNIP stations (Figure 4.53). The LMWL for Kericho GNIP station follows the equation $\delta\text{D} = 7.7 \text{ }^{18}\text{O} + 12.2$ with $R^2 = 0.90$. The LMWL for Soroti follows the equation $\delta\text{D} = 8.5 \text{ }^{18}\text{O} + 13.8$ with $R^2 = 0.99$ while the LMWL for Moyale GNIP station follows the equation $5.6947 \text{ }^{18}\text{O} + 8.3$ with $R^2 = 0.98$. These results indicated that the Soroti GNIP station in Uganda, though not completely relating to the observation data of the study area, was the best regression model for correlating with the isotopic data. Soroti station also represents rainfall characteristics upstream of the study area,

that is, the Mt. Elgon region which is the source of the Turkwel river. It is also important to note that the three regression lines for the GNIP stations intercepted at $\delta^{18}\text{O} = -2.28$ and $\delta^2\text{H} = -5.5$, suggesting similar processes of isotope fractionation in the region.



Regression Statistics	Kericho	Soroti	Moyale
Multiple R	0.9563	0.99751	0.991153
R Square	0.904902	0.995026	0.982384
Adjusted R Square	0.899308	0.994612	0.973575
Standard Error	6.64381	1.775293	3.714175
Observations	19	14	4

Figure 4.53: Regression lines of $\delta^2\text{H}$ versus $\delta^{18}\text{O}$ for the nearby GNIP stations; Kericho, Moyale and Soroti with their respective regression statistics

b) $\delta^{18}\text{O}$ and $\delta^2\text{H}$ ratio in rainfall and surface water

The isotopic compositions of the rainfall and surface water in Lodwar and its environs displayed varied isotopic compositions (Figure 4.54). The rain sample of the Lodwar town plotted above the LMWL, contrasting with the isotope composition of Turkwel River samples that plotted below the meteoric water lines. One river sample of the flowing water of the Kawalase River plotted below the LMWL, and slightly below that of the Turkwel River. The scoop holes of the streams in the eastern section of Lodwar all plotted along the LMWL, while those in the western part (Kawalase and Nakutan areas) plotted slightly below the meteoric water line, indicating $\delta^{18}\text{O}$ enrichment. All the water pan samples are below the LMWL while

that of the Eliye spring is located on the meteoric water line. The Lake Turkana samples showed enriched isotope ratios ($\delta^{18}\text{O}$ and $\delta^2\text{H}$) relative to the local meteoric water line and relative to all the types of water samples in the study area. By comparing the two lake samples, the one collected on its shores at Eliye Spring (2461) is more enriched than that obtained at the Turkwel delta (2462).

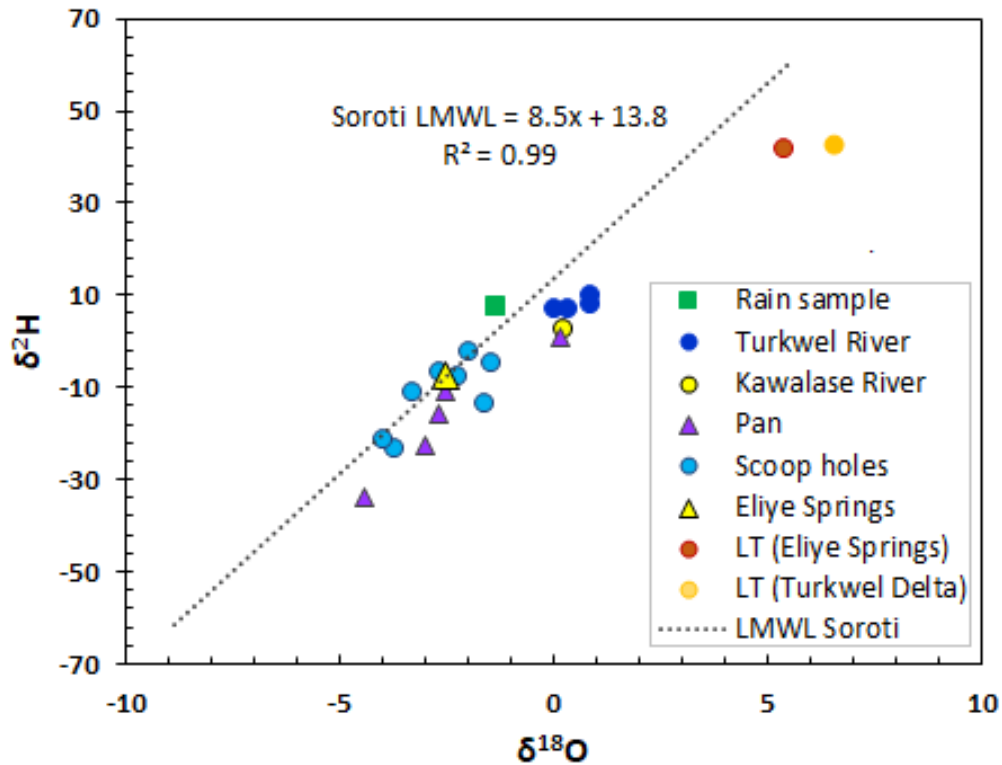


Figure 4.54: Relationship between $\delta^{18}\text{O}$ and $\delta^2\text{H}$ for the rain sample, Turkwel River, Kawalase River, scoop holes, water pans and springs in the study area

c) $\delta^{18}\text{O}$ and $\delta^2\text{H}$ ratio in groundwater

The relationship between $\delta^{18}\text{O}$ and $\delta^2\text{H}$ was determined for groundwater samples of the SAA, TGSA, IA, DA, and for the wells whose depth was unknown (Figure 4.55). The water samples of the SAA plotted generally below the Soroti LMWL indicating $\delta^{18}\text{O}$ enrichment relative to the meteoric water (Figure 4.55a). The groundwater of the TGSA plotted along the LMWL except for two samples (3394 and 3396) located at the contact zone of the Turkana grits and the nepheline-phonolite at Lodwar town that exhibited $\delta^{18}\text{O}$ enrichment and deviated from the LMWL (Figure 4.55c). As compared to the SAA, the groundwater of the TGSA and showed depleted $\delta^{18}\text{O}$ and $\delta^2\text{H}$ isotopes. The samples of the intermediate aquifer plotted around and along the LMWL except for three samples (3341, 3374 and 3392) that were plotted in the SAA field and two samples (3366 and 3368) that plotted above the meteoric water line, indicating

depleted $\delta^{18}\text{O}$ ratio relative to that of the meteoric water. The $\delta^2\text{H}/\delta^{18}\text{O}$ plot of the wells with unknown depth resulted in three distinct groups; group A that exhibited isotopic compositions of the SAA; group B that plotted in the region of the IA, and group C that comprised only two samples and plotted in the region of the TGSA (Figure 4.55d).

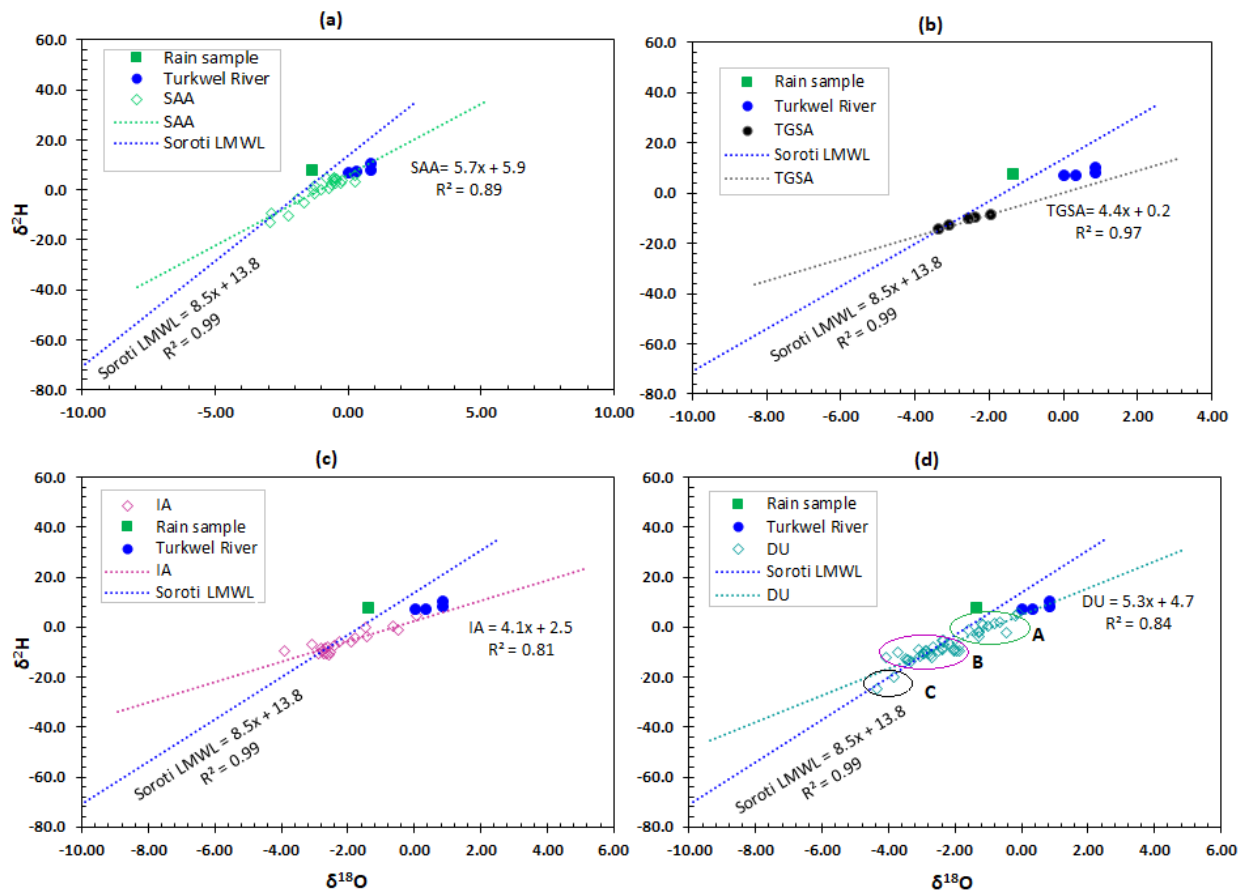


Figure 4.55: Regression analysis for $\delta^{18}\text{O}$ and $\delta^2\text{H}$ for SAA (<30m), IA (31-100m), and the TGSA (<30m) in relation to the Soroti LMWL and the GMWL. The graph also shows the position of the rain sample, Turkwel River samples, spring sample, samples of the DA (>100), and the TGSA samples

4.2.3.3 Age of groundwater and recharge sources

a) Age of groundwater

Qualitative and quantitative techniques were used to determine the age of groundwater of the Lodwar aquifers based on Clark and Fritz (1997, see section 3.4.3). The tritium values suggest that the groundwater of the study area comprises recharge before the 1950s (< 0.8TU) and a mixture of sub-modern and modern water (0.8 to 4.0 TU) (Clark and Fritz, 1997). The SAA, IA and DA are characterised by sub-modern recharge (1.1 to 2.20 TU) with pockets of older groundwater (<0.8) in the intermediate aquifer south-west of Lodwar town at Naotin, Nabuin

and Nachomin areas, and may extend further south-westwards. The TGSA primarily consists of older (before the 1950s) groundwater with tritium <0.8 TU. Figure 4.57 shows the distribution of tritium in the study area, showing relatively younger water located closer to the Turkwel River. The tritium values ranged from 1.10 to 2.20 TU in the water samples of the study area. Similar values have been observed by Sklash and Mwangi, (1991) in the north eastern region of Kenya, including Marsabit county. Values between 0.17 to 1.82 TU have been reported in Tanzania (McKenzie *et al.*, 2001) and between 3.00 to 9.00 TU in Uganda (Onugba and Aboh, 2009). Thus, although the East African waters are expected to have low levels of tritium (< 1.0 TU), higher values can be recorded in various regions.

The age of groundwater was calculated using Equation 3.23 (section 3.4.3) for the water samples with detectable levels of tritium – recharged after 1950. A detectable level of tritium was found in 24 groundwater samples in the SAA, IA, DA and some of the DU wells. The results revealed that recharge occurred for these samples between 2004 and 2018, indicating about 0 to 14 years. Of the 24 groundwater samples used in age calculation, 16 samples showed that they were recharged after 2010 (<10 years old) while the remaining eight are regarded to be older (recharged between 2004 and 2009). Figure 4.56 shows the tritium trends in groundwater of the LAAS (excluding the TGSA), indicating levels approaching pre-bomb levels (1.0 TU) in 2018. No relationship was observed between tritium and depth of the wells in the LAAS. See Appendix 4-18 for the specific ages of each of the 24 samples discussed above.

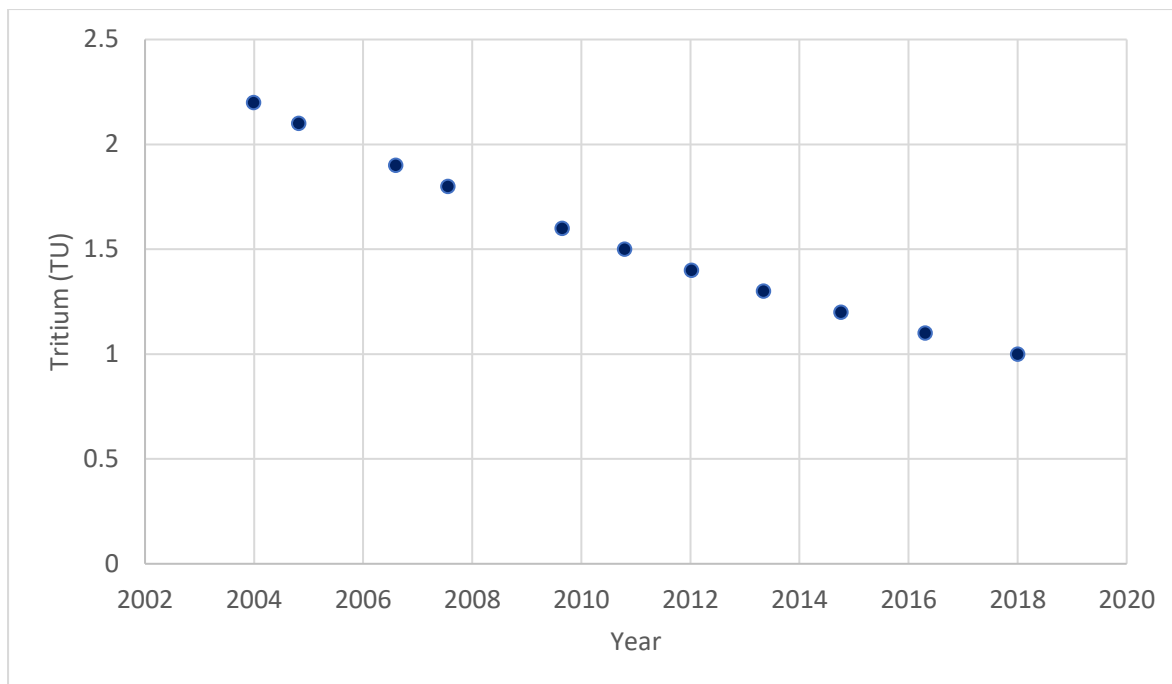


Figure 4.56: Tritium trend in the groundwater of the LAAS between 2004 and 2018, indicating ^3H values approaching pre-bomb levels

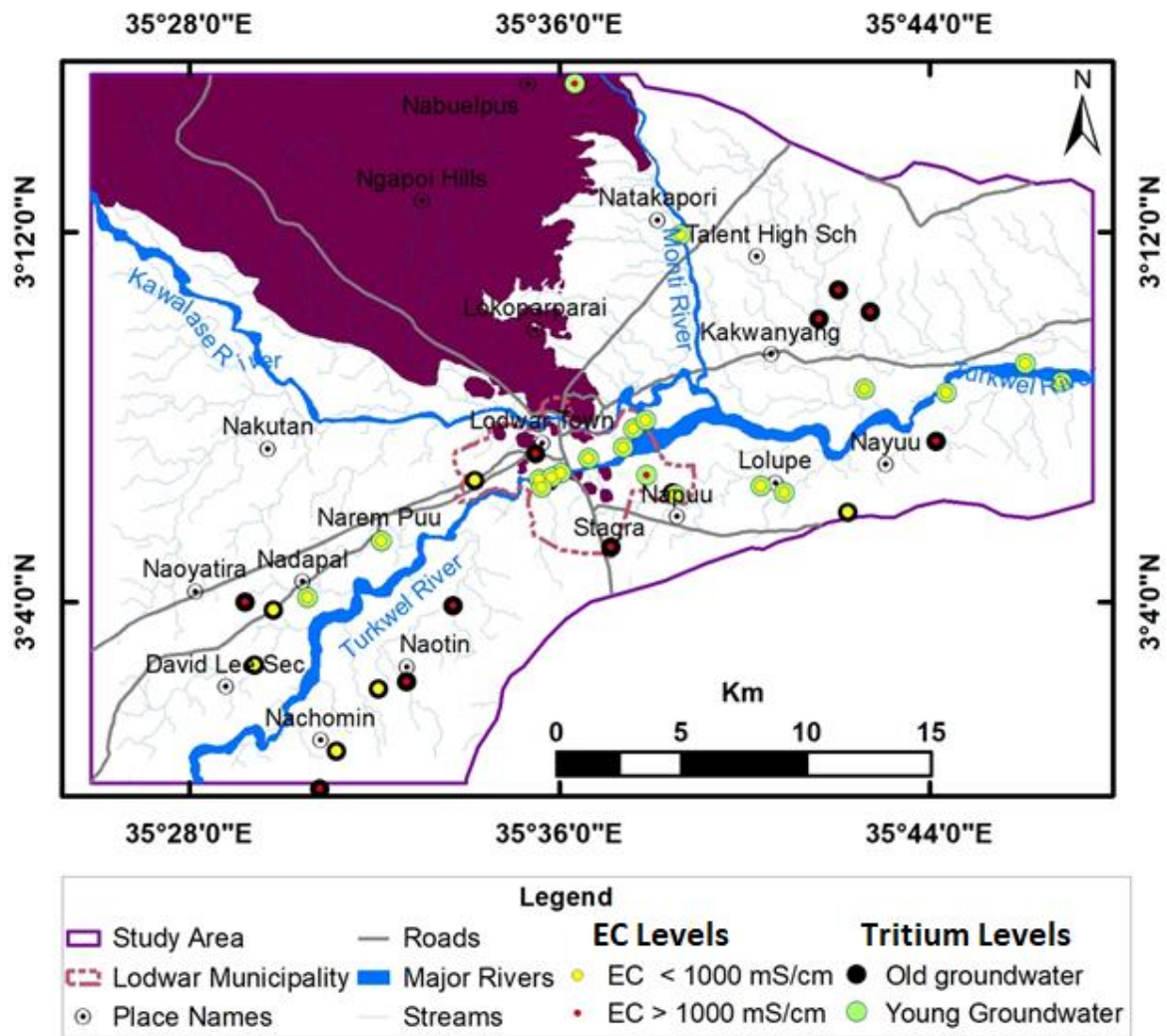


Figure 4.57: Spatial distribution of tritium in groundwater in the Lodwar Alluvial Aquifer System (LAAS); older groundwater is saline unless within the proximity of the Turkwel River while the younger groundwater is fresh

b) Recharge sources

The Soroti LMWL has a slope and intercept ($\delta D = 8.5^{18}\text{O} + 13.8$), which is relatively higher than that of the GMWL ($\delta D = 8^{18}\text{O} + 10$), indicating humid conditions (Taylor and Howard, 1996). The $\delta^{18}\text{O}$ and $\delta^2\text{H}$ isotopes of the rainfall in Lodwar plotted above the LMWL, suggesting continental effects resulting in rainfall enriched in deuterium. The more enriched values of oxygen-18 and deuterium in the Turkwel River over the local precipitation in Lodwar town indicate rainfall characteristics in a highland catchment (H. Yeh *et al.*, 2014). Evaporation processes in the water pans, scoop holes, Turkwel and Kawalase Rivers resulted in depleted isotope ratios (^{18}O and ^2H) relative to the LMWL. The Turkwel River originates south-east of Lodwar town in the Mount Elgon region while the Kawalase River emanates from the western

part of Lodwar in the Loima Hills. Flow regulation and frequency of dam release, and groundwater baseflows in the dry season may contribute to the depleted isotopic composition of the Turkwel River relative to that of the precipitation. The scoop hole samples plotted along the meteoric water lines, except for those in the Kawalase River, indicating isotopic compositions of local rainfall.

The $\delta^{18}\text{O}$ and $\delta^2\text{H}$ isotopes in the groundwater of the SAA slightly deviated from that of the local meteoric water line. Therefore, the groundwater of the SAA might be a mixture of Turkwel River water and local rainfall, causing the effect of the river water recharge being larger than that the infiltration of rainfall (Chen *et al.*, 2019; Yeh *et al.*, 2014). The spatial distribution of $\delta^{18}\text{O}$ and $\delta^2\text{H}$ in groundwater samples (SAA, IA, DA, TGSA and DU) (Figure 4.58) shows enriched values of $\delta^{18}\text{O}$ and $\delta^2\text{H}$ closer to the Turkwel River and become depleted away from the river channel. Water samples of the SAA and IA that plotted above the LMWL are linked to direct recharge from local rainfall. These samples were few and sparsely distributed within Nayuu and Lolupe areas of the study area. The analysis of the d-excess indicates that the SAA has a relatively higher value ($d = 5.9$), indicating its association with recent rainfall recharge as compared to that of the IA ($d = 2.5$). The lower d-excess value of the IA than that of the SAA suggests fractionation of oxygen and hydrogen isotopes along the groundwater flow path from the shallow alluvial aquifer to the intermediate aquifer through time (Taylor and Howard, 1996). The d-excess of the wells with unknown depth ($d = 4.7$) slightly deviated from that of the SAA demonstrating that their majority in the shallow alluvial aquifer, while the others are either in the IA and TGSA. The d-excess value of the TGSA ($d\text{-excess} = 0.2$) represents that of groundwater associated with significant evaporation processes (Levin *et al.*, 2009). These findings indicate that the average recharge waters of this system are significantly depleted compared to modern-day rainfall recharge waters (Acworth *et al.*, 2014).

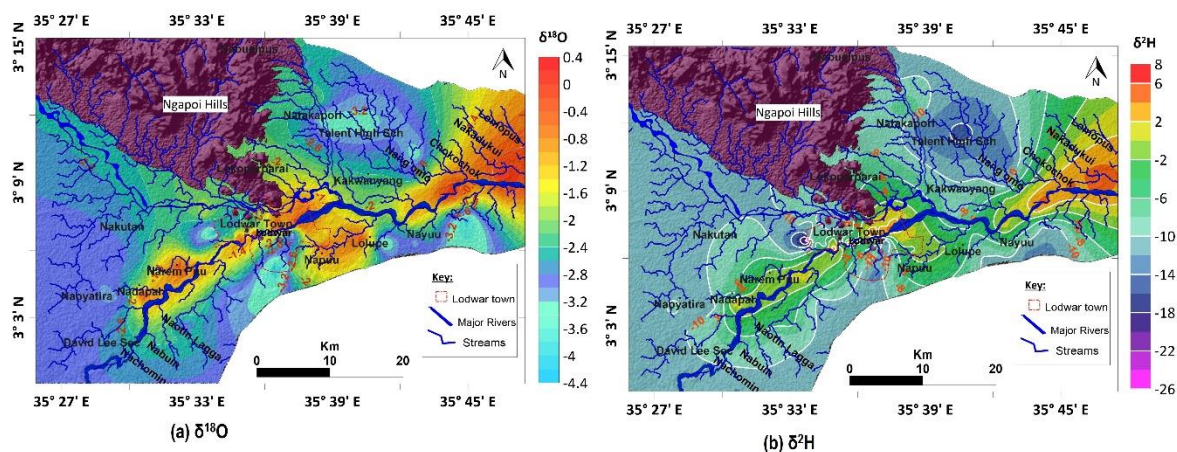


Figure 4.58: Spatial distribution of (a) $\delta^{18}\text{O}$ and (b) $\delta^2\text{H}$ for all the groundwater samples showing isotope enrichment along the Turkwel River, suggesting diffuse recharge

Table 4.29: Regression results from the shallow alluvial aquifer (SAA), Turkana grits shallow aquifer (TGSA), intermediate aquifer and for the wells with unknown depth (DU) relative to the GMWL and LWML

Data Source	Line Slope (a)	D-Excess (b)	MWL Equation ($\delta\text{D} = a^{18}\text{O} + b$)	R ²
GMWL	8	10	$\delta\text{D} = 8^{18}\text{O} + 10$	1
LMWL (Moyale)	5.7	8.3	$\delta\text{D} = 5.7^{18}\text{O} + 8.3$	0.98
Shallow alluvial aquifer	5.7	5.9	$\delta\text{D} = 5.7^{18}\text{O} + 5.9$	0.87
Turkana grit shallow aquifer	4.4	0.2	$\delta\text{D} = 4.4^{18}\text{O} + 0.2$	0.97
Intermediate aquifer	4.1	2.5	$\delta\text{D} = 4.1^{18}\text{O} + 2.5$	0.81
Depth Unknown (wells)	5.3	4.7	$\delta\text{D} = 5.3^{18}\text{O} + 4.7$	0.84

4.2.4 Development of Conceptual aquifer model

An aquifer conceptual model has been prepared based on information derived from a variety of sources; (i) DEM profiles (ii) Borehole depth information of selected boreholes contained in secondary data (iii) aquifer thickness derived from geophysics (ii) water type of each aquifer based on Piper diagram, and (iii) surface geology and geological structures in the study area obtained from geological mapping.

(a) Geological cross-sections

Four profiles were obtained from the digital terrain model of the study area to prepare geological cross-sections (Figure 4.59);

(a) Line AB is oriented N-S and passes through the central part of Lodwar town. It traverses the Precambrian Quartzo-feldspathic gneiss, Miocene nepheline-phonolite and, Cretaceous Turkana grits. Holocene sediments are not exposed along line AB profile. From the secondary data, the wells in this section are mainly in the SAA while the few in the IA are < 40 m deep.

(b) Line CD oriented N-S passes is 21 km located to the east of Lodwar town and through Napuu area traversing the Cretaceous Turkana grits, Alluvial deposits on the Turkwel River, Holocene sediments (both 4,000 and 10,000 Yr BP) on the southern part of the Turkwel River that extends southwards into the Turkana grits. The secondary data indicated that the majority of the boreholes in this section are in the intermediate aquifer and one borehole in the deep aquifer (Napuu Bh).

(c) Line EF also running in an N-S trend passing through the nepheline-phonolite, Cretaceous Turkana grits, a thin layer of alluvial sediments in the Turkwel River, Holocene sediments (4,000 Yr BP) and again the Turkana grits south of the Turkwel River. Few wells have been dug along this profile in the SAA within the Turkwel River, and the boreholes at the end of the line (Nachomin area) are in the IA.

(d) Line GH is approximately 41 km running from the west to the east of the study area covering areas with the majority of borehole and handpumps, indicating increased groundwater abstraction. Cretaceous Turkana grits, Holocene sediments and Alluvial deposits describe the surface geology along this line. The up-doming along this profile south of Lodwar town represents underlying volcanic rocks. West of the profile line, the wells are situated in the SAA and become deeper outwards of the Turkwel River into the IA. All the wells in the east of Lodwar town along this profile are in the intermediate aquifer.

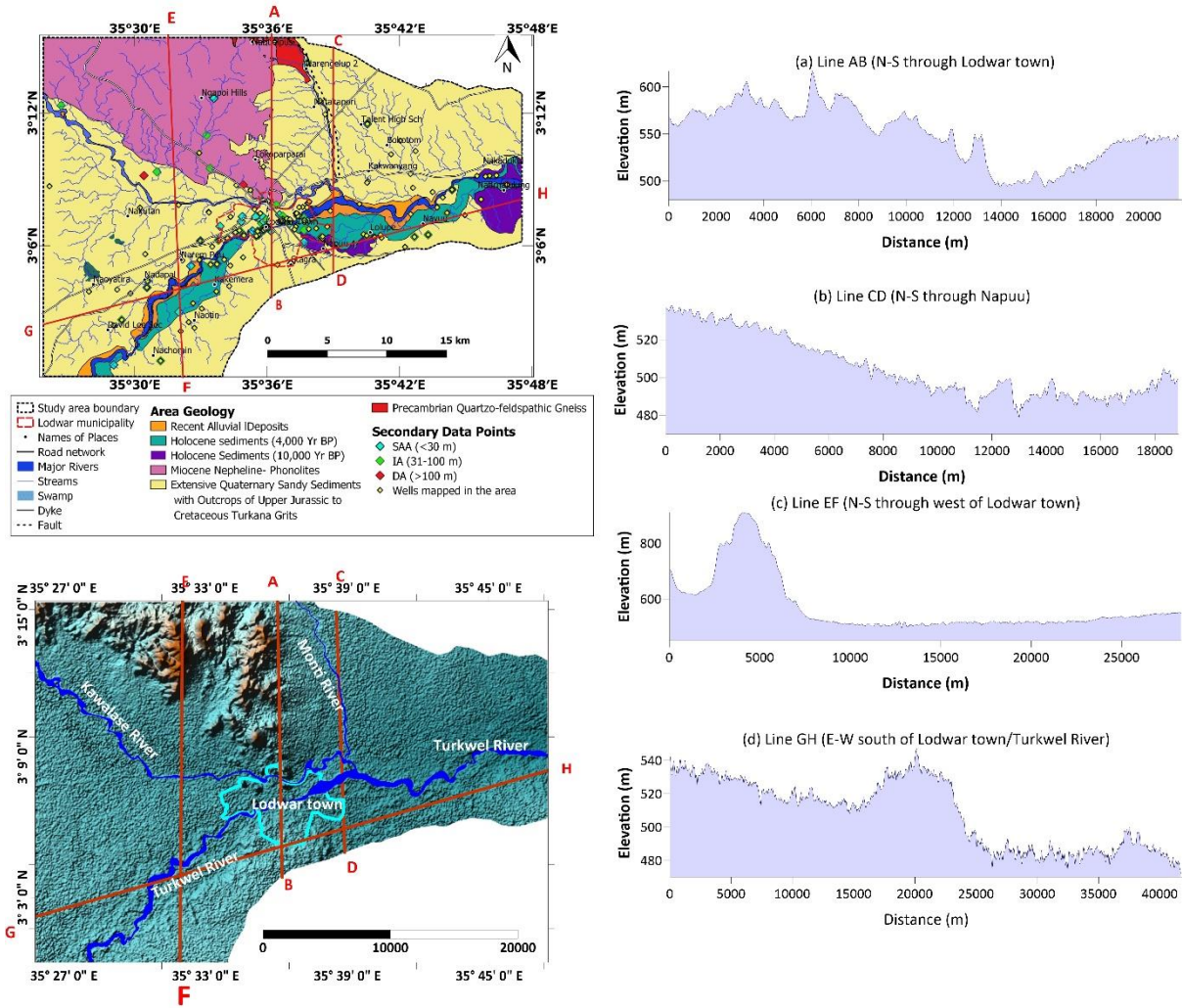


Figure 4.59: Cross-section lines (AB, CD, EF, and GH) representing different part of the study area indicating variations in surface geology and topography

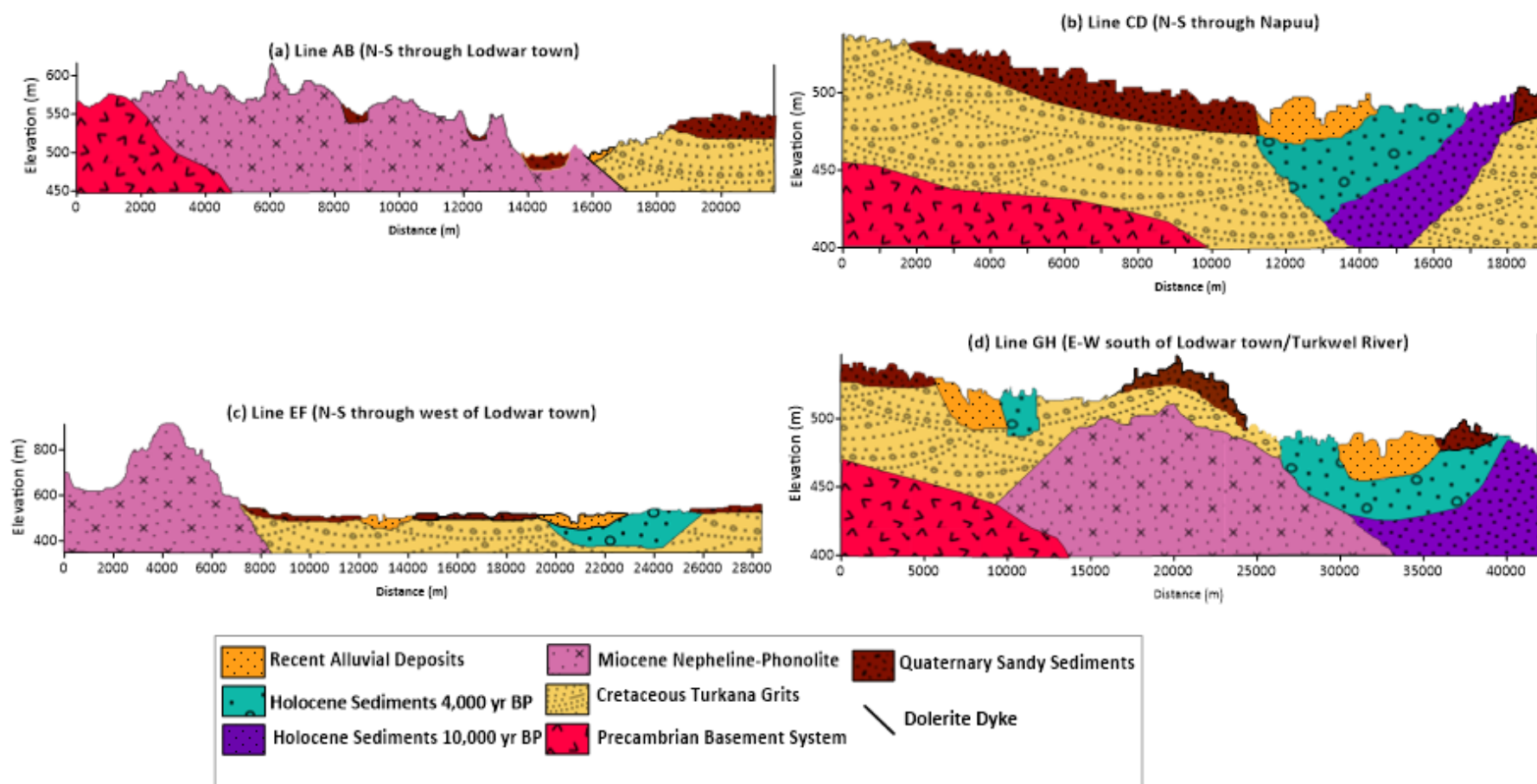


Figure 4.60: Geological cross-sections along for selected profiles in the study area, showing changes in the surface geology with depth

(b) Aquifer Conceptual model – Lodwar Alluvial Aquifer System

The Lodwar Alluvial Aquifer system comprises three sub-systems categorised based on depth as follows; shallow alluvial aquifer (<30 m), intermediate aquifer (31-100 m), and the deep aquifer (> 100) (cf. Olago 2018). The source of recharge to the aquifer is mainly through diffuse recharge by the Turkwel River and from the surface water of the Kawalase River during the wet season. Direct recharge from rainfall infiltration in the study area is expected to contribute aquifer recharge during rainfall events. The conceptual model (Figure 4.61) outlines the shallow alluvial aquifer as an unconfined system at depth < 30 m on either side of the Turkwel River. The intermediate and the deep aquifer are both semi-confined with the highly permeable semi-confining layer. Groundwater discharge mechanisms in the study area are mainly through groundwater abstraction and evaporation.

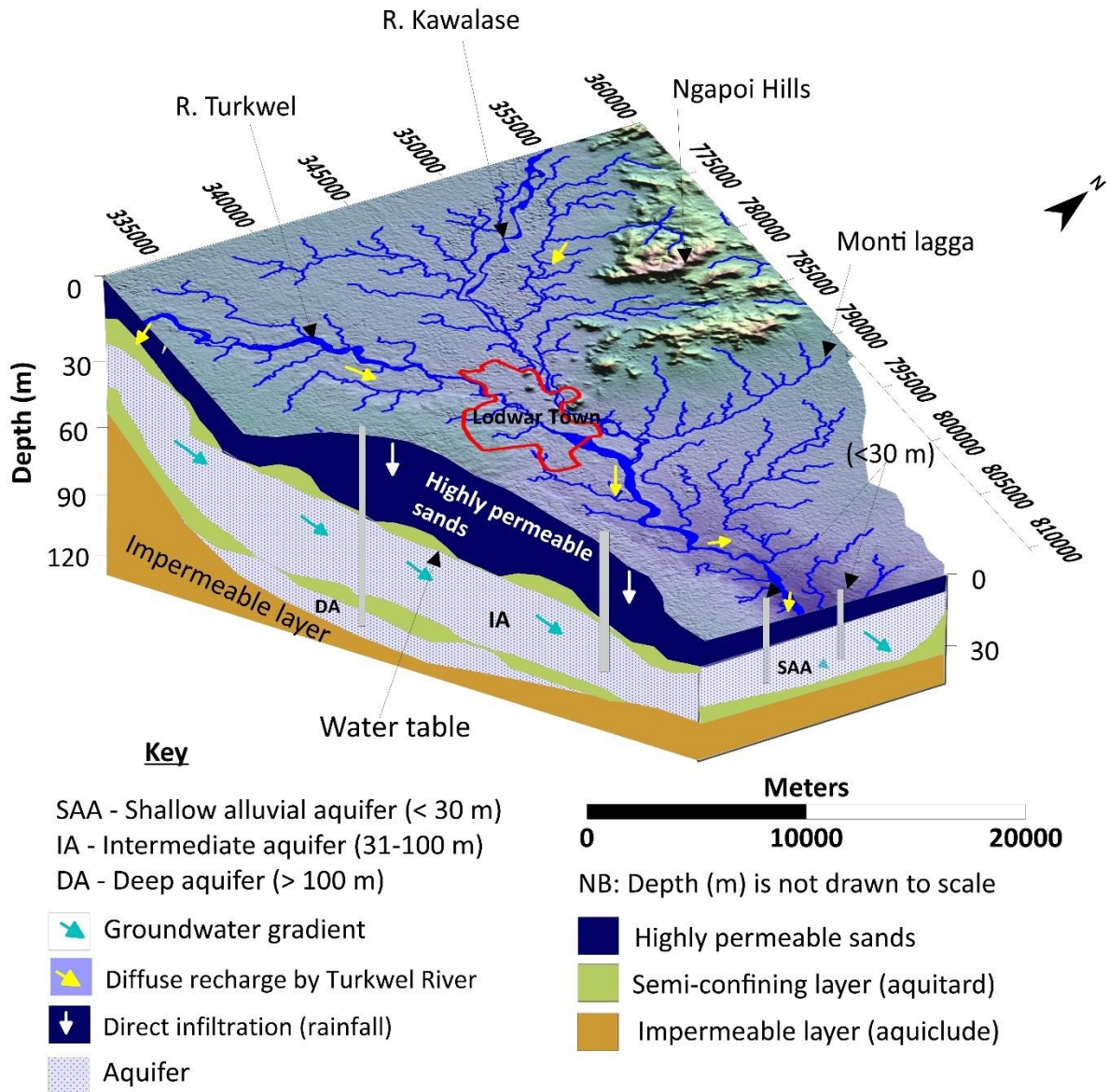


Figure 4.61: Conceptual aquifer model of the Lodwar Alluvial Aquifer System showing the three sub-systems; shallow alluvial aquifer (SAA), intermediate aquifer (IA) and deep aquifer (DA). The SAA is unconfined while the IA and DA are semi-confined and are separated by semi-impervious layers (aquitard)

4.3 Discussion

4.3.1 Lodwar Alluvial Aquifer System

Statistical and various geochemical methods were used to investigate the study area and to analyze the datasets obtained from primary and secondary sources. .

4.3.1.1 Hydrogeological characteristics

(i) Surficial geology and the geological structures

The geology of the area is characterized by the four rock types (i) Basement system rocks – mainly the quartzo-felspathic gneiss, (ii) sedimentary formations that comprise the Cretaceous Turkana grits and sandstones, and the Quaternary to Holocene sediments, (iii) Paleogene and Neogene volcanics that includes the augite basalts and the nepheline-phonolite and (iv) the alluvial deposits. Geological mapping in Lodwar and its environs revealed that the groundwater sources have been developed within the alluvial deposits and the Holocene sediments

Various factors such as physiography, climate, geology, and structural features such as lineaments and dykes govern the occurrence and movement of groundwater (Senthilkumar *et al.*, 2015). Dykes are very common geological discontinuities recognised in occurrence of aquifers as altering the flow of groundwater (Appleyard and Cook, 2009; Babiker and Gudmundsson, 2004; Comte *et al.*, 2017). Dolerite dykes were recorded in the Turkana grits and the quartzo-felspathic gneiss following the NW-SE trending control the groundwater flow in the study area. Of interest in the dolerite dyke in the Turkana grits within Lodwar town of about 1.5 m thickness and relatively dense in nature than the surrounding grits. The dyke dissects the Lodwar alluvial aquifer system into two major parts; the western part and the eastern section relative to the position of Lodwar town in the study area. The groundwater sources developed near the dyke in the western section of the LAAS are saline, suggesting limited flow of groundwater supporting mineral dissolution. For much of the topography-driven groundwater flow, long and thick low-permeability dykes serve as barriers (Babiker and Gudmundsson, 2004). The groundwater gathered by these dykes is transported along their margins to the topographic depressions occupied fault zones of higher permeability (Comte *et al.*, 2017).

(ii) Petrography and rock geochemistry

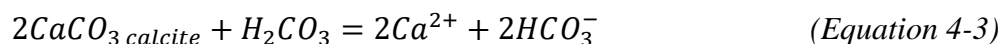
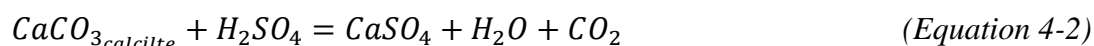
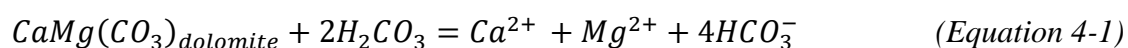
The petrographic analysis and rock geochemistry of the rocks in the study area revealed that the rock-forming minerals include pyroxenes, olivine, feldspars (plagioclase and orthoclase)

aluminosilicates, ferromagnesian minerals, amphiboles, quartz, micas and carbonates. As in all arid areas physical and mechanical weathering is predominant.

Groundwater chemistry largely depends on the mineral composition of the rocks its flow paths due to rock-water interactions (Lakshmanan and Kannan, 2007). Depending on the chemical composition of the initial water, geological conditions, and time of residence, these chemical reactions vary spatially and temporally. By hydrating the surface of minerals, hydrolyzing minerals and replacing some of their exposed surface cations with hydrogen ions, and dissolving minerals to remove mineral matter as solutes, water serves as a chemical weathering agent. Ferrous iron is preferentially soluble in minerals, including ferromagnesian silicates, carbonates, and magnetite (Enkin *et al.*, 2020). This study found that Ca, Na, Fe, Mg, Al and K are the elements that can be released to the groundwater through weathering of carbonates and silicates minerals and oxidation reactions. Carbonate weathering, silicate weathering, halite and gypsum dissolution and precipitation are common aquifer processes in arid areas (Lakshmanan and Kannan, 2007). The compositions of trace elements on the other hand were generally low, indicating that they are unlikely to be found in undesirable concentrations in groundwater.

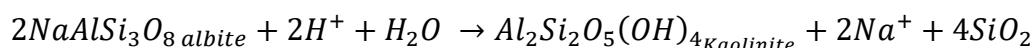
(a) Carbonate weathering

Ca^{2+} and Mg^{2+} is realised to groundwater by dolomite (Equation 4-1) and calcite (Equation 4-2; 4-3) dissolution. The addition of HCO_3^- to groundwater is due to the dissolution of carbonates and the reaction of silicates with carbonic acid (M. Kumar *et al.*, 2006). ‘Kankar’ carbonates were found in the Turkana grits, Holocene sediments and alluvial deposits within the study area, suggesting they are the potential source of Ca^{2+} and HCO_3^- .

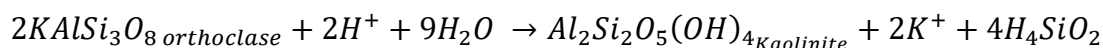


(b) Silicate weathering

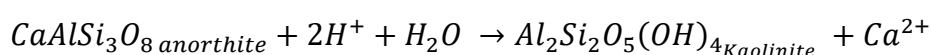
Silicate weathering involves hydrolysis reactions that use primary minerals and protons to form silicate minerals (K, Ca, Fe and Mg) (Bhattacharya *et al.*, 2008). All rocks in the study area are rich in silica ($\text{SiO}_2 = >40 \text{ wt } \%$), suggesting a high potential for silicate weathering and ion leaching in aquifers. The presence of kaolinite in the Cretaceous Turkana grits suggests plagioclase feldspar weathering involving albite ($\text{NaAlSi}_3\text{O}_8$). decomposition releasing Na^+ and SiO_2 to groundwater (Equation 4-4). The increased K concentrations in the shallow alluvial aquifer and the intermediate aquifer (Tanui *et al.*, 2020) is linked to the high compositions of K_2O (average = 1.88 wt %) and K (average = 0.35 wt %) in the Holocene sediments suggesting hydrolytic reaction in favour of orthoclase feldspar ($\text{KAl}_3\text{Si}_3\text{O}_8$) (Equation 4-5) releasing K^+ and soluble silica (H_4SiO_4). Additional Ca^{2+} concentrations in groundwater is related to weathering of mineral anorthite ($\text{CaAl}_2\text{Si}_2\text{O}_8$) (Equation 4-6). The occurrence of silicate weathering in the study area is subject to spatial and temporal variations, dominating the Turkana grits and the Holocene sediments.



(Equation 4-4)



(Equation 4-5)



(Equation 4-6)

Silicate weathering has been linked to higher concentration of Na^+ in groundwater (M. Kumar *et al.*, 2006), a characteristic observed in the TGSA.

(iii) Sub-surface characteristics

The use of geophysics for subsurface investigations in groundwater studies has increased in the recent years (Bello *et al.*, 2017; Egai and Douglas, 2015; Kana *et al.*, 2015). Vertical Electrical sounding measurements utilizing Schlumberger array has also been applied by many researchers

(Bello *et al.*, 2017; Egai and Douglas, 2015; Kana *et al.*, 2013). The results of the resistivity soundings in the LAAS revealed heterogenous sub-surface formations. Vertical and lateral variations in the apparent resistivity values reflect changes in the geological units in the aquifer (Bello *et al.*, 2017). The modelled VES data revealed up to five geoelectric layers in the section A of the LAAS, three layers in section B and C and four within the Napuu (section D). In all the four aquifer sections, the medium resistivities ranging between 20-65 Ohm- m were interpreted an aquifer unit hosting fresh groundwater at varying depths between 15 to up to 130 m. In contrast, the low resistivity values (< 10 Ohm-m) were associated with saline groundwater in the area as determined by (Tanui *et al.*, 2020). Saline groundwater in Lodwar and its environs are associated with occurrence of Turkana grits and the Miocene volcanic rocks.

(iv) LAAS aquifer properties

The characteristics of the aquifers play a major role in the identification of potential groundwater zones because they represent the rock structures through which the water flows (Kumar *et al.*, 2016). The hydrogeological conditions of the area were assessed based on the results of the pump test records of boreholes previously drilled in the study area. Important aquifer characteristics such as aquifer depth, transmissivity, yields, aquifer thickness and storage were determined.

The transmittivity of soil or rock is frequently determined by physical factors such as porosity, particle size, and particle distribution and arrangement (Fabbri and Piccinini, 2013). The transmittivity values reflect the variability in the thickness and permeability of the aquifer levels (Kumar *et al.*, 2016). Average transmissivity values indicate that the deep aquifer in Napuu has a high groundwater potential (1316.11 m²/day), followed by the shallow aquifer (440.00 m²/day) and then the intermediate aquifer (115.18 m²/day) (Kuria, 2013). The average optimum yields in the shallow alluvial aquifer was 16.87 m³/h, 8.23 m³/h in the intermediate aquifer and 100.00 m³/h in the DA within the Napuu area, reflecting the distribution of the transmissivity values. Optimum yield is a unique aquifer parameter that can be used to establish a groundwater discharge and management plan. It is closely related to subsurface lithology and other aquifer parameters (Fabbri and Piccinini, 2013; Kumar *et al.*, 2016). It helps control the depletion of the water level and maintains a long-term stability in the aquifer. As far as groundwater is concerned, the aquifer thickness is closely related to the transmission and storability of any soil (Shekhar, 2017). Based on test pumping data obtained from the secondary sources and the geophysical measurements, the thickness of the aquifer varied at each section of the aquifer; Section A (37 m), Section B (40 m), Section C (30 m), and Section D (45 m). These values suggest that the high yields observed in the

Napuu area (section D) is associated with the prevailing aquifer thickness. The yields and the aquifer thickness in the Turkana grits aquifer was not determined by this study due to unavailable borehole logs and test pumping data. The Lodwar Alluvial Aquifer System covers 104.93 km² of land east and west of the Municipality of Lodwar with an estimated aquifer storage was 1.3 Billion Cubic Meter (BCM), considered to be renewable in nature.

4.3.1.2 Hydrogeochemical characteristics

The evaluation of the water quality of the LAAS revealed that the system mainly hosts good groundwater quality in wet and dry seasons except for a few wells, that included LOWASCO Bh 2C. The water quality index was used to evaluate the seasonal changes in water quality in the LAAS and in the TGSA. The TGSA revealed poor groundwater quality unfit for human consumption in both seasons, therefore, it is not further discussed in terms of quality in the next sections. The water quality index has widely been used to evaluate drinking water quality of groundwater (Ansari and Hemke, 2013; Badmus *et al.*, 2015; Heiß *et al.*, 2020). Deteriorating trends in water quality was observed in all the sub-systems of the LAAS during the wet season, linked to mineral dissolution and flushing of contaminated recharge water into the aquifer by recharge water. The contamination was due to high Fe²⁺ and Mn²⁺ ions in the shallow alluvial aquifer linked to oxidizing conditions in the wet season (Yadav *et al.*, 2020) while high F and EC were the major factors affecting the water quality in the intermediate aquifer, suggesting predominant mineral dissolution.

Shallow alluvial aquifers are known as highly pollution-prone (Muhammad *et al.*, 2015; Yidana *et al.*, 2010a). In order to assess the anthropogenic effect on the quality of groundwater, nitrate concentrations in groundwater samples were assessed. High levels of nitrate in drinking water are undesirable due to the possible reduction in nitrite that may be hazardous to health, especially in infants and pregnant women (Ramaroson *et al.*, 2018). Furthermore, nitrate in groundwater is primarily due to pollution, such as fertiliser or manure leaching, wastewater disposal, leakage from septic tanks, etc., and thus suggests the potential presence of other harmful pollutants, such as bacteria or pesticides (Guo *et al.*, 2019; Lathamani *et al.*, 2015). In arid urban areas, nitrate contamination in shallow groundwater is linked to poor waste disposal and leaky sewerage networks (Goni *et al.*, 2019; Lapworth *et al.*, 2017). Lodwar town lacks a functional sewerage network (Hirpa *et al.*, 2018; Olago, 2018), posing threat to the groundwater quality in the area (Tanui *et al.*, 2020). Increasing trends of nitrates were observed in the SAA and IA during the wet season, an indication of potential aquifer pollution, with values approaching the water quality

guidelines within the town. Lapworth *et al.* (2017) determined that nitrate pollution is an underlying issue in urban arid areas, always associated with poor sanitation and irrigation sources.

The water groundwater chemistry of the shallow alluvial aquifer during the wet season reflected that of the river water indicating a high degree of connectivity. Similar findings have been observed shallow alluvial aquifers in the sub-Saharan Africa (Walker *et al.*, 2019). In addition, evaluation of hydrochemical facies revealed that just as the Turkwel River, the shallow alluvial aquifer was dominated by Ca-HCO₃ water type. The calcium bicarbonate waters are associated with recent recharge (Walker *et al.*, 2019). The Intermediate (samples from depths between 31-100 m) and deep groundwater (samples from wells with depths >100 m) is of a NaHCO₃ type indicating higher mineralization due to longer residence times and greater distance of flow (Walker *et al.*, 2019). Pockets of Mg-HCO₃ water were observed within the shallow alluvial and intermediate aquifers. Aquifer chemistry in the SAA and IA is highly affected by seasonal recharge pulses from the Turkwel flow, whereas direct rainfall recharge has a similar impact on TGSA (Tanui *et al.*, 2020). However, in the DA, there are no substantial variations in physico-chemical parameters in the wet-dry season, indicating that recharge occurs over longer timescales than the seasonal cycles for this aquifer. The Turkana grit shallow aquifer was Na-Cl water type and became Na-HCO₃ near the Holocene sediments, indicating substantial mineralization in the grits due to mineral dissolution and evaporation processes. Minimal dilution of groundwater by recharge water occurs in this aquifer near the Holocene sediments (Tanui *et al.*, 2020).

This study compares with the findings of (Kumar *et al.*, 2006) where the predominant hydrochemical processes in an arid aquifer system were dissolution, weathering of carbonate and silicate minerals, ion exchange, and surface water interaction.

4.3.1.3 Rainfall-surface water-groundwater interactions

The isotopes widely used in groundwater investigations are stable isotopes of the water molecule, ²H and ¹⁸O, and radioactive isotopes, tritium and carbon-14 (Sappa *et al.*, 2012). This study utilized ²H, ¹⁸O and ³H isotopes to understand rainfall-surface water-groundwater interactions in Lodwar and its environs. Mechanistic knowledge of the fundamental mechanisms for managing the spatial patterns and temporal dynamics of groundwater-surface water interactions is essential to maintaining drinking water supplies and ecological processes (Lewandowski *et al.*, 2020). The isotopic compositions of O and H in water, modified by meteoric processes, are useful tracers for the determination of groundwater origin and movement, since they do not usually change as a result of rock-water interactions (Clark and Fritz, 1997; Chen *et al.*, 2018, 2019).

The groundwater recharge system in the alluvial plain consists of three complementary processes: vertical rainfall infiltration, lateral infiltration through the fracture network and altered rocks, and vertical drainage of the surface hydrographic network (Ramaroson *et al.*, 2018). As compared to the precipitation in Lodwar, the groundwater of the LAAS was isotopically depleted. Consequently, precipitation may not be the primary mechanism for recharging the Lodwar Alluvial Aquifer System. The proximity of the groundwater and river composition suggested that the Turkwel river was a significant contributor to recharge in the SAA. Lateral infiltration of groundwater from the SAA and the Turkwel River contributes recharge to the IA and the DA. The EC values and the overall aquifer mineralization was observed to increase away from the river (i.e. Turkwel river < SAA < IA < DA < TGSA) Tanui *et al.*, 2020 where the EC value in the Turkwel River is < 250 $\mu\text{S}/\text{cm}$ and > 5000 $\mu\text{S}/\text{cm}$ in the TGSA. Three recharge mechanisms are identified to contribute recharge to the LAAS sub-systems; recharge of the SAA by the Turkwel River related to mixing in the IA, recharge by Kawalase river in Napuu, Lolupe and Nayuu areas, and direct rainfall recharge in few locations. This study also revealed that the groundwater of the TGSA is not associated with modern rainfall.

Tritium is a radioactive hydrogen isotope. It has unique characteristics that make it distinctive among the environmental tracers of groundwater pollution: it does not interfere with aquifer materials when passing through porous media and is considered conservative geochemically (Ramaroson *et al.*, 2018). Qualitative and quantitative techniques were used to determine the age of groundwater of the Lodwar aquifers based on Clark and Fritz (1997, see section 3.4.3) using tritium. The tritium values in groundwater suggest that the groundwater of the study area comprises recharge before the 1950s (< 0.8 TU) and a mixture of sub-modern and modern water (0.8 to 4.0 TU) – post 1950s. The water samples with detectable levels of tritium in the SAA, IA and DA (1.1 to 2.2) with more enriched values occurring closer to the Turkwel River. Groundwater samples in the intermediate aquifer with no detectable levels of tritium were located away from the river channel and had depths > 50 m, suggesting longer residence time as compared to near the Turkwel River. Spatial distribution of tritium in the plain suggests a dynamic mechanism for groundwater flow (Bayari *et al.*, 2006), especially in the intermediate and deep aquifers; some parts of intermediate aquifer had no measurable levels of tritium, while other parts had values had values in range with that of the SAA. In addition, the tritium levels in the deep aquifer were > 2.0, contradicting the average values of the intermediate aquifer. High and low

hydraulic conductivity units with rapid and slow groundwater velocity appear to exist side by side in the aquifer (Bayari *et al.*, 2006).

4.3.1.4 *Development of Conceptual aquifer model*

Rural communities in the sub-Saharan Africa utilize shallow aquifers for water supply. Increased use of shallow groundwater can help to achieve multiple sustainable development goals (SDGs) by having a positive effect on poverty, hunger and health (Walker *et al.*, 2019). However, these shallow aquifers are little studied and misunderstood, partially because of the lack of existing hydrogeological evidence in many regions of sub-Saharan Africa (Walker *et al.*, 2019; Xu *et al.*, 2019). Like many urban arid areas in the SSA, Lodwar town in Turkana county depends on shallow aquifers (<30 m) to intermediate depth (31-100 m) (c.f. Olago 2018) for water supply.

The development of a hydrogeological conceptual model is crucial to a better understanding of the hydrogeological system (Umar, 2006). Developing a conceptual model usually involves the evaluation of existing topographic, geological and hydrometeorological data, which would generally require, to varying degrees depending on the location of the study site, the addition of new field investigations, laboratory analyses and additional monitoring (Walker *et al.*, 2019). Due to the complex distribution of lithological units in the plain, it is very difficult. A computational model of a hydrogeological system is difficult to construct. Absence of this information limits the use of numerical flow models that could be used to describe the aquifer's recharging process (Bayari *et al.*, 2006).

This study therefore developed a hydrogeological conceptual model for Lodwar Alluvial Aquifer System, based on extensive field investigation of surface and sub-surface geology, geochemical surveys, review of secondary data and investigation of surface-groundwater interaction in the region. The secondary data and geophysics revealed that the depth of boreholes in the area range between 5 to 110 m, reflecting groundwater abstraction in the shallow, intermediate and deep aquifer systems. The hydrogeochemistry and water quality data suggested that fresh groundwater is hosted in the alluvial deposits on the floodplains of the Turkwel River and in the adjacent Holocene sediments (intermediate aquifer), suggesting interconnection between the two systems. This evidence suggests that shallow groundwater flows laterally in directions that do not generally coincide with surface water flow paths, as demonstrated by Walker (2019). Thus, recharging deeper aquifers. The deep groundwater (> 100 m) was observed to mirror that of the IA within the Napuu areas and that of the SAA at Natir, indicating possible hydrological gradients as in the case of (Walker *et al.*, 2019). This aquifer, therefore, determined that the sub-systems of the

LAAS; SAA, IA and the DA are separated from each other by a highly permeable aquiclude that acts as a semi-confining layer. Besides, HCA demonstrates that there is some interaction between the IA and the Napuu bh (Tanui *et al.*, 2020). The oxygen and hydrogen isotopes revealed rainfall associated with modern rainfall in most parts of the aquifer, especially within the SAA.

4.3.2 *Implications for sustainable groundwater use, demand, and aquifer protection*

The consequence of unsustainable use of groundwater is increasingly evident across many parts of the world. Groundwater management is a serious problem that threatens groundwater availability in many arid and semi-arid parts of the world. Cost-effective and easy to use methods for augmenting groundwater resources in arid alluvial aquifers ensure sustainable management of the water supply (Guo *et al.*, 2019). Global water demand is highly influenced by population expansion, urbanization, food, and energy security policies, as well as macroeconomic activities such as trade globalization, changing diets, and increased consumption. According to the UN (2015), the projected global water demand by 2050 is expected to increase by 55% related to growing industrial and domestic water demands. Thus, competing demands make it difficult for allocation decisions that will, in turn, threaten sustainable development. The investigation of the LAAS presents a vulnerable system to both human activities (Tanui *et al.*, 2020) and climate risks (Hirpa *et al.*, 2018).

The isotopic compositions of ^{18}O and ^2H in surface water and groundwater of the study area provide evidence of recharge sources. The positive d-excess values in the Turkwel river (6.47) and SAA (2.18) suggest that they are interlinked. The plots of the groundwater samples below the LMWL indicate that the recharge water has undergone slight evaporation (Mckenzie *et al.*, 2010; Ochungo *et al.*, 2019; Sklash and Mwangi, 1991). In addition, direct rainfall recharge also occurs in the study area as indicated by the water samples above the LMWL. However, determining isotopic compositions of more rainfall samples in the study area will help understand the isotopic composition of rainfall in the region and generate a new local meteoric water line relevant to future similar studies.

Water quality indices have been used by several studies as a tool for communicating complex groundwater quality information (Dhanasekarapandian *et al.*, 2016; Hamlat and Guidoum, 2018; Kumar and James, 2013a). The WQI of the study area has indicated areas of good groundwater quality for expansion of groundwater supplies and areas of poor groundwater quality to be considered for piped network. Furthermore, the tritium results revealed that the SAA comprises fully modern groundwater with ^3H levels between 1.0 to 2.2 TU. The decreasing d-excess values

from the SAA (2.18) to the intermediate aquifer (-6.81) and TGSA (-8.14) indicate isotope fractionation during the lateral groundwater flow (Bershaw *et al.*, 2018). Thus, tritium-bearing groundwater of the IA results from the dilution of originally tritium-free groundwater by a lateral flow of diffuse river recharge through the alluvial aquifer (Hamutoko *et al.*, 2017, 2018; Vu *et al.*, 2020). Therefore, conservation of the Turkwel River catchment is critical in the sustainability of the LAAS. The long-term approaches need to incorporate evidenced-based groundwater management policies that will address three key issues including (Guo *et al.*, 2019); (i) management of supply sources to improve water availability in time and space, (ii) management of water demand needs including the efficiency of water use, sectoral interaction with economic activities, and (iii) balancing of competing demands and preservation of the integrity of water-dependent eco-system.

Chemical and isotopic analysis was used to characterize the groundwater of the study area. The relatively depleted values of $\delta^2\text{H}$ corresponds to the water chemistry in river water, where the Kawalase river samples are slightly mineralised than in the Turkwel river (Fig 5). This is linked to the prevailing climatic conditions of the rainfall source areas; Mt Elgon comprises a cool and wet climate with relief rainfall Loima is hot and dry with convectional rainfall (Oiro *et al.*, 2018; Yusuf *et al.*, 2018).

Aquifer mineralization is also observed to increases from the SAA, which is hydraulically connected to the Turkwel River, to the intermediate aquifer in the Holocene sediments and into the Turkana grits (Tanui *et al.*, 2020). Thus, the most negative values of $\delta^2\text{H}$ are associated with highest EC values. The mixing of the Kawalase and Turkwel River water result in relatively depleted $\delta^{18}\text{O}$ and $\delta^2\text{H}$ signatures in groundwater at Napuu-Lolupe areas. The more depleted values of the $\delta^{18}\text{O}$ and $\delta^2\text{H}$ in the TGSA and lack of tritium in its waters is consistent with the highly mineralised groundwater (Tanui *et al.*, 2020), suggesting long groundwater residence time. However, closer to the Holocene sediments, the groundwater in the Cretaceous Turkana grits displays similar chemical and isotopic signatures with the tritium-free groundwater of the intermediate, indicating that the tow systems are inter-connected. This evidence suggests that the Turkwel river recharges the TGSA through lateral flow via subsurface channels and buried geological structures (Sklash and Mwangi, 1991) in the Holocene sediments and the Turkana grits.

CHAPTER FIVE: CONCLUSIONS AND RECOMMENDATIONS

5.1 Conclusions

This study was conducted to determine and characterize the Lodwar Alluvial Aquifer System in terms of its hydrogeological characteristics, water quality determination and to evaluate the natural and anthropogenic factors influencing its groundwater chemistry, and to investigate its rainfall-surface water-groundwater interaction regimes by use of stable environmental isotopes. The data collected from hydrogeological, hydrogeochemistry and isotope studies were used to develop a conceptual aquifer model, providing scientific evidence for sustainable, safe exploitation and management. The conclusions drawn from each of the study objectives are presented below.

(a) Hydrogeological characteristics of the LAAS

Four distinct aquifer systems underlie Lodwar, and its environs are; three subsystems of the Lodwar alluvial aquifer system (LAAS) (i) the shallow alluvial aquifer which is less than 30 m deep with an average aquifer yield of 16.87 m³/h, (ii) the intermediate aquifer with depths ranging from 31 to 100 m and average yield of 8.28 m³/h, and (iii) the deep aquifer with a depth greater than 100 m and yields > 100 m³/h. The fourth aquifer system is in the Turkana grits with depth < 30 m and is characterised by highly saline and non-potable water. The shallow depths and good aquifer yield of the LAAS present an opportunity to address the water security challenges in Lodwar and its environs. The Lodwar Alluvial Aquifer System covers 104.93 km² of land area. It is aligned east-west, and Lodwar Municipality is in the central portion. Based on borehole drilling and test pumping records and the geophysical measurements, the thickness of the aquifer varies as follows; Section A (37 m), Section B (40 m), Section C (30 m), and Section D (45 m). The total estimated aquifer storage is 1.3 Billion Cubic Meter (BCM). The transmissivities range from 21.60 to 116.64 m²/day. Within the Napuu region, high yielding boreholes can therefore be struck.

Water availability is directly linked to economic development and expansion of investment opportunities. The evidence obtained from the study suggests that the LAAS is a strategic aquifer with medium to high borehole yields and that it is cheap to exploit because of its shallow nature (< 30 m to 110 m). Thus, the growth and expansion of Lodwar town depend on the sustainability of the underlying aquifers (the LAAS). Therefore, the hydrogeological data collected and analysed provides the basis for informed decisions during the development of new groundwater sources and sustainable management of the Lodwar Alluvial Aquifer System and the process can apply to other

arid regions in Kenya. Furthermore, the study contributes the much needed scientific knowledge for better understanding of ASAL alluvial aquifers in sub-Saharan Africa and other similar regions worldwide.

(b) Aquifer hydrogeochemistry and vulnerability to pollution

The water quality index revealed that the LAAS has good drinking water quality during the dry season. Although the water quality indices are within the drinking water quality during the wet season, they deteriorate slightly relative to the dry season across all the sub-systems of the LAAS. In the SAA during the wet season, high Fe^{2+} and Mn^{2+} are observed with Bh 2C, one of the LOWASCO supply boreholes records high Mn^{2+} (0.5 mg/L). High fluoride concentrations characterize the IA in the wet season. The water quality of the TGSA is not suitable for drinking in all seasons due to its high alkalinity ($\text{pH} > 8.50$) and very high salinity with cation and anion concentrations that are well in excess of drinking water guidelines. Generally, the LAAS presents a vulnerable groundwater resource with regard to anthropogenic contamination, though currently, anions that are used to track anthropogenic pollution, such as NO_3 , are still below the guideline values for drinking water, elevated concentrations of NO_3 occur in the groundwater within the town region as compared to the groundwater in the rural sections of the LAAS. The lack of a sewerage network and poor sanitation poses a threat to the water quality of the LAAS, particularly, because the population of the town is rapidly growing hence potential point-source pollutant sources such as on-site sanitation facilities are becoming more and more widespread.

The water quality index maps in groundwater quality studies are used by decision-makers to identify areas of groundwater abstraction (good quality) and areas for piped water supply (poor groundwater quality) as has been demonstrated for the LAAS. The lack of sewerage networks in small towns in sub-Saharan Africa has contributed immensely to contamination of their shallow aquifers. The evidence presented by the low NO_3 levels in the LAAS indicates an opportunity to protect the aquifer from potential human contamination risks.

(c) Rainfall-surface water-groundwater interactions

The environmental isotopes (oxygen and hydrogen) point to the Turkwel River as a vital recharge source to the underlying shallow alluvial aquifer. The data confirm the existing linkage between the Turkwel River and the Lodwar Alluvial Aquifer System as hypothesized by Olago (2018) and Hirpa *et al.* (2018). Other recharge sources include direct infiltration of rainfall and flowing water of the Kawalase River during the wet season that recharges the eastern areas of the LAAS,

including the Napuu area. Qualitative determination of the age of groundwater in the LAAS indicates that recharge occurs in two regimes; (1) pre-1950 recharge consisting of non-detectable tritium levels (< 0.8 TU) within some parts of the IA adjacent to the Turkana grits, and (2) recharge after the 1950s with tritium levels ranging from 1.1 to 2.20 TU found in the Holocene sediments, and with higher values recorded in close proximity to the Turkwel River. The young groundwater occurs mainly in the SAA, vast parts of the IA and the DA, and was recharged between 2004 and 2018, with the SAA having the most recent recharge. The TGSA comprises older groundwater recharged before the 1950s and this, in part, accounts for its highly mineralised groundwater chemistry.

The existence of rainfall-surface water-groundwater interaction in the LAAS based on the close association of the stable isotopes (^{18}O , ^2H and ^3H) illustrates the aquifer's renewable nature by the modern recharge. However, numerous studies have demonstrated that aquifers associated with the recent rainfall (directly or indirectly) suffer vast impacts of climate variability, especially in arid areas characterised by low rainfall usually < 250 mm. Thus, decision-makers require effective interventions in terms of management, protection, and planning for informed and sustainable aquifer use.

(d) Conceptual aquifer model

Comprehensive aquifer studies involving the development of accurate hydrogeological conceptual models ensure sustainable development and use of groundwater. The conceptual aquifer model was developed for the LAAS based on the data derived from the hydrogeological, hydrogeochemistry and isotope studies. The conceptual model outlines the shallow alluvial aquifer as an unconfined system at depth < 30 m on either side of the Turkwel River. The intermediate and the deep aquifer are both semi-confined with a highly permeable semi-confining layer. The aquifer obtains its recharge from rainfall (direct infiltration through the highly permeable sands) and primarily through Turkwel River water infiltration (diffuse recharge). The hydrogeological model provides essential information about the depth variation of each sub-system of the LAAS, recharge mechanisms, and helps to predict the water quality within the aquifer sections. Generally, it presents important hydrogeological and hydrogeochemical findings of the LAAS in a simplified manner for informed groundwater development. The hydrogeological model obtained contributes to the ongoing studies of the alluvial aquifers in the SSA that involve developing aquifer conceptual models.

This study demonstrated that vigorous groundwater research involving the investigation of hydrogeological properties of an aquifer, water quality and its hydrogeochemistry, as well as understanding of recharge characteristics helps to provide evidence-based groundwater management at local, regional and international levels. The study revealed important hydrogeological characteristics of the LAAS such as the aquifer recharge, discharge mechanisms, depth of the three aquifer sub-systems, and aquifer yields. Although the water quality results indicated good drinking water quality for most wells in the LAAS, the rising trends of nitrates in the shallow alluvial aquifer and the intermediate sub-system indicates their susceptibility to anthropogenic contamination. The stable isotopes of oxygen-18, deuterium and tritium in groundwater showed a close linkage with modern to sub-modern recharge, suggesting vulnerability of the aquifers in Lodwar to climate variability. Overall, the study objectives were achieved, but the lack of long-term groundwater times series in the study area limited utilization of the water table fluctuation method to estimate the amount of recharge within the LAAS. This reflects the importance of initiating groundwater monitoring across the sub-Saharan African region to improve on evidence-informed sustainable management outcomes.

5.2 Recommendations

From the detailed findings presented by this study, the following recommendations are made:

- (i) **It is important to record accurate geologs during drilling and maintain these in a database to improve on the understanding of the aquifer system, which will then support more sustainable use and management models.** This research was limited to a greater extent by the lack of comprehensive data on borehole logging and test pumping. The Water Resources Authority (WRA) should ensure ultimate compliance by the drilling contractors on submission of full borehole completion reports for the newly developed boreholes in the area.
- (ii) **There is a need for prudent water quality monitoring and management of groundwater resources in Lodwar and its environs to ensure their sustainability and safe use.** Prior to this study, detailed water quality studies in the study area had not been carried out, making it difficult to determine the past groundwater quality status in the LAAS. However, this study indicated changes in water quality and aquifer chemistry between the wet and the dry season. With the growing population and human

activities in the region, and the increasing variability of the climate, the aquifer's water quality may be adversely affected. The datasets presented by this study provide a strong basis for building a future sustainable water quality monitoring program by the WRA.

- (iii) **Urgent protection of the Lodwar Alluvial Aquifer System is critical to ensure the elimination of potential contamination sources.** Aquifer protection and sustainable use – the water quality and aquifer geochemistry data indicated that the LAAS hosts good drinking water quality and anthropogenic pollution effects are low. However, the lack of a functional sewerage network in Lodwar municipality and poor sanitation distribution continue to threaten the aquifer's future water quality. Improve sanitation in the area should be improved as well as around the water points to minimize human pollution. The evaluation of groundwater isotopes indicated aquifer recharge by the Turkwel River. Thus, the suitability of the LAAS is dependent on the continuous existence of the Turkwel River, suggesting the urgent need for catchment conservation and regulation of upstream activities (within and outside the Turkana county). This calls for multi-stakeholder approach and collaboration by all the parties involved. Within the study area, the LAAS system boundary has been outlined based on the hydrogeological, hydrochemical and isotope studies. Prevention of land encroachment in the aquifer will help minimize pollution risks and the development of groundwater well-fields in the area. Aquifer protection is also part of the Vision 2030 environmental protection goal. Furthermore, there is need for accurate water quality index maps for other aquifers in the Turkana County areas. The development of groundwater supply sources is capital intensive and sometimes result in dry or saline water sources. The water quality index maps are easily understood and will facilitate the determination of areas of good groundwater quality for informed decisions regarding the groundwater development sites, especially in arid regions where groundwater development challenges in terms of water quality are dominant.
- (iv) **The understanding of groundwater interaction regimes enhances understanding of the recharge characteristics and quantification of recharge, enabling groundwater resource managers to plan for sustainable supply and adopt management options that consider the extent of climate variability being experienced in their region.** into the. Groundwater level monitoring of the Lodwar Alluvial Aquifer System by the Turkana County Government and the Water Resources

Authority is required to allow for adequate and long-term data for the development of the forward and inverse groundwater models. These models will be useful tools for abstraction allocation in the area. More generally, such approaches will add to the very few rainfall-surface water-groundwater interaction studies currently undertaken in Sub-Saharan Africa.

5.3 Recommendations For Future Research

To further understand the extent of impacts of climate variability of the Lodwar aquifers and to generate more information for decision making, future research areas include but not limited to;

- **Climate variability continues to pose a threat to the sustainability of groundwater resources globally.** Its impacts on aquifers can be accurately measured using long-term rainfall and groundwater time series. Groundwater level monitoring is non-existent in the area. As part of the preparation for a future hydro-climatic study in the area, there is a need to develop a groundwater monitoring program. The derived datasets will help a future study quantify the extent of climate variability and assess the long-term impacts of climate variability on the groundwater system. The Water Table Fluctuation (WTF) data will aid in developing forward and inverse models for allocation of groundwater abstraction accurate estimation of groundwater recharge.
- **Geophysical models and lithostratigraphic logs can be used synergistically to improve aquifer conceptual models.** However, there was a lack of geological logs throughout the study area and a lack of adequate rock outcrops to define the 3D lithostratigraphy of the study area accurately. Although this study utilised geological mapping, hydrocensus, geophysical measurements, water quality and isotope studies of rain samples, surface water and groundwater to develop the aquifer conceptual model, a future study involving the use of geological logs for boreholes in the study area will help to improve the current aquifer model by application of numerical modelling.
- **Seasonal measurements of groundwater isotopes help to estimate the amount of recharge in an aquifer quantitatively.** Due to this study's limited timelines, a future study involving analysis of seasonal groundwater isotopes of oxygen-18, deuterium, and tritium will help quantify the amount of recharge in the LAAS. Analysis of rainfall and surface

water samples in this research will help distinguish the amount of recharge attributed to rainfall and that of surface water in the area, and accurately predict the impacts of climate variability on recharge of the LAAS.

REFERENCES

- Abdelshafy, M., Saber, M., Abdelhaleem, A., Abdelrazek, S. M., and Seleem, E. M. (2019). Hydrogeochemical processes and evaluation of groundwater aquifer at Sohag city, Egypt. *Scientific African*, 6, e00196. <https://doi.org/10.1016/j.sciaf.2019.e00196>
- Abid, K., Zouari, K., Dulinski, M., Chkir, N., and Abidi, B. (2011). Hydrologic and geologic factors controlling groundwater geochemistry in the Turonian aquifer (southern Tunisia). *Hydrogeology Journal*, 19(2), 415–427. <https://doi.org/10.1007/s10040-010-0668-z>
- Abiye, T., Masindi, K., Mengistu, H., and Demlie, M. (2018). Understanding the groundwater-level fluctuations for better management of groundwater resource: A case in the Johannesburg region. *Groundwater for Sustainable Development*, 7, 1–7. <https://doi.org/10.1016/j.gsd.2018.02.004>
- Aboubaker, M., Jalludin, M., and Razack, M. (2013). Hydrochemistry of a complex volcano-sedimentary aquifer using major ions and environmental isotopes data: Dalha basalts aquifer, southwest of Republic of Djibouti. *Environmental Earth Sciences*, 70(7), 3335–3349. <https://doi.org/10.1007/s12665-013-2398-8>
- Acharyya, S. K. (2002). *Arsenic contamination in groundwater affecting major parts of southern West Bengal and parts of western Chhattisgarh: Source and mobilization process*. 82(6), 22–24.
- Acworth, R. I., Rau, G. C., McCallum, A. M., Andersen, M. S., and Cuthbert, M. O. (2014). Comprendre les systèmes connectés eaux de surface/eaux souterraines en utilisant l'analyse de Fourier sur les variations de charge journalières et infra journalières. *Hydrogeology Journal*, 23(1), 143–159. <https://doi.org/10.1007/s10040-014-1182-5>
- Adelana, S., Fantong, W., Nedaw, D., and Duah, A. (2011). *Groundwater and Health: Meeting Unmet Needs in Sub-Saharan Africa*. <https://doi.org/10.1007/978-90-481-3426-7>
- Adimalla, N., Dhakate, R., Kasarla, A., and Taloor, A. K. (2020). Appraisal of groundwater quality for drinking and irrigation purposes in Central Telangana, India. *Groundwater for Sustainable Development*, 10, 100334. <https://doi.org/10.1016/j.gsd.2020.100334>

- Adomako, D., Maloszewski, P., Stumpp, C., Osae, S., Akiti, T. T., Adomako, D., Maloszewski, P., Stumpp, C., Osae, S., and Akiti, T. T. (2010). Estimating groundwater recharge from water isotope (δH , δO) depth profiles in the Densu River basin, Ghana Estimating groundwater recharge from water isotope ($\delta 2 H$, $\delta 18 O$) depth. *Hydrological Sciences Journal – Journal Des Sciences Hydrologiques*, 8(55), 2150–3435. <https://doi.org/10.1080/02626667.2010.527847>
- Afzali, A., Shahedi, K., Habib, M., Roshan, N., Solaimani, K., and Vahabzadeh, G. (2015). *Groundwater Quality Assessment in Haraz Alluvial Fan, Iran Full Length Research Paper Groundwater Quality Assessment in Haraz Alluvial Fan, Iran. October 2014.* <https://doi.org/10.12983/ijres-2014-p0346-0360>
- Aggarwal, P. K., and Froehlich, K. (2016). ENVIRONMENTAL ISOTOPS IN GROUNDWATER STUDIES. *Groundwater, II.*
- Aghazadeh, N., Chitsazan, M., and Golestan, Y. (2017). Hydrochemistry and quality assessment of groundwater in the Ardabil area, Iran. *Applied Water Science*, 7(7), 3599–3616. <https://doi.org/10.1007/s13201-016-0498-9>
- Águila, J. F., Samper, J., and Pisani, B. (2019). Parametric and numerical analysis of the estimation of groundwater recharge from water-table fluctuations in heterogeneous unconfined aquifers. *Hydrogeology Journal*, 27(4), 1309–1328. <https://doi.org/10.1007/s10040-018-1908-x>
- Agyemang, P. C. O., Roberts, E. M., Downie, B., and Sertich, J. J. W. (2019). Sedimentary provenance and maximum depositional age analysis of the Cretaceous? Lapur and Muruanachok sandstones (Turkana Grits), Turkana Basin, Kenya. *Geological Magazine*, 156(8), 1334–1356. <https://doi.org/10.1017/S0016756818000663>
- Ahmed, M., Talukder, M., Mojid, M. A., and Samad, M. (1998). A study of hydrogeological characteristics and properties of Muktagacha aquifer. *Bangladesh Journal of Agricultural Engineering*, 9, 11–16.
- Alam, K., and Ahmad, N. (2014). Determination of aquifer geometry through geophysical methods: A case study from Quetta Valley, Pakistan. *Acta Geophysica*, 62(1), 142–163. <https://doi.org/10.2478/s11600-013-0171-8>

- Alhawdar, Z. (2014). *Method Development for the Analysis of Aluminum, Calcium, Magnesium and Iron in Sedimentary Rocks Recommended Citation*. Pittsburg State University.
- Allison, G. B., and Hughes, M. W. (1978). The use of environmental chloride and tritium to estimate total recharge to an unconfined aquifer. *Soil Research*, 16(2), 181–195. <https://doi.org/10.1071/sr9780181>
- Al-Ruwaih, F. M. (2017). Hydrogeology and Groundwater Geochemistry of the Clastic Aquifer and Its Assessment for Irrigation, Southwest Kuwait. In *Aquifers—Matrix and Fluids*. InTech. <https://doi.org/10.5772/intechopen.71577>
- Al-Shaibani, A. M. (2008). Hydrogeology and hydrochemistry of a shallow alluvial aquifer, western Saudi Arabia. *Hydrogeology Journal*, 16(1), 155–165. <https://doi.org/10.1007/s10040-007-0220-y>
- Anderson, M. P., and Woessner, W. W. (1992). *Applied groundwater modeling: Simulation of flow and advective transport*. Academic Press. https://books.google.co.ke/books/about/Applied_Groundwater_Modeling.html?id=vVIneqegO4QCandredir_esc=y
- Andrés-Doménech, García-Bartual, R., Montanari, A., and Marco, J. B. (2015). Climate and hydrological variability: The catchment filtering role. *Hydrol. Earth Syst. Sci*, 19, 379–387. <https://doi.org/10.5194/hess-19-379-2015>
- Ansari, J. A., and Umar, R. (2019). Evaluation of hydrogeochemical characteristics and groundwater quality in the quaternary aquifers of Unnao District, Uttar Pradesh, India. *HydroResearch*, 1, 36–47. <https://doi.org/10.1016/J.HYDRES.2019.01.001>
- Ansari, K., and Hemke, N. M. (2013). *Water Quality Index for Assessment of Water Samples Of Different Zones In Chandrapur City*. 3(3), 233–237.
- APHA, A. P. H. A. (1995). *Standard Methods for the Examination of Water and Wastewater Part 1000 Standard Methods for the Examination of Water and Wastewater*. https://www.mwa.co.th/download/file_upload/SMWW_1000-3000.pdf
- Appleyard, S., and Cook, T. (2009). Reassessing the management of groundwater use from sandy aquifers: Acidification and base cation depletion exacerbated by drought and groundwater

- withdrawal on the Gnangara Mound, Western Australia. *Hydrogeology Journal*, 17(3), 579–588. <https://doi.org/10.1007/s10040-008-0410-2>
- Arambourg, C. (1933). *Mammifères Miocènes du Turkana (Afrique Orientale)*. Masson et Cie.
- Arambourg, C., and Wolff, R. (1969). *Nouvelles Données Paleontologiques Sur L'age Des 'Gres Du Lubur' (Turkana Grits) A L'ouest Du Lac Rodolphe*.
- Ashley, G. M., Mworia, J. M. A., Muasya, A. M., Owen, R. B., and Driese, S. G. (2004). *Sedimentation and recent history of a freshwater wetland in a semi-arid environment: Loboï Swamp, Kenya, East Africa*. 1–21. <https://doi.org/10.1111/j.1365-3091.2004.00671.x>
- Ashraf, M. A. M., Yusoh, R., Sazalil, M. A., and Abidin, M. H. Z. (2018). Aquifer Characterization and Groundwater Potential Evaluation in Sedimentary Rock Formation. *Journal of Physics: Conference Series*, 995, 012106. <https://doi.org/10.1088/1742-6596/995/1/012106>
- Atuahene, B. (2017). Interaction of Surface Water and Groundwater in the Nile River Basin and Peizometric Evidence. *We Want What's Ours: Learning from South Africa's Land Restitution Program*, 18. <https://doi.org/10.1590/S1516-18462008000300012>
- Avery, S. T. (2013). What future for Lake Turkana? *African Studies Centre*, 1–56.
- Avery, S. T., and Tebbs, E. J. (2018). Lake Turkana, major Omo River developments, associated hydrological cycle change and consequent lake physical and ecological change. *Journal of Great Lakes Research*, 44(6), 1164–1182. <https://doi.org/10.1016/j.jglr.2018.08.014>
- Aynew, T. (2008). *The distribution and hydrogeological controls of fluoride in the groundwater of central Ethiopian rift and adjacent highlands*. 1313–1324. <https://doi.org/10.1007/s00254-007-0914-4>
- Baalousha, H. (2011). *Fundamentals of Groundwater Modelling* (pp. 113–130).
- Babiker, M., and Gudmundsson, A. (2004). The effects of dykes and faults on groundwater flow in an arid land: The Red Sea Hills, Sudan. *Journal of Hydrology*, 297(1), 256–273. <https://doi.org/10.1016/j.jhydrol.2004.04.018>

- Badmus, B. S., Ozebo, V. C., Idowu, O. A., Ganiyu, S. A., and Olurin, O. T. (2015). Seasonal variations of physico chemical properties and quality index of groundwater of hand-dug wells around Ajakanga Dump Site in Southwestern Nigeria. *Research Journal of Physics*, 9(1), 1–10. <https://doi.org/10.3923/rjp.2015.1.10>
- Bai, L., Wang, Y., Zhou, Y., Liu, L., Yan, Z., and Li, F. (2016). Research on the process-based risk evaluation method of groundwater pollution for contaminated site. *Water Science and Technology: Water Supply*, 16(1), 150–162. <https://doi.org/10.2166/ws.2015.118>
- Barilari, A., Quiroz Londoño, M., Paris, M. del C., Lima, M. L., and Massone, H. E. (2020). Groundwater contamination from point sources. A hazard index to protect water supply wells in intermediate cities. *Groundwater for Sustainable Development*, 10, 100363. <https://doi.org/10.1016/j.gsd.2020.100363>
- Batelaan, O., and Smedt, F. D. E. (2001). *WetSpas: A flexible, GIS based, distributed recharge methodology for regional groundwater modelling*. 269, 11–17.
- Bates, B., Kundzewicz, Z. W., and IPCC (Eds.). (2008). *Climate change and water*.
- Bayari, S., Ozyurt, N. N., Hatipoglu, Z., and Kilani, S. (2006). Groundwater age: A vital information in protecting the groundwater dependent ecosystem. In A. Baba, K. W. F. Howard, and O. Gunduz (Eds.), *Groundwater and Ecosystems* (pp. 33–46). Springer Netherlands. https://doi.org/10.1007/1-4020-4738-X_3
- Bekesi, G., and Mcconchie, J. (1998). *Regional Groundwater Recharge Modelling Using the Monte-Carlo Technique in the Manawatu Region, New Zealand*. 1–18.
- Bello, R., Emujakporue, G. O., Mkpese, U. U., and Gladman, B. G. (2017). The use of Vertical Electrical Sounding (VES) to investigate the extent of groundwater contamination and lithology delineation at a dumpsite in Aluu Community, Rivers State. *Scientia Africana*, 16(1), Article 1. <https://doi.org/10.4314/sa.v16i1>.
- Belt, C. J. (1964). Atomic Absorption Spectrophotometry. *Journal of Economic Geology*, 59, 240–258.
- Bershaw, J., Bershaw, and John. (2018). Controls on Deuterium Excess across Asia. *Geosciences*, 8(7), 257. <https://doi.org/10.3390/geosciences8070257>

- Bhattacharya, P., Ramanathan, A. L., Mukherjee, A. B., Bundschuh, J., Chandrasekharam, D., and Keshari, A. K. (2008). *Groundwater for Sustainable Development: Problems, Perspectives and Challenges*. CRC Press.
- Birkle, P., Torres Rodríguez, V., and González Partida, E. (1998). The water balance for the Basin of the Valley of Mexico and implications for future water consumption. *Hydrogeology Journal*, 6(4), 500–517. <https://doi.org/10.1007/s100400050171>
- Boah, D. K., Twum, S. B., and Pelig-ba, K. B. (2015). Mathematical Computation of Water Quality Index of Vea Dam in Upper East Region of Ghana. *Environmental Sciences*, 3(1), 11–16. <https://doi.org/10.12988/es.2015.4116>
- Boulton, S., and Whittaker, A. (2009). Quantifying the slip rates, spatial distribution and evolution of active normal faults from geomorphic analysis: Field examples from an oblique-extensional Graben, Southern Turkey. *Geomorphology*, 104, 299–316. <https://doi.org/10.1016/j.geomorph.2008.09.007>
- Brassington, and Younger. (2010). A proposed framework for hydrogeological conceptual modelling. *Water and Environment Journal*, 24(4), 261–273. <https://doi.org/10.1111/j.1747-6593.2009.00173.x>
- Brears, E., and Post, R. (2014). *NVCA Water Table Fluctuation Study. I*(Figure 1), 1–17.
- Brindha, K., Rajesh, R., Murugan, R., and Elango, L. (2011). Fluoride contamination in groundwater in parts of Nalgonda District, Andhra Pradesh, India. *Environmental Monitoring and Assessment*, 172(1–4), 481–492. <https://doi.org/10.1007/s10661-010-1348-0>
- Bruthans, J., Kůrková, I., and Kadlecová, R. (2019). Factors controlling nitrate concentration in space and time in wells distributed along an aquifer/river interface (Káraný, Czechia). *Hydrogeology Journal*, 27(1), 195–210. <https://doi.org/10.1007/s10040-018-1854-7>
- Burnham, C. (2019). (PDF) *A Study of UAV Photogrammetry Software*. ResearchGate. https://www.researchgate.net/publication/335749992_A_Study_of_UAV_Phogrammetry_Software

- Butler, L. R. P., and Kokot, M. L. (1971a). ATOMIC ABSORPTION. In *National Physical Research Laboratory* (pp. 205–206).
- Research Laboratory* (pp. 205–206).
- Calvache, M. L., Duque, C., Gomez Fontalva, J. M., and Crespo, F. (2011). Processes affecting groundwater temperature patterns in a coastal aquifer. *International Journal of Environmental Science and Technology*, 8(2), 223–236. <https://doi.org/10.1007/BF03326211>
- Carter, J. F., and Barwick, V. J. (2011). *Good Practice Guide for Isotope Ratio Mass Spectrometry FIRMS*. [http://www.forensic-isotopes.org/assets/IRMS Guide Finalv3.1_Web.pdf](http://www.forensic-isotopes.org/assets/IRMS%20Guide%20Finalv3.1_Web.pdf)
- Casanova, J., Devau, N., and Pettenati, M. (2016). Managed Aquifer Recharge: An Overview of Issues and Options. In A. J. Jakeman, O. Barreteau, R. J. Hunt, J.-D. Rinaudo, and A. Ross (Eds.), *Integrated Groundwater Management* (pp. 413–434). Springer International Publishing. https://doi.org/10.1007/978-3-319-23576-9_16
- Chacha, R. (2014). *Method for analysing soil samples for mineral composition using XRD* (pp. 1–12).
- Chae, G.-T., Kim, K., Yun, S.-T., Kim, K.-H., Kim, S.-O., Choi, B.-Y., Kim, H.-S., and Rhee, C. W. (2004). Hydrogeochemistry of alluvial groundwaters in an agricultural area: An implication for groundwater contamination susceptibility. *Chemosphere*, 55(3), 369–378. <https://doi.org/10.1016/J.CHEMOSPHERE.2003.11.001>
- Chen, X., Wang, G., and Wang, F. (2019). Classification of Stable Isotopes and Identification of Water Replenishment in the Naqu River Basin, Qinghai-Tibet Plateau. *Water*, 11(1), 46. <https://doi.org/10.3390/w11010046>
- Chen, Z., Grasby, S. E., and Osadetz, K. G. (2004). *Relation between climate variability and groundwater levels in the upper carbonate aquifer , southern Manitoba , Canada*. 290, 43–62. <https://doi.org/10.1016/j.jhydrol.2003.11.029>
- Chenini, I., Farhat, B., and Ben Mammou, A. B. (2010). Identification of major sources controlling groundwater chemistry from a multilayered aquifer system. *Chemical Speciation and Bioavailability*, 22(3), 183–189. <https://doi.org/10.3184/095422910X12829228276711>

- Chilton, J., Dahi, E., Lennon, M., and Jackson, P. (2006). *Fluoride in Drinking-water*.
- Chilton, J., and Seiler, K.-P. (2006). Groundwater occurrence and hydrogeological environments. In *Protecting Groundwater for Health. Managing the Quality of Drinking-water Sources*. IWA Publishing,. <http://www.bvsde.paho.org/bvsacd/cd59/protecting/sect1-2.pdf>
- Clark, I. D. (Ian D., and Fritz, P. (Peter). (1997). *Environmental isotopes in hydrogeology*. CRC Press/Lewis Publishers. <https://www.crcpress.com/Environmental-Isotopes-in-Hydrogeology/Clark-Fritz/p/book/9781566702492>
- Cloutier, V., Lefebvre, R., Savard, M. M., Bourque, É., and Therrien, R. (2006). Hydrogeochemistry and groundwater origin of the Basses-Laurentides sedimentary rock aquifer system, St. Lawrence Lowlands, Québec, Canada. *Hydrogeology Journal*, 14(4), 573–590. <https://doi.org/10.1007/s10040-005-0002-3>
- Cobbing, J. (2020). Groundwater and the discourse of shortage in Sub-Saharan Africa. *Hydrogeology Journal*, 28(4), 1143–1154. <https://doi.org/10.1007/s10040-020-02147-5>
- Coetsiers, M., Kilonzo, F., and Walraevens, K. (2009). *Hydrochemistry and source of high fluoride in groundwater of the Nairobi area , Kenya*. 53(December 2008).
- Comte, J. C., Cassidy, R., Obando, J., Robins, N., Ibrahim, K., Melchioly, S., Mjemah, I., Shauri, H., Bourhane, A., Mohamed, I., Noe, C., Mwegu, B., Makokha, M., Join, J. L., Banton, O., and Davies, J. (2016). Challenges in groundwater resource management in coastal aquifers of East Africa: Investigations and lessons learnt in the Comoros Islands, Kenya and Tanzania. *Journal of Hydrology: Regional Studies*, 5, 179–199. <https://doi.org/10.1016/j.ejrh.2015.12.065>
- Comte, J.-C., Wilson, C., Ofterdinger, U., and González-Quirós, A. (2017). Effect of volcanic dykes on coastal groundwater flow and saltwater intrusion: A field-scale multiphysics approach and parameter evaluation. *Water Resources Research*, 53(3), 2171–2198. <https://doi.org/10.1002/2016WR019480>
- Craig, H. (1961). Isotopic Variations in Meteoric Waters. *Science*, 133(3465), 1702. <https://doi.org/10.1126/science.133.3465.1702>

- Dandar, O., Okamoto, A., Uno, M., Batsaikhan, U., Ulziiburen, B., and Noriyoshi, T. (2018). Drone brings new advance of geological mapping in Mongolia: Opportunities and challenges. *Mongolian Geoscientist*, 53–57. <https://doi.org/10.5564/mgs.v0i47.1063>
- Dash, S., Borah, S. S., and Kalamdhad, A. (2018). Monitoring and assessment of Deepor Beel water quality using multivariate statistical tools. *Water Practice and Technology*, 13(4), 893–908. <https://doi.org/10.2166/wpt.2018.098>
- Dennehy, K. F., Reilly, T. E., and Cunningham, W. L. (2015). Disponibilité des eaux souterraines aux Etats-Unis d'Amérique: La valeur des évaluations quantitatives régionales. *Hydrogeology Journal*, 23(8), 1629–1632. <https://doi.org/10.1007/s10040-015-1307-5>
- Dhanasekarapandian, M., Chandran, S., Devi, D. S., and Kumar, V. (2016). Spatial and temporal variation of groundwater quality and its suitability for irrigation and drinking purpose using GIS and WQI in an urban fringe. *Journal of African Earth Sciences*, 124, 270–288. <https://doi.org/10.1016/j.jafrearsci.2016.08.015>
- Dhungel, R., and Fiedler, F. (2016). Water Balance to Recharge Calculation: Implications for Watershed Management Using Systems Dynamics Approach. *Hydrology*, 3(1), 13. <https://doi.org/10.3390/hydrology3010013>
- Dodson, R. G. (Ministry of N. R. (1971). *Geology the Area Area South of Lodwar*. 87.
- Douglas, K. S. O. R. K. (2015). Evaluation of major factors influencing the geochemistry of groundwater using graphical and multivariate statistical methods in Yenagoa city , Southern Nigeria. *Applied Water Science*, 27–37. <https://doi.org/10.1007/s13201-014-0166-x>
- Doust, H., and Sumner, H. S. (2007). Petroleum systems in rift basins – a collective approach in Southeast Asian basins. *Petroleum Geoscience*, 13(2), 127–144. <https://doi.org/10.1144/1354-079307-746>
- Ducrocq, S., Boisserie, J.-R., Tiercelin, J.-J., Delmer, C., Garcia, G., Kyalo, M. F., Leakey, M. G., Marivaux, L., Otero, O., Peigné, S., Tassy, P., and Lihoreau, F. (2010). New Oligocene vertebrate localities from Northern Kenya (Turkana basin). *Journal of Vertebrate Paleontology*, 30(1), 293–299. <https://doi.org/10.1080/02724630903413065>

- Edmunds, W. M., and Smedley, P. L. (2013). Fluoride in Natural Waters. In *Fluoride in Natural Waters*. <https://doi.org/10.1007/978-94-007-4375-5>
- Egai, A. O., and Douglas, R. K. (2015). Aspects of Geophysical Survey Using Vertical Electrical Sounding (VES) for Groundwater Exploration in Parts of Ahoada West LGA of Rivers State, Southern Nigeria. *Geosciences*, 5(1), 31–38.
- Egan, P., and Price, M. (2014). *Our Global Water Towers: Ensuring Ecosystem Services From Mountains Under Climate Change – A Policy Brief (UNESCO)*.
- Elango, L., and Kannan, R. (2007). Chapter 11 Rock–water interaction and its control on chemical composition of groundwater. In *Developments in Environmental Science (Vol. 5)*, pp. 229–243). Elsevier. [https://doi.org/10.1016/S1474-8177\(07\)05011-5](https://doi.org/10.1016/S1474-8177(07)05011-5)
- Engelen, V. V. (1984). *Kenya Soil Survey: An Assessment of the Irrigation Suitability of the Soils of The Nakwamoru Area (Turkana District)* (pp. 1–25). Ministry of Agriculture - National Agricultural Laboratory. <https://edepot.wur.nl/480078>
- Enkin, R. J., Hamilton, T. S., and Morris, W. A. (2020). The Henkel Petrophysical Plot: Mineralogy and Lithology from Physical Properties. *Geochemistry, Geophysics, Geosystems*, 21(1), e2019GC008818. <https://doi.org/10.1029/2019GC008818>
- Fabbri, P., and Piccinini, L. (2013). Assessing transmissivity from specific capacity in an alluvial aquifer in the middle Venetian plain (NE Italy). *Water Science and Technology*, 67(9), 2000–2008. <https://doi.org/10.2166/wst.2013.074>
- Falkenmark, M. (2019). Rapid Population Growth and Water Scarcity: The Predicament of Tomorrow’ s Africa. *Population and Development Review*, 16(1990), 81–94.
- Famiglietti, J. S. (2014). The global groundwater crisis. *Nature Climate Change*, 4(11), 945–948. <https://doi.org/10.1038/nclimate2425>
- FAO. (2018). *Southern Africa Resilience Strategy 2018–2021* (p. 36). Food Agricultural Organization (FAO).
- Faye, S. C., Diongue, M. L., Pouye, A., Gaye, C. B., Travi, Y., Wohnlich, S., Faye, S., and Taylor, R. G. (2019). Tracing natural groundwater recharge to the Thiaroye aquifer of Dakar,

- Senegal. *Hydrogeology Journal*, 27(3), 1067–1080. <https://doi.org/10.1007/s10040-018-01923-8>
- Feibel, C. S. (2011). A Geological History of the Turkana Basin. *Evolutionary Anthropology*, 20(6), 206–216. <https://doi.org/10.1002/evan.20331>
- Foster, S. S. D., and Chilton, P. J. (2003). Groundwater: The processes and global significance of aquifer degradation. *Philosophical Transactions of the Royal Society B: Biological Sciences*, 358(1440), 1957–1972. <https://doi.org/10.1098/rstb.2003.1380>
- Foster, S., Tuinhof, A., and Steenbergen, F. V. (2012). *Managed groundwater development for water-supply security in Sub-Saharan Africa: Investment priorities*. 38(3), 359–366.
- Garba Abdullahi, M., Nasiru Usman, U., Ekhwan Toriman, M., Juahir, H., Auwalu Rabi, A., and Isiyaka, H. (2014). Assessment of Groundwater Quality Using Multivariate Statistical Techniques in Terengganu Groundwater Pattern Recognition Based on Rainfall Distribution in Terengganu Malaysia View project Effect of Light Pollution View project Assessment of Groundwater Quality Using Multivariate Statistical Techniques in Terengganu. *Science and Technology*, 4(3), 42–49. <https://doi.org/10.5923/j.scit.20140403.02>
- Gardner, K. K., and Vogel, R. M. (2005). *Predicting Ground Water Nitrate Concentration from Land Use*. 43(3), 343–352.
- Garrels, R. M., and Berner, R. A. (1983). The Global Carbonate-Silicate Sedimentary System—Some Feedback Relations. In P. Westbroek and E. W. de Jong (Eds.), *Biomineralization and Biological Metal Accumulation: Biological and Geological Perspectives Papers presented at the Fourth International Symposium on Biomineralization, Renesse, The Netherlands, June 2–5, 1982* (pp. 73–87). Springer Netherlands. https://doi.org/10.1007/978-94-009-7944-4_6
- Gates, J. B., Edmunds, W. M., Ma, J., and Sheppard, P. R. (2008). A 700-year history of groundwater recharge in the drylands of NW China. *Holocene*, 18(7), 1045–1054. <https://doi.org/10.1177/0959683608095575>

- Gaye, C. B., and Edmunds, W. M. (1996). Groundwater recharge estimation using chloride, stable isotopes and tritium profiles in the sands of northwestern Senegal. *Environmental Geology*, 27(3), 246–251. <https://doi.org/10.1007/BF00770438>
- Geological map of Kenya (MERD)*. (1987).
- Ghaffar, A., Tariq, T., Mashiatullah, A., and Ali, S. M. (2017). Hydrological and environment tritium investigation to evaluate groundwater in capital territory of Pakistan. *Water Science and Technology: Water Supply*, 17(2), 433–451. <https://doi.org/10.2166/ws.2016.149>
- Ghoraba, S. M., and Khan, A. D. (2013). Hydrochemistry and groundwater quality assessment in Balochistan province, Pakistan. *International Journal of Research and Reviews in Applied Sciences*, 17(2), 185–199.
- Giménez-Forcada, E. (2010a). *Dynamic of Seawater Interface using Hydrochemical Facies Evolution Diagram (HFE-D)*. <https://doi.org/10.1111/j.1745-6584.2009.00649.x>
- Gleeson, T., Allen, D. M., and Ferguson, G. (2012). *Teaching hydrogeology: A review of current practice*. 2159–2168. <https://doi.org/10.5194/hess-16-2159-2012>
- Glover, E. T., Akiti, T. T., and Osae, S. (2012a). Geoscience Major ion chemistry and identification of hydrogeochemical processes of groundwater in the Accra Plains. *Geoscience*, 50, 10279–10288.
- Glover, E. T., Akiti, T. T., and Osae, S. (2012b). Geoscience Major ion chemistry and identification of hydrogeochemical processes of groundwater in the Accra Plains. *Geoscience*, 50, 10279–10288.
- Goni, I. B., Sheriff, B. M., Kolo, A. M., and Ibrahim, M. B. (2019). Assessment of nitrate concentrations in the shallow groundwater aquifer of Maiduguri and environs, Northeastern Nigeria. *Scientific African*, 4, e00089. <https://doi.org/10.1016/j.sciaf.2019.e00089>
- González-Trinidad, J., Pacheco-Guerrero, A., Júnez-Ferreira, H., Bautista-Capetillo, C., and Hernández-Antonio, A. (2017). Identifying groundwater recharge sites through environmental stable isotopes in an alluvial aquifer. *Water (Switzerland)*, 9(8), 1–12. <https://doi.org/10.3390/w9080569>

- Goudarzi, S., Jozi, S. A., Monavari, S. M., Karbasi, A., and Hasani, A. H. (2017). Assessment of groundwater vulnerability to nitrate pollution caused by agricultural practices. *Water Quality Research Journal of Canada*, 52(1), 64–77. <https://doi.org/10.2166/wqrjc.2017.031>
- Green, T. R. (2016). Linking Climate Change and Groundwater. In A. J. Jakeman, O. Barreteau, R. J. Hunt, J.-D. Rinaudo, and A. Ross (Eds.), *Integrated Groundwater Management* (pp. 97–141). Springer International Publishing. https://doi.org/10.1007/978-3-319-23576-9_5
- Grundmann, G., and Scholz, H. (2015). *Preparation methods in Mineralogy and Geology: The preparation of thin sections, polished sections, acetate foil prints, preparation for elutriation analysis and staining tests for the optical and electron microscopy.*
- Guo, Q., Zhou, Z., Huang, G., and Dou, Z. (2019). Variations of groundwater quality in the multi-layered aquifer system near the Luanhe river, China. *Sustainability (Switzerland)*, 11(4). <https://doi.org/10.3390/su11040994>
- Haile-Meskale, M. (2017). An Overview of Saturation State of Groundwater with Respect to Some Common Minerals in South Central Ontario. *International Journal of Sciences: Basic and Applied Research (IJSBAR)*, Volume 36(5), 32–47.
- Hamlat, A., and Guidoum, A. (2018). Assessment of groundwater quality in a semiarid region of Northwestern Algeria using water quality index (WQI). *Applied Water Science*, 8(8), 1–13. <https://doi.org/10.1007/s13201-018-0863-y>
- Hamutoko, J. T., Wanke, H., Beyer, M., Gaj, M., and Koeniger, P. (2018). Spatio-temporal variations of hydrochemical and isotopic patterns of groundwater in hand-dug wells: The Cuvelai-Etосha Basin, Namibia. *Proceedings of the International Association of Hydrological Sciences*, 378, 29–35. <https://doi.org/10.5194/piahs-378-29-2018>
- Hamutoko, J. T., Wanke, H., Koeniger, P., Beyer, M., and Gaj, M. (2017). Hydrogeochemical and isotope study of perched aquifers in the Cuvelai-Etосha Basin, Namibia. *Isotopes in Environmental and Health Studies*, 53(4), 382–399. <https://doi.org/10.1080/10256016.2016.1273913>

- Hawkins, S. (2016). *Using a drone and photogrammetry software to create orthomosaic images and 3D models of aircraft accident sites*. 26.
- Healy, R. W. (2010). *Estimating Groundwater Recharge*. Cambridge University Press.
- Heiß, L., Bouchaou, L., Tadoumant, S., and Reichert, B. (2020). Index-based groundwater vulnerability and water quality assessment in the arid region of Tata city (Morocco). *Groundwater for Sustainable Development*, 10, 100344. <https://doi.org/10.1016/j.gsd.2020.100344>
- Hemker, K., and Bakker, M. (2005). *Calibration and Reliability in Groundwater Modelling: From Uncertainty to Decision Making (Proceedings of ModelCARE' Complex groundwater whirl systems (Vol. 304)*. IAHS Publ. <https://iahs.info/uploads/dms/13505.50-281-287-IAHS304-07-181.pdf>
- Henkes, G. A., Moreira, M. C., Yang, D., and Thomas, E. (2018). *A modern isotope hydrology of the Turkana Basin*. 2018, PP31B-1654.
- Hinkle, B. S. R., and Survey, U. S. G. (1997). *Quality of Shallow Ground Water in Alluvial Aquifers of the Willamette Basin, Oregon*,.
- Hinzman, L. D., Wegner, M., and Lilly, M. R. (2000). Hydrologic Investigations of groundwater and surface-water interactions in subarctic Alaska. *Nordic Hydrology*, 31(4–5), 339–356. <https://doi.org/10.2166/nh.2000.0020>
- Hirpa, F. A., Dyer, E., Hope, R., Olago, D. O., and Dadson, S. J. (2018). Journal of Hydrology: Regional Studies Finding sustainable water futures in data-sparse regions under climate change: Insights from the Turkwel River basin, Kenya. *Journal of Hydrology: Regional Studies*, 19(August), 124–135. <https://doi.org/10.1016/j.ejrh.2018.08.005>
- Hove, A. R. T., and Ongweny, G. S. O. (1974). AN OUTLINE OF KENYA'S GROUNDWATER QUALITY. *Journal of Eastern African Research and Development*, 4(1), 67–97.
- Hughes, M. (1933). *Notes on the Geological Succession, Tectonics, and Economic Geology of the Western Half of Kenya Colony*. 3.

- Irvine, T. N., and Baragar, W. R. A. (1971). A Guide to the Chemical Classification of the Common Volcanic Rocks. *Canadian Journal of Earth Sciences*, 8(5), 523–548. <https://doi.org/10.1139/e71-055>
- Islam, Md. M., Lenz, O. K., Azad, A. K., Ara, M. H., Rahman, M., Hassan, N., Islam, Md. M., Lenz, O. K., Azad, A. K., Ara, M. H., Rahman, M., and Hassan, N. (2017). Assessment of Spatio-Temporal Variations in Water Quality of Shailmari River, Khulna (Bangladesh) Using Multivariate Statistical Techniques. *Journal of Geoscience and Environment Protection*, 05(01), 1–26. <https://doi.org/10.4236/gep.2017.51001>
- Jang, W., Engel, B., Harbor, J., and Theller, L. (2017). Aquifer Vulnerability Assessment for Sustainable Groundwater Management Using DRASTIC. *Water*, 9(10), 792. <https://doi.org/10.3390/w9100792>
- Jaroslav, V., and Van der Gun, J. (2004). *The world's groundwater resources* (p. Report Nr IP 2004-1). International Groundwater Resources Assessment Centre (IGRAC). <http://geocompendium.grid.unep.ch/index.htm>
- Jassas, H., and Merkel, B. (2014). Estimating groundwater recharge in the semiarid Al-Khazir: Gomal basin, north Iraq. *Water (Switzerland)*, 6(8), 2467–2481. <https://doi.org/10.3390/w6082467>
- JICA. (2012). *Water Potential Study in Turkana County* (pp. 231–256).
- Jimenez, B., and Chávez, A. (2004). Quality assessment of an aquifer recharged with wastewater for its potential use as drinking source: “El Mezquital Valley” case. *Water Science and Technology*, 50(2), 269–276. <https://doi.org/10.2166/wst.2004.0141>
- Joshi, S. K., Rai, S. P., Sinha, R., Gupta, S., Densmore, A. L., Rawat, Y. S., and Shekhar, S. (2018). Tracing groundwater recharge sources in the northwestern Indian alluvial aquifer using water isotopes ($\delta^{18}\text{O}$, $\delta^2\text{H}$ and ^3H). *Journal of Hydrology*, 559, 835–847. <https://doi.org/10.1016/j.jhydrol.2018.02.056>
- Kana, J. D., Djongyang, N., Dadjé, A., and Raïdandi, D. (2013). Vertical Electrical Soundings for Subsurface Layers and Groundwater Investigations in the Mayo Kani Area in Cameroon. *International Journal of Science and Research (IJSR)*, 396–401.

- Kanda, I., and Suwai, J. (2013). *Hydrogeochemistry of Shallow and Deep Water Aquifers of Menengai Geothermal Area, Kenya Rift Valley*. 37, 8.
- Karegi, S., Macharia, K., Muthengia, W., and Mwiti, M. (2018). Hydrogeochemistry of Ground Water in Mbeere South Sub-County, Kenya. *International Journal of Chemistry*, 10, 173. <https://doi.org/10.5539/ijc.v10n4p173>
- Kaufmann, G. (2009). Modelling karst geomorphology on different time scales. *Geomorphology*, 106(1), 62–77. <https://doi.org/10.1016/j.geomorph.2008.09.016>
- Kebede, S. (2005). Groundwater recharge, circulation and geochemical evolution in the source region of the Blue Nile River , Ethiopia. *Applied Geochemistry*, 20(2005), 1658–1676. <https://doi.org/10.1016/j.apgeochem.2005.04.016>
- Kebede, S., Travi, Y., and Asrat, A. (2008). *Groundwater origin and flow along selected transects in Ethiopian rift volcanic aquifers*. 55–73. <https://doi.org/10.1007/s10040-007-0210-0>
- Kebede, S., Travi, Y., and Stadler, S. (2010a). Groundwaters of the Central Ethiopian Rift: Diagnostic trends in trace elements, $\delta^{18}\text{O}$ and major elements. *Environmental Earth Sciences*, 61(8), 1641–1655. <https://doi.org/10.1007/s12665-010-0479-5>
- Kebede, S., Travi, Y., and Stadler, S. (2010b). Groundwaters of the Central Ethiopian Rift: Diagnostic trends in trace elements, $\delta^{18}\text{O}$ and major elements. *Environmental Earth Sciences*, 61(8), 1641–1655. <https://doi.org/10.1007/s12665-010-0479-5>
- Kendall, C., and Holland, H. D. (2003). Stable Isotope Applications in Hydrologic Studies. In H. D. Holland and K. K. Turekian (Eds.), *Treatise on Geochemistry* (pp. 319–364). Pergamon. <https://doi.org/10.1016/B0-08-043751-6/05081-7>
- Khatri, N., and Tyagi, S. (2014). Influences of natural and anthropogenic factors on surface and groundwater quality in rural and urban areas. *Frontiers in Life Science*, 8(1), 23–39. <https://doi.org/10.1080/21553769.2014.933716>
- KNBS. (2009). *The 2009 Kenya Population and Housing Census* (Census Report VOLUME IC; Counting Our People for the Implementation of Vision 2030”, pp. 1–546). Kenya National Bureau of Statistics. <https://s3-eu-west-1.amazonaws.com/s3.sourceafrica.net/documents/21195/Census-2009.pdf>

- KNBS. (2019). *Kenya Population and Housing Census (Population By County and Subcounty Volume 1; pp. 1–49)*. Kenya National Bureau of Statistics. <http://housingfinanceafrica.org/app/uploads/VOLUME-I-KPHC-2019.pdf>
- Koskei, E. C., Kitetu, J. J., and Recha, C. W. (2018). *Analysis of spatial variability in rainfall trends in Baringo County, Kenya*. *12*(September), 296–304. <https://doi.org/10.5897/AJEST2016.2214>
- Kotchoni, D. O. V., Vouillamoz, J. M., Lawson, F. M. A., Adjomayi, P., Boukari, M., and Taylor, R. G. (2018). Relationships between rainfall and groundwater recharge in seasonally humid Benin: A comparative analysis of long-term hydrographs in sedimentary and crystalline aquifers. *Hydrogeology Journal*, 1–11. <https://doi.org/10.1007/s10040-018-1806-2>
- Kumar, Balasubramanian, A., Kumar, R. S., Dushiyanthan, C., Thiruneelakandan, B., Suresh, R., Karthikeyan, K., and Davidraju, D. (2016). Assessment of groundwater potential based on aquifer properties of hard rock terrain in the Chittar–Uppodai watershed, Tamil Nadu, India. *Applied Water Science*, *6*(2), 179–186. <https://doi.org/10.1007/s13201-014-0216-4>
- Kumar, M., Ramanathan, AL., Rao, M. S., and Kumar, B. (2006). Identification and evaluation of hydrogeochemical processes in the groundwater environment of Delhi, India. *Environmental Geology*, *50*(7), 1025–1039. <https://doi.org/10.1007/s00254-006-0275-4>
- Kumar, P. (2013a). Interpretation of groundwater chemistry using piper and chadhas diagrams: A comparative study from perambalur taluk. *Elixirpublishers.Com*, *54*, 12208–12211.
- Kumar, P. (2013b). Interpretation of groundwater chemistry using piper and chadhas diagrams: A comparative study from perambalur taluk. *Elixirpublishers.Com*, *54*, 12208–12211.
- Kumar, P. J. S., and James, E. J. (2013a). Development of Water Quality Index (WQI) model for the groundwater in Tirupur district, South India. *Chinese Journal of Geochemistry*, *32*(3), 261–268. <https://doi.org/10.1007/s11631-013-0631-5>
- Kumar, P. J. S., and James, E. J. (2013b). Development of Water Quality Index (WQI) model for the groundwater in Tirupur district, South India. *Chinese Journal of Geochemistry*, *32*(3), 261–268. <https://doi.org/10.1007/s11631-013-0631-5>

- Kumar, S., Thirumalaivasan, D., and Radhakrishnan, N. (2014). GIS Based Assessment of Groundwater Vulnerability Using Drastic Model. *Arabian Journal for Science and Engineering*, 39(1), 207–216. <https://doi.org/10.1007/s13369-013-0843-3>
- Kumari, B., Mondal, M. R., Tiwary, R., and Srivastava, K. K. (2014). Physico-chemical characterization and water quality index of ground water of Dhanbad town area. *Advances in Applied Science Research*, 5(3), 286–292.
- Kundzewicz, Z. W., Mata, L. J., Arnell, N. W., Doll, P., Jimenez, B., Miller, K., Oki, T., Sen, Z., and Shiklomanov, I. (2008). The implications of projected climate change for freshwater resources and their management. *Hydrological Sciences Journal*, 1(53), 2–10. <https://doi.org/10.1623/hysj.53.1.3>
- Kuria, Z. (2011). Kenya: A Natural Outlook: Groundwater Distribution and Aquifer Characteristics in Kenya. In *Kenya: A Natural Outlook: Geo-Environmental Resources and Hazards* (1st ed., **Vol. 16**, pp. 83–105). Elsevier B.V.
- Kuria, Z. (2013). Chapter 8—Groundwater Distribution and Aquifer Characteristics in Kenya. In P. Paron, D. O. Olago, and C. T. Omuto (Eds.), *Developments in Earth Surface Processes* (**Vol. 16**, pp. 83–107). Elsevier. <https://doi.org/10.1016/B978-0-444-59559-1.00008-6>
- Kurniawan, A. (2009). *BASIC IP2 WIN TUTORIAL*. 32.
- Kuroda, K., and Fukushi, T. (2008). Groundwater Contamination in Urban Areas. In S. Takizawa (Ed.), *Groundwater Management in Asian Cities: Technology and Policy for Sustainability* (pp. 125–149). Springer Japan. https://doi.org/10.1007/978-4-431-78399-2_7
- Lakshmanan, E., and Kannan, R. (2007). Chapter 11 Rock–water interaction and its control on chemical composition of groundwater. *Developments in Environmental Science*, 5. [https://doi.org/10.1016/S1474-8177\(07\)05011-5](https://doi.org/10.1016/S1474-8177(07)05011-5)
- Lapworth, D. J., Nkhuwa, D. C. W., Okotto-Okotto, J., Pedley, S., Stuart, M. E., Tijani, M. N., and Wright, J. (2017). Urban groundwater quality in sub-Saharan Africa: Current status and implications for water security and public health. *Qualité des eaux souterraines urbaines en Afrique sub-saharienne: État actuel et implications pour la sécurité de*

- l'approvisionnement en e. *Hydrogeology Journal*, 25(4), 1093–1116.
<https://doi.org/10.1007/s10040-016-1516-6>
- Lathamani, R., Janardhana, M. R., Mahalingam, B., and Suresha, S. (2015a). Evaluation of Aquifer Vulnerability Using Drastic Model and GIS: A Case Study of Mysore City, Karnataka, India. *Aquatic Procedia*, 4(Icwrcoe), 1031–1038.
<https://doi.org/10.1016/j.aqpro.2015.02.130>
- Lautze, J., Holmatov, B., Saruchera, D., and Villholth, K. G. (2018). Conjunctive management of surface and groundwater in transboundary watercourses: A first assessment. *Water Policy*, 20(1), 1–20. <https://doi.org/10.2166/wp.2018.033>
- Lee, C. H., Chen, W. P., and Lee, R. H. (2006). Estimation of groundwater recharge using water balance coupled with base-flow-record estimation and stable-base-flow analysis. *Environmental Geology*, 51(1), 73–82. <https://doi.org/10.1007/s00254-006-0305-2>
- Lerner, D. N., Issar, A. S., and Simmers, I. (1990). *Groundwater recharge: A guide to understanding and estimating natural recharge*.
- Levin, N. E., Zipser, E. J., and Cerling, T. E. (2009). Isotopic composition of waters from Ethiopia and Kenya: Insights into moisture sources for eastern Africa. *Journal of Geophysical Research (Atmospheres)*, 114, D23306. <https://doi.org/10.1029/2009JD012166>
- Lewandowski, J., Meinikmann, K., and Krause, S. (2020). Groundwater–Surface Water Interactions: Recent Advances and Interdisciplinary Challenges. *Water*, 12(1), 296. <https://doi.org/10.3390/w12010296>
- Li, B. D., Zhang, X. H., Xu, C. Y., Zhang, H., and Song, J. X. (2015). Water balance between surfacewater and groundwater in the withdrawal process: A case study of the Osceola watershed. *Hydrology Research*, 46(6), 943–953. <https://doi.org/10.2166/nh.2015.137>
- Li, X., Wu, H., Qian, H., and Gao, Y. (2018). Groundwater chemistry regulated by hydrochemical processes and geological structures: A case study in Tongchuan, China. *Water (Switzerland)*, 10(3). <https://doi.org/10.3390/w10030338>
- Liu, C., Chia, Y., Chuang, P., Chiu, Y., and Tseng, T. (2018). *Impacts of hydrogeological characteristics on groundwater-level changes induced by earthquakes*. 451–465.

- Lokhande, P. B., and Mujawar, H. A. (2016a). Graphic Interpretation and Assessment of Water Quality in the Savitri River Basin. *International Journal of Scientific and Engineering Research*, 7(3), 1113–1123.
- Lokhande, P. B., and Mujawar, H. A. (2016b). Graphic Interpretation and Assessment of Water Quality in the Savitri River Basin. *International Journal of Scientific and Engineering Research*, 7(3), 1113–1123.
- MacDonald, A. M., Bonsor, H. C., Dochartaigh, B. É. Ó., and Taylor, R. G. (2012). Quantitative maps of groundwater resources in Africa. *Environmental Research Letters*, 7(2), 024009. <https://doi.org/10.1088/1748-9326/7/2/024009>
- Macdonald, A. M., Davies, J., Nations, U., Programme, E., Olorunfemi, F., Rilwanu, T. Y., Inkani, A. I., Olasehinde, P. I., Journal, K., Abdul, Solomon, S., Nwankwoala, H. O., Danert, K., Gesti Canuto, J., British Geological Survey, Nanbakhsh, H., Tasi ', O, I. E., Mallam I, ... Decision, M. (2016). Surface Water and Groundwater Resources Assessment In Wajir County For Decision Making Final Report Water Resources Management Authority in Collaboration with the State Department For Devolution. *Journal of Environment and Earth Science*, 1(May), 1–17. <https://doi.org/10.13140/RG.2.2.21914.64964>
- MacDonald, and Adelana, S. (2008). Groundwater research issues in Africa. In S. Adelana and MacDonald (Eds.), *Applied Groundwater Studies in Africa* (Vol. 20086152). Taylor and Francis. <https://doi.org/10.1201/9780203889497.ch1>
- MacDonald, and Davies, J. (2000). *A brief review of groundwater for rural water supply in sub-Saharan Africa* (Technical Report WC/00/33; Overseas Geology Series, p. 30). British Geological Survey.
- Maina, J. W., and Gaciri, S. J. (2010). Contributions to the hydrogeochemistry of the area to the immediate north of Nairobi Conservation Area, Kenya. *Journal of African Earth Sciences* (1983), 2(3), 227–232. [https://doi.org/10.1016/S0731-7247\(84\)80017-8](https://doi.org/10.1016/S0731-7247(84)80017-8)
- Makokha, M. (2019). Groundwater Quality Analyses along Kenyan Coastal Region, Case Study of Kilifi County. *International Journal of Environment and Geoinformatics*, 6, 1–14. <https://doi.org/10.30897/ijegeo.466933>

- Malvić, T., Velić, J., and Peh, Z. (2005). *Geologia Croatica Qualitative – Quantitative Analyses of the Influence of Depth and Lithological Composition on Lower Pontian Sandstone Porosity in the Central Part of Bjelovar Sag (Croatia)*. 73–86.
- Martínez, D. E., and Bocanegra, E. M. (2002). Hydrogeochemistry and cation-exchange processes in the coastal aquifer of Mar Del Plata, Argentina. *Hydrogeology Journal*, 10(3), 393–408. <https://doi.org/10.1007/s10040-002-0195-7>
- Mason, P., and Gibson, A. B. (1957). *GEOLOGY OF THE KALOSSIA-TIATI AREA: DEGREE SHEET 26, N.E. AND S.E. QUARTERS*. Geological Survey of Kenya.
- Maurice, L., Taylor, R. G., Tindimugaya, C., Macdonald, A. M., Johnson, P., Kaponda, A., Owor, M., and Sanga, H. (2018). *Characteristics of high-intensity groundwater abstractions from weathered crystalline bedrock aquifers in East Africa*. <https://doi.org/10.1007/s10040-018-1836-9>
- Mbithi, F. M., Kariuki, P. C., and Gikuma-Njuru, P. (2017). *Assessment of the Impact of Groundwater Fluoride on Human Health: A Case Study of Makindu District in Kenya*.
- Mckenzie, J. M., Mark, B. G., Thompson, L. G., Schotterer, U., and Lin, P.-N. (2010). A hydrogeochemical survey of Kilimanjaro (Tanzania): Implications for water sources and ages. *Hydrogeology Journal*, 18(4), 985–995. <https://doi.org/10.1007/s10040-009-0558-4>
- McKenzie, J. M., Siegel, D. I., Patterson, W., and McKenzie, D. J. (2001). A geochemical survey of spring water from the main Ethiopian rift valley, southern Ethiopia: Implications for well-head protection. *Hydrogeology Journal*, 9(3), 265–272. <https://doi.org/10.1007/s100400100134>
- Meng, F., Xiao, C., Liang, X., Wang, G., and Sun, Y. (2019). Regularity and a statistical model of surface water and groundwater interaction in the Taoer River alluvial fan, China. *Water Supply*, 1–12. <https://doi.org/10.2166/ws.2019.118>
- Miljević, N., Boreli-Zdravković, D., Obradović, V., Golobočanin, D., and Mayer, B. (2012). Evaluation of the origin of nitrate influencing the Ključ groundwater source, Serbia. *Water Science and Technology*, 66(3), 472–478. <https://doi.org/10.2166/wst.2012.179>

- Mook, W. G. (2000). Environmental isotopes in the hydrological cycle. **Volume I**.pdf. *Technical Documents in Hydrology*, 1(39), 1–291.
- Moore, J. E. (2011). *Field Hydrogeology: A Guide for Site Investigations and Report Preparation, Second Edition*. CRC Press.
- Morán-Ramírez, J., Ledesma-Ruiz, R., Mahlknecht, J., and Ramos-Leal, J. A. (2016). Rock–water interactions and pollution processes in the volcanic aquifer system of Guadalajara, Mexico, using inverse geochemical modeling. *Applied Geochemistry*, 68, 79–94. <https://doi.org/10.1016/J.APGEOCHEM.2016.03.008>
- Moridi, A., Tabatabaie, M. R. M., and Esmaealzade, S. (2018). Holistic Approach to Sustainable Groundwater Management in Semi-arid Regions. *International Journal of Environmental Research*, 12(3), 347–355. <https://doi.org/10.1007/s41742-018-0080-4>
- Mostafa, M. G., Uddin, S. M. H., and Haque, A. B. M. H. (2017). Assessment of hydro-geochemistry and groundwater quality of Rajshahi City in Bangladesh. *Applied Water Science*, 7(8), 4663–4671. <https://doi.org/10.1007/s13201-017-0629-y>
- Motzer, W. E. (2007). *Age Dating Groundwater*. 1–4.
- Mrklas, O., Bentley, L. R., Lunn, S. R. D., and Chu, A. (2006). Principal component analyses of groundwater chemistry data during enhanced bioremediation. *Water, Air, and Soil Pollution*, 169(1–4), 395–411. <https://doi.org/10.1007/s11270-006-2817-5>
- Mugerwa, T. (2015). *Field and Petrographic Study of Rocks from Vada Mamandur, Vilupuram District, Tamil Nadu, India*. 3, 2321–2527.
- Muhammad, A. M., Zhonghua, T., Dawood, A. S., and Earl, B. (2015). Evaluation of local groundwater vulnerability based on DRASTIC index method in Lahore, Pakistan. *Geofísica Internacional*, 54(1), 67–81. <https://doi.org/10.1016/J.GI.2015.04.003>
- Muia, G. (2015). George Muia The “Turkana Grits”: Potential Hydrocarbon Reservoirs of the Northern and Central Kenya Rifts. *PhD Thesis*, 1–207.
- Muthuka, M. M. (1994). *The hydrogeochemistry of the Ndavaya-Mrima area Coast Province Kenya* [Thesis]. <http://erepository.uonbi.ac.ke/handle/11295/20943>

- MWI, M. of W. (2013). *National Water Master Plan 2030* (October). The Republic Of Kenya Ministry Of Environment, Water And Natural Resources Water Resources Management Authority.
- Mzuga, J. M., Tole, M. P., and Ucauwun, E. K. (2001). Contamination of groundwater resources by pit latrines in Kwale District, Kenya. *Discovery and Innovation*, 13(3), 203–212.
- NDMA, (2016). *Turkana county*. National Drought Management Authority.
- Newman, C. P. (2019). Variation in groundwater recharge and surface-water quality due to climatic extremes in semi-arid mountainous watersheds. *Hydrogeology Journal*, 1627–1643. <https://doi.org/10.1007/s10040-019-01967-4>
- Nyende, J. (2013). Application of Isotopes and Recharge Analysis in Investigating Surface Water and Groundwater in Fractured Aquifer under Influence of Climate Variability. *Journal of Earth Science and Climatic Change*, 04. <https://doi.org/10.4172/2157-7617.1000148>
- Nyilytya, B., Mureithi, S., and Boeckx, P. (2020). Tracking sources and fate of groundwater nitrate in Kisumu City and Kano Plains, Kenya. *Water*, 12(2), 401.
- Ochungo, E. A., Ouma, G. O., Obiero, J. P. O., and Odero, N. A. (2019). The Implication of Unreliable Urban Water Supply Service: The Case of Vendor Water Cost in Langata Sub County, Nairobi City, Kenya. *Journal of Water Resource and Protection*, 11(07), 896–935. <https://doi.org/10.4236/jwarp.2019.117055>
- Ocra. (2015). Good practice principles on planning for water and irrigated crop agriculture in the drylands of the Horn of Africa. *2013, May*, 1–16.
- Oiro, S., Comte, J., Soulsby, C., and Walraevens, K. (2018). Using stable water isotopes to identify spatio-temporal controls on groundwater recharge in two contrasting East African aquifer systems. *Hydrological Sciences Journal*, 63(6), 862–877. <https://doi.org/10.1080/02626667.2018.1459625>
- Okiongbo, K., and Soronnadi-Ononiwu, G. (2004). Ife journal of science. In *Ife Journal of Science* (Vol. 17). Obafemi Awolowo University <https://www.ajol.info/index.php/ijs/article/view/131760/121361>

- Olago, D. O. (2018). Constraints and solutions for groundwater development, supply and governance in urban areas in Kenya. *Hydrogeology Journal*, 27(3), 1031–1050. <https://doi.org/10.1007/s10040-018-1895-y>
- Olaka, L. A., Wilke, F. D., Olago, D. O., Odada, E. O., Mulch, A., and Musolff, A. (2016). Groundwater fluoride enrichment in an active rift setting: Central Kenya Rift case study. *Science of the Total Environment*, 545, 641–653.
- Onugba, A., and Aboh, H. O. (2009). The tritium content of precipitation and groundwater at Yola, Nigeria. *Science World Journal*, 4(2), Article 2. <https://doi.org/10.4314/swj.v4i2.51842>
- Opiyo. (2014). *Climate Variability and Change on Vulnerability and Adaptation among Turkana Pastoralists in North-Western Kenya* (Issue November) [PhD Thesis]. [http://erepository.uonbi.ac.ke/bitstream/handle/11295/77661/Omondi_Climate variability and change on vulnerability and adaptation among Turkana pastoralists in north-western Kenya.pdf?sequence=3](http://erepository.uonbi.ac.ke/bitstream/handle/11295/77661/Omondi_Climate%20variability%20and%20change%20on%20vulnerability%20and%20adaptation%20among%20Turkana%20pastoralists%20in%20north-western%20Kenya.pdf?sequence=3)
- Opiyo, F., Wasonga, O., Nyangito, M., Schilling, J., and Munang, R. (2015). Drought Adaptation and Coping Strategies Among the Turkana Pastoralists of Northern Kenya. *International Journal of Disaster Risk Science*, 6(3), 295–309. <https://doi.org/10.1007/s13753-015-0063-4>
- Potts, P. J. (1987). Atomic absorption spectrometry. In *A Handbook of Silicate Rock Analysis* (pp. 106–152). Springer Netherlands. https://doi.org/10.1007/978-94-015-3988-3_4
- Prinz, D., and Singh, A. K. (2000). *Water Resources In Arid Regions And Their Sustainable Management*. <https://pdfs.semanticscholar.org/f9e4/5c17f9acf9d04db5516eb4e09e94fe88011a.pdf>
- Raghunath, H. M. (2007). *Ground Water*. New Age International.
- Raiber, M., Webb, J. A., Jacobsen, G. E., Chisari, R., and Williams, A. A. (2008). *Geological controls on the spatial variability of groundwater recharge and salinity in a regional-scale basalt aquifer in western. Joyce 2003*, 1279–1283.
- Ramaroson, V., Rakotomalala, C. U., Rajaobelison, J., Fareze, L. P., Razafitsalama, F. A., and Rasolofonirina, M. (2018). Tritium as tracer of groundwater pollution extension: Case

- study of Andralanitra landfill site, Antananarivo–Madagascar. *Applied Water Science*, 8(2), 57. <https://doi.org/10.1007/s13201-018-0695-9>
- Ramesh, K., and Gowri, V. S. (2012). *Silicate or calcite weathering in wet-dry climate in lower Varahanadi basin, Tamilnadu , India – A determinant in global warming*. 2(4), 2155–2166. <https://doi.org/10.6088/ijes.00202030098>
- Ravikumar, P., Aneesul, M. M., and Somashekar, R. K. (2013). Water quality index to determine the surface water quality of Sankey tank and Mallathahalli lake, Bangalore urban district, Karnataka, India. *Applied Water Science*, 3(1), 247–261. <https://doi.org/10.1007/s13201-013-0077-2>
- Ravikumar, P., and Somashekar, R. K. (2015). Principal component analysis and hydrochemical facies characterization to evaluate groundwater quality in Varahi river basin, Karnataka state, India. *Appl Water Sci*, 2017(7), 745–755. <https://doi.org/10.1007/s13201-015-0287-x>
- Ravikumar, P., Somashekar, R. K., and Prakash, K. L. (2015). A comparative study on usage of Durov and Piper diagrams to interpret hydrochemical processes in groundwater from SRLIS river basin, Karnataka , India. *Elixir International Journal*, 80(2015), 31073–31077.
- REACH. (2015). *Country Diagnostic Report, Kenya. REACH Working Paper 3*.
- Rhemtulla, S. (1970). The South Turkana Expedition: Scientific Papers III. A Geological Reconnaissance of South Turkana Author (s): Sultan Rhemtulla Source: The Geographical Journal , **Vol. 136** , No. 1 (Mar ., 1970), pp. 61-73 Published by: The Royal Geographical Soc. *Royal Geographical Society*, 136(1), 61–73.
- Rocca, R. (2017). *Low Cost 3D Mapping Using a Commercial Drone / UAV: Application in Structural Geology* *. 42054.
- RTI. (2013). *Advanced Survey of Groundwater Resources of Northern and Central Turkana County , Kenya*.
- Russell, C. E., and Kluesner, T. L. (2007). *Recharge to Selected Hydrographic Basins of Eastern Nevada and Western Utah using the Chloride Mass-balance Method*. 41232.

- Salako, A. O., and Adepelumi, A. A. (2018). Aquifer, Classification and Characterization. In *InTechOpen*. <http://dx.doi.org/10.5772/intechopen.72692>
- Sappa, G., Barbieri, M., Ergul, S., and Ferranti, F. (2012). *Hydrogeological Conceptual Model of Groundwater from Carbonate Aquifers Using Environmental Isotopes (^{18}O , ^2H) and Chemical Tracers: A Case Study in Southern Latium Region, Central Italy*. 2012. <https://doi.org/10.4236/jwarp.2012.49080>
- Selvakumar, S., Chandrasekar, N., and Kumar, G. (2017). Hydrogeochemical characteristics and groundwater contamination in the rapid urban development areas of Coimbatore, India. *Water Resources and Industry*, 17(February), 26–33. <https://doi.org/10.1016/j.wri.2017.02.002>
- Senthilkumar, M., Arumugam, R., Gnanasundar, D., Thambi, D. S. C., and Sampath Kumar, E. (2015). Effects of geological structures on groundwater flow and quality in hardrock regions of northern Tirunelveli district, Southern India. *Journal of Earth System Science*, 124(2), 405–418. <https://doi.org/10.1007/s12040-015-0538-0>
- Shamsuddin, M. K. N., Sulaiman, W. N. A., Ramli, M. F., Mohd Kusin, F., and Samuding, K. (2018). Assessments of seasonal groundwater recharge and discharge using environmental stable isotopes at Lower Muda River Basin, Malaysia. *Applied Water Science*, 8(5). <https://doi.org/10.1007/s13201-018-0767-x>
- Sharma, S., and Chhipa, R. C. (2016). Seasonal variations of ground water quality and its agglomerates by water quality index. *Global J. Environ. Sci. Manage. Global J. Environ. Sci. Manage*, 2(21), 79–86. <https://doi.org/10.7508/gjesm.2016.01.009>
- Shekhar, S. (2017). *GEOLOGY Module: Aquifer Properties*. November.
- Shekhar, S., Shukla, A., and Kumar, P. (2018). *Geochemical and petrographic interpretation of Sandhan Formation: An insight into provenance, tectonics and paleoclimatic conditions*.
- Shiferaw, B., Tesfaye, K., Kassie, M., Abate, T., Prasanna, B. M., and Menkir, A. (2014). Managing vulnerability to drought and enhancing livelihood resilience in sub-Saharan Africa: Technological, institutional and policy options. *Weather and Climate Extremes*, 3, 67–79. <https://doi.org/10.1016/j.wace.2014.04.004>

- Shirazi, S. M., Adham, Md. I., Zardari, N. H., Ismail, Z., Imran, H. M., and Mangrio, M. A. (2015). Groundwater quality and hydrogeological characteristics of Malacca state in Malaysia. *Journal of Water and Land Development*, 24(1), 11–19. <https://doi.org/10.1515/jwld-2015-0002>
- Singh, B. P. (2017). Original isotopic composition of water in precipitation by different methods. *Applied Water Science*, 7(6), 3385–3390. <https://doi.org/10.1007/s13201-016-0500-6>
- Singh, S., Hussain, A., and Khobragade, S. D. (2016). Analysis of isotope element by electrolytic enrichment method for ground water and surface water in Saurashtra region, Gujarat, India. *Cogent Engineering*, 3(1), 1164789. <https://doi.org/10.1080/23311916.2016.1164789>
- Sklash, M. G., and Mwangi, M. P. (1991). An isotopic study of groundwater supplies in the Eastern Province of Kenya. *Journal of Hydrology*, 128(1), 257–275. [https://doi.org/10.1016/0022-1694\(91\)90141-4](https://doi.org/10.1016/0022-1694(91)90141-4)
- Sombroek, W. G., Braun, H. M. H., and Pouw, B. J. A. van der. (1982). Exploratory soil map and agro-climatic zone map of Kenya, 1980. *Exploratory Report - Kenya Soil Survey (Kenya)*. https://scholar.google.com/scholar_lookup?title=Exploratory+soil+map+and+agro-climatic+zone+map+of+Kenya%2C+1980andauthor=Sombroek%2C+W.G.andpublication_year=1982
- Sophocleous, M. (2002). Interactions between groundwater and surface water: The state of the science. *Hydrogeology Journal*, 52–67. <https://doi.org/10.1007/s10040-001-0170-8>
- Stambuk-Giljanovic, N. (1999a). Water quality evaluation by index in Dalmatia. *Water Research*, 33(16), 3423–3440. [https://doi.org/10.1016/S0043-1354\(99\)00063-9](https://doi.org/10.1016/S0043-1354(99)00063-9)
- Stambuk-Giljanovic, N. (1999b). Water quality evaluation by index in Dalmatia. *Water Research*, 33(16), 3423–3440. [https://doi.org/10.1016/S0043-1354\(99\)00063-9](https://doi.org/10.1016/S0043-1354(99)00063-9)
- Stave, J., Oba, G., Stenseth, N. Chr., and Nordal, I. (2005). Environmental gradients in the Turkwel riverine forest, Kenya: Hypotheses on dam-induced vegetation change. *Forest Ecology and Management*, 212(1), 184–198. <https://doi.org/10.1016/j.foreco.2005.03.037>
- Subramani, T., Rajmohan, N., and Elango, L. (2009). Groundwater geochemistry and identification of hydrogeochemical processes in a hard rock region, Southern India.

Environmental Monitoring and Assessment, 162(1–4), 123–137.
<https://doi.org/10.1007/s10661-009-0781-4>

Subyani, A., and Sen, Z. (2006). *Refined chloride mass-balance method and its application*. 4380(August 2005), 4373–4380. <https://doi.org/10.1002/hyp.6172>

Suwardhan, K., Suresh Kumar, K., Reddy, K., and Chiranjeevi, P. (2003a). *Determination Of Trace Element By Atomic Absorption Spectroscopy (Aas) After Preconcentration On A Support Impregnated With Coniine Dithiocarbamate* (pp. 15–17). http://www.yorku.ca/bunchmj/ICEH/proceedings/Suwardhan_K_ICEH_papers_562to569.pdf

Suwardhan, K., Suresh Kumar, K., Reddy, K., and Chiranjeevi, P. (2003b). *Determination Of Trace Element By Atomic Absorption Spectroscopy (Aas) After Preconcentration On A Support Impregnated With Coniine Dithiocarbamate*.

Tague, C., Grant, G., Farrell, M., Choate, J., and Jefferson, A. (2008). *Deep groundwater mediates streamflow response to climate warming in the Oregon Cascades*. 189–210. <https://doi.org/10.1007/s10584-007-9294-8>

Tanui, F., Olago, D., Dulo, S., Ouma, G., and Kuria, Z. (2020). Hydrogeochemistry of a strategic alluvial aquifer system in a semi-arid setting and its implications for potable urban water supply: The Lodwar Alluvial Aquifer System (LAAS). *Groundwater for Sustainable Development*, 11, 100451. <https://doi.org/10.1016/j.gsd.2020.100451>

Taylor, R. G. (2013). *Ground water and climate change*. November, 1–8. <https://doi.org/10.1038/NCLIMATE1744>

Taylor, R. G., and Howard, K. W. F. (1996). *Stable isotope tracers and flow modelling*. 180, 31–53.

Taylor, R. G., and Howard, K. W. F. (2000). *A tectono-geomorphic model of the hydrogeology of deeply weathered crystalline rock: Evidence from Uganda*. 8, 279–294.

Taylor, R. G., Koussis, A. D., and Tindimugaya, C. (2009). Groundwater and climate in Africa—A review. *Hydrological Sciences*, 54(August), 655–664.

- Taylor, R. G., Todd, M. C., Kongola, L., Maurice, L., Nahozya, E., Sanga, H., and Macdonald, A. M. (2012). Evidence of the dependence of groundwater resources on extreme rainfall in East Africa. *Nature Climate Change*, 3(4), 374–378. <https://doi.org/10.1038/nclimate1731>
- Teng, Y., Hu, B., Zheng, J., Wang, J., Zhai, Y., and Zhu, C. (2018). Water quality responses to the interaction between surface water and groundwater along the Songhua River, NE China. *Hydrogeology Journal*, 26(5), 1591–1607. <https://doi.org/10.1007/s10040-018-1738-x>
- Thomas, A., and Tellam, J. (2006). *Modelling of recharge and pollutant fluxes to urban groundwaters*. 360, 158–179. <https://doi.org/10.1016/j.scitotenv.2005.08.050>
- Tirogo, J., Jost, A., Biao, A., Valdes, D., Koussoube, Y., and Ribstein, P. (2016). Climate Variability and Groundwater Response: A Case Study in Burkina Faso (West Africa). *Water*, 8, 171. <https://doi.org/10.3390/w8050171>
- Tlili-zrelli, B., Gueddari, M., and Bouhlila, R. (2018). *Spatial and Temporal Variations of Water Quality of Mateur Aquifer (Northeastern Tunisia) : Suitability for Irrigation and Drinking Purposes*. 2018.
- Török, Á., Bögöly, G., Somogyi, Á., and Lovas, T. (2020). Application of UAV in Topographic Modelling and Structural Geological Mapping of Quarries and Their Surroundings—Delineation of Fault-Bordered Raw Material Reserves. *Sensors (Basel, Switzerland)*, 20(2), 489. <https://doi.org/10.3390/s20020489>
- Touber, L. (1990). *Landforms and Soils of Turkana District, Kenya* (No. 41; pp. 1–56). The Ministry of Livestock Development, Range Department. <https://edepot.wur.nl/494277>
- Turkana County. (2013). *Turkana County Integrated Development Plan (CIDP), 2013—2017*. 336.
- Turkana County. (2017). *Turkana County Water, Sanitation Services Sector Strategic Plan* (pp. 1–48). Turkana County Government. https://turkana.go.ke/wp-content/uploads/2018/03/The-Turkana-County-Water-Sector-Plan-Final_23022018.pdf#page=7andzoom=100,0,129
- Turkana County. (2018). *Intergrated Development Plan 2018-2022* (p. 70).

- Twarakavi, N. K. C., and Kaluarachchi, J. J. (2005). *Aquifer Vulnerability Assessment to Heavy Metals Using Ordinal Logistic Regression*. 43(2), 200–214.
- Umar, R. (2006). Hydrogeological environment and groundwater occurrences of the alluvial aquifers in parts of the Central Ganga Plain, Uttar Pradesh, India. *Hydrogeology Journal*, 14(6), 969–978. <https://doi.org/10.1007/s10040-005-0019-7>
- UNESCO. (1998). Monitoring for groundwater management in (Semi-)arid regions. *Studies and Reports in Hydrology*, 57.
- UNHCR, U. N. H. C. F. R. (2018). *Kalobeyei Integrated Socio-Economic Development Plan In Turkana West* (pp. 1–36) [Strategic Overview]. Turkana County Government. <https://www.unhcr.org/ke/wp-content/uploads/sites/2/2018/12/KISED-Strategic-Overview.pdf>
- Van der Gun, J. (2010). Climate change and alluvial aquifers in arid regions: Examples from Yemen. *Climate Change Adaptation in the Water Sector*, 159–176.
- van Dijk, G., Nijp, J. J., Metselaar, K., Lamers, L. P. M., and Smolders, A. J. P. (2017). Salinity-induced increase of the hydraulic conductivity in the hyporheic zone of coastal wetlands. *Hydrological Processes*, 31(4), 880–890. <https://doi.org/10.1002/hyp.11068>
- Vandecasteele, I., Nyssen, J., Clymans, W., Deckers, J., and Walraevens, K. (2007). *Hydrogeology and groundwater flow in a basalt-capped Mesozoic sedimentary series of the Ethiopian highlands*. <https://doi.org/10.1007/s10040-010-0667-0>
- Varol, S., and Şekerci, M. (2018). Hydrogeochemistry, water quality and health risk assessment of water resources contaminated by agricultural activities in Korkuteli (Antalya, Turkey) district center. *Journal of Water and Health*, 16(4), 574–599. <https://doi.org/10.2166/wh.2018.003>
- Vasu, D., Singh, S. K., Tiwary, P., Sahu, N., Ray, S. K., Butte, P., and Duraisami, V. P. (2017). Influence of geochemical processes on hydrochemistry and irrigation suitability of groundwater in part of semi-arid Deccan Plateau, India. *Applied Water Science*, 7(7), 3803–3815. <https://doi.org/10.1007/s13201-017-0528-2>

- Vivona, R., Preziosi, E., Madé, B., and Giuliano, G. (2007). Occurrence of minor toxic elements in volcanic-sedimentary aquifers: A case study in central Italy. *Hydrogeology Journal*, 15(6), 1183–1196. <https://doi.org/10.1007/s10040-007-0169-x>
- Vu, H., Merkel, B. J., and Weise, S. M. (2020). Origin of groundwater in Hanoi, Vietnam, revealed by environmental isotopes. *Isotopes in Environmental and Health Studies*, 56(4), 370–386. <https://doi.org/10.1080/10256016.2020.1788548>
- Walker, D., Parkin, G., Gowing, J., and Haile, A. (2019). Development of a Hydrogeological Conceptual Model for Shallow Aquifers in the Data Scarce Upper Blue Nile Basin. *Hydrology*, 6, 43. <https://doi.org/10.3390/hydrology6020043>
- Walsh, J., and Dodson, R. G. (Ministry of N. R. (1969). *Geology of Northern Turkana* (December).
- WASREB. (2018). *A Performance Report of Kenya's Water Services Sector 2015 / 16 and 2016 / 17*. https://wasreb.go.ke/downloads/WASREB_IMPACT_Issue10_FINAL.pdf
- Wescott, W. A., Morley, C. K., and Karanja, F. M. (1993). Geology of the “Turkana Grits” in the Lariu range and Mt. Porr areas, southern Lake Turkana, Northwestern Kenya. *Journal of African Earth Sciences (and the Middle East)*, 16(4), 425–435. [https://doi.org/10.1016/0899-5362\(93\)90101-U](https://doi.org/10.1016/0899-5362(93)90101-U)
- WHO (2011). Guidelines for Drinking Water Quality. *Reference and Research Book News*, 26(3). [https://doi.org/10.1016/S1462-0758\(00\)00006-6](https://doi.org/10.1016/S1462-0758(00)00006-6)
- Winter, T. C., Harvey, J. W., Franke, O. L., and Alley, W. M. (2005). *Protecting Our Rivers from the Groundwater Up Case Study: 15(3)*.
- Wirmvem, M. J., Mimba, M. E., Kamtchueng, B. T., Wotany, E. R., Bafon, T. G., Asaah, A. N. E., Fantong, W. Y., Ayonghe, S. N., and Ohba, T. (2017). Shallow groundwater recharge mechanism and apparent age in the Ndop plain, northwest Cameroon. *Applied Water Science*, 7(1), 489–502. <https://doi.org/10.1007/s13201-015-0268-0>
- World Bank. (2018). *Annual report 2018* (pp. 1–90).

- Wright, E. P. (1992). The hydrogeology of crystalline basement aquifers in Africa. *Geological Society, London, Special Publications*, 66(1), 1–27. <https://doi.org/10.1144/GSL.SP.1992.066.01.01>
- Wu, H., Chen, J., Qian, H., and Zhang, X. (2015). Chemical Characteristics and Quality Assessment of Groundwater of Exploited Aquifers in Beijiao Water Source of Yinchuan, China: A Case Study for Drinking, Irrigation, and Industrial Purposes. *Journal of Chemistry*, 2015, 1–14.
- Xi, H., Feng, Q., Zhang, L., Si, J., and Yu, T. (2018). Groundwater storage changes and estimation of stream lateral seepage to groundwater in desert riparian forest region. *Hydrology Research*, 49(3), 861–877. <https://doi.org/10.2166/nh.2017.279>
- Xu, P. Y., and Adams, S. (2005). *A Water Balance Approach to Groundwater Recharge Estimation In Montagu Area Of The Western Klein Karoo*
- Xu, Y., and Beekman, H. E. (2003). *Groundwater Recharge Estimation in Southern Africa*.
- Xu, Y., Seward, P., Gaye, C., Lin, L., and Olago, D. O. (2019). Preface: Groundwater in Sub-Saharan Africa. *Hydrogeology Journal*, 27(3), 815–822. <https://doi.org/10.1007/s10040-019-01977-2>
- Xu, Y., and Tonder, G. J. V. (2001). *Estimation of recharge using a revised CRD method*. 27(3), 341–344.
- Yadav, A., Nanda, A., Sahu, Y., Sahu, B., Patel, K. S., Pervez, S., Gulgundi, M., Cuchí, J., Martín-Ramos, P., and Bhattacharya, P. (2020). *Groundwater hydrochemistry of Rajnandgaon district, Chhattisgarh, Central India*. <https://doi.org/10.1016/j.gsd.2020.100352>
- Yamazaki, S., Neo, N., and Miyashita, S. (2009). Data report: Whole-rock major and trace elements and mineral compositions of the sheeted dike and gabbro transition in ODP Hole 1256D. *Proceedings of the IODP*, 309/312, 309. <https://doi.org/10.2204/iodp.proc.309312.203.2009>
- Yang, Q., Mu, H., Wang, H., Ye, X., Ma, H., and Martín, J. D. (2018). Quantitative evaluation of groundwater recharge and evaporation intensity with stable oxygen and hydrogen isotopes

- in a semi-arid region, Northwest China. *Hydrological Processes*, 32(9), 1130–1136. <https://doi.org/10.1002/hyp.11474>
- Yeh, H., Lin, H., Lee, C., Hsu, K., and Wu, C. (2014). Identifying Seasonal Groundwater Recharge Using Environmental Stable Isotopes. *Water*, 6(2014), 2849–2861. <https://doi.org/10.3390/w6102849>
- Yeh, H.-F., and Lee, J.-W. (2018). Stable Hydrogen and Oxygen Isotopes for Groundwater Sources of Penghu Islands, Taiwan. *Geosciences*, 8(84), 6–13. <https://doi.org/10.3390/geosciences8030084>
- Yidana, S. M., Banoeng, Yakubo, B., and Akabzaa, T. M. (2010a). Analysis of groundwater quality using multivariate and spatial analyses in the Keta basin, Ghana. *Journal of African Earth Sciences*, 58(2), 220–234. <https://doi.org/20103264217>
- Yidana, S. M., Banoeng, Yakubo, B., and Akabzaa, T. M. (2010b). Analysis of groundwater quality using multivariate and spatial analyses in the Keta basin, Ghana. *Journal of African Earth Sciences*, 58(2), 220–234. <https://doi.org/20103264217>
- Yusuf, M. A., Abiye, T. A., Butler, M. J., and Ibrahim, K. O. (2018). Origin and residence time of shallow groundwater resources in Lagos coastal basin , south- west Nigeria: An isotopic approach. *Heliyon*, 4(October), 1–33. <https://doi.org/10.1016/j.heliyon.2018.e00932>
- Zaheeruddin, and Khurshid, S. (2004). Aquifer geometry and hydrochemical framework of the shallow alluvial aquifers in the western part of the Yamuna River Basin, India. *Water Quality Research Journal of Canada*, 39(2), 129–139. <https://doi.org/10.2166/wqrj.2004.020>
- Zhang, D., Cui, L., Madani, R. M. A., Wang, H., Zhu, H., and Liang, J. (2019). Effect of nitrite and nitrate on sulfate reducing ammonium oxidation. *Water Science and Technology*, 1–10. <https://doi.org/10.2166/wst.2019.277>
- Zhang, J., and Satake, H. (2003). The chemical characteristics of submarine groundwater seepage in Toyama Bay, Central Japan. In *Land and Marine Hydrogeology* (pp. 45–60). Elsevier. <https://doi.org/10.1016/B978-044451479-0/50016-9>

Zhao, L. J., Eastoe, C. J., Liu, X. H., Wang, L. X., Wang, N. L., Xie, C., and Song, Y. X. (2018). Origin and residence time of groundwater based on stable and radioactive isotopes in the Heihe River Basin, northwestern China. *Journal of Hydrology: Regional Studies*, 18, 31–49. <https://doi.org/10.1016/j.ejrh.2018.05.002>

APPENDICES

Appendix 3.1: Analytical rational – hydrogeological characteristics of the LAAS

a) Geological mapping and remote sensing

Geological mapping is the process of identifying the overlying geological materials, lithological characteristics, as well as mapping of the geological structures for preparation of a detailed local geological map and a detailed report. It takes into consideration regional geology, existing reports of local geology, landforms, and geological structures such as faults/fractures, and rock and soil samples are collected from the study area for petrographic and geochemical analyses. The geology of the area controls its hydrogeology; therefore, it is essential to understand the types of rocks present in the area of interest, their lithologies and their structural inter-relationships (Brassington and Younger, 2010). Knowledge of subsurface geology is important for defining the three-dimensional variations in permeability and storage properties (Brassington and Younger, 2010) and how they affect the directions and rates of groundwater flow and recharging processes. Information may be derived from existing geological maps and reports that are interpreted in the context of elevations provided by topographic maps and may also include records from boreholes drilled for study purposes or other purposes and geophysical surveys (Brassington and Younger, 2010). Geology also makes it possible to understand the relationship between groundwater and surface water systems.

Remote sensing is a fundamental technique for groundwater exploration in areas of scarce groundwater resources. It involves the use of remote sensing data to identify the potential sites for groundwater exploration. Various geographic information system (GIS) tools are used to prepare and analyse resultant digital layers of the geological structure, lithology, drainage, and topography. Remotely sensed images (aerial or satellite photographs) are analysed before the fieldwork to determine the geological contacts more quickly than their actual identification in the field (Barnes and Lisle, 2004). Once a potential contact zone is identified remotely, it is targeted in the field for actual demarcation and description. One approach for determining groundwater exploration potential sites is by analysing the frequency of lineament, length, and drainage lines density to determine different probabilities of groundwater potential in an area. Another approach is through the analysis of hydro-geomorphological characteristics to identify potential zones for

groundwater recharge after applying a qualitative classification to the layer. This method is often suitable for identifying areas of artificial recharge, which is not covered by this study.

Aerial photography and remote sensing provide important information of the context for the field-based investigations, especially for the topography and landform features that are too large to observe at ground level. Drones flown at low altitudes (up to 500 m) can capture information that can also be captured from Airborne Light Detection and Ranging (LiDAR) or terrestrial Laser Scanning (TLS). LiDAR surveys are most preferred for larger areas, while drone surveys are useful for small areas such as the current study area. Drones are lightweight and highly mobile and are most suitable for capturing short-lived events such as floods, debris flows, earthquakes, sandstorms, or used for repeat photography for long-lived events such as stream erosion and active landslides. The use of drones for geological mapping is an evolving technique, and only a few studies have been conducted over the last two decades (Tziavou *et al.*, 2017). The utilization of the unmanned aerial vehicles (UAVs) permits the decrease in costs and time for the data acquisition and the enhancement of the capacity for data processing to produce effectively large volumes of information (Fernández-lozano, 2017; Rocca, 2017; Tziavou *et al.*, 2017).

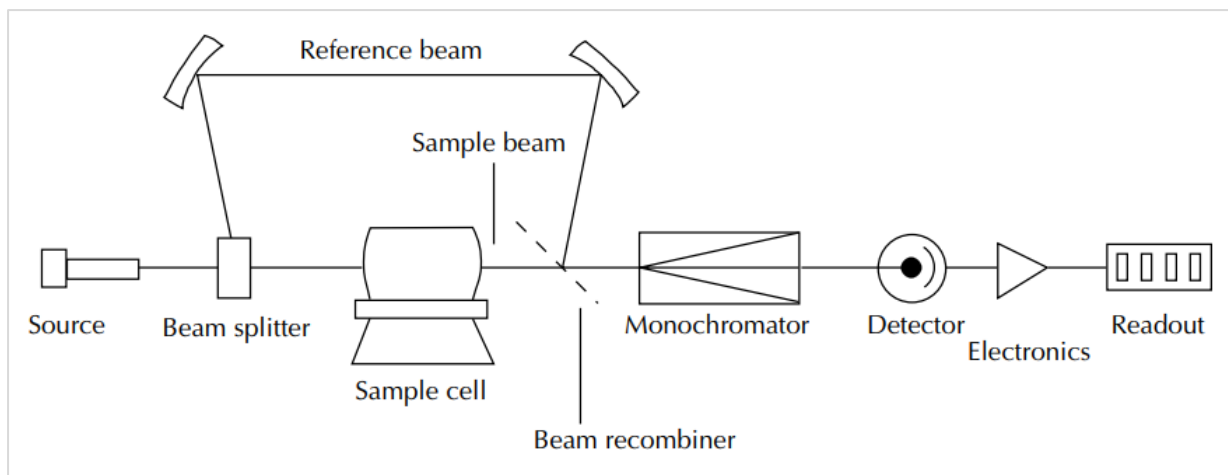
b) X-ray fluorescence

X-ray fluorescence is a technique in which photons emitted from an x-ray source interact effectively with the atoms in the sample, triggering an electron to be removed from the inner shell of a given atom leaving the inner shell to become “unstable”. The resultant space left by the electron is then filled with another electron from a higher shell, releasing energy (fluorescence) in the form of another photon, and is characteristic not only to each element but also to each shell transition (Chacha, 2014). The XRF instruments have a detector that picks up the distinctive fluorescent energies of elements and identifies using their wavelengths. The photons at higher energy state create data useful in quantifying the trace elements. The new vacuum pump technology allows quick and easy analysis of non-uniform materials and concentration analysis of uniform materials consisting of elements from Sodium to Uranium.

c) Atomic absorption spectrometry

Atomic absorption spectrometry (AAS) is a modern method for the determination of a wide range of elements for many types of materials accurately and precisely (Butler and Kokot, 1971b). This method is suitable for the analysis of rocks, ores, and brines, and Butler and Kokot (1971) described its application for geological materials. Due to its high sensitivity, AAS has been applied

widely for the determination of major and trace elements (Kebede *et al.*, 2010b; Suvardhan *et al.*, 2003b; Yamazaki *et al.*, 2009). However, the method has also been regarded as adequately precise and accurate for the determination of major elements (Butler and Kokot, 1971; Suvardhan *et al.*, 2003b). The requirement that the sample must be brought into the solution is maybe time-consuming. However, sample dissolution of silicate-based materials is generally not considered difficult (Butler and Kokot, 1971b; Potts, 1987). Potts (1987) gives an account of the application of this technique for the analysis of geological materials. The AAS technique is based on the ability of a ground-state atom to absorb light with specific energy causing it to be excited and achieve a higher energy state. The light intensity absorbed by an element is proportional to its concentration (Belt, 1964; Suvardhan *et al.*, 2003). As the number of atoms increases in the light path, the intensity of the absorbed light at a specific wavelength increases (Alhawdar, 2014). The commonly used light source is the hollow cathode lamp that contains a cylindrical hollow cathode and tungsten anode made of the element to be determined. The cylinders are sealed in a glass tube filled with inert gas (argon) at a pressure range of 1-5 N/m². A potential difference between 300 and 400 V is applied between the anode and the cathode, where the gaseous ions bombard the cathode and eject metal atoms through sputtering. The monochromator is used to determine the specific wavelength of light absorbed by the sample. The selection of specific light allows for the determination of the selected element in the presence of others. The selected light is directed to the detector that, in turn, produces an electrical signal proportional to the light intensity. The crucial components of a typical atomic absorption spectrometer are shown in the schematic diagram found in (Figure 3-8)



Schematic diagram for AAS (Alhawdar, 2014)

(c) Vertical electrical sounding

The vertical electrical sounding (VES) aims to measure the vertical variation of ground resistivity with depth at a fixed station by gradually increasing the spacing of the electrodes at about a fixed centre of array. The conventional Schlumberger array uses four electrodes arranged linearly with difference inter-electrode spacing, and the potential electrode remains partially fixed at the centre of the spread. The current electrode is expanded symmetrically about the centre of the spread. The limitation of vertical resistivity sounding is that lateral changes in the subsurface result in changes in the apparent resistivity values often misinterpreted as changes in the subsurface resistivity.

Resistivities of common rocks formations (Loke, 2000)

Material	Resistivity (Ω Ohm-m)	Conductivity (S/m)
<i>Igneous and metamorphic</i>		
Granite	$5 \times 10^3 - 10^6$	$10^{-6} - 2.5 \times 10^{-4}$
Basalt	$10^3 - 10^6$	$10^{-6} - 10^{-4}$
Slate	$6 \times 10^2 - 4 \times 10^7$	$2.5 \times 10^{-8} - 1.7 \times 10^{-3}$
Marble	$10^2 - 2.5 \times 10^8$	$4 \times 10^{-9} - 10^{-2}$
Quartzite	$10^2 - 2 \times 10^6$	$5 \times 10^{-9} - 10^{-2}$
<i>Sedimentary Rocks</i>		
Sandstone	$8 - 4 \times 10^3$	$2.5 \times 10^{-4} - 0.125$
Shale	$20 - 2 \times 10^3$	$5 \times 10^{-4} - 0.05$
Limestone	$50 - 4 \times 10^2$	$2.5 \times 10^{-3} - 0.02$
<i>Soils and Waters</i>		
Clay	$1 - 100$	$0.01 - 1$
Alluvium	$10 - 800$	$1.25 \times 10^{-3} - 0.1$
Groundwater (fresh)	$10 - 100$	$0.01 - 0.1$
Sea water	0.2	5

Appendix
3-2:

Appendix 3.2 Analytical rationale – hydrogeochemistry of the LAAS

Access to safe drinking water is vital to health, a fundamental human right and an integral part of effective policies on health protection (WHO, 2011). Groundwater suitability for drinking has become a global concern (WHO, 2011)(Sarath Prasanth *et al.*, 2012; WHO, 2011; Wu *et al.*, 2015), particularly in arid and semi-arid areas where water shortages are a major concern (Falkenmark, 2019). The World Health Organization (WHO) has provided physiological, chemical and bacteriological parameters for international drinking water guidelines (WHO, 2011). In addition to the WHO guidelines, each country has developed its own drinking water quality guidelines due to regional variations of chemical constituents in water and needs to comply with country-specific public health policies and practices. In Kenya, drinking water quality standards are determined by the Kenya Bureau of Standards (KEBS), the standards, that are also used within the East Africa Community (EAC) (KEBS, 2014). With this regard, WHO (2011) and KEBS (2014) guideline values of various constituents in water are used to determine its suitability for drinking. Table 3-8 provides the guideline values for WHO (2011), and KEBS (2014) used to determine the drinking water quality of groundwater sources.

Drinking water guideline values for WHO (2011) and KEBS (2014)

Parameter	Unit	WHO	KEBS
pH	PH Scale	6.5-8.5	6.5-8.6
Turbidity	N.T. U	5.0	5.0
Total Hardness	mgCaCO ₃ /l	500.0	600.0
Total Alkalinity	mgCaCO ₃ /l	500.0	500.0
EC	μS/cm	2500.0	1500.0
Fe	mg/L	0.3	0.3
Mn	mg/L	0.1	0.1
Ca	mg/L	100.0	150.0
Mg	mg/L	100.0	100.0
Na	mg/L	200.0	200.0
K	mg/L	50.0	50.0
Cl	mg/L	500.0	500.0
F	mg/L	1.5	1.5
NO ₃	mgN/l	10.0	10.0
NO ₂	mgN/l	0.1	0.003

SO ₄	mg/L	450.0	400.0
CO ₃	mg/L	None	None
TDS	mg/L	1500	1000

The main objective of water quality monitoring is to assess the suitability for a particular use. The water quality index (WQI) is a mathematical tool that is used to transform large quantities of water quality data into a single number, which represents the water quality level (Ravikumar *et al.*, 2013; Sharma and Chhipa, 2016). In fact, developing WQI in an area is a fundamental process in the planning of land use and water resources management (Kumar and James, 2013; Stambuk-Giljanovic, 1999; Yidana *et al.*, 2010). The water quality index is regarded as the most effective way of communicating water quality trends to the public and to policymakers (Kumari *et al.*, 2014). A water quality index summarizes large amounts of water quality data into simple terms (Boah *et al.*, 2015) such as excellent, suitable, or unsuitable for drinking. The water quality index (WQI) was calculated by adopting the Weighted Arithmetic Index method to reflect the influence of water quality parameters on the overall quality of water (Ravikumar *et al.* .2015).

A variety of graphical methods for representations of water chemistry and hydrochemical facies exist (Giménez-Forcada, 2010b). Triangle diagrams show concentrations of the major cations and anions as percentage meq/L of the total anions and cations, in which a point represents waters with different chemical composition at different positions in each triangle (Ghoraba and Khan, 2013; Glover *et al.*, 2012a). The majority of the hydrochemical studies use piper trilinear diagrams (Glover *et al.*, 2012a; P. Kumar, 2013b; Lokhande and Mujawar, 2016a; Ravikumar *et al.*, 2015a) to represent the groundwater facies. The limitation of the Piper diagram is that it is not merely that a single point represents a unique facies, but that the point also takes on the corresponding interpretation (Giménez-Forcada, 2010b). According to Giménez-Forcada (2010), The sum or representation of the two ions in the same field of the diagram implies a similar behaviour of both water types, and the value of a parameter in the interpretation of a process is reinforced.

Mineral saturation index helps to determine the equilibrium state of water for a mineral phase using analytical data (Aghazadeh *et al.*, 2017); Garrels and Mackenzie, 1967). Changes in the saturation state are used to identify the geochemical reactions controlling the water chemistry and to differentiate between different stages of hydrochemical evolution (Aghazadeh *et al.*, 2017; Al-Ruwaih, 2017). The saturation index (SI) is given by (Garrels and Mackenzie 1967);

$$SI = \text{Log} \frac{IAP}{KT}$$

Where IAP represents the ion activity product of the dissociated chemical species in solution, KT is the equilibrium solubility product for the chemical involved at the sample temperature (Garrels and Mackenzie 1967).

Positive and negative saturation indices may be obtained as saturation indices (Appelo and Postma, 2005). Positive SI shows that the groundwater is oversaturated with respect to a particular mineral, i.e., unable of dissolving more of the mineral while the negative saturation indices (SI) indicate that the groundwater is under-saturated with respect to a particular mineral (Aghazadeh *et al.*, 2017; Al-Ruwaih, 2017). SI values close to zero indicate an equilibrium state between groundwater and the mineral (Appelo and Postma, 2005). Zero index values reflect groundwater discharging from an aquifer containing an ample amount of the mineral with sufficient resident time to reach equilibrium (Aghazadeh *et al.*, 2017).

Multivariate statistical techniques are widely used to evaluate groundwater chemistry and to determine prevailing aquifer processes (Dash *et al.*, 2018; Garba Abdullahi *et al.*, 2014; Islam *et al.*, 2017). Principal Component Analysis (PCA) and Hierarchical Cluster Analysis (HCA) are the mostly used statistical methods for determining the most important contributing parameters that decides the geochemistry of groundwater samples (Li *et al.*, 2018). PCA is useful for the identification of correlated variables as well as the process and grouping of types of water quality. (Mrklas *et al.*, 2006; Wu *et al.*, 2015). HCA on the other hand groups similar observations together to reveal different chemical characteristics of the various groups of groundwater samples (Dash *et al.*, 2018; Garba Abdullahi *et al.*, 2014; Islam *et al.*, 2017).

Point sources of pollution refer to the discharge of contaminants into the groundwater through a pipe, ditch, discrete fissure, tunnels, concentrated animal feed, and municipal wastewater. (Garba Abdullahi *et al.*, 2014; Islam *et al.*, 2017) while nonpoint sources may results from agricultural chemicals (fertilizers and pesticides) through surface runoff, precipitation, atmospheric deposition, seepage, drainage, or hydrological modification (Islam *et al.*, 2017). Sound management of nonpoint sources of pollution groundwater requires a thorough scientific understanding of these sources and the linkages between nonpoint sources and groundwater discharges to users or affected well and streams (Lathamani *et al.*, 2015)..

Appendix 3-3: Analytical rationale – Rainfall-Surface water -Groundwater Interactions

Groundwater is part of the hydrological cycle, and the potential links between surface and groundwater systems in the study area must be identified (Kotchoni *et al.*, 2018). A comparison of information from the geological maps and watercourses shown on topographical maps allow for an initial assessment of their relationships. Stable isotopes of oxygen and hydrogen are often used to study the origin and chemical evolution of groundwater (Cloutier *et al.*, 2006; Miljević *et al.*, 2012; Yusuf *et al.*, 2018; Zhao *et al.*, 2018). Deuterium excess (d-excess = $\delta D - 8 \times \delta^{18}O$) is often used to describe the effect of evaporation on water bodies compared to precipitation (X. Li *et al.*, 2018). In addition, a deviation from a slope of 8 on a plot of δD versus $\delta^{18}O$ may also indicate mixing between different water groups or water-rock interactions (Yusuf *et al.*, 2018; Zhao *et al.*, 2018). Tritium has a half-life of 12.3 years, making it useful to trace and date groundwater, calculation of the rate of water circulation in the hydrologic cycle and assess how long a groundwater source has been stored out of contact with tritium laden recharge. Groundwater systems with recharge occurring before the 1950s will have tritium levels at or below 1 TU. These groundwater systems are considered “not vulnerable” to anthropogenic contamination (Moore, 2011; Ghaffar *et al.*, 2017). Conversely, groundwater systems recharged after the early 1950s will contain tritium levels at, or significantly above, the natural "pre-bomb" background concentrations and are considered “vulnerable” to human pollution (Moore, 2011).

Drinking water guideline values for WHO (2011) and KEBS (2014)

Parameter	Unit	WHO	KEBS
pH	PH Scale	6.5-8.5	6.5-8.6
Turbidity	N.T. U	5.0	5.0
Total Hardness	mgCaCO ₃ /l	500.0	600.0
Total Alkalinity	mgCaCO ₃ /l	500.0	500.0
EC	μS/cm	2500.0	1500.0
Fe	mg/L	0.3	0.3
Mn	mg/L	0.1	0.1
Ca	mg/L	100.0	150.0
Mg	mg/L	100.0	100.0
Na	mg/L	200.0	200.0
K	mg/L	50.0	50.0
Cl	mg/L	500.0	500.0
F	mg/L	1.5	1.5
NO ₃	mgN/l	10.0	10.0
NO ₂	mgN/l	0.1	0.003
SO ₄	mg/L	450.0	400.0
CO ₃	mg/L	None	None
TDS	mg/L	1500	1000

The main objective of water quality monitoring is to assess the suitability for a particular use. The water quality index (WQI) is a mathematical tool that is used to transform large quantities of water quality data into a single number, which represents the water quality level (Ravikumar *et al.*, 2013; Sharma and Chhipa, 2016). In fact, developing WQI in an area is a fundamental process in the planning of land use and water resources management (P. J. S. Kumar and James, 2013a; Stambuk-Giljanovic, 1999b; Yidana *et al.*, 2010a)(Kumar and James, 2013; Stambuk-Giljanovic, 1999; Yidana *et al.*, 2010). The water quality index is regarded as the most effective way of communicating water quality trends to the public and to policymakers (Kumari *et al.*, 2014). A water quality index summarizes large amounts of water quality data into simple terms (Boah *et al.*, 2015) such as excellent, suitable, or unsuitable for drinking. The water quality index (WQI) was calculated by adopting the Weighted Arithmetic Index method to reflect the influence of water quality parameters on the overall quality of water (Ravikumar *et al.* .2015).

A variety of graphical methods for representations of water chemistry and hydrochemical facies exist (Giménez-Forcada, 2010). Triangle diagrams show concentrations of the major cations and anions as percentage meq/L of the total anions and cations, in which a point represents waters with different chemical

composition at different positions in each triangle (Ghoraba and Khan, 2013; Glover *et al.*, 2012). The majority of the hydrochemical studies use piper trilinear diagrams (Glover *et al.*, 2012; Kumar, 2013; Lokhande and Mujawar, 2016; Ravikumar *et al.*, 2015) to represent the groundwater facies. The limitation of the Piper diagram is that it is not merely that a single point represents unique facies, but that the point also takes on the corresponding interpretation (Giménez-Forcada, 2010). According to Giménez-Forcada (2010), The sum or representation of the two ions in the same field of the diagram implies a similar behaviour of both water types, and the value of a parameter in the interpretation of a process is reinforced.

Mineral saturation index helps to determine the equilibrium state of water for a mineral phase using analytical data (Aghazadeh *et al.*, 2017; Garrels and Mackenzie, 1967). Changes in the saturation state are used to identify the geochemical reactions controlling the water chemistry and to differentiate between different stages of hydrochemical evolution (Aghazadeh *et al.*, 2017; Al-Ruwaih, 2017). The saturation index (SI) is given by (Garrels and Mackenzie 1967);

$$SI = \text{Log} \frac{IAP}{KT}$$

Where IAP represents the ion activity product of the dissociated chemical species in solution, KT is the equilibrium solubility product for the chemical involved at the sample temperature (Garrels and Mackenzie 1967).

Positive and negative saturation indices may be obtained as saturation indices (Appelo and Postma, 2005). Positive SI shows that the groundwater is oversaturated with respect to a particular mineral, i.e., unable of dissolving more of the mineral while the negative saturation indices (SI) indicate that the groundwater is under-saturated with respect to a particular mineral (Aghazadeh *et al.*, 2017; Al-Ruwaih, 2017). SI values close to zero indicate an equilibrium state between groundwater and the mineral (Appelo and Postma, 2005). Zero index values reflect groundwater discharging from an aquifer containing an ample amount of the mineral with sufficient resident time to reach equilibrium (Aghazadeh *et al.*, 2017).

Multivariate statistical techniques are widely used to evaluate groundwater chemistry and to determine prevailing aquifer processes (Dash *et al.*, 2018; Garba Abdullahi *et al.*, 2014; Islam *et al.*, 2017). Principal Component Analysis (PCA) and Hierarchical Cluster Analysis (HCA) are the mostly used statistical methods for determining the most important contributing parameters that decides the geochemistry of groundwater samples (Li *et al.*, 2018). PCA is useful for the identification of correlated variables as well as the process and grouping of types of water quality (Mrklas *et al.*, 2006; Wu *et al.*, 2015). HCA on the other hand groups similar observations together to reveal different chemical characteristics of the various groups of groundwater samples (Dash *et al.*, 2018; Garba Abdullahi *et al.*, 2014; Islam *et al.*, 2017).

Point sources of pollution refer to the discharge of contaminants into the groundwater through a pipe, ditch, discrete fissure, tunnels, concentrated animal feed, and municipal wastewater (Garba Abdullahi *et al.*, 2014;

Islam *et al.*, 2017) while nonpoint sources may result from agricultural chemicals (fertilizers and pesticides) through surface runoff, precipitation, atmospheric deposition, seepage, drainage, or hydrological modification (Islam *et al.*, 2017). Sound management of nonpoint sources of pollution groundwater requires a thorough scientific understanding of these sources and the linkages between nonpoint sources and groundwater discharges to users or affected well and streams (Lathamani *et al.*, 2015).

Appendix 3.3: Analytical rationale – Rainfall-Surface water -Groundwater Interactions

Groundwater is part of the hydrological cycle, and the potential links between surface and groundwater systems in the study area must be identified (Kotchoni *et al.*, 2018). A comparison of information from the geological maps and watercourses shown on topographical maps allow for an initial assessment of their relationships. Stable isotopes of oxygen and hydrogen are often used to study the origin and chemical evolution of groundwater (Cloutier *et al.*, 2006; Miljević *et al.*, 2012; Yusuf *et al.*, 2018; Zhao *et al.*, 2018). Deuterium excess (d-excess = $\delta D - 8 \times \delta^{18}O$) is often used to describe the effect of evaporation on water bodies compared to precipitation (Li *et al.*, 2018). In addition, a deviation from a slope of eight on a plot of δD versus $\delta^{18}O$ may also show mixing between different groups of water or water-rock interactions (Yusuf *et al.*, 2018; Zhao *et al.*, 2018). Tritium has a half-life of 12.3 years, making it useful to trace and date groundwater, calculation of the rate of water circulation in the hydrologic cycle and assess how long a groundwater source has been stored out of contact with tritium laden recharge. Groundwater systems with recharge occurring before the 1950s will have tritium levels at or below 1 TU. These groundwater systems are considered “not vulnerable” to anthropogenic contamination (Moore, 2011; Ghaffar *et al.*, 2017). Conversely, groundwater systems recharged after the early 1950s will contain tritium levels at, or significantly above, the natural "pre-bomb" background concentrations and are considered “vulnerable” to human pollution (Moore, 2011).

Appendix 4.1: Field description for the quartzo-feldspathic gneiss

Sample No.	Latitude	Longitude	Elev.	Description	Occurrence	Mineralogy
3841	3.2748	35.5944	582	Light grey with Fe and Mn nodules	Outcrop observed only at Nabuelpus area with debris transported and deposited along the Monti lagga up to Katapakori area	Predominantly quartz and feldspars. Other minerals include biotite, hornblende and micas
3843	3.2748	35.5944	582	Altered dark-coloured gneiss		
3846	2.8575	35.6146	616	Dark coloured with visible quartz grains		

Appendix 4.2: Field description of the Turkana grits samples collected from the study area

Sample No.	Latitude	Longitude	Elevation	Field Description	Locality
1646	3.0798	35.5401	509	Partly coarse-grained and fine-grained grit	Nakutan area
1649	3.1084	35.5933	497	Fine-grained grit at LOWASCO Bh 6	LOWASCO Bh 6
1651	3.1095	35.5948	499	Medium to fine-grained grit at contact zone (nepheline-phonolite)	Nabulon area
1652	3.1622	35.6192	508	Gravelly grit mostly unconsolidated	north-east of Lodwar town at Kakwanyang
1654	3.1915	35.8344	482	Fine-grained grit	Lodwar town
1655	3.1336	35.6007	488	Grit sample above the dolerite dyke	Lodwar next to Kawalase River
1671	3.1095	35.7868	517	Semi-consolidated gravelly formation	Lolupe
1672	3.1095	35.7868	517	Upper part - Thin and highly consolidated layer	Lokoparpai
1673	3.0946	35.5333	516	Middle part - sandy semi-consolidated grit	Turkwel River at Nayuu area
3830	3.0899	35.5567	483	Grit capped by calcareous material	Nachomin
3831	3.0077	35.5163	536	Grit at Nachomin stream	Nachomin stream
3835	3.0063	35.5171	542	Fine-grained grit	Nadapal
3836	3.0399	35.4839	516	Sandy grit next to Holocene sediments	David Lee Secondary school
3838	3.2749	35.6269	583	Grit sample (thin section sample)	Naotin stream
3839	3.2749	35.6269	583	Semi-consolidated sandy gravel	Naoyatira area
3848	3.1974	35.7690	479	Unconsolidated gravelly grit	the east of Talent High school
3849	3.1974	35.7690	479	Consolidated grit exposure	Nakadukui
3856	3.1421	35.7843	457	Grit exposure capped by calcareous material	Natirnalulung

Appendix 4.3: Field description of the Holocene sediments between Napuu and Lolupe, east of Lodwar, Natir and at Turkwel Riverbank at Kakwanyang area

Lab No.	Latitude	Longitude	Elev .	Locality	Field Description	Thickness (m)	Grain size
3820	3.1502	35.4910	509	Napuu/Lolupe (4, 000 YR BP)	Compacted light coloured sediment (A); No reaction with acid (10% HCl)	0.5	fine-grained
3821	3.1502	35.4910	509		Dark coloured sediment (B); No reaction with acid (10% HCl)	1.5	fine-grained
3822	3.1502	35.4910	509		Slightly light-coloured sediment (C); Fizzles with acid (10% HCl)	0.5	medium-grained
3823	3.1502	35.4910	509		Very fine-grained sandy layer (D); Fizzles with acid (10% HCl)	0.5	fine-grained
3824	3.1229	35.5394	503	Lodwar East (4, 000 YR BP)	Dark coloured calcite layer (A); Fizzles with acid (10% HCl)	0.5	medium-grained
3825	3.1229	35.5394	503		Light-coloured sediment with calcite grains (B); Fizzles with acid (10% HCl)	1.5	fine-grained
3826	3.0857	35.5573	510	Natir (4, 000 YR BP)	Bottom layer (C) silty gravel; Fizzles with acid (10% HCl)	1	coarse-grained
3827	3.0857	35.5573	510		Middle layer (B) light coloured bed - absent quartz grains; No reaction with acid (10% HCl)	0.5	medium-grained
3829	3.0857	35.5573	510		The top layer (A) red-brown sediment; Fizzles with acid (10% HCl)	0.5	fine-grained
3852	3.1830	35.8036	451	Turkwel Riverbank at Kakwanyang (10,000 YR BP)	Layer A Fe-dominant; No reaction with acid (10% HCl)	1.5	fine-grained
3853	3.1830	35.8036	451		Layer B- light coloured silty gravel; Fizzles with acid (10% HCl)	1	medium to fine
3854	3.1417	35.7358	496		Layer C – Clays; Fizzles with acid (10% HCl)	0.5	fine-grained
3855	3.1420	35.7838	461		Layer D -Very fine-grained light-coloured bed with calcite grains; Fizzles with acid (10% HCl)	1.5	fine-grained

Appendix 4.4: Field description of the Sandstone outcrops in the study area

Sample No.	Latitude	Longitude	Elev.	Lab No.	Field Description	Thickness
1645	3.0946	35.5336	516	1645	Sandstone with shale at Nadapal	0.5
1658	3.1136	35.5810	497	1658	Gravelly calcite-cemented sandstone at Nakwamekwi	0.3
1659	3.1136	35.5810	497	1659	Fine-grained sandstone with laminations	0.4
1668	3.1304	35.8579	460	1668	Coarser sandstone and gravel at Turkwel River east of Natir	0.3
1669	3.1304	35.8579	460	1669	Pebbly sandstone	0.2
1670	3.1095	35.7868	517	1670	Greenish fine-grained sandstone	1.8
1675	3.1420	35.8630	429	1675	White moist sandstone with Fe stain	0.2
1676	3.1420	35.8630	429	1676	Weakly unconsolidated coarse sandstone with gravel-sized clasts	0.5
1678	3.1420	35.8630	429	1678	White sandstone mixed with thin clay layers	0.50-0.70
3832	3.0077	35.5163	536	3832	Conglomeratic sandstone at Nachomin	0.4
3833	3.0063	35.5171	542	3833	Grey gravelly sandstone	0.4
3842	3.2748	35.5944	582	3842	Altered sandstone near Nabuelpus	0.7
3847	3.1427	35.7389	441	3847	Micaceous sandstone with clays located at natir	0.5
3850	3.1830	35.8036	451	3850	Unconsolidated gravelly sandstone	0.3
3858	3.1263	35.6475	462	3858	Fine-grained laminated sandstone	0.5

Appendix 4.5: Field description of conglomerate and grainstone samples

Lab No.	Field Description	Latitude	Longitude	Elevation	Occurrence
1657	Grainstone -medium-fine grained	3.13044	35.85792	460	Rock outcrop at Natir
1667	Pebbly grainstone	3.13044	35.85792	460	Rock outcrop at Natir
1677	Conglomerate grading to silty grains	3.14196	35.86303	429	Layer capped the Turkana Grit at contact zone with nepheline phonolite
3857	Conglomerate grading to fine-grained with coarsening-upward bedding structures. Sediment cemented by calcium carbonate	3.14179	35.78517	462	Layer occurring within the sandstone unit

Appendix 4.6: Field description of volcanic rocks (augite basalt, nepheline-phonolite, and dolerite dyke found in Turkana grits and basement rocks

Field Description	Augite Basalt	Nepheline-Phonolite	Nepheline-Phonolite	Nepheline Phonolite	Dolerite (TG)	Dolerite (MB)
Lab No.	1648	1650	1653	1674	1656	3845
Latitude	3.1878	3.1139	3.1093	3.1138	3.1336	3.2748
Longitude	35.8381	35.5858	35.5947	35.5856	35.6007	35.5944
Elevation	497	502	498	497	488	582
Colour	White-grey	Grey-black	Light coloured	Black	Dark grey to black	Black-coloured
Texture	Well-polished fine-grained surface	Fine to medium and unweathered fine-grained	Medium to coarse-grained, highly brecciated phonolite	Fine-grained	Medium to coarse-grained with Ophitic texture	fine-grained
Mineralogy	A mixture of lava and sand	Tiny quartz crystals, haematite,	Prism-shaped minerals, quartz grains and haematite	Visible haematite and quartz grains	Plagioclase and pyroxene minerals with inclusions of the grits indicating the Turkana Grit is older	Deformed minerals and not visible
Occurrence	Occurred on a volcanic hill east of Talent High school	Occurred on the Ngapoi Hills and comprised the volcanic cones within Lodwar town.	Formed contact with Turkana grit at Nabulon and is highly weathered	Collected on one of the cone-shaped features in Lodwar	Dyke in the Turkana grits displaying contact metasomatism features	Dyke in the Basement system

Appendix 4.7: Results of the whole rock analysis for samples collected from the study area (1645 -3858)

Rock Type	Lab No.	Field Code	Latitude	Longitude	Elev.	SiO ₂	Al ₂ O ₃	CaO	MgO	Na ₂ O	K ₂ O	TiO ₂	MnO	Fe ₂ O ₃	LOI
Alluvial	3851	Stop 93B	3.1830	35.8036	451	74.64	10.39	3.15	3.97	0.91	1.81	0.19	0.07	2.51	1.14
Augite Basalt	1648	Lod_002	3.1878	35.8381	497	53.79	18.00	5.69	3.22	0.64	2.06	1.09	0.12	6.08	9.22
Conglomerate	1677	Lod_033	3.1420	35.8630	429	71.60	9.72	4.99	2.25	0.79	2.13	0.31	0.09	2.03	5.99
Conglomerate	3857	Stop 133	3.1418	35.7852	462	60.07	9.15	12.15	0.04	1.70	3.52	0.26	0.70	2.51	8.68
Dolerite (MB)	3845	Stop 71	3.2748	35.5944	582	74.09	4.98	4.99	7.31	0.15	0.94	0.35	0.16	5.01	1.46
Dolerite (TG)	1656	Lod/010	3.1336	35.6007	488	50.59	15.87	4.70	1.71	0.27	7.01	1.89	0.28	8.12	8.62
Grainstone	1657	Lod_011	3.1304	35.8579	460	58.07	5.80	23.00	0.02	0.20	1.06	0.18	0.32	1.50	9.83
Grainstone	1667	Lod/023	3.1304	35.8579	460	64.30	8.30	7.84	5.19	0.73	2.95	0.15	0.13	1.13	9.13
Holocene sediments	3820	Stop 5A	3.1502	35.4910	509	66.90	16.05	2.74	1.50	0.15	2.43	0.76	0.10	3.78	5.50
Holocene sediments	3821	Stop 5B	3.1502	35.4910	509	55.10	14.70	2.55	1.47	0.10	1.87	1.34	0.19	7.70	14.16
Holocene sediments	3822	Stop 5C	3.1502	35.4910	509	51.80	16.42	2.62	0.11	0.17	1.84	1.24	0.20	7.71	17.09
Holocene sediments	3823	Stop 5D	3.1502	35.4910	509	80.85	10.92	2.61	0.12	0.12	1.68	0.14	0.17	1.11	2.07
Holocene sediments	3824	Stop 8A	3.1229	35.5394	503	57.97	16.52	2.06	1.37	0.14	1.39	0.94	0.12	7.97	11.26
Holocene sediments	3825	Stop 8B	3.1229	35.5394	503	69.97	11.89	5.34	1.97	0.09	2.02	0.43	0.08	3.14	4.10
Holocene sediments	3826	Stop 14A	3.0857	35.5573	510	24.91	4.89	27.15	7.01	0.08	0.72	0.27	0.30	2.14	32.00
Holocene sediments	3827	Stop 14B	3.0857	35.5573	510	12.89	2.01	45.78	0.07	0.04	0.06	0.14	0.52	1.99	36.31
Holocene sediments	3829	Stop 14C	3.0857	35.5573	510	68.97	10.21	1.82	2.67	0.05	1.81	0.62	0.09	4.73	8.48
Holocene sediments	3852	Stop 93C	3.1830	35.8036	451	48.79	18.90	1.25	1.93	1.30	3.24	1.20	0.14	9.53	13.16
Holocene sediments	3853	Stop 93D	3.1830	35.8036	451	43.69	18.70	1.01	0.08	1.96	3.41	1.41	0.17	13.15	15.97
Holocene sediments	3854	Stop 126	3.1417	35.7358	496	46.51	13.95	8.15	3.05	0.99	2.41	0.14	0.15	6.51	16.72
Holocene sediments	3855	Stop 130	3.1420	35.7838	461	46.07	9.87	19.50	2.87	0.87	1.57	0.75	0.60	3.90	12.91
Basement	3841	Stop 50	3.2748	35.5944	582	53.71	18.20	1.52	1.07	4.03	6.52	0.19	0.27	3.92	9.63
Basement	3843	Stop 50	3.2748	35.5944	582	52.83	19.95	2.15	0.01	4.93	5.87	0.18	0.25	4.31	8.66
Basement	3846	Stop 71	2.8575	35.6146	616	53.21	19.89	2.49	0.09	5.01	5.50	0.23	0.24	4.49	8.84

Nepheline-phonolite	1650	Lod_004	3.1139	35.5858	502	48.24	12.81	8.01	3.50	1.28	2.01	4.11	0.16	10.08	8.80
Nepheline-phonolite	1674	Lod/030	3.1138	35.5856	497	52.30	13.79	7.09	2.41	1.12	1.31	2.60	0.70	9.61	9.06
Nepheline-phonolite	1653	Lod_007	3.1093	35.5947	498	54.81	15.31	8.20	2.30	0.90	2.50	3.03	0.28	10.01	2.09
Sandstone	1645	Stop 1	3.0946	35.5336	516	40.01	7.70	25.15	1.81	0.89	1.13	0.40	0.31	3.40	18.19
Sandstone	1658	Lod/013	3.1136	35.5810	497	55.80	13.41	7.60	3.15	1.55	2.61	0.92	0.13	5.15	9.08
Sandstone	1659	Lod/014	3.1136	35.5810	497	47.61	9.03	24.42	0.04	0.37	1.32	0.50	0.38	6.15	10.11
Sandstone	1668	Lod/024	3.1304	35.8579	460	49.40	5.87	18.61	4.13	0.65	1.12	0.30	0.12	1.90	17.49
Sandstone	1669	Lod/025	3.1304	35.8579	460	52.60	5.15	24.91	4.70	0.53	0.84	0.19	0.07	1.60	9.25
Sandstone	1670	Lod/026	3.1095	35.7868	517	64.02	11.87	4.87	4.31	0.72	1.51	0.70	0.06	3.92	8.01
Sandstone	1675	Lod_031	3.1420	35.8630	429	62.07	10.92	10.91	0.02	1.86	2.14	0.42	0.17	2.40	8.99
Sandstone	1676	Lod_032	3.1420	35.8630	429	72.00	10.93	4.60	1.41	0.80	2.30	0.39	0.09	2.40	5.06
Sandstone	1678	Lod_034	3.1420	35.8630	429	65.10	13.69	1.72	2.82	0.49	1.95	0.64	0.09	4.05	9.44
Sandstone	3832	Stop 25	3.0077	35.5163	536	47.84	5.92	25.01	0.02	0.06	1.32	0.17	0.50	1.50	17.20
Sandstone	3833	Stop 25	3.0063	35.5171	542	48.09	5.32	24.91	0.03	0.13	1.51	0.16	0.18	1.18	18.47
Sandstone	3842	Stop 50	3.2748	35.5944	582	26.67	12.31	8.05	21.01	5.04	6.31	0.17	0.05	0.92	19.03
Sandstone	3847	Stop 90	3.1427	35.7389	441	57.50	20.15	8.59	6.79	0.12	0.43	0.13	0.09	5.47	0.46
Sandstone	3850	Stop 93A	3.1830	35.8036	451	30.91	6.51	27.90	0.10	0.21	1.35	0.64	1.21	8.53	22.59
Sandstone	3858	Stop 139	3.1263	35.6475	462	40.01	7.50	26.20	0.05	0.87	1.09	0.41	0.32	3.61	18.86
Turkana Grit	1646	Stop 2	3.0798	35.5401	509	49.15	4.78	17.15	6.10	0.92	1.51	0.14	0.17	1.32	17.37
Turkana Grit	1649	Lod/003	3.1084	35.5933	497	60.13	3.89	14.01	6.65	0.87	1.25	0.17	0.19	1.95	9.89
Turkana Grit	1651	Lod/005	3.1095	35.5948	499	60.48	5.03	12.00	9.21	1.44	1.35	0.17	0.09	1.35	7.88
Turkana Grit	1652	Lod/006	3.1622	35.6192	508	48.36	4.03	37.00	1.06	0.58	0.65	0.23	0.13	1.17	6.81
Turkana Grit	1654	Lod_008	3.1915	35.8344	482	58.45	9.49	18.24	0.02	0.02	2.80	0.31	0.13	2.07	7.95
Turkana Grit	1655	Lod_009	3.1336	35.6007	488	46.21	16.40	7.80	3.01	1.98	4.03	2.40	0.19	7.90	9.89
Turkana Grit	1671	Lod/027	3.1095	35.7868	517	71.06	11.60	2.76	0.03	0.16	2.15	0.40	0.08	2.40	9.26
Turkana Grit	1672	Lod/028	3.1095	35.7868	517	62.80	10.60	9.80	2.50	0.14	1.80	0.89	0.14	4.90	6.28
Turkana Grit	1673	Lod/029	3.0946	35.5333	516	65.30	15.87	3.00	1.82	0.12	2.51	0.62	0.08	3.95	6.69

Turkana Grit	3830	Stop 15	3.0899	35.5567	483	24.51	3.41	38.15	0.05	0.03	0.54	0.23	0.71	2.73	29.49
Turkana Grit	3831	Stop 24	3.0077	35.5163	536	60.80	4.81	4.31	0.04	0.09	0.94	0.32	0.31	2.71	24.91
Turkana Grit	3835	Stop 39	3.0063	35.5171	542	56.92	10.98	14.12	0.03	0.04	2.53	0.17	0.37	1.73	12.75
Turkana Grit	3836	Stop 39	3.0399	35.4839	516	70.86	12.15	3.15	2.01	0.11	2.09	0.51	0.08	3.41	5.47
Turkana Grit	3838	Stop 49	3.2749	35.6269	583	62.77	10.98	7.15	3.02	0.21	2.03	0.41	0.32	3.21	8.85
Turkana Grit	3839	Stop 50	3.2749	35.6269	583	45.70	9.12	11.72	8.71	0.09	0.98	0.77	2.01	3.51	16.62
Turkana Grit	3848	Stop 91	3.1974	35.7690	479	53.70	4.21	30.14	6.01	0.20	0.61	0.19	0.15	1.81	1.88
Turkana Grit	3849	Stop 91	3.1974	35.7690	479	21.83	4.21	30.14	6.01	0.20	0.61	0.19	0.15	1.81	34.27
Turkana Grit	3856	Stop 132	3.1421	35.7843	457	40.09	4.20	15.80	9.15	0.57	1.12	0.18	0.19	1.65	25.87

Appendix 4.8: Results of the major elements obtained from X-fluorescence spectrometry (XRF) at ICRAF lab (1648-3858); the results have been arranged in order of rock samples where “nd” refers to not detected while “-“ were not measured

Rock Type	Lab No.	Field Code	Lat	Long	Elev.	Na	Mg	Al	P	S	K	Ca	Mn	Fe
Alluvial	3851	Stop 93B	3.1830	35.8036	451	nd	0.95	5.96	0.04	0.09	0.84	0.16	0.09	7.83
Augite Basalt	1648	Lod_002	3.1878	35.8381	497	nd	1.26	4.70	0.18	nd	0.48	4.99	0.17	5.09
Conglomerate	1677	Lod_033	3.1420	35.8630	429	nd	1.08	3.98	0.02	0.01	0.19	2.63	0.05	2.06
Conglomerate	3857	Stop 133	3.1418	35.7852	462	0.00	2.20	1.45	0.04	0.02	0.16	14.86	0.22	0.99
Dolerite (MB)	3845	Stop 71	3.2748	35.5944	582	0.00	2.32	3.71	0.02	0.01	0.02	8.56	0.14	4.12
Dolerite (TG)	1656	Lod/010	3.1336	35.6007	488	-	-	-	-	-	-	-	-	-
Grainstone	1657	Lod_011	3.1304	35.8579	460	0.05	0.43	1.37	0.03	0.02	0.14	17.18	0.41	1.22
Grainstone	1667	Lod/023	3.1304	35.8579	460	-	-	-	-	-	-	-	-	-
Holocene sediments	3820	Stop 5A	3.1502	35.4910	509	nd	0.64	3.76	0.07	0.01	0.39	2.51	0.09	3.03
Holocene sediments	3821	Stop 5B	3.1502	35.4910	509	nd	0.73	4.87	0.07	0.00	0.64	1.88	0.14	5.16
Holocene sediments	3822	Stop 5C	3.1502	35.4910	509	nd	0.69	4.69	0.06	nd	0.62	1.88	0.14	4.80
Holocene sediments	3823	Stop 5D	3.1502	35.4910	509	0.11	0.09	1.72	0.03	0.01	0.11	2.50	0.03	1.23
Holocene sediments	3824	Stop 8A	3.1229	35.5394	503	nd	1.18	5.32	0.04	0.18	0.69	1.49	0.09	5.67
Holocene sediments	3825	Stop 8B	3.1229	35.5394	503	nd	0.84	3.01	0.05	0.00	0.26	4.93	0.07	2.40
Holocene sediments	3826	Stop 14A	3.0857	35.5573	510	0.00	2.83	1.62	0.03	0.02	0.09	18.98	0.23	1.18
Holocene sediments	3827	Stop 14B	3.0857	35.5573	510	nd	0.34	1.13	nd	0.02	0.07	25.23	0.87	0.88
Holocene sediments	3829	Stop 14C	3.0857	35.5573	510	nd	1.36	4.04	0.02	nd	0.27	1.25	0.05	3.32
Holocene sediments	3852	Stop 93C	3.1830	35.8036	451	0.00	1.80	4.23	0.06	0.06	0.36	5.22	0.12	3.96
Holocene sediments	3853	Stop 93D	3.1830	35.8036	451	nd	0.75	1.79	0.09	0.07	0.26	14.79	0.71	2.29
Holocene sediments	3854	Stop 126	3.1417	35.7358	496	0.00	4.53	2.06	0.03	0.08	0.12	13.32	0.13	1.17
Holocene sediments	3855	Stop 130	3.1420	35.7838	461	0.19	0.37	1.31	0.08	0.02	0.40	9.36	0.26	1.84
Basement	3841	Stop 50	3.2748	35.5944	582	0.00	1.96	1.71	0.03	0.07	0.37	12.63	0.07	1.12
Basement	3843	Stop 50	3.2748	35.5944	582	0.00	2.89	1.82	0.05	nd	0.17	5.34	0.18	4.26
Basement	3846	Stop 71	2.8575	35.6146	616	0.00	2.42	3.38	0.03	0.01	0.14	7.82	0.20	6.32

Nepheline-phonolite	1650	Lod/004	3.1139	35.5858	502	0.22	nd	5.46	0.08	nd	0.52	1.69	0.13	3.62
Nepheline-phonolite	1674	Lod/030	3.1138	35.5856	497	-	-	-	-	-	-	-	-	-
Nepheline-phonolite	1653	Lod/007	3.1093	35.5947	498	0.00	1.37	3.87	0.33	nd	0.87	6.80	0.20	6.01
Sandstone	1645	Stop 1	3.0946	35.5336	516	-	-	-	-	-	-	-	-	-
Sandstone	1658	Lod/013	3.1136	35.5810	497	-	-	-	-	-	-	-	-	-
Sandstone	1659	Lod/014	3.1136	35.5810	497	-	-	-	-	-	-	-	-	-
Sandstone	1668	Lod/024	3.1304	35.8579	460	-	-	-	-	-	-	-	-	-
Sandstone	1669	Lod/025	3.1304	35.8579	460	-	-	-	-	-	-	-	-	-
Sandstone	1670	Lod/026	3.1095	35.7868	517	-	-	-	-	-	-	-	-	-
Sandstone	1675	Lod_031	3.1420	35.8630	429	nd	1.09	2.68	0.04	0.03	0.15	11.09	0.15	1.70
Sandstone	1676	Lod_032	3.1420	35.8630	429	nd	1.07	2.63	0.06	0.01	0.22	7.74	0.11	1.91
Sandstone	1678	Lod_034	3.1420	35.8630	429	nd	1.09	4.37	0.03	nd	0.30	1.18	0.05	3.68
Sandstone	3832	Stop 25	3.0077	35.5163	536	0.19	0.24	0.95	0.04	0.03	0.22	19.13	0.22	0.99
Sandstone	3833	Stop 25	3.0063	35.5171	542	0.22	0.24	0.94	0.03	0.04	0.21	18.21	0.22	0.97
Sandstone	3842	Stop 50	3.2748	35.5944	582	0.27	0.29	4.73	0.03	0.01	0.74	1.37	0.19	3.41
Sandstone	3847	Stop 90	3.1427	35.7389	441	0.00	2.67	1.49	0.01	0.08	0.07	19.70	0.15	0.97
Sandstone	3850	Stop 93A	3.1830	35.8036	451	nd	1.26	5.89	0.07	0.02	0.88	0.62	0.09	6.88
Sandstone	3858	Stop 139	3.1263	35.6475	462	0.00	3.91	2.04	0.05	0.02	0.12	12.65	0.11	0.97
Turkana Grit	1646	Stop 2	3.0798	35.5401	509	-	-	-	-	-	-	-	-	-
Turkana Grit	1649	Lod/003	3.1084	35.5933	497	-	-	-	-	-	-	-	-	-
Turkana Grit	1651	Lod/005	3.1095	35.5948	499	-	-	-	-	-	-	-	-	-
Turkana Grit	1652	Lod/006	3.1622	35.6192	508	-	-	-	-	-	-	-	-	-
Turkana Grit	1654	Lod_008	3.1915	35.8344	482	0.19	0.26	1.24	0.05	0.02	0.39	19.53	0.15	1.29
Turkana Grit	1655	Lod_009	3.1336	35.6007	488	nd	1.04	4.10	0.26	nd	0.84	6.25	0.27	6.32
Turkana Grit	1671	Lod/027	3.1095	35.7868	517	-	-	-	-	-	-	-	-	-
Turkana Grit	1672	Lod/028	3.1095	35.7868	517	-	-	-	-	-	-	-	-	-
Turkana Grit	1673	Lod/029	3.0946	35.5333	516	-	-	-	-	-	-	-	-	-

Turkana Grit	3830	Stop 15	3.0899	35.5567	483	nd	0.48	1.14	0.02	0.02	0.16	22.67	1.19	1.35
Turkana Grit	3831	Stop 24	3.0077	35.5163	536	nd	0.41	0.89	0.03	0.04	0.20	22.12	0.32	1.06
Turkana Grit	3835	Stop 39	3.0063	35.5171	542	0.19	0.35	1.49	0.03	0.02	0.39	11.41	0.36	1.50
Turkana Grit	3836	Stop 39	3.0399	35.4839	516	nd	0.74	3.39	0.04	nd	0.23	1.91	0.05	2.77
Turkana Grit	3838	Stop 49	3.2749	35.6269	583	0.00	3.38	2.62	0.05	0.01	0.10	9.08	0.18	2.22
Turkana Grit	3839	Stop 50	3.2749	35.6269	583	0.21	0.49	4.62	0.03	0.01	0.75	0.92	0.21	3.34
Turkana Grit	3848	Stop 91	3.1974	35.7690	479	nd	0.60	1.96	0.08	0.04	0.23	17.31	1.62	2.90
Turkana Grit	3849	Stop 91	3.1974	35.7690	479	nd	0.78	2.10	0.04	0.00	0.18	2.75	0.06	2.25
Turkana Grit	3856	Stop 132	3.1421	35.7843	457	nd	0.70	1.78	0.06	0.03	0.15	17.08	0.33	1.53

Appendix 4.9: Results of the trace elements obtained from X-fluorescence spectrometry (XRF) at ICRAF lab (1648-3858); the results have been arranged in order of rock samples where “nd” refers to not detected while “-“were not measured

Rock Type	Lab No.	Field Code	Lat	Long	Elev.	Ti	Cr	Co	Ni	Cu	Zn	As	Se	Mo	Pb
Alluvial	3851	Stop 93B	3.1830	35.8036	451	0.17	0.01	0.00	0.01	0.00	0.02	nd	nd	0.00	nd
Augite Basalt	1648	Lod_002	3.1878	35.8381	497	0.26	0.01	0.00	0.00	0.00	0.01	nd	0.00	nd	nd
Conglomerate	1677	Lod_033	3.1420	35.8630	429	0.04	0.00	nd	0.00	0.00	0.01	nd	nd	0.00	nd
Conglomerate	3857	Stop 133	3.1418	35.7852	462	nd	0.01	nd	0.00	nd	0.01	nd	nd	0.00	nd
Dolerite (MB)	3845	Stop 71	3.2748	35.5944	582	nd	0.03	0.00	0.00	nd	0.01	nd	nd	0.00	nd
Dolerite (TG)	1656	Lod/010	3.1336	35.6007	488	-	-	-	-	-	-	-	-	-	-
Grainstone	1657	Lod_011	3.1304	35.8579	460	nd	0.01	nd	0.00	nd	0.01	nd	0.00	0.00	nd
Grainstone	1667	Lod/023	3.1304	35.8579	460	-	-	-	-	-	-	-	-	-	-
Holocene sediments	3820	Stop 5A	3.1502	35.4910	509	0.14	0.01	0.00	0.00	0.00	0.01	nd	nd	0.00	nd
Holocene sediments	3821	Stop 5B	3.1502	35.4910	509	0.19	0.01	0.00	0.00	0.00	0.02	nd	nd	0.00	nd
Holocene sediments	3822	Stop 5C	3.1502	35.4910	509	0.19	0.01	0.00	0.00	0.00	0.02	nd	nd	0.00	nd

Holocene sediments	3823	Stop 5D	3.1502	35.4910	509	0.02	0.01	nd	0.00	0.00	0.01	nd	nd	0.00	nd
Holocene sediments	3824	Stop 8A	3.1229	35.5394	503	0.13	0.01	0.00	0.00	0.01	0.02	nd	nd	0.00	nd
Holocene sediments	3825	Stop 8B	3.1229	35.5394	503	0.05	0.01	0.00	0.00	nd	0.01	nd	nd	0.00	nd
Holocene sediments	3826	Stop 14A	3.0857	35.5573	510	0.02	0.00	nd	0.00	nd	0.01	nd	nd	0.00	nd
Holocene sediments	3827	Stop 14B	3.0857	35.5573	510	nd	0.01	nd	0.02	nd	0.01	nd	0.00	0.00	nd
Holocene sediments	3829	Stop 14C	3.0857	35.5573	510	0.06	0.01	0.00	0.00	0.00	0.01	nd	nd	0.00	nd
Holocene sediments	3852	Stop 93C	3.1830	35.8036	451	0.10	0.01	0.00	0.00	0.02	0.02	nd	nd	0.00	nd
Holocene sediments	3853	Stop 93D	3.1830	35.8036	451	0.10	0.01	0.00	0.00	0.00	0.01	nd	nd	0.00	nd
Holocene sediments	3854	Stop 126	3.1417	35.7358	496	0.01	0.01	nd	0.00	nd	0.01	nd	nd	0.00	nd
Holocene sediments	3855	Stop 130	3.1420	35.7838	461	0.01	0.01	0.00	0.00	0.00	0.01	nd	nd	0.00	nd
Basement	3841	Stop 50	3.2748	35.5944	582	0.01	0.01	nd	0.00	0.03	0.01	nd	nd	0.00	nd
Basement	3843	Stop 50	3.2748	35.5944	582	0.01	0.08	0.00	0.02	nd	0.01	nd	nd	0.00	nd
Basement	3846	Stop 71	2.8575	35.6146	616	nd	0.08	0.00	0.01	nd	0.01	nd	0.00	0.00	nd
Nepheline-phonolite	1650	Lod_004	3.1139	35.5858	502	0.10	0.00	0.00	0.00	nd	0.02	nd	0.00	0.00	nd
Nepheline-phonolite	1674	Lod/030	3.1138	35.5856	497	-	-	-	-	-	-	-	-	-	-
Nepheline-phonolite	1653	Lod_007	3.1093	35.5947	498	0.71	0.01	0.00	0.00	0.02	0.02	nd	0.00	nd	nd
Sandstone	1645	Stop 1	3.0946	35.5336	516	-	-	-	-	-	-	-	-	-	-
Sandstone	1658	Lod/013	3.1136	35.5810	497	-	-	-	-	-	-	-	-	-	-
Sandstone	1659	Lod/014	3.1136	35.5810	497	-	-	-	-	-	-	-	-	-	-
Sandstone	1668	Lod/024	3.1304	35.8579	460	-	-	-	-	-	-	-	-	-	-
Sandstone	1669	Lod/025	3.1304	35.8579	460	-	-	-	-	-	-	-	-	-	-
Sandstone	1670	Lod/026	3.1095	35.7868	517	-	-	-	-	-	-	-	-	-	-
Sandstone	1675	Lod_031	3.1420	35.8630	429	0.01	0.00	nd	0.00	nd	0.01	nd	nd	0.00	nd
Sandstone	1676	Lod_032	3.1420	35.8630	429	0.01	0.01	0.00	0.00	0.00	0.01	nd	nd	0.00	nd
Sandstone	1678	Lod_034	3.1420	35.8630	429	0.07	0.01	0.00	0.00	0.00	0.01	nd	nd	0.00	nd
Sandstone	3832	Stop 25	3.0077	35.5163	536	0.00	0.01	nd	0.00	nd	0.01	nd	nd	0.00	nd
Sandstone	3833	Stop 25	3.0063	35.5171	542	0.01	0.01	nd	0.00	nd	0.01	nd	nd	0.00	nd

Sandstone	3842	Stop 50	3.2748	35.5944	582	nd	0.00	0.00	0.00	nd	0.03	nd	nd	0.00	nd
Sandstone	3847	Stop 90	3.1427	35.7389	441	0.01	0.00	nd	0.00	0.00	0.01	nd	nd	0.00	nd
Sandstone	3850	Stop 93A	3.1830	35.8036	451	0.18	0.01	0.00	0.01	0.00	0.02	nd	nd	0.00	nd
Sandstone	3858	Stop 139	3.1263	35.6475	462	nd	0.00	nd	0.00	0.00	0.01	nd	nd	0.00	nd
Turkana Grit	1646	Stop 2	3.0798	35.5401	509	-	-	-	-	-	-	-	-	-	-
Turkana Grit	1649	Lod/003	3.1084	35.5933	497	-	-	-	-	-	-	-	-	-	-
Turkana Grit	1651	Lod/005	3.1095	35.5948	499	-	-	-	-	-	-	-	-	-	-
Turkana Grit	1652	Lod/006	3.1622	35.6192	508	-	-	-	-	-	-	-	-	-	-
Turkana Grit	1654	Lod_008	3.1915	35.8344	482	0.01	0.00	nd	0.00	nd	0.01	nd	nd	0.00	nd
Turkana Grit	1655	Lod_009	3.1336	35.6007	488	0.74	0.01	0.00	0.00	0.01	0.02	nd	0.00	nd	nd
Turkana Grit	1671	Lod/027	3.1095	35.7868	517	-	-	-	-	-	-	-	-	-	-
Turkana Grit	1672	Lod/028	3.1095	35.7868	517	-	-	-	-	-	-	-	-	-	-
Turkana Grit	1673	Lod/029	3.0946	35.5333	516	-	-	-	-	-	-	-	-	-	-
Turkana Grit	3830	Stop 15	3.0899	35.5567	483	0.01	0.01	nd	0.00	nd	0.01	nd	nd	0.00	nd
Turkana Grit	3831	Stop 24	3.0077	35.5163	536	0.02	0.01	0.00	0.00	nd	0.01	nd	nd	0.00	nd
Turkana Grit	3835	Stop 39	3.0063	35.5171	542	0.01	0.01	0.00	0.00	0.00	0.01	nd	nd	0.00	nd
Turkana Grit	3836	Stop 39	3.0399	35.4839	516	0.05	0.01	0.00	0.00	0.00	0.01	nd	nd	0.00	nd
Turkana Grit	3838	Stop 49	3.2749	35.6269	583	0.08	0.01	0.00	0.00	0.01	0.01	nd	nd	0.00	nd
Turkana Grit	3839	Stop 50	3.2749	35.6269	583	nd	0.00	0.00	0.00	nd	0.02	nd	nd	0.00	nd
Turkana Grit	3848	Stop 91	3.1974	35.7690	479	0.07	0.01	0.00	0.01	nd	0.01	nd	0.00	0.00	nd
Turkana Grit	3849	Stop 91	3.1974	35.7690	479	0.00	0.01	0.00	0.00	nd	0.01	nd	nd	0.00	nd
Turkana Grit	3856	Stop 132	3.1421	35.7843	457	0.04	0.01	nd	0.00	nd	0.01	nd	nd	0.00	nd

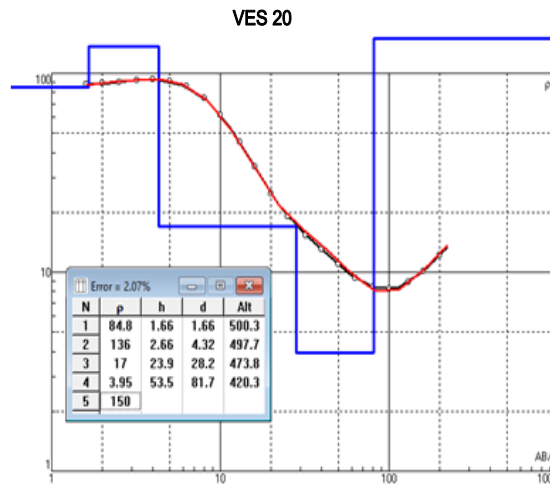
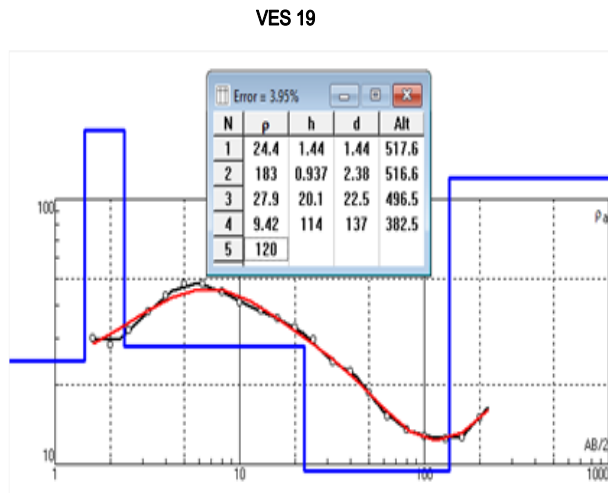
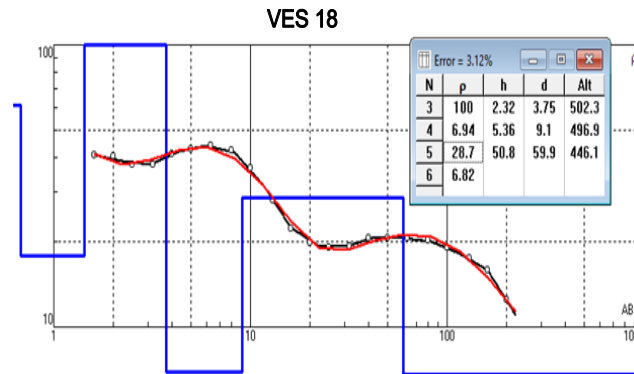
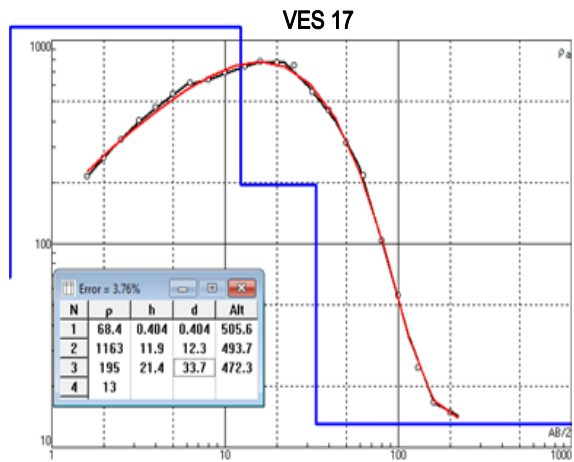
Appendix 4.10: Results of the vertical electrical soundings for VES 1 to VES 15

AB/2	MN/2	VES 1	VES 3	VES 4	VES 5	VES 6	VES 7	VES 8	VES 9	VES 10	VES 11	VES 12	VES 13	VES 14	VES 15
Latitude		3.11233	3.10599	3.10567	3.10711	3.11173	3.11299	3.10144	3.09746	3.10813	3.11773	3.12451	3.08444	3.0767	3.07674
Longitude		35.5964	35.6418	35.6432	35.6613	35.6528	35.6535	35.6673	35.7147	35.7192	35.7104	35.7244	35.5717	35.5663	35.5708
Elevation		474	479	472	467	476	474	470	485	482	466	457	492	494	501
1.6	0.5	1054	1065	1550	3822	265.1	134.7	2619	55.2	101.8	15.73	69.18	84.2	275.2	86.4
2	0.5	638.1	1039	1499	3401	169.4	103.4	2597	50.7	100.5	17.86	80.42	95.6	253.9	72
2.5	0.5	342.8	1001	1426	3209	135.5	80.89	2560	47	98.58	20.95	92.62	105	232.3	58.3
3.2	0.5	161.7	938.5	1307	2883	140.6	66.5	2480	44	95.38	26.04	106.6	107	209.1	44
4	0.5	96.01	866.5	1173	2317	161.4	62.5	2356	40.8	91.99	32.24	119.6	104	190.3	39.7
5	0.5	74.72	785	1029	1690	187.7	64.51	2158	35.7	89.29	40.2	132.5	100	172.4	36.2
6.3	0.5	69.95	697.3	885	1263	215.9	71.48	1857	31.7	89.34	50.64	145.4	88.3	151.9	36.7
8	0.5	68.17	606.9	754.6	943	244.8	83.11	1451	29.2	94.87	64.29	158.3	75	126.5	37
10	0.5	67.12	520.5	647	758	269.2	97.62	1032	26.3	106.6	80.35	170.2	64.8	98.42	39.5
13	0.5	65.92	411.7	522.3	583	292.5	118.6	584.5	23.3	128.4	104.4	185.2	62.3	64.22	42
16	0.5	64.64	322.2	417.8	423	305.6	137.7	325.5	19.6	151	128.5	199.7	64	40.86	43.1
20	0.5	62.59	231.8	303.8	238	314.5	160.3	155.3	16.5	179.4	160.6	220.5	68.3	23.01	40.7
25	0.5	59.42	159.9	201.9	108	319.7	185	70.95	13.5	211.5	200.7	250.6	83.1	13.44	36.5
32	10	54.28	109.1	125.5	48.3	324.7	214.1	31.05	10.7	250.6	256.8	299.8	106	8.976	30.4
40	10	48.2	85.32	91.96	28.6	333.1	241.7	16.54	8.02	287.9	320.9	363.4	127	7.733	19.3
50	10	41.32	73.68	83.52	23.4	350.4	270.3	10.85	7.71	324.9	400.8	448.3	147	7.274	16.7
63	10		67.23	89.03	21	382.3	301.5	8.855	8.12	360.1	504.7	562.2	177	6.965	12.6
80	10		61.9	99.19	19.3	434.6	336.9	8.616	8.12	386.9	640.3	712	215	6.68	11.2
100	10		57.24	109.4	18.9	502.4	376.1	9.054	8.74	394.1	799.4	887.9		6.443	12.3
130	10		52.32	120.5	19.3	604.4	436.4	10.18	9.5	391.4	1038	1150		6.213	13.5
160	10		49.21	128.8	19.5	698.8	502.6	11.67	10		1275	1411		6.078	17.6
200	10		46.82		20.7	810.5	600.8	13.98	11.3		1590	1756		5.975	21.3

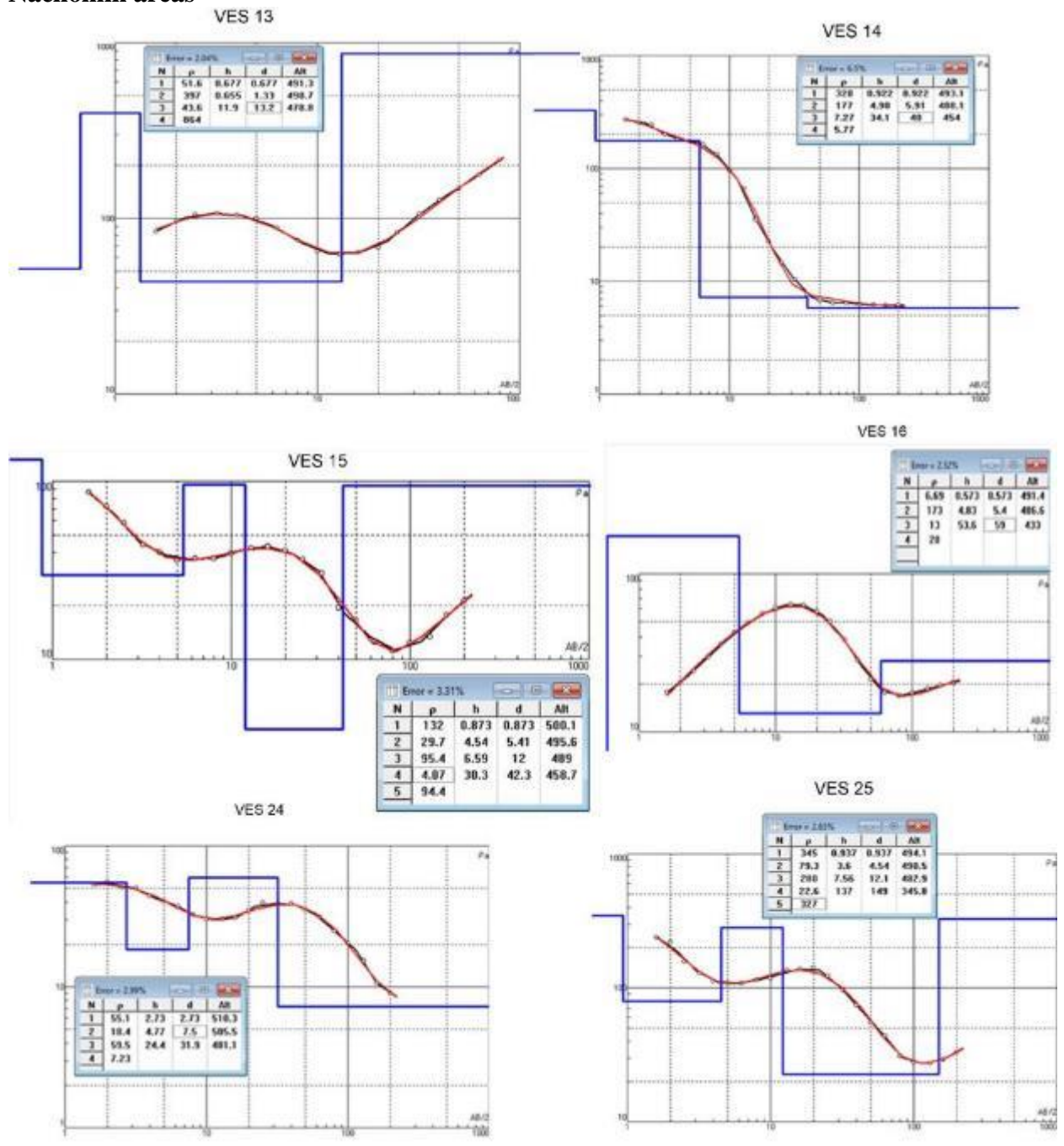
Appendix 4.11: Results of the vertical electrical soundings of VES 16 to VES 27

AB/2	MN/2	VES 16	VES 17	VES 18	VES 19	VES 20	VES 21	VES 22	VES 23	VES 24	VES 25	VES 26	VES 27
Latitude		3.0645	3.0712	3.0850	3.0514	3.1009	3.1448	3.1487	3.0140	3.0356	3.0544	3.1047	3.1107
Longitude		35.5587	35.5075	35.5287	35.4949	35.5378	35.7014	35.7251	35.5211	35.5302	35.5442	35.6902	35.6666
Elevation		492	506	506	518	502	466	462	534	513	495	471	469
1.6	0.5	17.7	213	40.7	29.8	87.6	102	62.69	23.2	53	238	69.7	2355
2	0.5	20.6	263	40.1	28.3	88.8	108	64.4	24.8	55.5	218	56.6	2510
2.5	0.5	24.3	323	37.6	32	90.4	115	66.97	24.4	50.8	156	58.3	2647
3.2	0.5	29.7	402	37.7	37.7	92.2	125	71.24	27.5	50.2	129	53.4	2762
4	0.5	35.5	465	41.2	43.3	92.9	135	76.14	30.8	43.9	112	49.5	2836
5	0.5	42	545	42.8	47.8	91.3	141	81.26	34.7	40.3	109	47.3	2878
6.3	0.5	48.9	620	44.1	48	85.8	140	85.48	39.3	37.2	109	43.8	2881
8	0.5	55.8	640	42.2	44.6	75.3	130	86.81	44.6	32.4	115	43.8	2827
10	0.5	60.8	689	36.6	40.7	62	111	83.84	52.3	30.3	117	41.1	2704
13	0.5	63.8	742	28.1	38.1	45.2	80.9	74.48	60.4	30.2	135	37.7	2436
16	0.5	62.8	789	22.4	35.7	33.7	56.9	63.46	67.1	30.8	138	32.9	2112
20	0.5	58	775	19.8	32.7	24.8	36.1	50.15	71.4	34.8	141	28.1	1664
25	0.5	49.6	747	19.2	29.4	19.1	23.7	37.89	70.6	39.2	123	24.7	1163
32	10	38.1	554	19.3	24.1	15.4	17.8	27.77	69.5	38.7	96.3	22.2	657
40	10	28.4	451	20.7	22.4	13	16.9	22.07	72.5	39.1	74.1	18.4	326
50	10	21.4	313	20.7	18.6	11	17.1	18.76	72.4	35.1	55.2	17.1	134
63	10	17.7	216	20.7	15.2	9.37	17.1	16.84	65.1	31.4	43.5	17	55.8
80	10	16.9	103	20.2	13.6	8.39	16.5	15.87	50.1	24.9	31	17.6	44.2
100	10	17.5	55.7	19.1	12.8	8.21	15.4	15.98	42.5	20.5	27.9	18.5	40.5
130	10	18.8	24.4	17.5	12.5	8.88	13.9	17.67	28.1	15.4	27.2	19.2	39.9
160	10	19.7	16.5	15.9	12.6	10.1	12.7	20.4	15.9	10.5	29.1	19	47
200	10	20.5	14.7	12.5	15	12.2	11.8	24.77	8.89	9.01	33.1	22.8	57.7

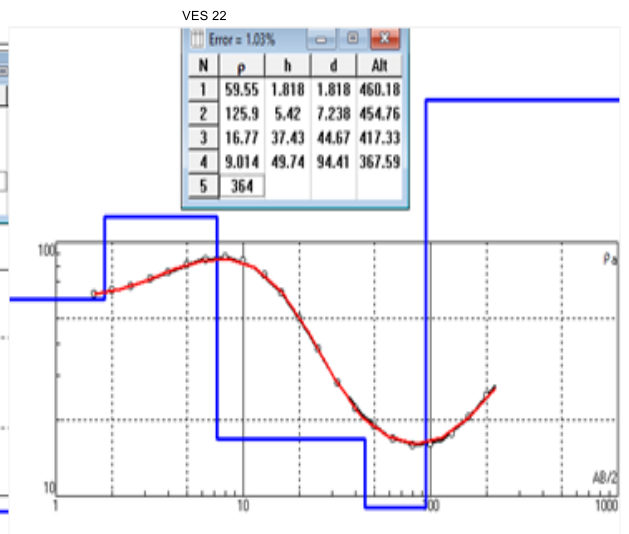
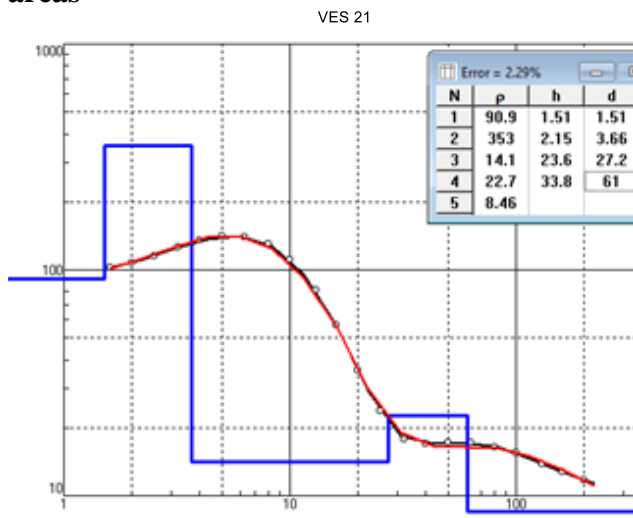
Appendix 4.12: VES graphs for VES 17 to 20 carried out on section A of the LAAS around Nadapal and Naoyatira areas



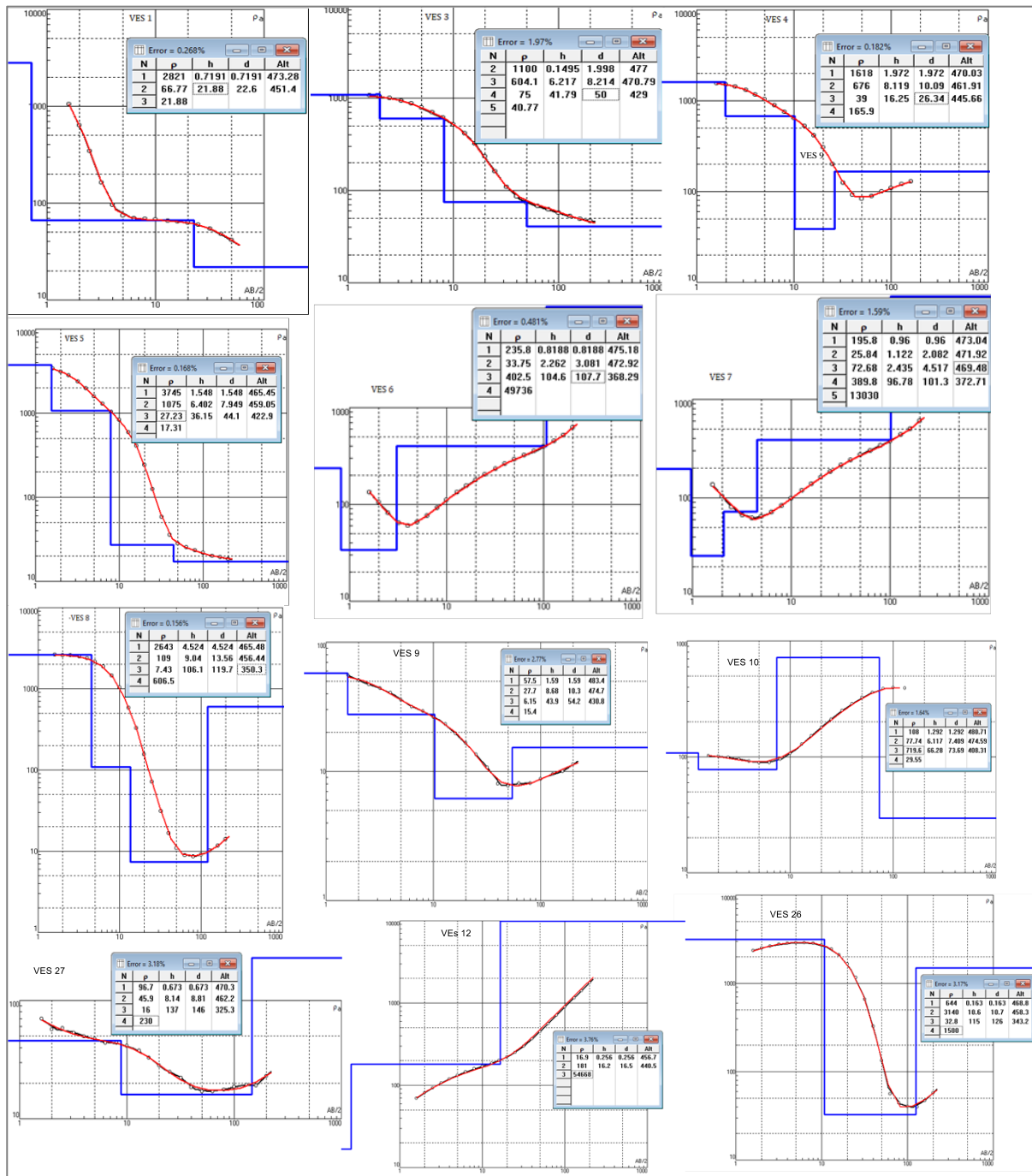
Appendix 4.13: VES graphs carried out in section B of the LAAS between Kakemera and Nachomin areas



Appendix 4.14: VES graphs for section C of the LAAS around Kakwanyang and Nang'omo areas



Appendix 4.15: VES graphs of section d of the LAAS covering Napuu, Lolupe and Nayuu areas



Appendix 4.16: Results for oxygen-18, deuterium and tritium for rainfall and surface water (Turkwel River = TR, Kawalase River = KR, water pans = pan, scoop holes = SH, Eliye sprong and Lake Turkana = LT) samples in Lodwar and its environs

No	Sample_Date	Sample ID	Lat	Long	Elevation (m)	Sample Code	Type	18O	2H	TU
1	18/02/2018	Rain Sample (REACH Office)	3.101107°	35.602050°	517	2442	Rain	-1.33	7.4	1.7
2	18/02/2018	Turkwel at KEFRI near Bh 1	3.1124	35.5990	485	2440	TR	0.37	6.6	2.1
3	18/02/2018	Turkwel at Kangangetei	3.1440	35.8593	410	2437	TR	0.89	9.8	nm
4	18/02/2018	Turkwel at Nangolekuruk	3.1096	36.0502	387	2441	TR	0.90	7.6	nm
5	18/02/2018	Turkwel_Namupoth	3.1590	35.8243	430	2438	TR	0.06	6.5	nm
6	21/05/2018	Kalawase Tri	3.1302	35.5219	510	3293	KR	0.25	2.6	nm
7	21/05/2018	Nakutan Pan	3.1249	35.4871	511	3296	Pan	-3.01	-22.5	nm
8	27/05/2018	Monti Water pan	3.1924	35.6387	512	3320	Pan	-4.40	-33.9	nm
9	29/05/2018	Namuthia Water Pan	3.1954	35.6732	489	3332	Pan	-2.67	-15.9	nm
10	30/05/2018	Nakariong'ora Water Pan	3.2217	35.7798	482	3342	Pan	-2.52	-10.7	nm
11	03/06/2018	Kerio water Pan	3.0909	35.6851	482	3375	Pan	0.19	0.9	nm
12	21/05/2018	Nakutan Lagga 1	3.1338	35.4834	505	3294	SH	-1.57	-14.0	nm
13	21/05/2018	Kalawase Lagga	3.1502	35.4910	510	3295	SH	-1.43	-5.2	nm
14	01/06/2018	Monti Lagga	3.2383	35.6293	516	3324	SH	-3.27	-11.4	nm
15	28/05/2018	Kawalase Bridge	3.1329	35.6011	462	3326	SH	-3.65	-23.7	nm
16	28/05/2018	Nakutan Lagga 2	3.1331	35.4997	497	3327	SH	-3.95	-21.6	nm
17	02/06/2018	Monti Lagga	3.1672	35.6496	492	3330	SH	-2.63	-6.9	nm
18	31/05/2018	Nakadukui Lagga	3.1824	35.7582	419	3347	SH	-2.21	-8.0	nm
19	31/05/2018	Chokochok lagga	3.1580	35.7458	459	3348	SH	-1.96	-2.4	nm
20	18/02/2018	Eliye Springs	3.2525	36.0207	382	2436	Spring	-2.51	-7.4	nm
21	18/02/2018	Lake Turkana_Eliye	3.2536	36.0217	363	2461	LT	5.41	41.3	1.7
22	18/02/2018	Lake_Turkwel_Delta	3.0584	36.1433	373	2462	LT	6.60	42.4	1.8

Appendix 4.17: Results for oxygen-18, deuterium and tritium for groundwater samples in shallow alluvial aquifer (SAA), Turkana grit shallow aquifer (TGSA), intermediate aquifer (IA), deep aquifer (DA), and for wells with unknown depth (DU); (nm = not measured)

No.	Sample_Date	SampleID	Aquifer	Lat	Long	Elevation (m)	Sample Code	Type	18O	2H	TU
1	31/05/2018	Akibululu Hp	SAA	3.1527	35.7678	456	3344	Hp	-0.50	2.7	1.8
2	03/06/2018	Bh 1A	SAA	3.1131	35.5980	497	3381	Bh	-2.89	-9.5	nm
3	03/06/2018	Bh 1B	SAA	3.1127	35.5984	501	3380	Bh	-2.92	-13.1	nm
4	03/06/2018	Bh 2C	SAA	3.1108	35.5928	493	3382	Bh	0.25	3.5	nm
5	03/06/2018	Bh 3	SAA	3.1133	35.6005	489	3383	Bh	-1.33	-0.1	1.8
6	03/06/2018	Bh 5	SAA	3.1117	35.5972	486	3387	Bh	-0.41	4.2	nm
7	03/06/2018	Bh 7	SAA	3.1077	35.5824	482	3384	Bh	-0.51	3.6	1.8
8	03/06/2018	Bh 9	SAA	3.1122	35.5963	489	3388	Bh	-0.63	2.2	1.6
9	24/05/2018	Kakemera Pri Hp	SAA	3.0860	35.5621	524	3300	Hp	-1.28	1.4	nm
10	03/06/2018	KFS Hp	SAA	3.1128	35.6002	500	3390	Hp	-2.24	-10.5	1.1
11	31/05/2018	Locher A Akalale Hp	SAA	3.1525	35.7583	415	3298	Hp	-0.85	4.5	nm
12	31/05/2018	Lodwar Mixed Pri 1	SAA	3.1186	35.6104	500	3349	Hp	-0.24	3.9	1.4
13	31/05/2018	Lodwar Mixed Pri 2	SAA	3.1186	35.6116	496	3355	Hp	-0.51	4.7	nm
14	28/05/2018	Lokipetot Bh	SAA	3.0892	35.5488	500	3329	Bh	-1.02	0.0	nm
15	01/06/2018	Lolupe 3 Hp	SAA	3.1063	35.6809	434	3360	Hp	-1.68	-5.2	1.3
16	01/06/2018	Nabulon Drinking water well	SAA	3.1363	35.7325	486	3365	Hp	-0.60	4.1	nm
17	26/05/2018	Nadapal Hp	SAA	3.0684	35.5092	508	3313	Hp	-0.28	2.5	1.5
18	30/05/2018	Nakwalele Hp 2	SAA	3.1322	35.6312	460	3338	Hp	-0.74	0.8	1.3
19	26/05/2018	Nakwamekwi Pri Bh	SAA	3.1115	35.5790	509	3307	Bh	-1.29	-1.4	nm
20	26/05/2018	Naregai Bh	SAA	3.0992	35.5584	477	3312	Bh	-1.92	-3.4	nm
21	31/05/2018	Nasenyait Hp 2	SAA	3.1224	35.6230	480	3351	Hp	0.25	5.8	2.2
22	31/05/2018	Natotol	SAA	3.1178	35.6176	482	3354	Hp	-0.53	4.7	nm
23	05/06/2018	Al Noor Community Hp	TGSA	3.1218	35.5912	528	3396	Hp	-2.35	-9.9	<0.8
24	29/05/2018	Bokotom Hp	TGSA	3.1689	35.6934	481	3334	Hp	-2.53	-10.4	<0.8
25	05/06/2018	Loyo Pri Hp	TGSA	3.1219	35.5811	514	3399	Hp	-2.53	-10.7	nm

26	29/05/2018	Namuthia Hp	TGSA	3.1792	35.7004	493	3345	Hp	-3.05	-13.1	<0.8
27	29/05/2018	Talent High Sch Hp	TGSA	3.1918	35.6755	502	3331	Hp	-3.33	-14.8	nm
28	04/06/2018	Trumpet of Hope Ministries	TGSA	3.1206	35.5829	491	3394	Hp	-1.93	-8.8	<0.8
29	03/06/2018	Bh 6	IA	3.1080	35.5935	499	3389	Bh	-1.44	-3.7	nm
30	30/05/2018	Chokochok Pry	IA	3.1423	35.7394	453	3341	Hp	0.07	4.5	1.9
31	03/06/2018	Chukultom Hp	IA	3.1183	35.5802	497	3386	Hp	-2.82	-8.7	nm
32	05/06/2018	Comboni Girls	IA	3.1146	35.5643	532	3398	Bh	-2.54	-9.9	nm
33	01/06/2018	Eleleia Pri Hp	IA	3.1247	35.7357	465	3364	Hp	-2.77	-9.4	<0.8
34	24/05/2018	Kakemera Church	IA	3.0654	35.5616	513	3302	Hp	-2.61	-7.9	1.0
35	26/05/2018	Kochoda Hp	IA	3.1040	35.5631	482	3391	Hp	-2.24	-5.7	nm
36	25/05/2018	Limyounsim Bh	IA	2.9994	35.5137	549	3309	Bh	-2.89	-10.7	<0.8
37	01/06/2018	Loporkou-Eleleai Hp	IA	3.1231	35.7491	486	3366	Hp	-3.92	-9.7	nm
38	25/05/2018	Nachomin Bh	IA	3.0131	35.5195	547	3306	Bh	-2.74	-10.6	<0.8
39	26/05/2018	Nadapal Supply bh	IA	3.0734	35.5095	498	3314	Bh	-1.91	-5.8	nm
40	26/05/2018	Nagis Bakhita Bh	IA	3.0440	35.4902	527	3317	Bh	-2.67	-8.6	<0.8
41	26/05/2018	Nakwamekwi Hp	IA	3.1101	35.5759	509	3310	Hp	-2.40	-7.6	nm
42	02/06/2018	Napuu 2	IA	3.1061	35.6409	490	3373	Bh	-1.79	-4.1	nm
43	02/06/2018	Napuu 4 Resample	IA	3.1053	35.6417	480	3374	Bh	-0.63	0.3	1.5
44	27/05/2018	Nareng'elup 2	IA	3.2379	35.6301	535	3323	Hp	-2.63	-10.8	nm
45	01/06/2018	Natot Pri Bh	IA	3.1143	35.6452	508	3357	Bh	-1.47	-0.4	nm
46	04/06/2018	Nauren Puu	IA	3.0888	35.5359	516	3392	Bh	-0.50	-0.9	nm
47	01/06/2018	Nayuu Hp 4	IA	3.1066	35.7111	491	3368	Hp	-3.09	-7.0	nm
48	01/06/2018	Nayuu Hp Resample	IA	3.1082	35.7214	475	3363	Hp	-2.56	-11.3	nm
49	02/06/2018	Napuu 1 Resample	DA	3.1061	35.6407	502	3372	Bh	-1.17	-2.7	1.0
50	01/06/2018	Natirnalulung Bh	DA	3.1460	35.7809	462	3367	Bh	-0.23	3.9	2.1
51	01/06/2018	Akiremet Hp	DU	3.0990	35.7039	494	3369	Hp	-2.74	-11.2	<0.8
52	31/05/2018	Akwanga ECD	DU	3.1243	35.6214	469	3352	Hp	-0.80	1.3	nm
53	05/06/2018	Al Noor Academy	DU	3.1204	35.5914	521	3395	Bh	-2.50	-9.7	nm
54	05/06/2018	Al Noor Comboni Bh	DU	3.1136	35.5632	532	3400	Bh	-4.37	-24.7	nm

55	02/06/2018	Apuwa Bh	DU	3.0525	35.5506	527	3379	Bh	-2.40	-5.1	nm
56	02/06/2018	Canaan Bh	DU	3.0856	35.6076	523	3378	Bh	-4.09	-11.9	nm
57	26/05/2018	Frontier Ltd Bh	DU	3.0640	35.4968	522	3318	Bh	-2.91	-9.6	<0.8
58	25/05/2018	KAG Church Bh	DU	3.0005	35.5127	555	3308	Bh	-2.69	-12.3	nm
59	24/05/2018	Kakemera ECD Hp	DU	3.0695	35.5713	535	3301	Hp	-2.92	-10.4	nm
60	30/05/2018	Kakwanyang Dispensary Bh	DU	3.1314	35.6696	495	3339	Bh	-2.02	-9.5	nm
61	27/05/2018	Katapakori Hp	DU	3.1991	35.6437	513	3321	Hp	-3.47	-12.8	1.4
62	27/05/2018	Katapakori Hp 2	DU	3.2093	35.6398	518	3322	Hp	-2.18	-6.2	nm
63	05/06/2018	Kenya Redcross Bh	DU	3.1120	35.5878	491	3397	Bh	-1.88	-7.6	nm
64	29/05/2018	Km 62 Bh (Lotherere)	DU				3336	Bh	-3.86	-20.1	<0.8
65	24/05/2018	Loborot bh	DU	3.0911	35.5818	497	3356	Boreholes	nm	nm	nm
66	31/05/2018	Lochukae Hp	DU	3.1291	35.6267	488	3346	Hp	-0.63	2.1	1.4
67	26/05/2018	Lokipetot Hp	DU	3.1036	35.5496	502	3319	Hp	-2.96	-10.3	nm
68	01/06/2018	Lolupe Handpump Resample	DU	3.1059	35.6863	481	3361	Hp	-3.72	-9.9	nm
69	01/06/2018	Lolupe Hp 2	DU	3.1086	35.6726	482	3358	Hp	-0.45	-2.0	1.5
70	01/06/2018	Lolupe Pri Hp	DU	3.1076	35.6750	482	3359	Hp	-1.28	-2.3	nm
71	21/05/2018	Loyo Handpump	DU	3.1255	35.5558	462	3297	Hp	-1.87	-9.3	<0.8
72	26/05/2018	Missionary of St Paul	DU	3.1056	35.5699	485	3311	Bh	-1.27	-3.7	nm
73	27/05/2018	Nabuelpus Hp	DU	3.2537	35.6054	545	3325	Hp	-1.97	-9.6	1.5
74	25/05/2018	Nabuin Hp	DU	3.0355	35.5347	530	3305	Hp	-2.39	-8.4	<0.8
75	24/05/2018	Naiwotorong Water Supply	DU	3.0849	35.5721	493	3299	Bh	nm	nm	nm
76	31/05/2018	Nakadukui Bh	DU	3.1530	35.7730	476	3343	Bh	-0.12	5.9	nm
77	31/05/2018	Nakoporor Hp	DU	3.1204	35.6148	482	3353	Hp	-1.21	1.5	nm
78	31/05/2018	Namutheigalai Bh	DU	3.1522	35.7647	475	3340	Bh	nm	nm	nm
79	29/05/2018	Nang'omo 1 Hp	DU	3.1714	35.7119	477	3333	Hp	-3.41	-13.3	<0.8
80	29/05/2018	Nang'omo 2 Hp	DU	3.1540	35.7081	470	3335	Hp	-2.81	-10.6	nm
81	30/05/2018	Nang'omo 3 Hp	DU	3.1436	35.7099	474	3337	Hp	-1.29	-1.5	1.2
82	24/05/2018	Naotin Bh 2	DU	3.0423	35.5406	521	3303	Bh	-3.08	-8.8	nm
83	25/05/2018	Naotin Hp 3	DU	3.0380	35.5450	526	3304	Hp	-2.39	-9.0	<0.8

84	26/05/2018	Naoyatira Hp	DU	3.0669	35.4868	513	3315	Hp	-3.05	-11.4	nm
85	26/05/2018	Naoyatira Pri Bh	DU	3.0653	35.4654	516	3316	Bh	-2.84	-9.8	<0.8
86	02/06/2018	Napuu Pri Hp	DU	3.1126	35.6314	490	3371	Hp	-1.01	0.3	1.8
87	31/05/2018	Nasenyanaait Hp	DU	3.1233	35.6238	475	3350	Hp	-0.19	4.4	nm
88	28/05/2018	Natapeno Hp	DU	3.0936	35.5078	529	3328	Hp	-2.66	-8.0	nm
89	02/06/2018	Nawaitorong Mixed Sch Bh	DU	3.1122	35.6205	510	3370	Bh	-3.34	-13.6	nm
90	01/06/2018	Nayuu-Katilo Hp	DU	3.1238	35.7082	468	3362	Hp	-1.15	0.8	nm
91	03/06/2018	Ngilukomong' Hp	DU	3.1144	35.5822	506	3385	Hp	-1.61	-1.2	nm
92	02/06/2018	Opp Stagra Bh	DU	3.0867	35.6185	514	3376	Bh	-2.01	-8.9	<0.8
93	02/06/2018	Stegra Hotel Bh	DU	3.0869	35.6177	542	3377	Bh	-3.44	-13.4	nm
94	04/06/2018	Turkana Educational Centre	DU	3.1106	35.5695	490	3393	Hp	-2.36	-5.4	1.5

Appendix 4.18: Groundwater samples in the SAA, IA, DA and for wells with unknown depth (DU) used in the calculation of age of groundwater in the LAAS

No	SampleID	Lat	Long	Elevation (m)	Aquifer	Sample Code	Depth (m)	Tritium	Age of Groundwater	Age (Years)	Year
1	Nadapal Hp	3.0684	35.5092	508	SAA	3313	8	1.5	After 1950	7	2011
2	Nakwalele Hp 2	3.1322	35.6312	460	SAA	3338	22	1.3	After 1950	5	2013
3	Akibululu Hp	3.1527	35.7678	456	SAA	3344	9.5	1.8	After 1950	10	2008
4	Locher A Akalale Hp	3.1291	35.6267	488	SAA	3346	27	1.4	After 1950	6	2012
5	Nasenyait Hp 2	3.1224	35.6230	480	SAA	3351	7.5	2.2	After 1950	14	2004
6	Lodwar Mixed Pri 1	3.1186	35.6116	496	SAA	3355	20	1.4	After 1950	6	2012
7	Lolupe 3 Hp	3.1063	35.6809	434	SAA	3360	17	1.3	After 1950	5	2013
8	Bh 3	3.1133	35.6005	489	SAA	3383	22	1.8	After 1950	10	2008
9	Bh 7	3.1077	35.5824	482	SAA	3384	20	1.8	After 1950	10	2008
10	Bh 9	3.1122	35.5963	489	SAA	3388	30	1.6	After 1950	8	2010
11	KFS Hp	3.1128	35.6002	500	SAA	3390	17	1.1	After 1950	2	2016
12	Kakemera Church	3.0654	35.5616	513	IA	3302	45	1	After 1950	0	2018
13	Chokochock Pry	3.1423	35.7394	453	IA	3341	38	1.9	After 1950	11	2007
14	Napuu 4 Resample	3.1053	35.6417	480	IA	3374	52	1.5	After 1950	7	2011
15	Katapakori Hp	3.1991	35.6437	513	DU	3321		1.4	After 1950	6	2012
16	Nabuelpus Hp	3.2537	35.6054	545	DU	3325		1.5	After 1950	7	2011
17	Nang'omo 2 Hp	3.1436	35.7099	474	DU	3337		1.2	After 1950	3	2015
18	Nang'omo 3 Hp	3.1522	35.7647	475	DU	3340		1.2	After 1950	3	2015
19	Lochukae Hp	3.1186	35.6104	500	DU	3349		1.4	After 1950	6	2012
20	Lolupe Hp 2	3.1086	35.6726	482	DU	3358		1.5	After 1950	7	2011
21	Napuu Pri Hp	3.1126	35.6314	490	DU	3371		1.8	After 1950	10	2008
22	Turkana Educational Centre	3.1106	35.5695	490	DU	3393		1.5	After 1950	7	2011
23	Natirnalulung Bh	3.1460	35.7809	462	DA	3367	102	2.1	After 1950	13	2005
24	Napuu 1 Resample	3.1061	35.6407	502	DA	3372	110	1	After 1950	0	2018